2016

Archean Geodynamic Conditions Using P-T Constraints of the East Pilbara Craton TTGs

Andrew Kody Webb
Louisiana State University and Agricultural and Mechanical College

ARCHEAN GEODYNAMIC CONDITIONS USING P-T CONSTRAINTS OF THE EAST PILBARA CRATON TTGS

A Thesis

Submitted to the Graduate Faculty of the
Louisiana State University and
Agricultural and Mechanical College
in partial fulfillment of the
requirements for the degree of
Master of Science

in

the Department of Geology and Geophysics

by
Andrew Kody Webb
B.S. Louisiana State University, 2013
December 2016

Dedication

First, I would like to thank my advisor, Dr. Alex Webb, for working with me and believing in me. I would also like to thank my committee members, Dr. Clayton Loehn, Dr. Huiming Bao, and Dr. Carol Wicks for their extremely helpful advice and support throughout this process. I would also like to thank my collaborators on this project, Dr. T. Mark Harrison at UCLA for laying out the groundwork for this project, the members of the Geological Survey of Western Australia for the samples and insight they provided, Dr. Mark Pecha of the University of Arizona for processing my mineral separates, and Spencer Aertker, my undergraduate assistant for a time. Lastly, I would like to thank my mother and father for their love and support. This project would not exist without all of these people.

Table of Contents

List of Tables

List of Figures

Abstract

We know very little about the tectonic setting present during the Hadean, but based on studies of surviving Hadean zircons, we know that a Hadean protocrust must have been established by at least 4.4 Ga (Kemp et al. 2010), and it must have also been able to accommodate minimum melt conditions (Harrison 2005). Tectonic models for Earth during the Hadean and Archean follow two trends: uniformitarianism and non-uniformitarianism. Uniformitarian models (following the famed geological concept that the present is the key to the past) argue that Hadean zircons and Archean rocks formed via processes akin to modern-style oceanic crust production and subduction. Non-uniformitarian models speculate that a different style of tectonics, likely dominated by magmatism and vertical crustal / lithospheric kinematics, created the Hadean-Archean geological record. In order to help test these models, I studied the East Pilbara craton, an extremely well preserved Archean terrane. The craton consists of eight synclinic granitoid domes surrounded by greenstone belts. This dome-and-keel structure has been interpreted by most workers as the result of vertical tectonics, with prominent research teams arguing that it records buoyancy-driven partial convection within the crust caused by crustal heating by an underlying mantle plume. To examine the conditions present in the East Pilbara Craton and provide a direct point of comparison to the Hadean zircon record, I used titanium-in-zircon geothermometry and zircon U-Pb age dating of zircons from the granitoid domes. These approaches allow a direct comparison with published results from Hadean zircons. The Pilbara zircons show temperatures hotter than Hadean zircons by 400-700° C. The crystallization temperatures estimated from seven Pilbara samples of ages ranging from 3.40-3.21 Ga show a general cooling trend with a slight

increase in temperature c. 3.31 Ga, which could reflect cooling after a crustal heating event. The crustal conditions of the Paleoarchean East Pilbara craton are evidently different than those recorded by the preserved Hadean zircons, and thus may represent a tectonic regime change between the Hadean and Paleoarchean.

1. Introduction

1.1 Early Earth Geodynamic Models

The Hadean age is largely considered to be a time of extreme internal heat loss on Earth, due to high radioactive decay coupled with extraterrestrial collisions (Harrison 2009). This high rate of heat exchange on Earth has created a debate over what the dominant tectonic mechanism was during the Hadean. It is thought that Earth went through phases of heat loss as it gradually cooled after its coalescence as a planet. While several hypotheses about the progression of heat loss exist, geologists are confident that the Earth underwent a period of planet-wide magma ocean and differentiation before developing into modern-style tectonics.

The early Earth is considered to be an extremely hot, continuous magma ocean that, over time, eventually cooled and developed into the modern day style of plate tectonics. While the rate of cooling and crustal generation is debated, evidence from Hadean zircons suggests crust was generated prior to 4-4.4 Ga (Hopkins et al. 2008, 2010 and Kemp et al. 2010) with its rapid cooling resulting in the multiple common hypotheses for crustal formation. Some of these models include (1) Earth quickly cooling to develop modern-style tectonics in the Hadean (Hopkins et al. 2008, 2010, Harrison et al. 2008, Watson and Harrison 2005) (2) proto-plate tectonics, (3) stagnant lid, (4) heat-pipe Earth (Moore and Webb 2013), and (5) the convective overturn model. It is likely that Earth underwent a multistage process of cooling and crustal formation over time, and may have included several of these processes.

2. Tectonic Models

When investigating the tectonic history of Earth, the most basic theory is based on Charles Lyell and James Hutton's theory of Uniformitarianism. For Earth tectonics, this idea predicts that our *modern style of plate tectonics* existed as far back as the Hadean. According to this theory, soon after planetary accretion, Earth's lithosphere quickly cooled into large plates that float on the asthenosphere. These plates move and interact with each other, causing regions of crust destruction and crust creation like those seen today. This hypothesis is based on evidence collected from Hadean zircons, which provide evidence of crustal temperatures lower than the estimated geothermal gradient (Watson and Harrison 2005), show REE signatures that suggest global crust generation before 4.4 GA (Kemp et al. 2010), and mineral inclusions show low P-T conditions (Hopkins et al. 2008, 2010), thus they are inferred to represent slab refrigeration seen in modern-style subduction (Figure 1). This model has similar conditions to the modern Earth, but likely will show a higher geothermal gradient due to radioactive decay of elements and progressive heat loss of the inner planet. Thermally, the plate tectonic model predicts a thick, cold crust with areas of "slab refrigeration" along subduction boundaries.

Magmatic and tectonic evidence from the Archean to the Late Proterozoic suggests that modern day subduction-style tectonics began much later in Earth's history, during the Neoproterozoic (Stern 2008). A few tectonic models attempt to explain this idea, and they suggest that Earth underwent stages of different tectonic models during its transition from magma ocean to modern tectonics. Two of these models include Archean-Proterozoic proto-plate tectonics and stagnant lid tectonics models (Figure 2). The *proto-plate model* suggests that from the Archean until the Proterozoic, progressive cooling of the upper

mantle past the solidus of basalt and peridotite allowed small platelets and large cratons of oceanic crust to form and begin to partially melt into differentiated continental crust (Ernst 2007). This model implies that tectonics were minimal during this time, and that creation of the crust was slow and mantle-plume driven during this time.

Another model, the *stagnant lid*, is the dominant tectonic mechanism for silicate planets in our solar system, and Earth may have also undergone a time of lid tectonics. In this model, temperature and compositional differences in the mantle power its convection, and it is contained under a single, rigid tectonic plate that spans the entire planet. As the magmatic Earth cooled, it may have cause planet-wide crystallization of primitive crustal material, engulfing the planet in a single crustal plate. This model was developed to explain the tectonic setting on cooling, dying planets, but it may range in thermal settings from a cold and thick lithosphere with slow mantle convection, similar to the Moon, or a thin and hot lithosphere with fast mantle convection (Solomatov and Moresi 1996). While this model is viable on other hot planets with vigorous mantle convection, the presence of water on Earth weakens the crust and increases the chance of crustal breaking and destruction of the stagnant lid.

Another model, and the most recently proposed, offers an intermediate mechanism of heat transfer between the magma ocean and modern plate tectonics endmembers. Based on evidence from Jupiter's moon, Io, the *heat-pipe planet* model suggests that heat is lost through advection of mantle to the surface by volcanic channels, named heat pipes (Moore and Webb 2013). This model, similar to the stable stagnant lid model, predicts a single solid plate over the planet and allows for a thick lithosphere with heat loss multiple times that of modern Earth. However, unlike the stable stagnant lid model, it provides a

mechanism for crustal recycling and mantle differentiation. This model also predicts that during times of extreme heat loss, advection dominates conduction, and the cold lithosphere can sink further into the lower mantle before conduction heats and recycles it (Figure 3).

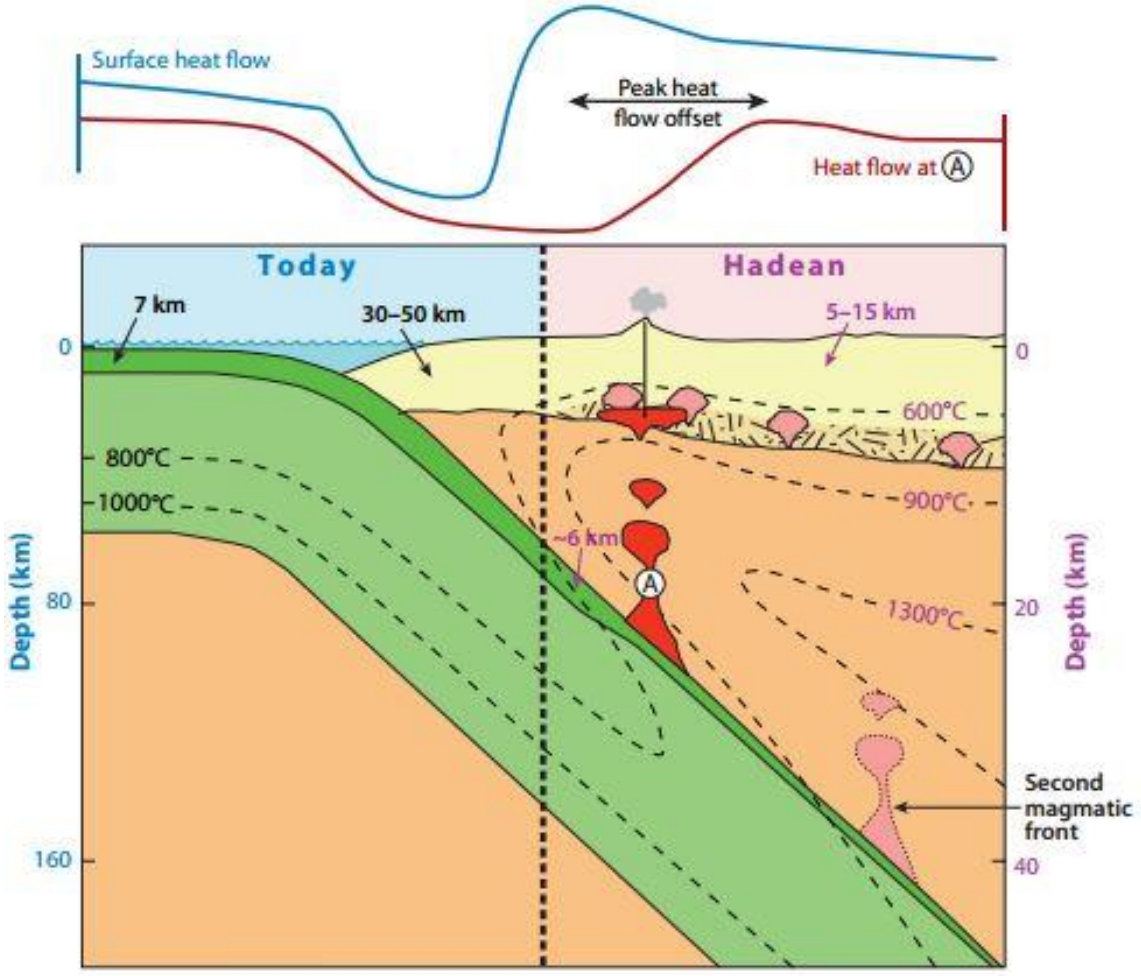

Figure 1. Cross-section showing both the modern and Hadean geotherms related to subduction tectonics. The left side shows geothermal gradient observed today, while the right shows those likely on Hadean Earth, based on zircon crystallization temperatures. The subduction refrigeration model explains how minimum melt zircons can be used to infer modern subduction-style settings. (A) shows melting of subducting slab and generation of zircon-bearing granite intrusions. From Harrison 2009.

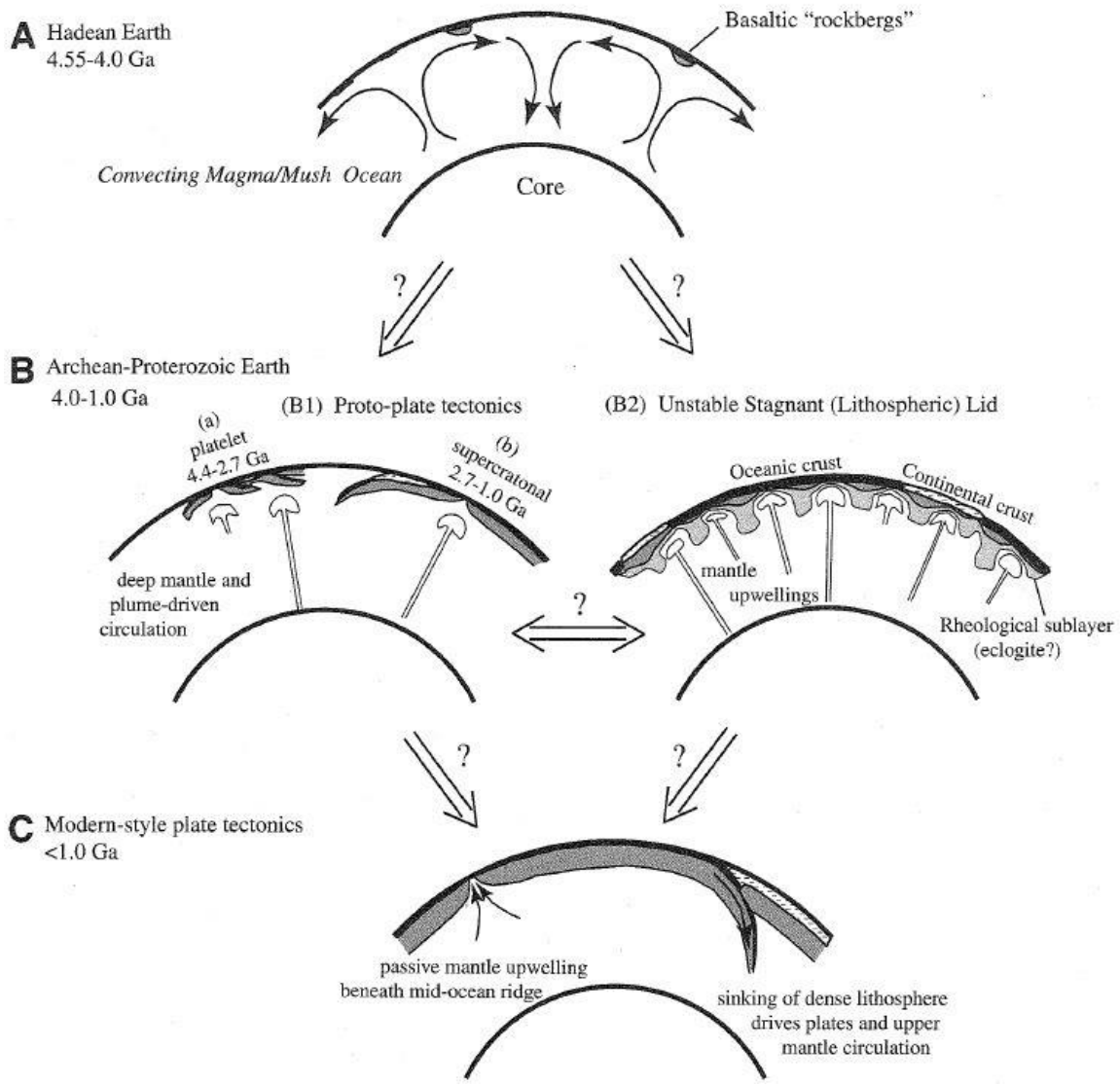

Figure 2. A Possible history of tectonic activity on Earth from (A) magma ocean with small primitive "rockbergs", to (B1) Proto-tectonics or plume generated crustal mini plates, and (B2) Stagnant Lid or a single plate, and eventually (C) modern-style tectonics. Modified from Stern 2008.

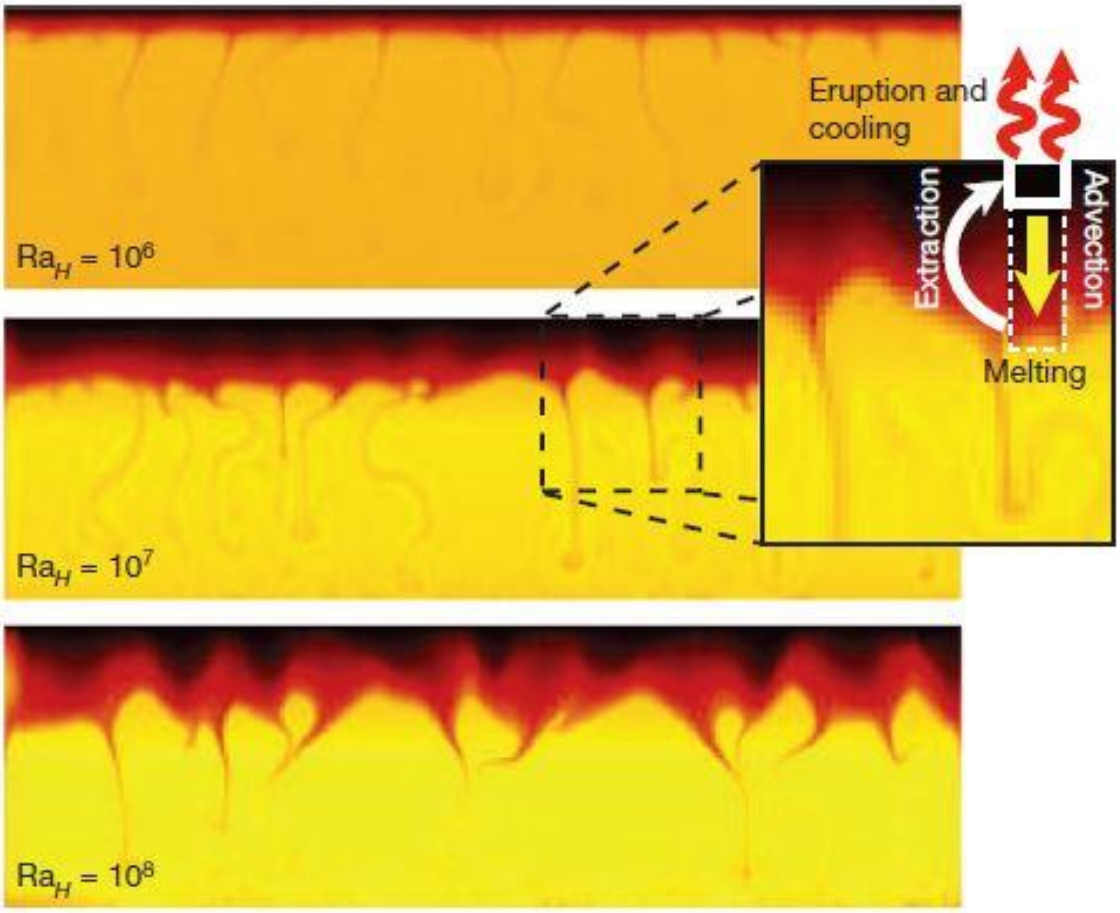

Figure 3. A model for mantle convection as proposed from the "heat-pipe Earth" model. Vigorous mantle convection creates a vertical tectonic setting. The top image shows a thin lithosphere model produced by a largely conduction driven model and the bottom image shows a dominantly advection driven heat-pipe planet resulting in a cold and thick lithosphere. From Moore and Webb 2013.

Lastly, the most broadly accepted mechanism explaining the formation of the East Pilbara Craton is the *partial convective overturn* model. As described later, this model explains the dome-and-keel structures seen in the area. Here, domes of ganitoids of Tonalite-Tronjhemite-Granodiorite (TTG) composition are enplaced, surrounded by bands of mafic greenstones. Granitoids from this area are hypothesized to have formed when wet mafic crust was partially melted from periodic mantle plumes, creating granitic plutons (Hickman and van Kranendonk 2004). Eventually, heating of the crust created a crustal overturn that caused the granites to migrate upwards in a diapir, displacing denser greenstones on the surface. This vertical tectonic, or crustal "dripping," mechanism is also suggested to explain the geometric orientation of Archean greenstone belts and granite domes found in Barberton, Africa. This model explains the crustal heating and density-driven movement as the result of periodic mantle plumes underlying the region. This idea explains the modern dome-and-keel structure in the region, and it suggests that a vertical tectonic mechanism was dominant during the Archean. Evidence found in the Barberton and the Pilbara Craton appears to be consistent with the presence of vertical tectonics in the Archean, but further data are required.

Each of the tectonic models presented provide a powerful explanation of the early lithospheric evolution of the Earth and can be used to construct a timeline of our planets thermal and geologic record. From magma ocean to modern plate tectonics, each of the nonuniformitarian models aim to describe a 'missing link' in Earth's history. Fortunately, these models provide predictions that are testable. The listed models can be grouped into two distinct, and easily differentiated groups based on their predictions: cool crust and hot crust. Based on the method of heat transfer, each model can be tested based one the crustal

temperatures they exhibit. Cool crust models include those that have low amounts of conductive heat transfer, such as low-heat stagnant lid or heat-pipe Earth. Warm crust models are those that mainly lose heat through conductive heat transfer, like those described in proto-plate tectonics and convective overturn. These predictions are testable using zircon thermometry and the results such a study can be directly compared to crystallization temperatures gleaned from Hadean zircons.

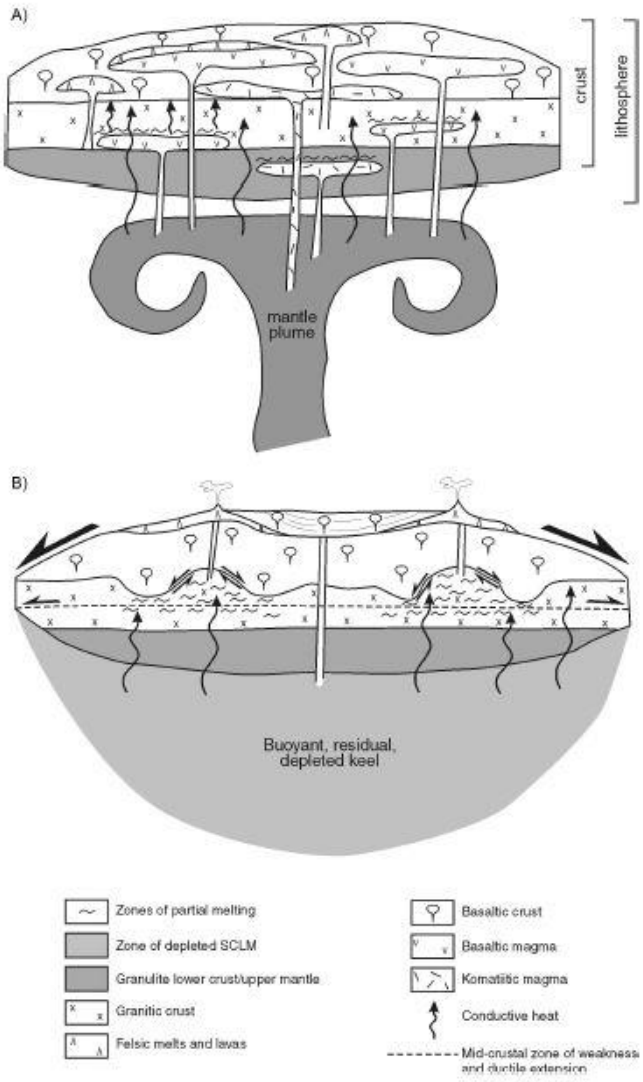

Figure 4. A model for the formation of the East Pilbara Craton through the convective overturn model. A) crustal thickening due to mantle upwelling and mafic volcanics, as well as the formation of felsic magmas as melts from older mafic crust. B) overthickening and internal melting of the crust, extensional collapse, and the formation of the buoyancy-driven dome-and-keel geometry of the crust. From Van Kranendonk et al 2007.

3. TTG Generation

To understand and test these hypotheses for the Hadean period, geologists are forced to turn to zircons, the only remaining piece of Hadean rock record. Zircons are useful minerals for evaluating crustal evolution because of their resistance to heat and pressure, their incorporation of several tracer elements, and their common appearance in nearly all granitoids. However, the method of generation of zircons from the Hadean to Archean is still debated. Several hypotheses have been considered to explain how the host granites of these zircons formed. These models correspond to the tectonic models discussed previously, as the zircon-bearing granites are a crucial piece of evidence seek to explain. Such models include (1) modern subduction melting of MORB-like basalts, (2) melting of primitive crust by deep mantle-plumes, (3) impact-generated melting, and (4) heat-pipe lithospheric melting. Each model for zircon generation in the early Earth intends to explain how a primitive magma may preferentially melt to form tonalite-trondhjemite-granodiorite (TTG) rocks, and thus create the zircons that have representative of early Earth conditions. Understanding how these granites and zircons formed is vital to fully understanding what information the zircon record shows.

The first, and most commonly supported model, was of *modern subduction-style melting of primitive crust*. This model uses the mechanism of modern subduction to explain how primitive crust (analogous to modern MORB basalts) melts to form TTG granitoids (Figure 1, A). This model is viable by Hadean zircon thermometry, which estimates that zircons from this time crystallized in cool conditions similar to those seen in modern subduction slab refrigeration (Harrison 2009, Figure 1). This model follows the uniformitarianism mindset that predicts modern processes persisted in the past.

A differing model utilizes zircon geochemistry to illustrate how zircon Lu/Hf isotopic compositions have remained near constant for over 4 billion years, and thus cannot be derived from the depleted upper mantle. This is explained by undifferentiated, *deep-mantle plumes* that rise through the upper mantle to partially melt primitive crust, yielding TTG granites (Guitreau et al. 2012). This model suggests that vertical tectonics is the main mechanism for TTG production. This suggestion has recently been expanded upon by the *heat-pipe Earth model*, which provides a mechanism for volcanism similar to such deep-mantle plumes (Moore and Webb 2013, Figure 3).

Another model for TTG production involves melting, burial, and mixing of Earth's primitive crust by *impacts with extraterrestrial bodies*. As we can see on the surface of the Moon, Earth likely underwent a time of rapid and violent bombardment from outside bodies. Indeed, the formation of the Moon is thought to have been formed by a massive collision and such an impact is also believed to have caused global melting on Earth. In this model, collisions across the surface of Earth are considered to have melted and buried much of the primitive crust, introducing new material and mixing the magma of the crust (Marchi et al. 2014).

The last model for TTG generation is through *heat-pipe lithospheric melting*. This model corresponds to the heat-pipe Earth tectonic model. Through this mechanism, granitic rocks can form by conduction-driven heating of the subducted lithosphere. As crust is generated through volcanism at the surface, the crust is pushed deeper into the mantle, where it heats, partially melts, and intrudes into the overlying crust.

3.1 Zircon

The only minerals durable enough to survive on Earth since the Hadean are zircon crystals, and because of this, the interpretation of their geochemistry is extremely important to our knowledge of the Hadean. These minerals are also very useful for radiometric dating because of their ability to incorporate several radioactive elements such as Uranium and Thorium. Because of their potential to survive the high-temperature conditions of the Hadean, zircons are also able to crystallize around other minerals and melts, shielding them from extreme conditions that would otherwise destroy them. However, aside from radiometric dating, little information has been gleaned from these included minerals. Hopkins et al. (2008, 2010) showed that Hadean zircon inclusion can essentially act as a time capsule, revealing pressure and temperature conditions on early Earth. Using the inclusion mineralogy of Hadean zircons as pressure and temperature indicators, they were able to estimate the conditions at which the included minerals crystallized. This was then used as evidence to infer the geologic setting of the rocks, proving a new dataset to further constrain the tectonic and thermal setting of the Hadean. This can also be done with inclusions found in Archean granitoids.

3.2 Archean

The geologic record of the Archean is much more extensive than that of the Hadean, and includes regions of Australia, Africa, Brazil, Canada, Greenland, India, Scandinavia, Scotland, and the United States. The record from the Archean consists largely of greenstone belts, tonalite-trondhjemite-granodiorite (TTG), and komatiite volcanic rocks. Studies of Archean lithologies in locations such as Australia, South Africa, and Greenland have led

to different interpretations about how they formed and their importance to the beginnings of plate tectonics. Previously, these locations were believed to be evidence of modern-style subduction zones as early as 3.8 Ga in the Archean. This idea continues to be the standard model for how the rocks of the Isua Greenstone belt formed (Nutman et al. 2007). However, new ideas have circulated proposing methods of non-subduction style creation. For example, in Barberton, Africa local dome and keel geometry lead to the hypothesis that a different mechanism of vertical tectonics created granitic domes by the dripping of the cool, dense overlying greenstones into lighter melting granites (Van Kranendonk 2011). This hypothesis offers a mechanism that supports vertical tectonic models and can potentially be applied to several of these Archean locations. Geochemistry and geometry of the East Pilbara Craton suggest that this area did not form in a modern subduction setting (Champion and Smithies 2007), but rather from mantle plumes that partial melt previously placed basaltic crust (Hickman and Van Kranendonk 2004). Even though the Archean rock record is still hotly debated, it provides us with regional rock records that can be studied and compared to the small amount of evidence of the Hadean that is available.

3.3 Geologic Setting

In order to establish a comparison to Hadean zircons, we look to the Pilbara Craton in Western Australia. The Pilbara Craton is an almost circular region located on the Northwest coast of Australia and is comprised of 3 superterranes (Figure 5). These three superterranes are all Archean in age and each are described by unique syn and post-depositional histories. However, out of these superterranes, the East Pilbara Terrane is the oldest and, along with the Kaapvaal Craton of southern Africa, one of the best preserved

Archean greenstone terranes in the world. The Eastern Pilbara Craton is generally composed of ca. 3.525-3.225 Ga granitic domes and greenstone belts. The greenstones include autochthonous volcano-sedimentary rocks deposited in distinct pulses from 3.53-3.19 Ga. The greenstones are distributed in arc-shaped belts that wrap around large, synclinic granitic domes that were intruded from ca. 3.5-3.165 Ga. After emplacement, the entire craton experienced periods of deformation and metamorphism, as well as deposition of unconformably overlain sediments and granitic intrusions from 3.07-2.83 Ga (Van Kranendonk 2007, 2010).

Being one of the best preserved Archean terranes on Earth, our interest in the East Pilbara Craton is stemmed from the ability of comparing its known structure to the evidence provided by Hadean zircons. The dome-and-keel geometry of the granitoids and surrounding greenstones provides evidence of a later mechanism of lithosphere generation, and allows us to compare the crystallization conditions of Hadean zircons with the observable rock record. Prominent models explaining the geometry of the East Pilbara Craton are described the mechanism as partial convective overturn, which may or may not be the same setting that generated the Hadean zircons.

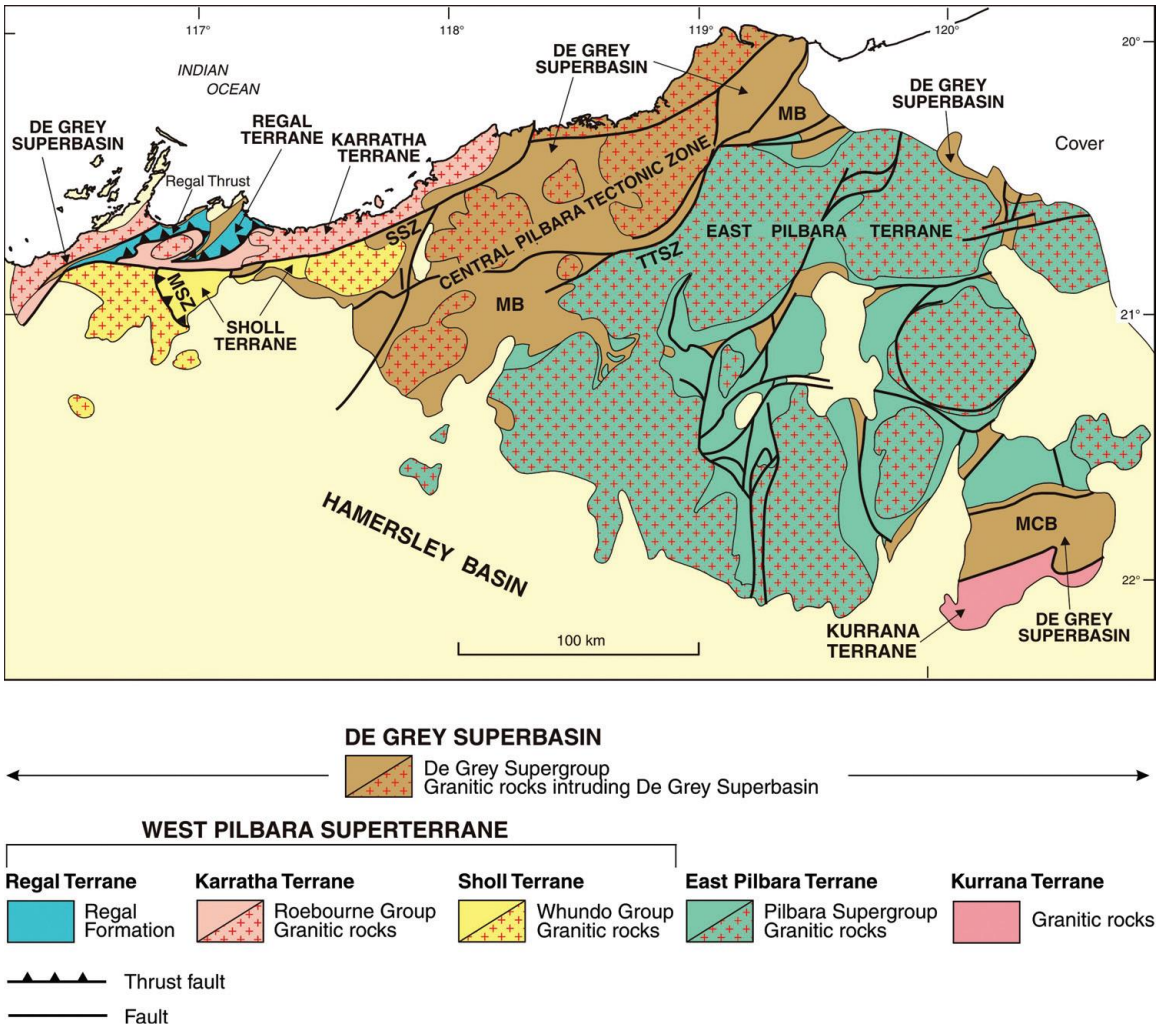

Figure 5. A simplified geologic map of the Pilbara Craton, with the 3 major terranes and structures. Abbreviations show the locations of groups and structures: MB = Mallina basin; MCB = Mosquito Creek basin; MSZ = Maitland Shear Zone; SSZ = Sholl Shear Zone; TTSZ = Tabba Tabba Shear Zone. From Van Kranendonk et al 2007, inset image showing location on Australian continent from Google Earth.

4. Methods

4.1 Data Source

In order to constrain the tectonic and thermal conditions during the Archean, two separate tests will be conducted on samples collected from the East Pilbara Craton in Western Australia. To do this, we will be borrowing previously dated (U-Pb SHRIMP) zircon mounts from the Geologic Survey of Western Australia from TTGs of the East Pilbara Craton that range in ages from ~3.5-3.0 Ga. A total of seven samples were chosen which represent a range of compositions of Archean TTGs and which also spatially represent several regional granitoid domes of the craton (Figure 6). Compositionally, the chosen samples include two tonalites, three granodiorites, one monzogranite, and one diorites. Spatially, the samples represent the Tamourah, Shaw, Corrunna Downs, and Mount Edgar domes. These samples were delivered as mineral separates, which were then sent to the University of Arizona Laserchron Center for mineral separation (according to Simpson, Pecha, and Gehrels 2012) and mounted on 1" epoxy discs (Pullen and Pepper 2009). Sample 169038 was mounted twice, on separate mounts to compare previously mounted GSWA separates with a newly separated sample.

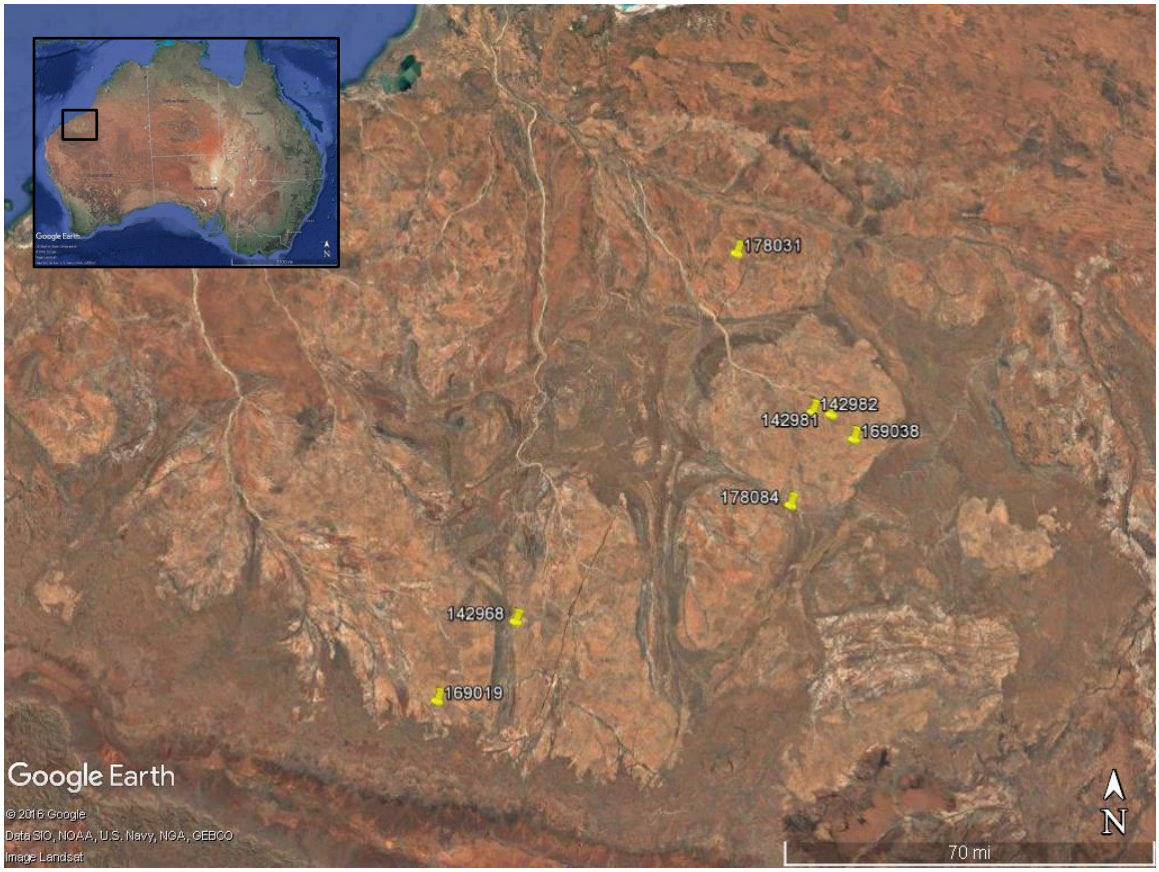

Figure 6. A satellite image map showing the location of the seven samples borrowed and tested in this study. The inset shows the location of the study area on the Australian continent. Images provided by Google Earth.

4.2 U-Pb ages

Once separated and mounted, the zircon crystals were analyzed for U-Pb ages and titanium content simultaneously using UCLA's Cameca IMS 1270 ion microprobe. 206/207 Pb ages, 207Pb/235U, and 206Pb/238U ages were calculated using measured Pb-content and the U-content of the zircon standards 91500 and AS3 standards. Concordia plots were quantified using the 91500 and AS3 standards (Paces and Miller 1993, Abbot et al. 2012, Weidenbeck et al 2004) to calculate titanium content as well as U-Th-Pb ages. Concordant grains were selected using the ZIPS program and ISOplot addon for excel to plot the 207Pb/206Pb vs. 206Pb/238U. Ti content was estimated in parts per million, then applied to an updated equation for the geothermometer (Ferry and Watson 2007).

4.3 Titanium-in-zircon Thermometry

To gather evidence, these zircons were examined to estimate crystallization conditions and melt compositions. For crystallization temperature, the zircons were analyzed using the Titanium-in-zircon geothermometer technique developed by Watson and Harrison (2005) and calibrated by Ferry and Watson (2007) in order to estimate crystallization temperature.

$$\text{Log (ppm Ti)} = 5.711 - 4800/T(K) - \log(a_{SiO2}) + \log(a_{TiO2})$$

In this thermometer, a_{SiO2} and a_{TiO2} represent the chemical activities of SiO_2 and TiO_2, respectively. Hand sample descriptions provided by the GSWA describe all the samples as containing titanite. Therefore, for this study, a_{TiO2} was estimated at 0.5 due to the samples containing titanite, and a_{SiO2} was assumed to be 1. No pressure calibrations were made, so the resulting temperatures calculated by the thermometer assume a pressure of 1 Gpa.

All zircons were analyzed for titanium content using a Cameca IMS 1270 ion microprobe using the Ti-U-Th-Pb methods described in Watson and Harrison's 2005 Science publication. Each grain was analyzed for both U/Pb ages for age correlations and the trace element titanium for temperature estimation.

4.4 Inclusions

In addition to the previous tests, any mineral or melt inclusions will be examined to further constrain the crystallization temperatures, pressures, and potentially the metamorphic grade (Rasmussen et al. 2011, Bell 2016) they may have experienced during crystal growth. Zircons determined to be concordant, and less likely to represent secondary inclusions, were analyzed using secondary electron imaging and backscatter electron imaging using LSU's electron microprobe, then compositionally analyzed using energy dispersive x-ray microanalysis. These inclusions were counted and used to infer temperature and pressure conditions during and after zircon crystallization. By estimating the conditions of the Archean, we hope to constrain the tectonic setting at the time and use it compare to previously established geodynamic hypotheses for the Precambrian.

Once age-dated, individual concordant grains were selected, imaged, and examined for any inclusions. This was done using a JEOL JSX-8230 electron microprobe at the LSU department of Geology & Geophysics. The grains were imaged using secondary electron imaging to show spots from SIMS analyses, then imaged using Energy-Dispersive Spectroscopy to show mineral inclusions. Due to contamination, only mineral inclusions that were isolated and not located near cracks or pits were counted and used to estimate metamorphic conditions (Harrison and Schmitt 2007).

5. Results

5.1 Zircon

Table 1 show the U-Pb ages of each sample. 207Pb/206Pb, 207Pb/235U, and 206Pb/238U ages measured for all zircons. Nearly all samples have consistent ages that are within error of each other, with the one exception: Sample 142968. Errors of each age are shown in the figure. Pb/Pb ages have the smallest errors. All the samples were plotted on traditional, 206Pb/238U vs 207Pb/235U Concordia plots. Overall, the zircons range from strongly concordant to strongly discordant. Discordant analyses, likely due to resetting during a post-crystallization metamorphic event, were not used for titanium thermometry or inclusion population counts because of possible mineral alterations and titanium contaminations. Zircons that were concordant were those that were within error of natural decay Concordia line (see Appendix for Concordia plots).

Table 1 also shows the mean temperature of each zircon measured in each sample. These temperatures were calculated using the titanium content of each zircon. The titanium temperatures were compiled into probability density functions to determine overall standard deviations and trends in each sample (Figure 7). Table 3 shows a summary of the U-Pb and titanium temperature data, complete with standard deviations of crystallization temperatures and errors of U-Pb ages. The crystallization temperature estimates exhibit large standard deviations due to a small sample size. Per sample, the titanium temperatures are tightly group (±50), except sample 169038, which shows a bimodal temperature distribution. This bimodal distribution is the result of the sample, a tonalite, being mounted twice. Overall, the zircons from the seven samples show a general cooling trend from ~3.40-3.22 Ga of 2.4° C/Ma with a noticeable high temperature peak around 3.31 Ga. The

cooling trend of the samples show a range in crystallization temperatures between 887-1356° C (Figure 10).

Table 1 Data table showing the U-Pb ages, Ti content (in ppm), and Ti-in-zircon temperature (° C) for the analyzed zircons of each sample.

U-Pb and Titanium Data per sample																			
142968																			
Grain	207Pb*/ 235U	207Pb*/ 235U	206Pb*/ 238U	206Pb*/ 238U	207Pb*/ 206Pb*	207Pb* /206Pb *	U O/U	U (ppm)	207Pb /235U Age (Ma)	207Pb/ 235U Age (Ma)	206Pb/ 238U Age (Ma)	206Pb/ 238U Age (Ma)	207Pb/ 206Pb Age (Ma)	207Pb /206P b Age (Ma)	49Ti/94Z r2 O	49Ti/94 Zr2 O	Ti (ppm)	Ti (ppm)	T(C)
		1 s.e.		1 s.e.		1 s.e.				1 s.e.		1 s.e.		1 s.e.		1 s.e.		1 s.e.	
2	26.87	1.56	0.6837	0.0396	0.2851	0.00102	8.44	4.26E+03	3379	56.7	3358	152	3391	5.57	9.35E-02	1.96E-03	75.2345	1.577	1254.96
4	24.7	1.31	0.6175	0.0319	0.2902	0.00158	8.6	6.58E+03	3297	51.6	3100	127	3419	8.49	1.45E-01	2.40E-03	117.0333	1.934	1354.37
5	21.92	1.16	0.5654	0.0282	0.2811	0.00276	9.08	3.42E+03	3180	51.3	2889	116	3369	15.3	1.67E-01	2.38E-03	134.0168	1.919	1387.50
6	25.49	1.38	0.6387	0.0337	0.2894	0.000708	8.83	3.84E+03	3327	52.8	3184	132	3415	3.8	6.84E-02	1.36E-03	55.0475	1.098	1191.70
7	25.57	1.14	0.6372	0.0294	0.2911	0.00158	8.81	5.97E+03	3330	43.7	3178	116	3423	8.46	2.82E-01	3.77E-03	226.9834	3.033	1530.25
9	23.66	0.944	0.6056	0.0241	0.2834	0.00165	9.24	3.69E+03	3255	38.9	3052	96.9	3382	9.07	2.10E-01	2.17E-02	168.8692	17.491	1447.24
13	25.73	1.05	0.6433	0.0267	0.2901	0.000729	9.24	3.49E+03	3336	39.9	3202	105	3418	3.91	1.74E-01	2.76E-03	139.6511	2.218	1397.84
14	22.3	1.03	0.5729	0.0256	0.2823	0.00185	9.01	2.77E+03	3197	44.8	2920	105	3376	10.2	1.46E-01	2.52E-03	117.5162	2.032	1355.35
15	25.48	1.55	0.6525	0.0367	0.2832	0.00231	9.32	2.02E+03	3327	59.5	3238	143	3381	12.7	1.07E-01	2.01E-03	85.8834	1.618	1283.45
16	23.63	1.13	0.6009	0.0306	0.2853	0.00264	9.47	4.07E+03	3253	46.6	3033	123	3392	14.4	1.12E-01	2.65E-03	89.9080	2.135	1293.55
22	26.41	1.13	0.6548	0.0273	0.2925	0.00159	9.23	3.47E+03	3362	42	3247	107	3431	8.45	1.42E-01	2.28E-03	114.1356	1.835	1348.38
25	26.13	1.02	0.6474	0.0253	0.2928	0.00196	9.33	4.55E+03	3352	38.3	3218	98.8	3432	10.4	2.66E-01	3.63E-03	213.9439	2.924	1513.01
26	27.58	1.37	0.6856	0.0329	0.2918	0.00153	8.98	4.24E+03	3404	48.7	3366	126	3427	8.14	1.77E-01	4.81E-03	142.7903	3.868	1403.47
29	24.04	1.14	0.6099	0.0279	0.2859	0.00126	9.5	2.45E+03	3270	46.2	3070	112	3395	6.86	1.56E-01	2.89E-03	125.8068	2.329	1371.88
30	25.26	1.12	0.6291	0.027	0.2913	0.00133	9.53	3.52E+03	3318	43.2	3146	107	3424	7.07	6.04E-02	1.31E-03	48.6002	1.055	1167.91
33	25.18	0.953	0.6368	0.0239	0.2868	0.000969	9.44	4.05E+03	3315	37	3176	94.1	3401	5.26	4.13E-02	1.04E-03	33.2587	0.835	1100.02
36	24.6	1.13	0.6381	0.0282	0.2796	0.00129	9.38	7.58E+03	3292	44.7	3181	111	3361	7.22	4.18E-01	9.46E-03	336.1286	7.614	1653.66
142981																			
3	28.4	3.66	0.7617	0.0983	0.2704	0.00115	7.76	4.41E+03	3433	126	3650	360	3309	6.64	0.0534	0.00145	9.6877	0.263	917.58

4	26.14	3.36	0.7074	0.0911	0.268	0.00168	7.6	4.27E+03	3352	126	3449	344	3295	9.82	0.1378	0.00175	24.9994	0.317	1052.99
6	28.06	3.62	0.7608	0.0982	0.2675	0.00102	7.77	3.96E+03	3421	127	3647	360	3291	6.01	0.077	0.00203	13.9692	0.368	966.45
7	26.08	3.36	0.7141	0.0919	0.2649	0.0015	7.54	3.92E+03	3349	126	3474	346	3276	8.92	0.07048	0.00103	12.7863	0.187	954.27
8	22.68	2.93	0.6294	0.0814	0.2613	0.00074	8.13	4.68E+03	3213	126	3147	322	3255	4.48	0.4741	0.0177	86.0102	3.211	1283.77
9	26.42	3.4	0.7018	0.0903	0.273	0.00080	7.58	4.74E+03	3362	126	3427	342	3323	4.62	0.05525	0.00113	10.0233	0.205	921.97
10	25.06	3.23	0.6792	0.0875	0.2676	0.0014	7.65	2.69E+03	3311	126	3341	336	3292	8.19	0.3504	0.00685	63.5688	1.243	1220.18
142982																			
2	22.15	2.86	0.6217	0.0804	0.2584	0.00092	7.36	4.31E+03	3190	126	3117	319	3237	5.62	0.02215	0.000987	4.0184	0.179	814.50
4	18.36	2.39	0.5143	0.067	0.2589	0.00074	7.43	5.78E+03	3009	126	2675	285	3240	4.55	0.04722	0.00136	8.5665	0.247	902.02
6	20.75	2.68	0.574	0.074	0.2621	0.00146	7.39	5.55E+03	3127	125	2924	303	3260	8.79	0.2693	0.0104	48.8558	1.887	1168.90
7	25.67	3.3	0.7161	0.092	0.2599	0.00032	8.21	8.89E+03	3334	126	3482	346	3246	1.96	0.03484	0.000708	6.3206	0.128	865.22
9	23.08	2.97	0.626	0.0808	0.2674	0.00086	7.2	7.26E+03	3230	125	3134	320	3291	5.05	0.09986	0.0017	18.1164	0.308	1003.67
10	24.71	3.2	0.6636	0.0859	0.27	0.00072	7.3	4.99E+03	3297	127	3281	333	3306	4.23	0.1279	0.00514	23.2033	0.932	1041.24
11	26.25	3.38	0.7087	0.0912	0.2686	0.00075	7.58	6.30E+03	3356	126	3454	344	3298	4.42	0.02208	0.00111	4.0057	0.201	814.16
12	23.19	3	0.6332	0.0819	0.2656	0.00096	7.58	2.99E+03	3235	126	3162	323	3280	5.7	0.1023	0.00202	18.5590	0.366	1007.24
169019																			
1	31.41	4.07	0.7705	0.0998	0.2957	0.00158	8.01	3.76E+03	3532	128	3683	363	3448	8.3	0.07797	0.00108	14.1451	0.196	968.19
2	23.11	3.02	0.6356	0.0829	0.2638	0.00174	8.19	4.14E+03	3232	127	3172	327	3269	10.3	0.5135	0.0157	93.1580	2.848	1301.47
3	31.03	4.01	0.7811	0.101	0.2881	0.00129	8.04	5.50E+03	3520	127	3721	365	3408	6.96	0.409	0.00897	74.1999	1.627	1252.04
5	31.3	4.17	0.7869	0.105	0.2885	0.00285	7.88	3.22E+03	3529	131	3742	377	3410	15.4	0.07198	0.000947	13.0585	0.172	957.15
6	32.07	4.14	0.7875	0.102	0.2954	0.00277	7.92	1.31E+03	3553	127	3744	367	3446	14.5	0.0672	0.00129	12.1913	0.234	947.81
7	29.77	3.84	0.7695	0.0993	0.2806	0.00117	8.2	3.10E+03	3479	127	3679	362	3366	6.5	0.1548	0.0043	28.0835	0.780	1071.76
8	30.43	4.03	0.7709	0.102	0.2862	0.00269	8.14	2.20E+03	3501	130	3684	372	3397	14.6	0.05957	0.000886	10.8071	0.161	931.77
9	26.38	3.46	0.6667	0.0874	0.2869	0.0036	7.53	2.30E+03	3361	128	3293	338	3401	19.5	0.1292	0.00199	23.4392	0.361	1042.82
11	30.52	4.01	0.7667	0.101	0.2887	0.00303	7.64	1.81E+03	3504	129	3669	370	3411	16.3	0.1088	0.0577	19.7383	10.468	1016.44

12	34.15	4.5	0.8797	0.115	0.2815	0.00386	8.69	2.74E+03	3614	130	4068	393	3371	21.4	0.106	0.00915	19.2303	1.660	1012.53
13	30.4	3.93	0.7956	0.104	0.2771	0.00317	8.34	2.41E+03	3500	127	3773	372	3347	17.9	0.2095	0.00291	38.0070	0.528	1123.16
14	19.17	2.49	0.5302	0.0686	0.2622	0.00265	7.94	4.52E+03	3050	125	2742	289	3260	15.9	0.9394	0.0202	170.4239	3.665	1449.70
16	28.77	3.71	0.7386	0.0954	0.2826	0.00143	8.15	2.52E+03	3446	126	3565	354	3377	7.87	0.1995	0.00484	36.1929	0.878	1114.59
17	29.88	3.85	0.7532	0.097	0.2877	0.000908	8	5.55E+03	3483	127	3619	357	3405	4.91	0.05048	0.00106	9.1580	0.192	910.41
19	24.03	3.1	0.6033	0.078	0.2889	0.00214	8.43	1.23E+03	3270	126	3043	314	3412	11.5	0.04758	0.000824	8.6319	0.149	902.96
20	38.89	5.04	0.9676	0.125	0.2915	0.00229	9.77	2.40E+03	3743	128	4363	409	3426	12.2	0.1035	0.00129	18.7767	0.234	1008.97
21	34.12	4.42	0.8559	0.111	0.2892	0.00187	9.19	1.94E+03	3614	128	3986	384	3413	10	0.2119	0.00255	38.4424	0.463	1125.17
22	23.17	2.99	0.6541	0.0844	0.2569	0.00125	10.8	3.14E+03	3234	125	3244	329	3228	7.68	0.7884	0.0412	143.0298	7.474	1403.90
23	31.94	4.18	0.8404	0.112	0.2757	0.00406	8.22	2.08E+03	3549	129	3932	392	3339	23	0.237	0.00269	42.9960	0.488	1145.26
24	35.21	4.57	0.891	0.117	0.2866	0.00421	8.5	2.82E+03	3645	128	4107	399	3399	22.9	0.5869	0.0109	106.4741	1.977	1332.02
26	31.16	4.01	0.7811	0.101	0.2893	0.00206	8.03	2.83E+03	3524	127	3721	365	3414	11.1	0.1743	0.00442	31.6211	0.802	1091.46
27	29.46	4.02	0.7092	0.0972	0.3012	0.00474	8.28	2.56E+03	3469	134	3455	367	3477	24.4	0.7494	0.0171	135.9545	3.102	1391.09
28	30.82	4.04	0.7745	0.101	0.2886	0.00443	8.19	1.69E+03	3513	129	3697	368	3410	23.9	0.3136	0.00713	56.8926	1.294	1198.13
29	33.73	4.41	0.8423	0.109	0.2905	0.00247	8.15	3.01E+03	3602	129	3939	383	3420	13.2	0.2717	0.0174	49.2912	3.157	1170.57
30	19.01	2.48	0.5823	0.0754	0.2368	0.00295	7.98	7.14E+03	3042	126	2958	307	3098	19.8	0.4529	0.0127	82.1641	2.304	1273.80
32	29.49	4.6	0.7522	0.114	0.2844	0.00528	8.07	5.15E+03	3470	153	3616	419	3387	29	0.2401	0.0214	43.5584	3.882	1147.63
33	31.49	4.07	0.7952	0.102	0.2872	0.00187	8.1	2.89E+03	3534	127	3772	368	3402	10.1	0.1516	0.00256	27.5029	0.464	1068.35
34	30.72	4.01	0.8032	0.104	0.2774	0.00286	9.28	1.76E+03	3510	128	3801	371	3348	16.1	7.588	0.188	1376.5983	34.107	2281.48
35	24.26	3.12	0.6543	0.0842	0.2689	0.00171	7.99	3.52E+03	3279	126	3245	328	3300	10	0.583	0.0191	105.7666	3.465	1330.47
36	31.12	4.05	0.7894	0.102	0.2859	0.00295	8.2	2.74E+03	3523	128	3751	367	3395	16.1	0.1218	0.00188	22.0967	0.341	1033.64
37	33.49	4.32	0.8411	0.109	0.2887	0.000849	8.16	2.79E+03	3595	127	3935	380	3411	4.58	0.08175	0.00115	14.8309	0.209	974.83
38	31.38	4.04	0.8129	0.105	0.28	0.00308	8.17	2.89E+03	3531	127	3835	373	3363	17.2	0.1676	0.00288	30.4056	0.522	1084.89
39	26.33	3.4	0.7087	0.0917	0.2695	0.00159	8.05	3.12E+03	3359	127	3453	346	3303	9.23	2.669	0.0685	484.2041	12.427	1784.59
40	28.35	3.77	0.7334	0.0957	0.2804	0.00402	8	4.24E+03	3431	130	3546	356	3365	22.4	0.07343	0.00283	13.3215	0.513	959.89
41	31.01	4.02	0.77	0.1	0.2921	0.00235	8.15	2.11E+03	3519	128	3681	365	3429	12.5	0.163	0.00534	29.5711	0.969	1080.26

169038																			
2	25.22	1.45	0.6759	0.0384	0.2706	0.00116	8.53	2.96E+03	3317	56.1	3329	148	3310	6.73	9.15E-01	1.02E-02	736.6497	8.194	1958.94
3	25.51	1.42	0.6779	0.0382	0.2729	0.00292	8.52	1.67E+03	3328	54.5	3336	147	3323	16.8	1.19E-01	1.72E-03	95.7838	1.386	1307.73
4	23.26	1.08	0.62	0.0297	0.2721	0.00256	8.76	3.06E+03	3238	45.3	3110	118	3318	14.7	6.66E-02	1.20E-03	53.6309	0.962	1186.66
6	23.01	0.994	0.6122	0.0273	0.2726	0.00155	8.88	3.34E+03	3227	42	3079	109	3321	8.9	8.46E-02	2.55E-03	68.0789	2.048	1234.14
9	23.51	1.4	0.6362	0.0372	0.268	0.00239	8.56	4.71E+03	3248	57.8	3174	147	3294	14	1.92E-01	2.88E-03	154.7834	2.318	1424.23
10	23.48	1.15	0.6289	0.0308	0.2708	0.000683	8.76	3.50E+03	3247	47.9	3145	122	3311	3.96	4.64E-02	9.72E-04	37.3235	0.782	1119.97
12	23.96	1.54	0.6409	0.0388	0.2711	0.0016	8.72	4.31E+03	3267	62.8	3193	153	3313	9.27	1.19E-01	1.75E-03	95.9448	1.411	1308.11
13	22.78	1.47	0.6104	0.0403	0.2707	0.00176	8.73	2.83E+03	3218	62.7	3072	161	3310	10.2	9.17E-02	1.51E-03	73.8420	1.215	1251.02
14	22.67	1.18	0.6041	0.0312	0.2722	0.00103	8.69	6.35E+03	3213	50.5	3047	126	3319	5.96	9.28E-02	1.48E-03	74.6711	1.193	1253.37
15	25.29	1.49	0.6741	0.0394	0.2721	0.00188	8.21	3.88E+03	3320	57.5	3322	152	3318	10.8	1.32E-01	3.82E-03	106.4085	3.074	1331.88
16	23.6	1.22	0.6285	0.0322	0.2723	0.00114	8.57	4.80E+03	3252	50.5	3144	127	3319	6.55	1.55E-01	4.74E-03	124.5189	3.812	1369.36
17	23.92	1.02	0.6439	0.0271	0.2694	0.00157	9.05	2.77E+03	3265	41.4	3204	106	3303	9.13	5.48E-02	1.06E-03	44.1330	0.852	1150.03
18	22.77	1.18	0.6127	0.0308	0.2695	0.00144	8.78	4.31E+03	3217	50.3	3081	123	3303	8.39	7.36E-02	1.29E-03	59.2089	1.038	1205.98
19	23.85	1.3	0.6383	0.0352	0.271	0.000548	8.74	5.72E+03	3262	53	3182	138	3312	3.17	2.69E-01	1.56E-02	216.6806	12.565	1516.68
22	23.39	1.04	0.6228	0.0276	0.2724	0.000904	8.89	2.97E+03	3243	43.4	3121	110	3320	5.2	6.08E-02	1.76E-03	48.9061	1.418	1169.09
23	23.87	1.53	0.639	0.0397	0.2709	0.000956	8.65	3.99E+03	3263	62.5	3185	156	3311	5.53	7.99E-02	1.37E-03	64.3039	1.101	1222.50
24	24.88	1.31	0.6677	0.0351	0.2703	0.00111	8.54	4.27E+03	3304	51.5	3297	136	3308	6.42	9.63E-02	1.53E-03	77.4963	1.228	1261.24
26	22.45	1.31	0.5978	0.0338	0.2724	0.00158	8.91	4.05E+03	3204	56.8	3021	136	3320	9.11	5.68E-02	1.09E-03	45.7508	0.873	1156.65
27	25.45	1.42	0.6749	0.0377	0.2735	0.00238	8.62	3.81E+03	3326	54.6	3325	145	3326	13.6	8.80E-02	1.44E-03	70.8076	1.156	1242.26
28	22.94	1.41	0.6116	0.0384	0.2721	0.00162	8.91	4.48E+03	3225	60	3076	153	3318	9.33	6.99E-02	1.22E-03	56.2388	0.984	1195.87
29	24.14	1.19	0.648	0.0327	0.2701	0.00154	8.62	3.30E+03	3274	48.2	3220	128	3307	8.93	5.29E-02	1.01E-03	42.5473	0.815	1143.35
30	23.43	1.56	0.6269	0.0416	0.271	0.00128	8.76	3.98E+03	3245	64.7	3137	165	3312	7.42	1.01E-01	1.52E-03	81.0540	1.226	1270.86
31	22.75	1.19	0.6135	0.0332	0.2689	0.00144	8.7	3.34E+03	3216	50.8	3084	133	3300	8.38	8.15E-02	1.33E-03	65.5837	1.071	1226.50
32	24.2	1.31	0.6459	0.0346	0.2717	0.000821	8.64	3.83E+03	3276	52.8	3212	135	3316	4.74	7.11E-02	1.21E-03	57.1885	0.976	1199.14
33	24.46	1.23	0.6598	0.0333	0.2688	0.000881	8.57	4.04E+03	3287	49	3266	129	3299	5.14	5.58E-02	1.16E-03	44.8735	0.935	1153.08
34	24.69	1.88	0.6574	0.0464	0.2724	0.00242	8.34	3.21E+03	3296	74.3	3257	180	3320	13.9	9.22E-02	1.42E-03	74.1882	1.143	1252.01

35	24.26	1.27	0.6449	0.0339	0.2729	0.00123	8.55	4.79E+03	3279	50.9	3208	133	3323	7.05	7.35E-02	1.22E-03	59.1928	0.980	1205.93
36	22.2	2.19	0.5948	0.0599	0.2706	0.00187	8.79	3.16E+03	3192	95.7	3009	242	3310	10.8	7.43E-02	1.25E-03	59.7884	1.002	1207.91
37	23.2	1.17	0.624	0.0304	0.2697	0.00168	8.67	2.84E+03	3235	48.9	3126	121	3304	9.75	6.37E-02	1.32E-03	51.2966	1.059	1178.13
38	24.79	1.45	0.6589	0.0384	0.2729	0.001	8.47	5.19E+03	3300	57	3263	149	3323	5.76	1.09E-01	1.56E-03	87.7347	1.256	1288.13
39	24.69	1.3	0.6603	0.0351	0.2712	0.00129	8.51	2.32E+03	3296	51.3	3268	136	3313	7.45	1.22E-01	1.69E-03	98.1985	1.364	1313.38
40	23.04	1.28	0.6145	0.0343	0.272	0.00141	8.79	5.47E+03	3229	54.3	3088	137	3317	8.14	1.90E-01	2.34E-03	153.1736	1.879	1421.51
41	23.14	1.05	0.6239	0.0277	0.269	0.00181	8.88	3.82E+03	3233	44	3125	110	3300	10.6	6.37E-02	1.14E-03	51.2564	0.914	1177.98
42	23.74	1.44	0.6348	0.0379	0.2712	0.000771	8.71	4.08E+03	3258	59.2	3168	149	3313	4.46	1.83E-01	2.28E-03	147.4587	1.838	1411.69
43	23.06	1.02	0.6127	0.0276	0.273	0.00117	8.86	5.39E+03	3230	43.2	3081	110	3323	6.71	8.59E-02	1.37E-03	69.1414	1.099	1237.33
44	23.7	1.09	0.6341	0.0289	0.2711	0.00184	8.79	4.04E+03	3256	44.8	3166	114	3312	10.6	4.91E-02	1.14E-03	39.5370	0.915	1130.16
45	22.98	1.06	0.6133	0.028	0.2717	0.00169	8.81	4.99E+03	3226	44.8	3083	112	3316	9.77	1.02E-01	1.51E-03	82.1809	1.219	1273.85
46	23.83	1.63	0.6309	0.0423	0.2739	0.000984	8.85	1.50E+03	3261	66.5	3153	167	3329	5.63	1.26E-01	1.76E-03	101.6596	1.419	1321.31
48	24.03	1.23	0.6442	0.0326	0.2706	0.001	8.52	6.89E+03	3270	49.7	3206	128	3309	5.79	1.51E-01	2.06E-03	121.8627	1.661	1364.11
49	24.1	1.73	0.6546	0.0464	0.267	0.00127	8.39	4.42E+03	3273	69.8	3246	181	3289	7.45	1.16E-01	1.69E-03	93.3691	1.356	1301.98
50	22.67	1.18	0.603	0.0314	0.2727	0.00129	8.9	3.34E+03	3213	50.7	3042	126	3322	7.4	7.17E-02	1.31E-03	57.6876	1.051	1200.85
51	23.97	1.2	0.6394	0.0322	0.2719	0.00142	8.73	3.25E+03	3267	48.8	3186	127	3317	8.17	6.45E-02	1.17E-03	51.9084	0.943	1180.39
52	24.53	1.36	0.6568	0.0369	0.2708	0.00203	8.65	4.04E+03	3290	54	3255	144	3311	11.8	5.74E-02	1.10E-03	46.2338	0.882	1158.60
54	24.25	1.48	0.6458	0.0401	0.2723	0.00317	8.68	3.16E+03	3278	59.6	3212	157	3319	18.2	1.46E-01	2.18E-03	117.3552	1.751	1355.03
55	22.65	1.34	0.6073	0.0362	0.2705	0.00125	9.03	2.86E+03	3212	57.3	3059	145	3309	7.24	7.37E-02	1.34E-03	59.3376	1.079	1206.41
56	22.17	1.28	0.5963	0.0326	0.2696	0.00279	8.83	2.41E+03	3191	56	3015	132	3304	16.2	1.35E-01	2.35E-03	108.6623	1.889	1336.78
57	23.8	1.18	0.6361	0.0311	0.2713	0.00231	8.77	2.50E+03	3260	48.3	3174	123	3314	13.4	7.08E-02	1.98E-03	56.9712	1.591	1198.40
58	23.47	1.26	0.6228	0.0347	0.2733	0.00171	8.74	2.76E+03	3246	52.5	3121	138	3325	9.79	6.83E-02	1.26E-03	54.9429	1.017	1191.33
59	23.41	1.32	0.6232	0.0343	0.2724	0.00428	8.82	3.29E+03	3244	54.9	3123	136	3320	24.6	1.07E-01	3.56E-03	86.3664	2.865	1284.68
60	24.52	1.38	0.6562	0.0364	0.271	0.00218	8.72	2.21E+03	3289	54.9	3253	142	3312	12.6	5.80E-02	1.17E-03	46.7006	0.945	1160.46
61	22.84	1.21	0.6076	0.0331	0.2726	0.0012	9.33	1.79E+03	3220	51.4	3060	133	3321	6.88	6.26E-02	1.30E-03	50.4112	1.048	1174.82
62	22.97	0.972	0.6153	0.0259	0.2707	0.00148	9.33	2.11E+03	3226	41.2	3091	103	3310	8.56	1.09E-01	1.94E-03	87.8152	1.562	1288.34
65	23.45	1.05	0.6268	0.0277	0.2714	0.00127	9.31	2.17E+03	3246	43.7	3137	110	3314	7.31	4.03E-02	1.04E-03	32.4457	0.840	1095.81

1b	27.15	3.5	0.7206	0.0928	0.2732	0.00183	7.57	2.05E+03	3389	126	3498	348	3325	10.5	0.04224	0.000768	721.4897	0.139	888.26
2b	27.79	3.59	0.7414	0.0959	0.2719	0.00151	7.69	1.40E+03	3412	127	3576	355	3317	8.69	0.04618	0.00128	729.5343	0.232	899.24
3b	26.12	3.37	0.6959	0.0898	0.2722	0.00196	7.59	1.79E+03	3351	126	3405	341	3319	11.3	0.0518	0.000859	740.0878	0.156	913.69
4b	27.87	3.59	0.7439	0.0957	0.2717	0.00115	7.79	1.70E+03	3415	126	3585	354	3316	6.65	0.07132	0.00111	770.6805	0.201	955.89
5b	28.35	3.67	0.7561	0.0979	0.272	0.00108	7.99	1.32E+03	3431	127	3630	359	3317	6.24	0.08479	0.00116	788.0137	0.210	979.99
6b	25.91	3.35	0.6984	0.0902	0.2691	0.00165	7.5	3.65E+03	3343	126	3415	342	3301	9.59	0.06687	0.00206	764.3693	0.374	947.15
7b	25.83	3.34	0.6911	0.0894	0.271	0.00243	8.65	1.39E+03	3340	126	3387	341	3312	14.1	0.04148	0.000735	719.8676	0.133	886.05
8b	28.14	3.64	0.7555	0.0976	0.2702	0.00174	7.84	1.79E+03	3424	127	3628	358	3307	10.1	0.04937	0.000834	735.6456	0.151	907.60
9b	26.06	3.37	0.6965	0.09	0.2713	0.00132	7.56	2.90E+03	3349	127	3407	342	3314	7.62	0.0542	0.00176	744.3111	0.319	919.49
10b	24.88	3.21	0.6628	0.0858	0.2722	0.00151	7.48	1.74E+03	3303	126	3278	333	3319	8.69	0.03481	0.000765	704.4741	0.139	865.12
11b	25.39	3.27	0.6812	0.0878	0.2704	0.00126	7.51	2.00E+03	3323	126	3349	337	3308	7.33	0.05293	0.00102	742.0957	0.185	916.45
12b	25.41	3.29	0.6857	0.0885	0.2688	0.00222	7.53	1.22E+03	3324	126	3366	338	3299	12.9	0.04747	0.000828	732.0460	0.150	902.68
13b	29.39	3.8	0.7854	0.102	0.2714	0.00159	8.03	1.80E+03	3467	127	3737	367	3314	9.18	0.06667	0.000997	764.0778	0.181	946.75
14b	26.02	3.38	0.7016	0.0913	0.269	0.0016	7.47	1.34E+03	3347	127	3427	346	3300	9.34	0.06435	0.00139	760.6426	0.252	942.00
15b	25.74	3.32	0.687	0.0886	0.2717	0.00166	7.57	1.77E+03	3337	126	3371	339	3316	9.6	0.03406	0.00107	702.5948	0.194	862.57
16b	24.83	3.23	0.6803	0.0882	0.2647	0.00164	7.75	2.27E+03	3302	127	3345	338	3275	9.75	0.06175	0.00365	756.6710	0.662	936.51
17b	27.32	3.51	0.7281	0.0936	0.2722	0.00106	7.73	2.64E+03	3395	126	3526	349	3319	6.1	0.1748	0.0134	867.2025	2.431	1091.94
18b	28	3.61	0.7469	0.0965	0.2719	0.00136	7.6	2.09E+03	3419	126	3596	356	3317	7.85	0.05029	0.00219	737.3480	0.397	909.94
19b	28.17	3.64	0.7521	0.0978	0.2716	0.00218	7.71	9.19E+02	3425	127	3615	360	3315	12.6	0.04779	0.00104	732.6604	0.189	903.52
178031																			
1	20.03	2.6	0.5672	0.0736	0.2562	0.00124	7.57	4.21E+03	3093	126	2896	303	3223	7.66	0.07525	0.00197	13.6517	0.357	963.26
2	17.33	2.25	0.4994	0.0645	0.2517	0.00124	7.42	7.14E+03	2953	124	2611	277	3195	7.82	0.07411	0.00101	13.4449	0.183	961.15
3	23.17	2.99	0.6401	0.0825	0.2625	0.00122	7.25	4.54E+03	3234	126	3189	324	3262	7.31	0.02207	0.000506	4.0039	0.092	814.11
4	22.46	2.92	0.627	0.0818	0.2598	0.00145	7.25	3.90E+03	3204	126	3138	324	3245	8.79	0.02731	0.000934	4.9545	0.169	837.38
5	23.28	3.01	0.6541	0.0845	0.2581	0.00144	7.22	3.56E+03	3239	126	3244	329	3235	8.78	0.02029	0.000733	3.6810	0.133	805.19

6	18.65	2.4	0.5164	0.0666	0.2619	0.00085	6.83	1.05E+04	3024	124	2684	283	3258	5.11	0.03878	0.000738	7.0354	0.134	877.92
9	16.83	2.19	0.4933	0.0645	0.2475	0.00215	7.15	6.94E+03	2925	125	2585	279	3169	13.8	0.04819	0.00167	8.7425	0.303	904.56
10	19.62	2.54	0.5512	0.0715	0.2582	0.00187	7.38	7.26E+03	3073	125	2830	297	3236	11.4	0.07906	0.00114	14.3429	0.207	970.13
11	19.47	2.51	0.558	0.0718	0.253	0.00112	7.15	6.07E+03	3065	125	2859	297	3204	7.03	0.05504	0.00191	9.9852	0.347	921.48
12	22.5	2.9	0.6373	0.0819	0.2561	0.00241	7.34	5.82E+03	3206	125	3179	322	3223	14.9	0.0324	0.000637	5.8779	0.116	856.77
13	22.6	2.92	0.6391	0.0825	0.2564	0.00108	7.61	2.92E+03	3210	125	3186	324	3225	6.65	0.02127	0.000737	3.8588	0.134	810.18
14	17.62	2.32	0.5314	0.0697	0.2405	0.00117	8.54	5.73E+03	2969	127	2747	293	3123	7.73	0.05296	0.00155	9.6079	0.281	916.52
178084																			
1	23	2.97	0.6089	0.0785	0.2739	0.00124	7.72	2.30E+03	3227	126	3066	315	3329	7.09	0.3023	0.0171	54.8426	3.102	1190.98
2	23.06	3.03	0.6131	0.0815	0.2728	0.0022	7.39	4.20E+03	3229	128	3083	326	3322	12.6	0.6173	0.0756	111.9892	13.715	1343.88
3	25.1	3.28	0.6698	0.0873	0.2718	0.00144	7.36	1.49E+03	3312	127	3305	337	3316	8.31	0.1303	0.0019	23.6387	0.345	1044.15
4	22.9	2.95	0.6169	0.0795	0.2692	0.00138	7.46	2.48E+03	3223	125	3098	317	3302	8.06	0.111	0.00246	20.1374	0.446	1019.46
5	25.19	3.27	0.6744	0.0876	0.2709	0.00202	7.46	1.98E+03	3316	127	3323	337	3311	11.7	0.1194	0.00226	21.6613	0.410	1030.58
7	24.92	3.22	0.6728	0.087	0.2687	0.00132	7.47	4.30E+03	3305	126	3317	335	3298	7.72	0.08531	0.00174	15.4768	0.316	980.86
8	21.28	2.73	0.5759	0.0741	0.268	0.00153	7.36	2.19E+03	3151	125	2932	303	3294	8.96	0.1234	0.00148	22.3870	0.268	1035.66
9	22.73	2.94	0.6219	0.0806	0.2651	0.00164	7.31	4.45E+03	3215	126	3117	321	3277	9.7	0.05977	0.000912	10.8433	0.165	932.21
10	23.92	3.09	0.6399	0.0826	0.2711	0.00126	7.24	3.52E+03	3265	126	3189	325	3313	7.26	0.06474	0.000963	11.7450	0.175	942.80
11	23.18	3.01	0.6058	0.0785	0.2775	0.00105	7.36	3.67E+03	3235	126	3053	315	3349	5.94	0.1969	0.00739	35.7212	1.341	1112.31
12	24.99	3.22	0.6722	0.0866	0.2697	0.00112	7.45	2.04E+03	3308	126	3315	334	3304	6.53	0.06337	0.000946	11.4964	0.172	939.95
15	20.04	2.67	0.5398	0.0713	0.2693	0.00189	6.82	3.80E+03	3093	129	2783	299	3302	11	0.0676	0.00168	12.2638	0.305	948.61

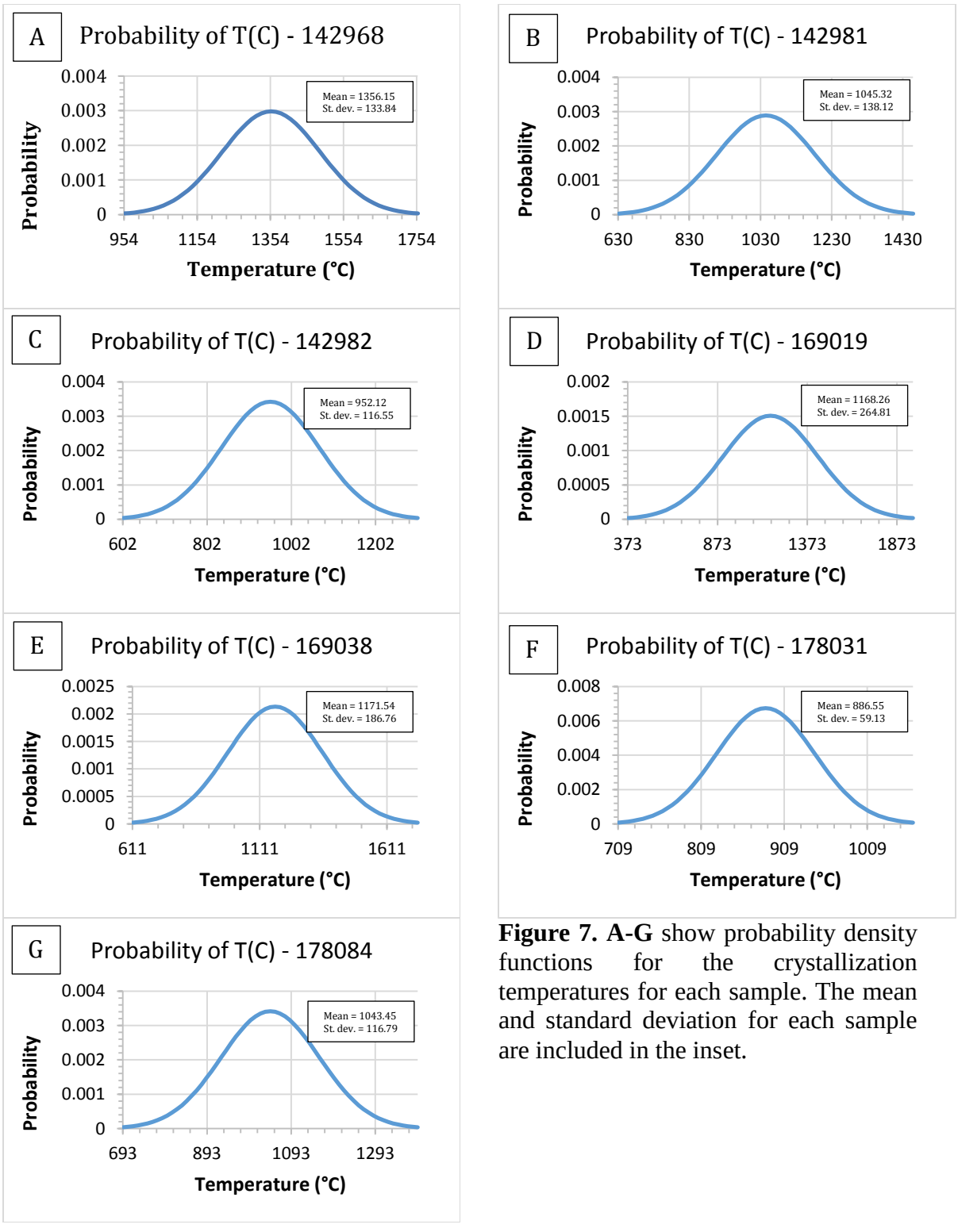

Figure 7. A-G show probability density functions for the crystallization temperatures for each sample. The mean and standard deviation for each sample are included in the inset.

5.2 Inclusions

Zircon crystals were further imaged and compositionally analyzed for mineral inclusions. A total of 84 grains were imaged for inclusions and 66 of those had inclusions. Overall, the samples contained many mineral inclusions, such as apatite, feldspars, epidote, quartz, plagioclase, and biotite. Of the samples imaged, all seven contained flourapatite inclusions, one contained chlorapatite, two contained potassium feldspar, two contained albite, two contained epidote as either mineral inclusions or fracture fills, two contained quartz, one contained plagioclase, and one contained biotite. These zircon inclusions provide us with a direct view of the Archean crust. However, the mineral assemblages seen in the East Pilbara Craton zircons do not provide evidence of the tectonic setting during the Archean without further investigation, which was not conducted in this study.

Table 2. . Total population counts of mineral inclusions, per sample. *Ap* apatite, *Plag* plagioclase, *Ksp* potassium feldspar, *Qtz* quartz, *Ep* epidote, *Biot* biotite.

Sample #	Zircons imaged	Zircons with inclusions	Ap	Plag	Ksp	Qtz	Ep	Biot	Fe-Ti
142968	17	11	16	2	0	1	0	1	0
142981	5	2	3	0	0	0	0	0	0
142982	3	3	2	0	2	0	0	0	0
169019	0	0	0	0	0	0	0	0	0
169038	51	44	206	2	5	1	3	0	1
178031	4	3	2	0	0	0	1	0	0
178084	5	5	9	0	0	0	1	0	0

Table 3. The U-Pb ages and in millions of years as well as mean temperatures in degrees C. The table also includes the SHRIMP ages measured by the GSWA after the samples were collected.

Sample #	GSWA 207Pb/ 206Pb		1 s.e.	207Pb/ 235U Age		1 s.e.	206Pb/ 238U Age		1 s.e.	207Pb/ 206Pb Age		1 s.e.	Mean T(C)		St Dev.
142968	3425	±	4	3305.53	±	46.23	3150.47	±	115.99	3402.18	±	8.55	1044.51	±	87.57
142981	3312	±	4	3348.71	±	126.14	3447.86	±	344.29	3291.57	±	6.95	832.87	±	96.31
142982	3305	±	3	3222.25	±	125.88	3153.63	±	321.63	3269.75	±	5.04	766.76	±	83.69
169019	3428	±	6	3464.57	±	128.54	3635.26	±	362.74	3373.00	±	14.49	914.62	±	169.51
169038	3315	±	2	3286.03	±	73.00	3245.53	±	192.93	3312.78	±	9.26	919.40	±	126.41
178031	3250	±	2	3099.58	±	125.33	2929.00	±	304.33	3216.50	±	8.92	719.92	±	43.39
178084	3311	±	3	3239.92	±	126.42	3131.75	±	322.00	3309.75	±	8.74	832.02	±	80.95

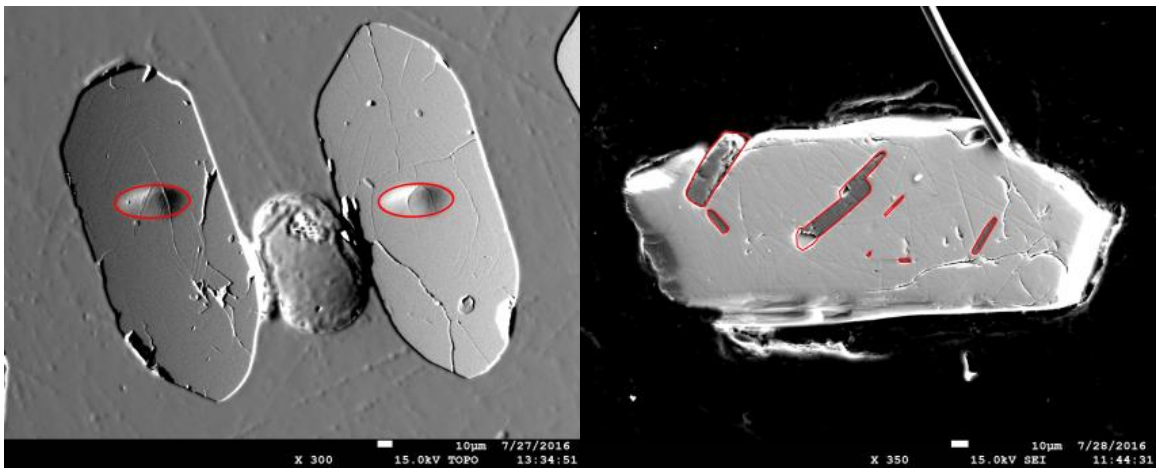

Figure 8. Left, shows examples of the spot size created by the SIMS probe. Spots vary in size between 40-50 µm. Right, a secondary electron image of a zircon from sample 169038 with many apatite inclusions, outlined in red.

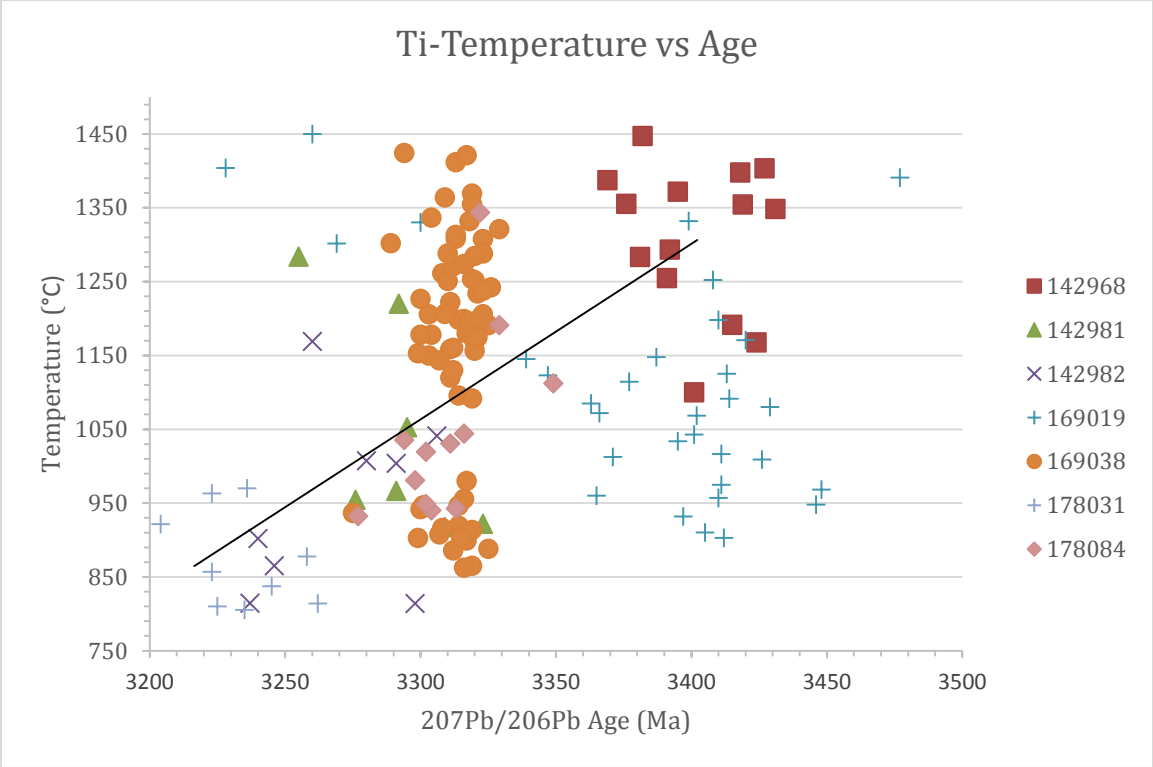

Figure 9. Plot showing temperature vs age for each measured zircon for each sample.

6. Discussion

6.1 Ages

Pb/Pb ages of the various granitic domes of the East Pilbara Craton are consistent to slightly inconsistent with previously SHRIMP measured ages by the GSWA (Table 3). SIMS ages vary from consistent to -55 Ma. This is likely because the newly tested zircon population is different than those previously examined by the GSWA, but it may also be caused by calibration errors with the SIMS probe. However, these age differences still provide insight into the conditions of the mid Archean. For one of the sampled granitic domes, Mt. Edgar, three samples were chosen. These three samples, while geographically close, have differing ages and crystallization temperatures. This may either represent a progressive cooling history, as there is a cooling trend as these samples young in age, or multiple granitic intrusions.

Previous models that explain the formation of the dome-and-keel geometry for the evolution of the Pilbara Craton put the ages of the studied samples (c. 3.40-3.22 Ga) during a period of crustal heating and thickening due to hundreds of millions of years of mantle plume interaction with the craton (Van Kranendonk 2006, Figure 11). Based on this model, a mantle plume beneath a mafic proto plate causes several granitic diapirs to intrude, thickening and heating the crust. Slightly before the formation of the studied areas, it is hypothesized that multiple mantle plumes began to thicken the crust some time before 3.50 Ga. The studied TTGs then formed between 3.40 and 3.22 Ga, and were followed by plume-driven rifting ca. 3.20 Ga.

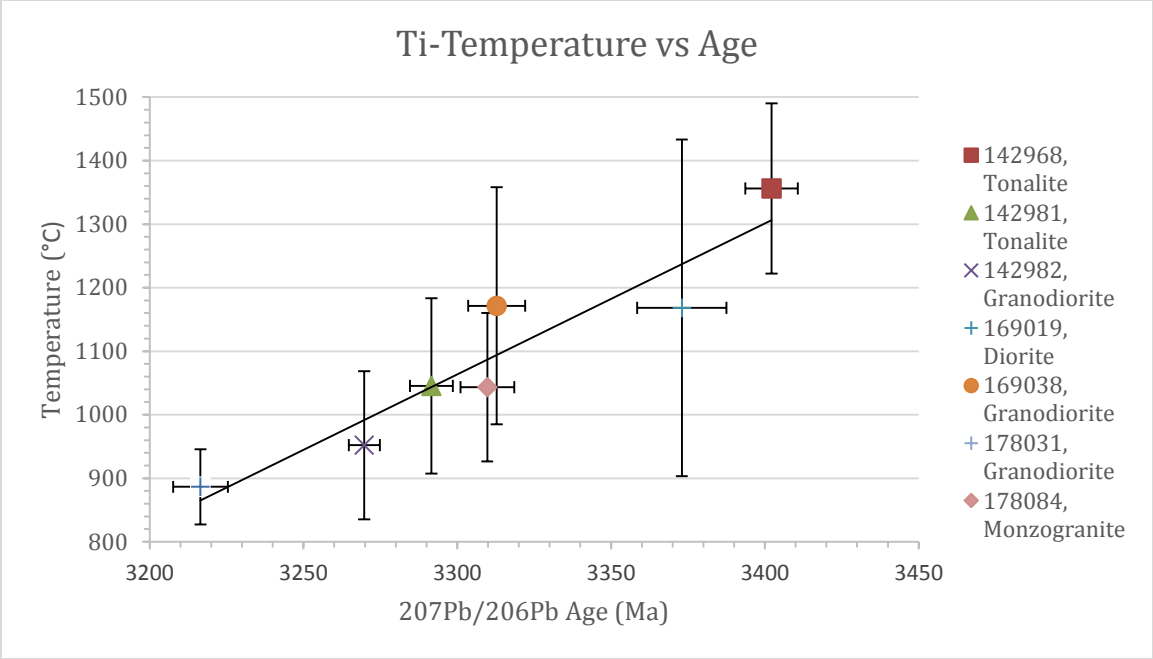

Figure 10. Plot showing the mean temperature and measured ages of each granitoid. Notice the cooling trend of all the samples, with a temperature peak just before 3300 Ma, at sample 169038. Age errors are 1σ, temperature error bars show 1 st. dev. The legend show the composition of each sample.

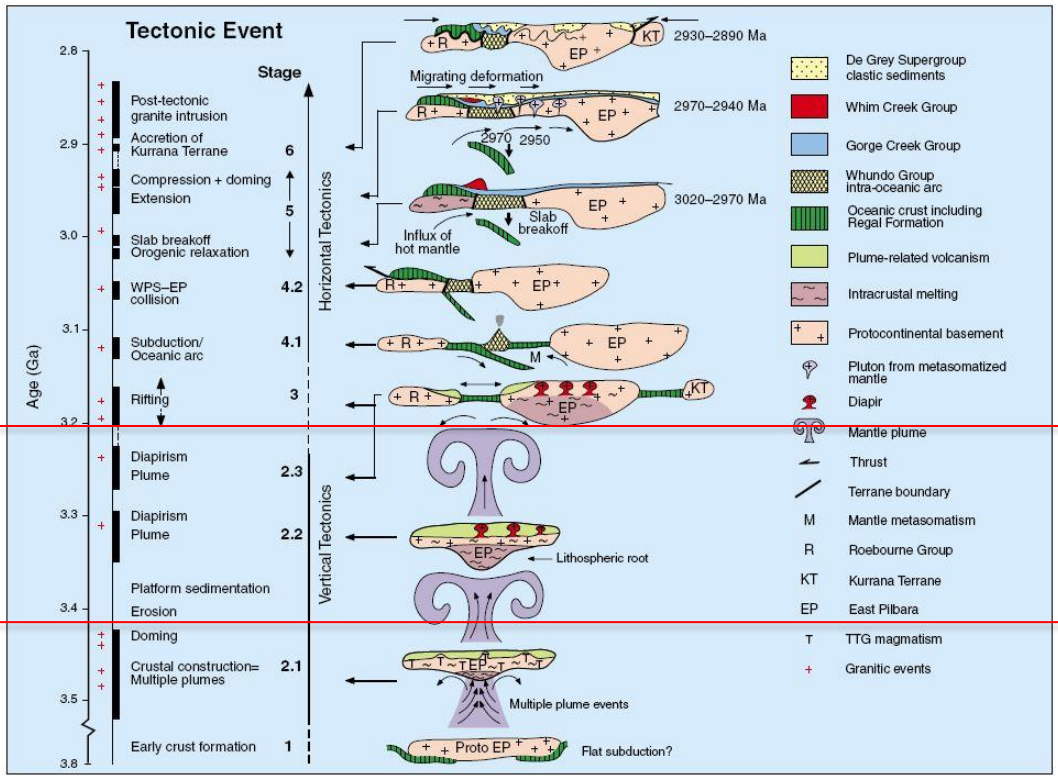

Figure 11. A history of events in the northern Pilbara Craton, starting with the formation of a proto plate via vertical tectonics, to the onset of horizontal tectonics with the onset of rifting at c. 3.20 Ga and modern-style subduction tectonics c. 3.10 Ga. The age range of the studied samples is inside the red box, which highlights the events that may contribute to the temperature estimates produced by the titanium thermometry. From Van Kranendonk 2006.

6.2 Temperature

When compared to Hadean zircons, which have been interpreted as showing hydrous, minimum melt conditions, the zircons of the East Pilbara Craton show a noticeably strong bias towards warmer crystallization conditions. In this data set, we see substantially higher (over 300° C) crystallization temperatures than those from the Hadean, which indicates a change in tectonic regimes between these two eras. The data set presented here includes seven different crystallization temperatures for five different granitic plutons of the East Pilbara Craton. These samples show a general cooling trend of 469° C, or about 2.4° C/Ma (Figure 10). While this may correspond with a cooling crust, the data points are spread across hundreds of millions of years. Instead, they likeley indicate several heating events that may be linked to the granitic intrusions the zircons are sourced from. These heating events could be mantle related (Van Kranendonk 2006) or linked a higher radiogenic heating of a younger planet (Kemp et al. 2010). Figure 12 shows the distribution of samples and their corresponding ages and temperatures.

The studied samples show a weak correlation of temperature with composition. Figure 10 shows the compositions of the samples, in combination with temperature estimates and U-Pb ages. The data shows a tendency for higher temperatures with granitic compositions that are lacking quartz (diorite, sample 169019) and lower temperatures for those bearing more alkali feldspars. While a weak correlation, this trend is appropriate for the granitoids studied and it suggests that the crystallization temperature is linked to the composition of the granitoid.

The temperature estimates from titanium-in-zircon thermometry suggest that, simply, the Paleoarchean crust was unlike the Hadean crust. Titanium-in-zircon

crystallization temperatures of the Hadean show minimum melt conditions and subchondritic Hf values which seem to indicate a planet-wide Hadean protocrust being established at or before 4.5 Ga. This combined with the preferential preservation of Archean terranes indicates a change in the mechanics in which the Earth generated crust from the Hadean to the Archean.

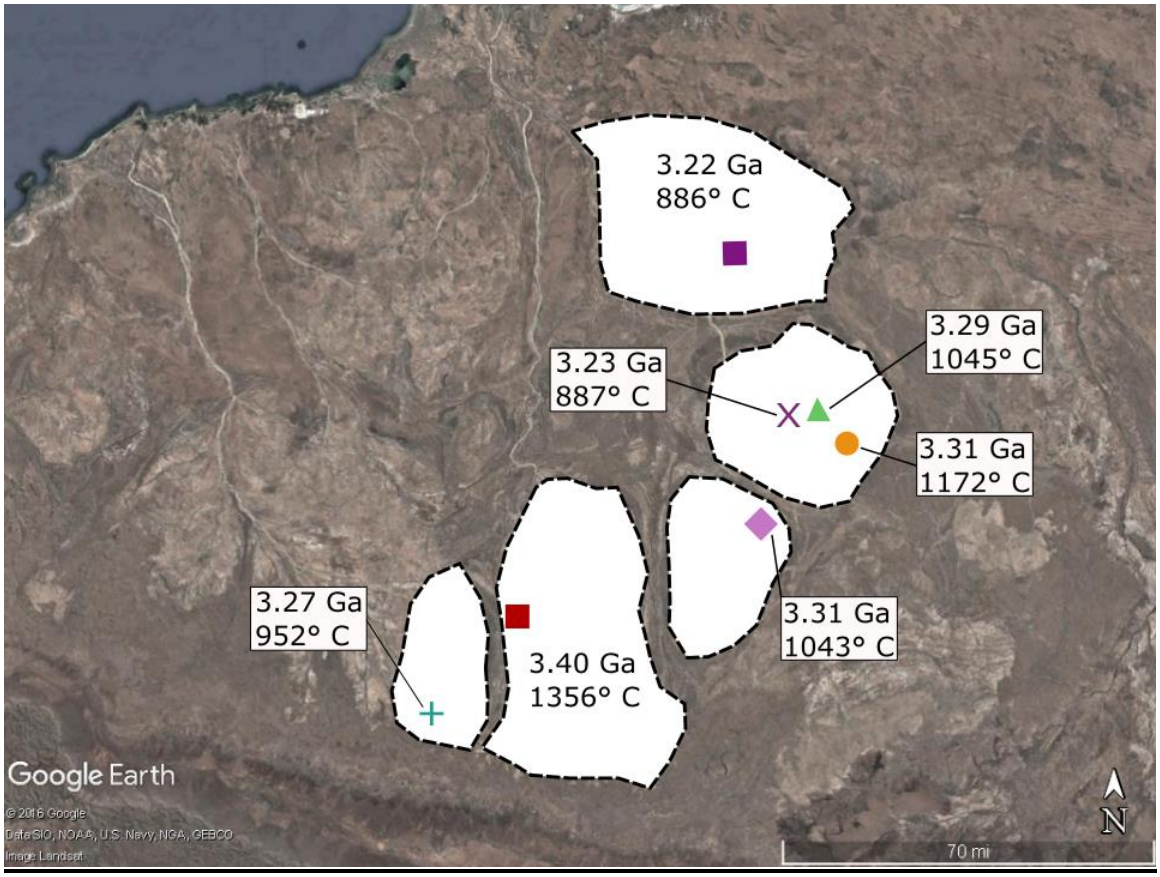

Figure 12. Map showing the distribution of samples with their 207Pb/206Pb ages and titanium crystallization temperatures. From this, we can see the ages and temperature estimates of each granitic dome. Note that the three samples from the Mt. Edgar dome have differing ages and temperatures.

7. **Conclusion**

Using titanium contents of zircons sourced from the Eastern Pilbara Craton, U-Pb ages and crystallization temperatures were estimated for five of the granitic domes of the craton. The seven data points collected show a general cooling trend across the domes of ~1350-880° C from about 3.40-3.21 Ga, but remain significantly higher than previous estimates of Hadean zircon crystallization temperatures. These estimates support an early Earth model with higher levels of heat released due to meteor impacts and increased radiogenic heating, which would have caused the early Earth to exhibit a higher geothermal gradient. The changing temperature estimates across the domes could be linked to several mantle plumes interacting with the crust across the ~200 million years seen in the samples, but may also be caused by progressive cooling of a hot, young crust. Tectonically, this data suggests that the Paleoarchean crust was significantly different than that of the Hadean and requires further investigation into the thermal and tectonic evolution seen from the Hadean and the Paleoarchean. For future work, mineral inclusions can be further studied to create a cooling history of the cratons, and can be combined with a larger dataset to constrain the ages of the remaining granitic domes.

References

Abbot, Sunshine, T. Mark Harrison, Axel K. Schmitt, and Stephen J. Mojzsis. "A search for thermal excursions from ancient extraterrestrial impacts using Hadean zircon Ti-U-Th-Pb depth profiles." *PNAS* vol. 109 no. 34. (Aug. 21, 2012): 13486-13492

Bell, Elizabeth A. "Preservation of primary mineral inclusions and secondary mineralization in igneous zircon: a case study in orthogneiss from the Blue Ridge, Virginia." *Contrib Mineral Petrol* 171:26 (2016).

Condie, Kent. Chapter 1.2 The Distribution of Paleoarchean Crust, In: Martin J. van Kranendonk, R. Hugh Smithies and Vickie C. Bennett, Editor(s), Developments in Precambrian Geology, Elsevier, 2007, Volume 15, Pages 9-18.

Champion, David C. and Smithies, R. Hugh. "Geochemistry of Paleoarchean granites of the East Pilbara Terrane, Pilbara Craton, Western Australia: Implications for Early Archean crustal growth." *Earths Oldest Rocks.* Elsevier, 2007: 369-409. Also published in *Developments in Precambrian Geology*, vol 15.

Ernst, W.G. "Speculations on evolution of the terrestrial lithosphere-asthenosphere system—Plumes and plates." *Gondwana Research.* Vol. 11 (2007): 38-49.

Ferry, J.M.; Watson, E.B. "New thermodynamic models and revised calibrations for the Ti-in-zircon and Zr-in-rutile thermometers". *Contributions to Mineralogy and Petrology* vol. 154**.**4 (Oct 2007): 429-437.

Guitreau, M., Blichert-Toft, J., Martin, H., Mojzsis, S.J., and Albarede, F. "Hafnium isotope evidence from Archean granitic rocks for deep-mantle origin of continental crust." *Earth and Planetary Science Letters.* (23 May 2012): 211-223.

Harrison TM, Schmitt AK (2007) Temperature spectra of zircon crystallization in plutonic rocks. Geology 35:635-638

Harrison, T. Mark. "The Hadean Crust: Evidence from >4 Ga Zircons." *Annual Review of Earth and Planetary Sciences.* 37 (2009): 479-505.

Harrison, T. Mark, Axel K. Schmitt, Malcolm T. McCulloch, Oscar M. Lovera. "Early (≥ 4.5 Ga) formation of terrestrial crust: Lu–Hf, δ18O, and Ti thermometry results for Hadean zircons", Earth and Planetary Science Letters, Volume 268, Issues 3–4, 30 April 2008, Pages 476-486.

Hickman, Arthur H., and van Kranendonk, Martin J. "Diapiric processes in the formation of Archean continental crust, East Pilbara Granite-Greenstone Terrane, Australia." *Developments in Precambrian Geology.* 12 (2004): 118-139

Hopkins, Michelle, Harrison, T. Mark, and Manning, Craig E. "Low heat flow inferred from >4 Gyr zircons suggests Hadean plate boundary interactions." *Nature. V*ol 456 (27 Nov 2008): 493-496.

Hopkins, Michelle, Harrison, T. Mark, and Manning, Craig E. "Constraints on Hadean geodynamics from mineral inclusions in >4 Ga zircons." *Earth and Planetary Science Letter.* Vol 298 (9 Aug 2010):367-376.

Hopkins, Michelle, Harrison, T. Mark, and Manning, Craig E. "Forum Comment: Metamorphic replacement of mineral inclusions in detrital zircon from Jack Hills, Australia: Implications for the Hadean Earth." *Geological Society of America: Geology Forum.* Dec 2012.

Kemp, A.I.S., S.A. Wilde, C.J. Hawkesworth, C.D. Coath, A. Nemchin, R.T. Pidgeon, J.D. Vervoort, and S.A. DuFrane. "Hadean crustal evolution revisited: New constraints from Pb–Hf isotope systematics of the Jack Hills zircons," Earth and Planetary Science Letters, Volume 296, Issues 1–2, 15 July 2010, Pages 45-56.

M.J. Bickle, Heat loss from the earth: A constraint on Archaean tectonics from the relation between geothermal gradients and the rate of plate production, Earth and Planetary Science Letters, Volume 40, Issue 3, 1978, Pages 301-315, ISSN 0012-821X

Marchi, S., Bottke, W.F., Elkins-Tanton, L.T., Bierhaus, M., Wuennemann, K., Morbidelli, A. and Kring, D.A. "Widespread mixing and burial of Earth's Hadean crust by asteroid impacts." *Nature.*Vol 511 (31 July 2014): 578-582.

Moore, William B and Webb, A. Alexander G. Webb. "Heat-pipe Earth." *Nature.* Vol 501 (26 Sep 2013): 501-505.

Nutman, Allen P., Friend, Clark R.L., Horie, Kenji, and Hidaka, Hiroshi. "The Itsaq Gneiss complex of Southern West Greenland and the Construction of Eoarchaean Crust at Convergent Plate Boundaries." *Earth's Oldest Rocks.* Vol. 15. Elsevier, 2007. 187-218.

Paces, J.B., Miller, J.D., 1993. Precise U–Pb ages of Duluth Complex and related mafic intrusions, northeastern Minnesota: geochronological insights into physical, petrogenetic, paleomagnetic and tectonomagmatic processes associated with the 1.1 Ga midcontinent rift system. Journal of Geophysical Research 98, 13997-14013.

Pullen, Alex and Martin Pepper. "Preparing & cleaning mounts for analysis at Arizona LaserChron Center." Arizona LaserChron Center, 2009.

R.-M. Bedini, J. Blichert-Toft, M. Boyet, F. Albarède, Isotopic constraints on the cooling of the continental lithosphere, Earth and Planetary Science Letters, Volume 223, Issues 1–2, 30 June 2004, Pages 99-111, ISSN 0012-821X, http://dx.doi.org/10.1016/j.epsl.2004.04.012.

Rasmussen, Birger, Fletcher, Ian R., Muhling, Janet R., Gregory, Courtney J., and Wilde, Simon A. "Metamorphic replacement of mineral inclusions in detrital zircon from Jack Hills,

Australia: Implications for the Hadean Earth." Geological Society of America. Vol 39, no. 12 (Dec 2011): 1143-1146.

Sandiford, M., M. J. Van Kranendonk, and S. Bodorkos (2004), Conductive incubation and the origin of dome-and-keel structure in Archean granite-greenstone terrains: A model based on the eastern Pilbara Craton, Western Australia,Tectonics, 23Simpson, Gayland, Mark Pecha, and George Gehrels. "Mineral separation instruction manual." Arizona LaserChron Center, 2012.

Simpson, Gayland, Mark Pecha, and George Gehrels. "Mineral separation instruction manual." Arizona LaserChron Center, 2012.

Smithies, R.H., Champion, D.C., Cassidy, K.F., 2003. Formation of Earth's early Archaean continental crust. Precambrian Res. 127, 89–101

Smithies, R.H., Champion, D.C., Van Kranendonk, M.J., 2009. Formation of Paleoarchaean continental crust through infracrustal melting of enriched basalt. Earth Planet. Sci. Lett. 281, 298–306

Solomatov, V.S. and Moresi, L.-N. "Stagnant lid convection on Venus." *Journal of Geophysical Research.* Vol. 101, no. E2 (25 Feb 1996): 4737-4753.

Stern, Robert J. "Modern-style plate tectonics began in Neoproterozoic time: An alternative interpretation of Earth's tectonic history." *Geologic Society of America Special Paper* 440 (2008): 265-280.

Turcotte, Donald L., and Gerald Schubert. "Geodynamics: Applications of continuum physics to geological problems, 450 pp." (1982).

Van Kranendonk, Martin J. "Two types of Archean continental crust: Plume and plate tectonics on early Earth." *American Journal of Science* 310.10 (2010): 1187-1209.

Van Kranendonk, Martin J. "Cool greenstone drips and the role of partial convective overturn in Barberton greenstone belt evolution." *Journal of African Earth Sciences 60 (2011): 346-352.*

Van Kranendonk, Martin J. , R. Hugh Smithies, Arthur H. Hickman, David C. Champion, Chapter 4.1 Paleoarchean Development of a Continental Nucleus: the East Pilbara Terrane of the Pilbara Craton, Western Australia, In: Martin J. van Kranendonk, R. Hugh Smithies and Vickie C. Bennett, Editor(s), Developments in Precambrian Geology, Elsevier, 2007, Volume 15, Pages 307-337.

Van Kranendonk, Martin J., Smithies, R. Hugh, Hickman, Arthur H., and Champion, D.C. "Secular tectonic evolution of Archean continental crust: interplay between horizontal and vertical processes in the formation of the Pilbara Craton, Australia." *Terra Nova* 19 (2007): 1-38.

Van, Kranendonk M. J."*Revised Lithostratigraphy of Archean Supracrustal and Intrusive Rocks in the Northern Pilbara Craton, Western Australia*." East Perth, W.A: Geological Survey of Western Australia, 2006.

Watson, E.B. and Harrison, T.M. "Zircon Thermometer Reveals Minimum Melting Conditions on Earliest Earth." *Science* 308 (6 May 2005): 841-844.

Wiedenbeck M, Hanchar JM, Peck WH, Sylvester P, Valley J, Whitehouse M, Kronz A, Morishita Y, Nasdala L (2004) Further characterization of the 91500 zircon crystal. Geostand Geoanal Res 28:9-39

Appendix

A. *Concordia Plots*

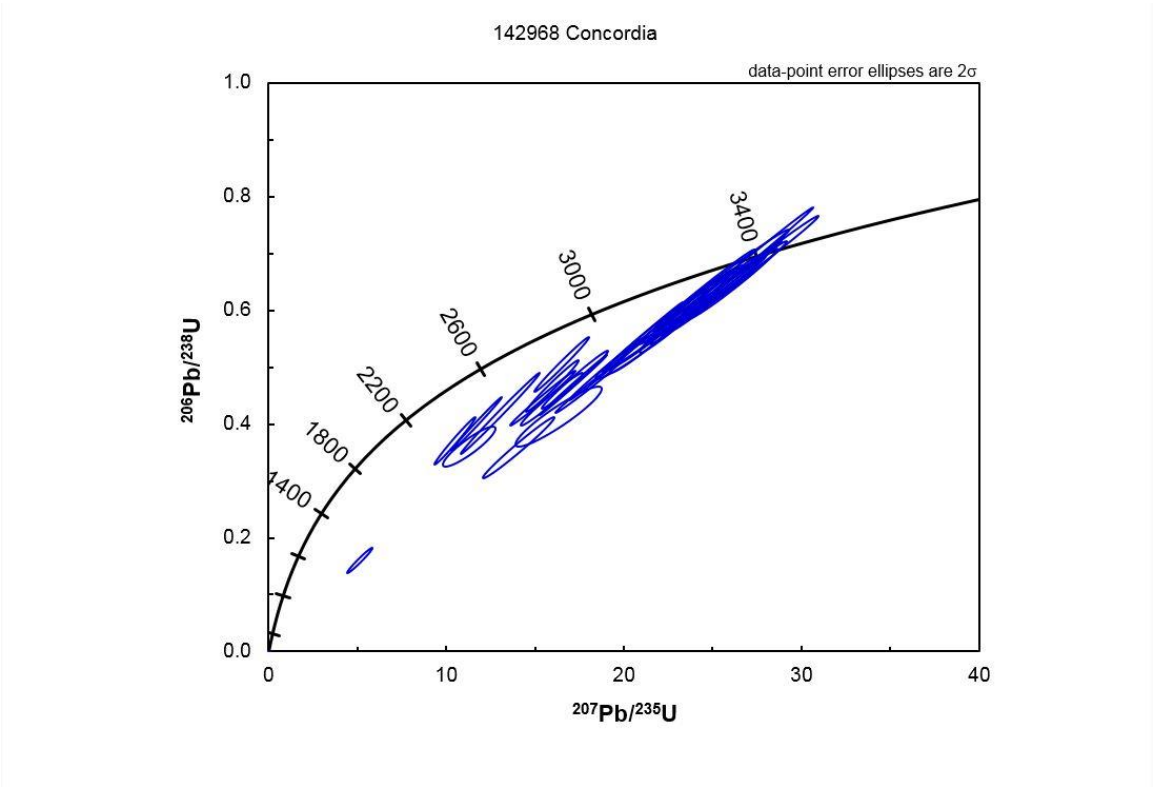

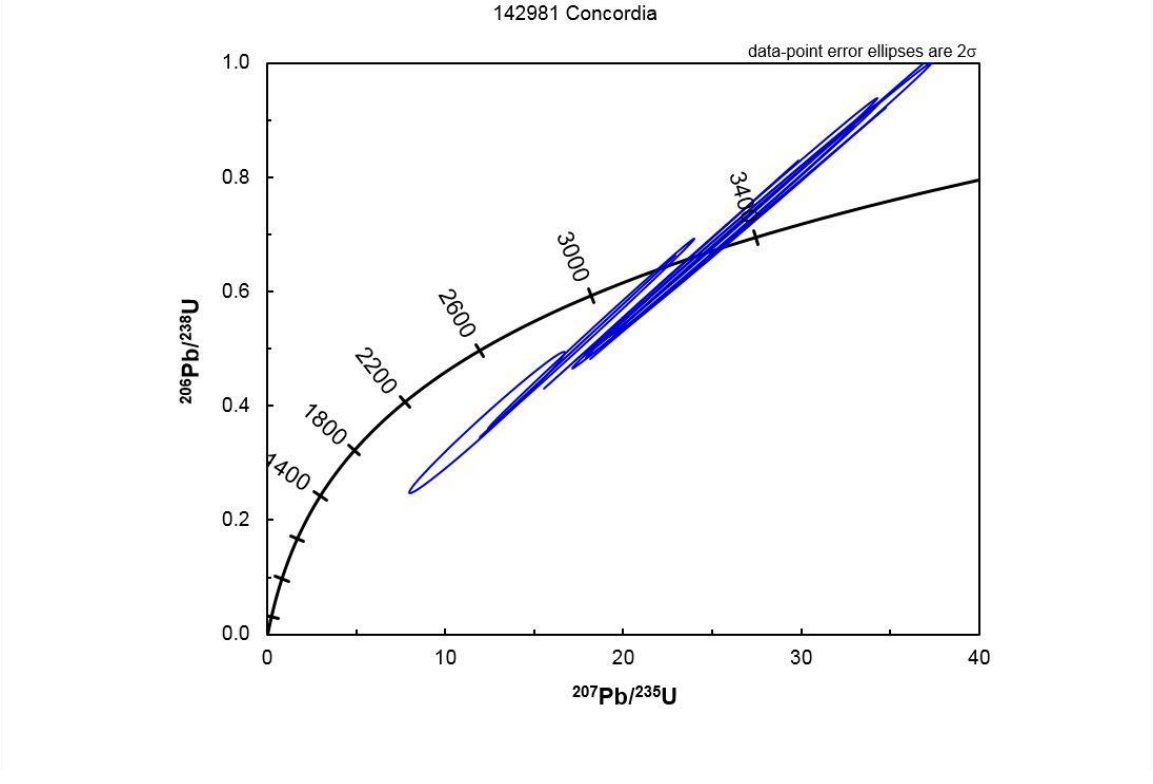

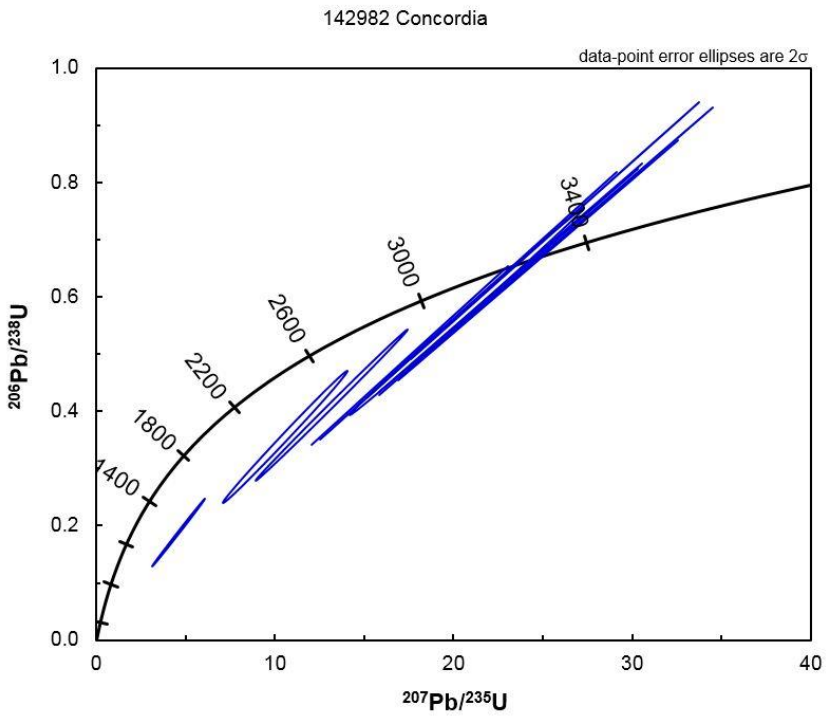
142982 Concordia
data-point error ellipses are 2σ
1.0
0.8
0.6
0.4
0.2
0.0
0
10
20
30
40
206Pb/238U
207Pb/235U
1400
1800
2200
2600
3000
3400

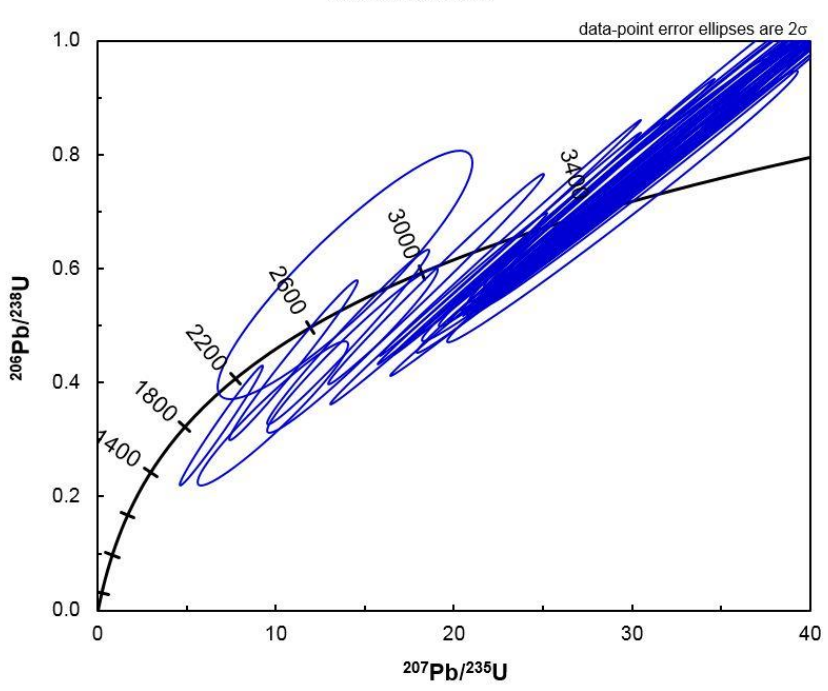
169019 Concordia
data-point error ellipses are 2σ
1.0
0.8
0.6
0.4
0.2
0.0
0
10
20
30
40
206Pb/238U
207Pb/235U
1400
1800
2200
2600
3000
3400

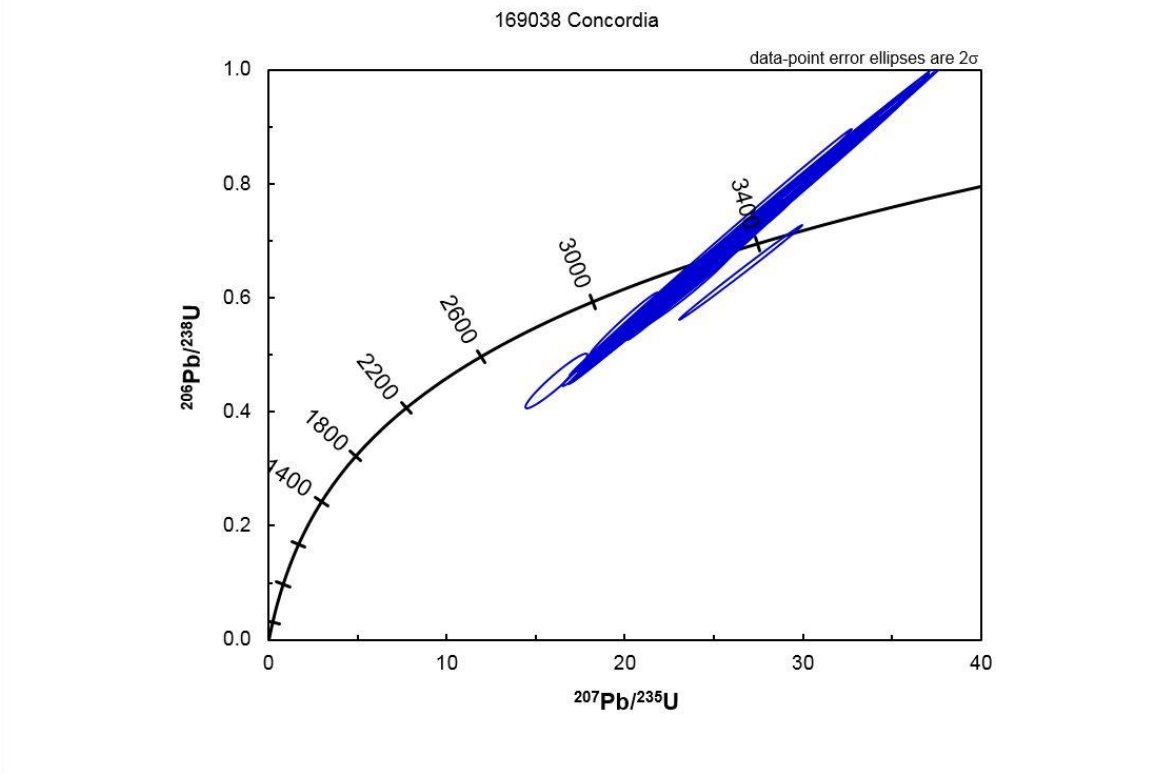
169038 Concordia
data-point error ellipses are 2σ
1.0
0.8
0.6
0.4
0.2
0.0
0
10
20
30
40
206Pb/238U
207Pb/235U
1400
1800
2200
2600
3000
3400

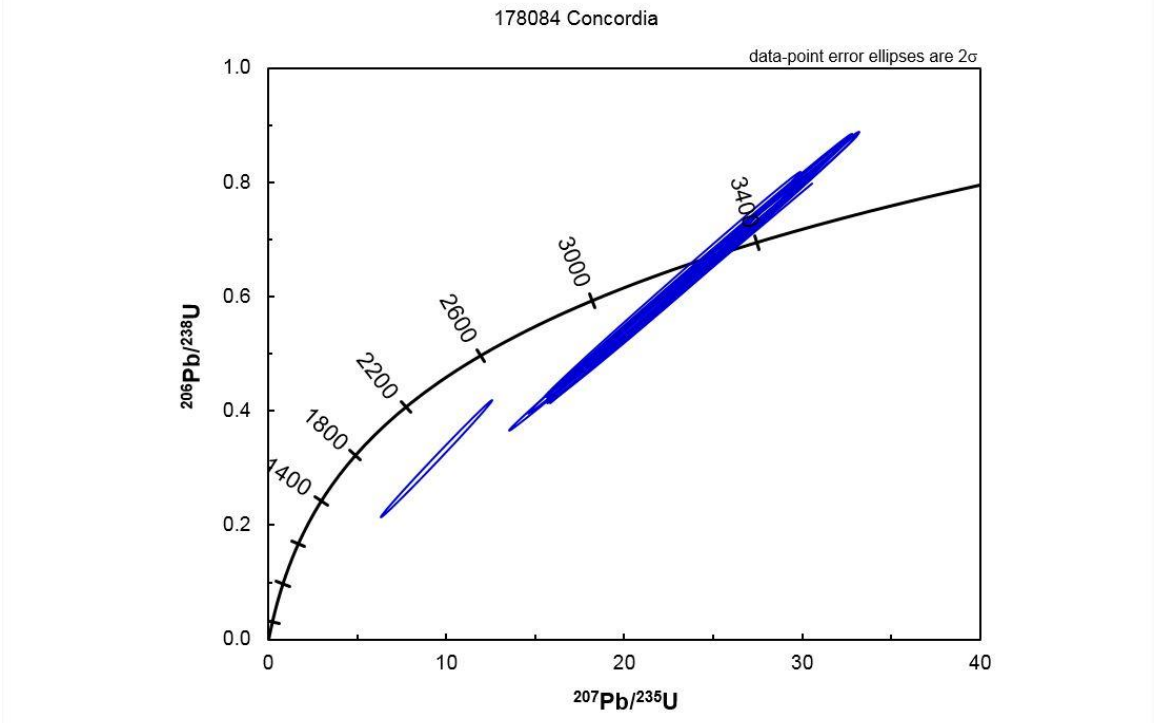
178084 Concordia
data-point error ellipses are 2σ
1.0
0.8
0.6
0.4
0.2
0.0
0
10
20
30
40
206Pb/238U
207Pb/235U
1400
1800
2200
2600
3000
3400

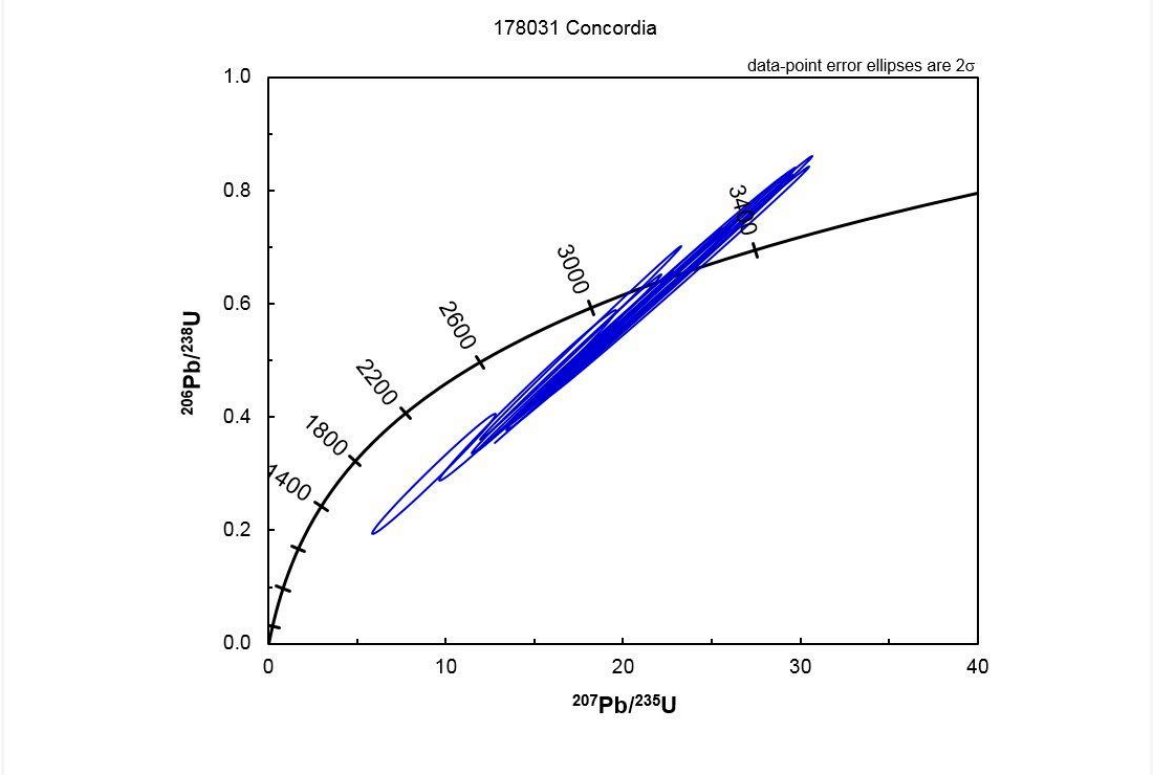

The above figures show the complete Concordia plots for all seven samples. From these plots, grains within error of Concordia were selected as viable samples for Ti-in-zircon thermometry and inclusion population analysis.

B. *Inclusion Images and Data*

142968

Grain 2

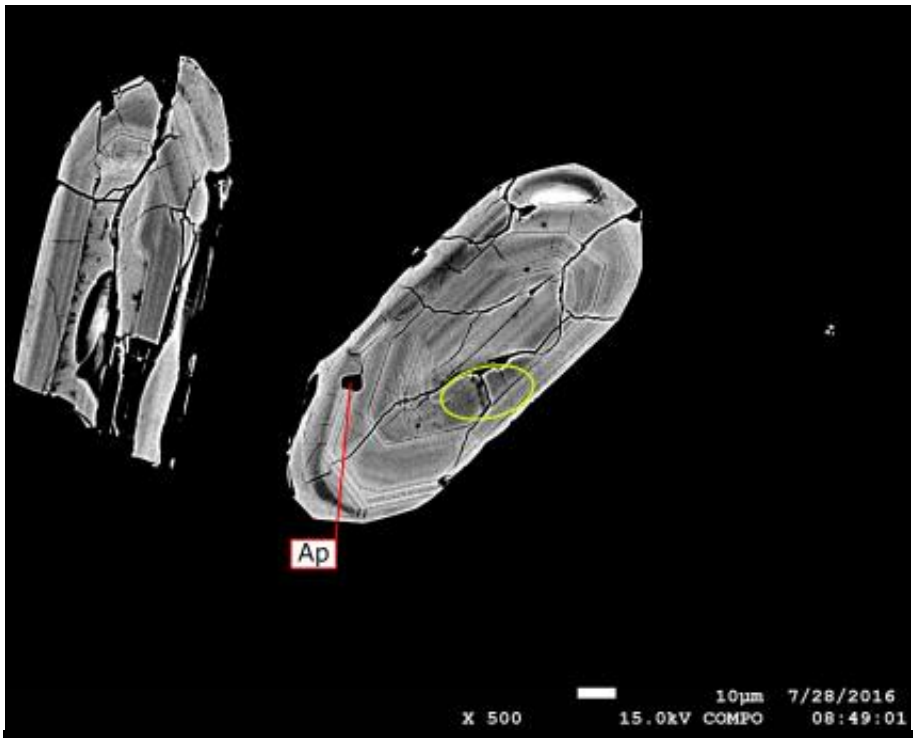

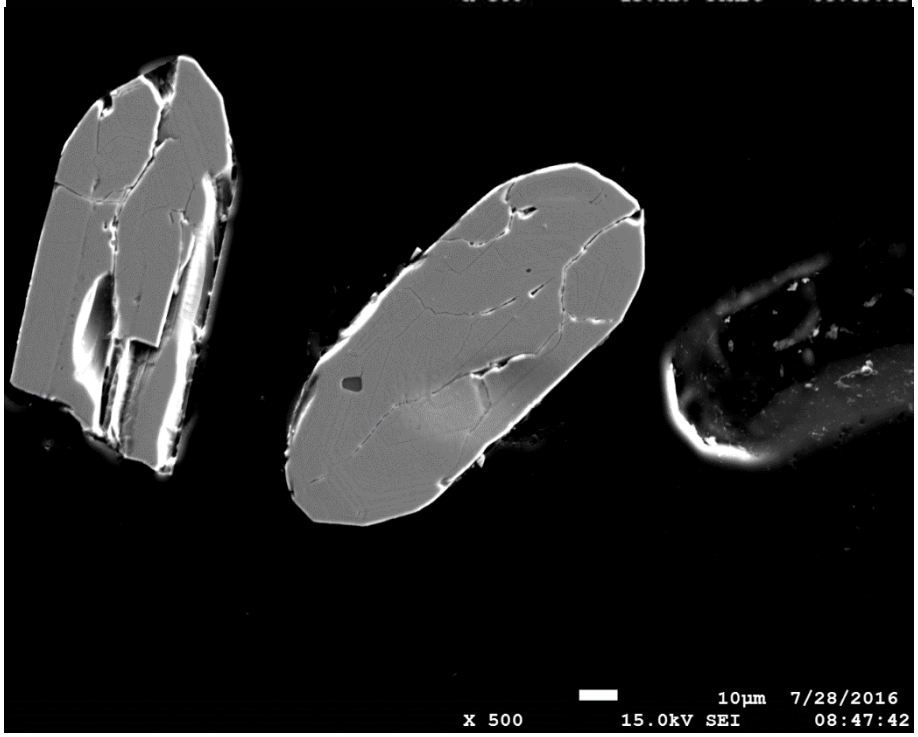

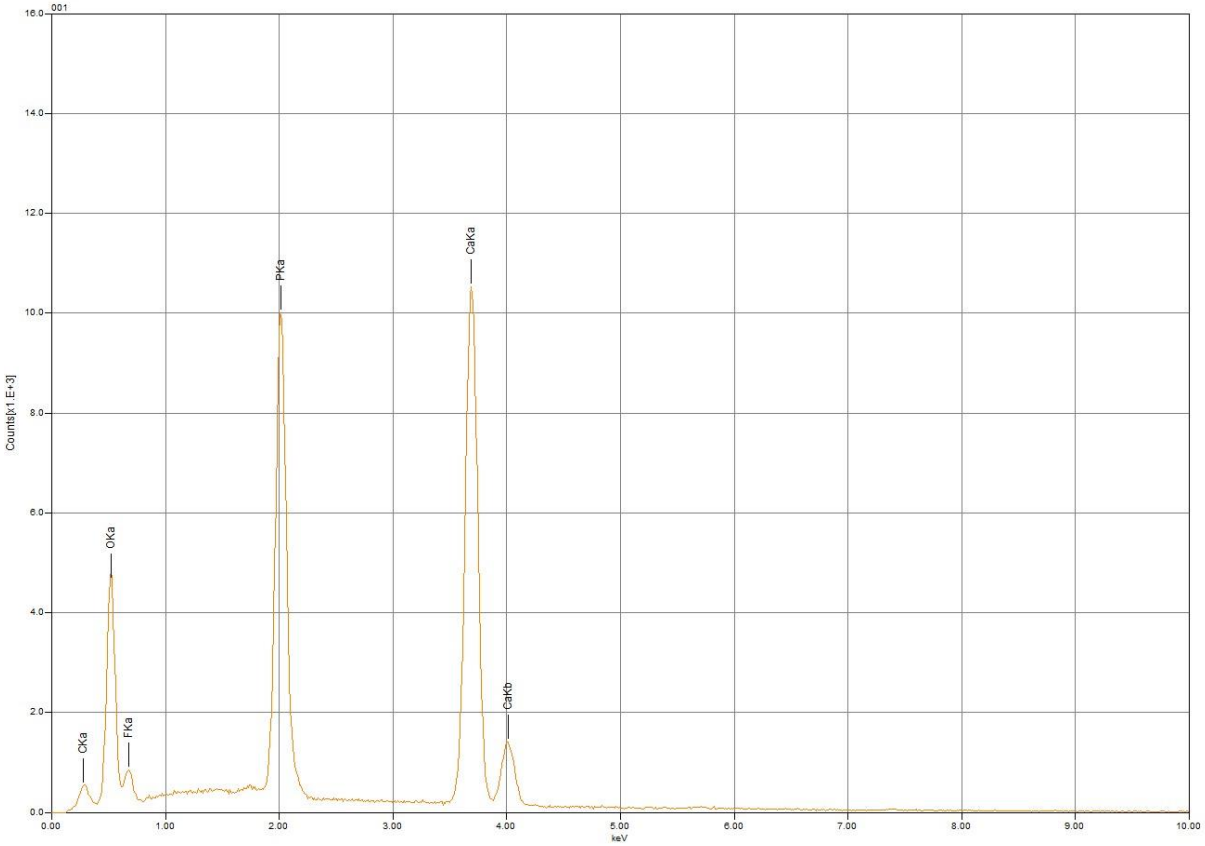
001
Counts[x1 E+3]
keV
CKa
OKa
FKa
PKa
CaKa
CaKb

Grain 5

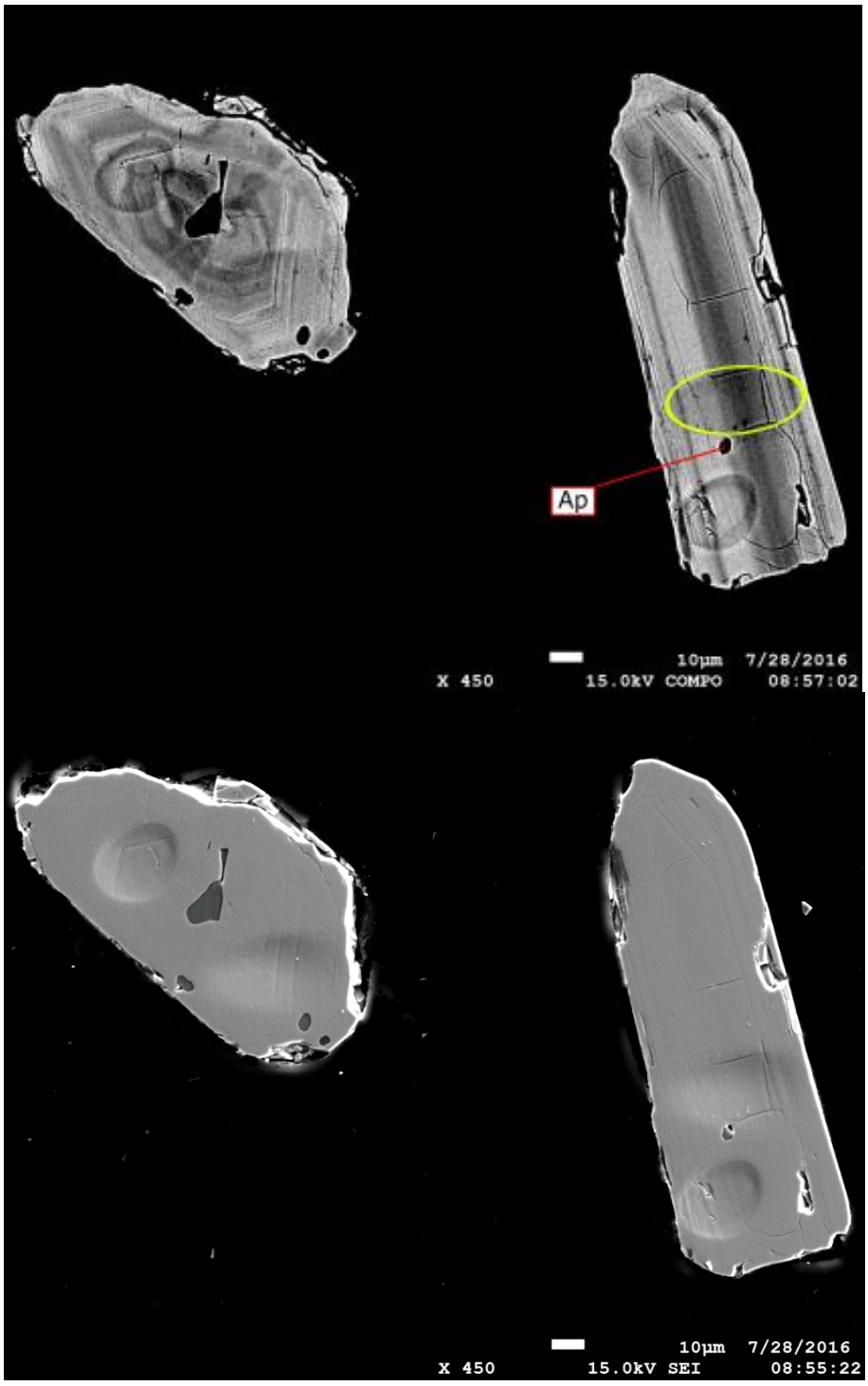
Ap
10µm 7/28/2016
X 450 15.0kV COMPO 08:57:02
10µm 7/28/2016
X 450 15.0kV SEI 08:55:22

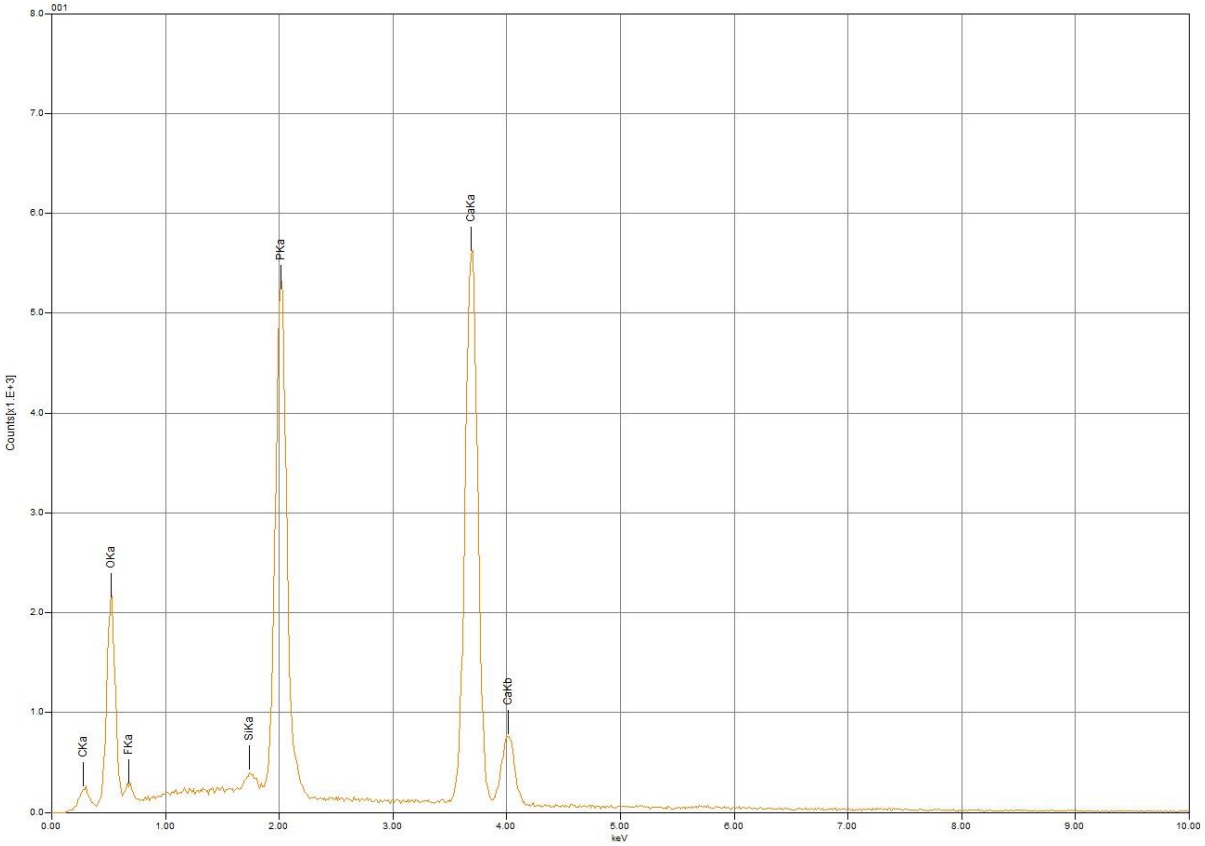
001
Counts[x1 E+3]
keV
CKa
OKa
FKa
SiKa
PKa
CaKa
CaKb

Grain 6

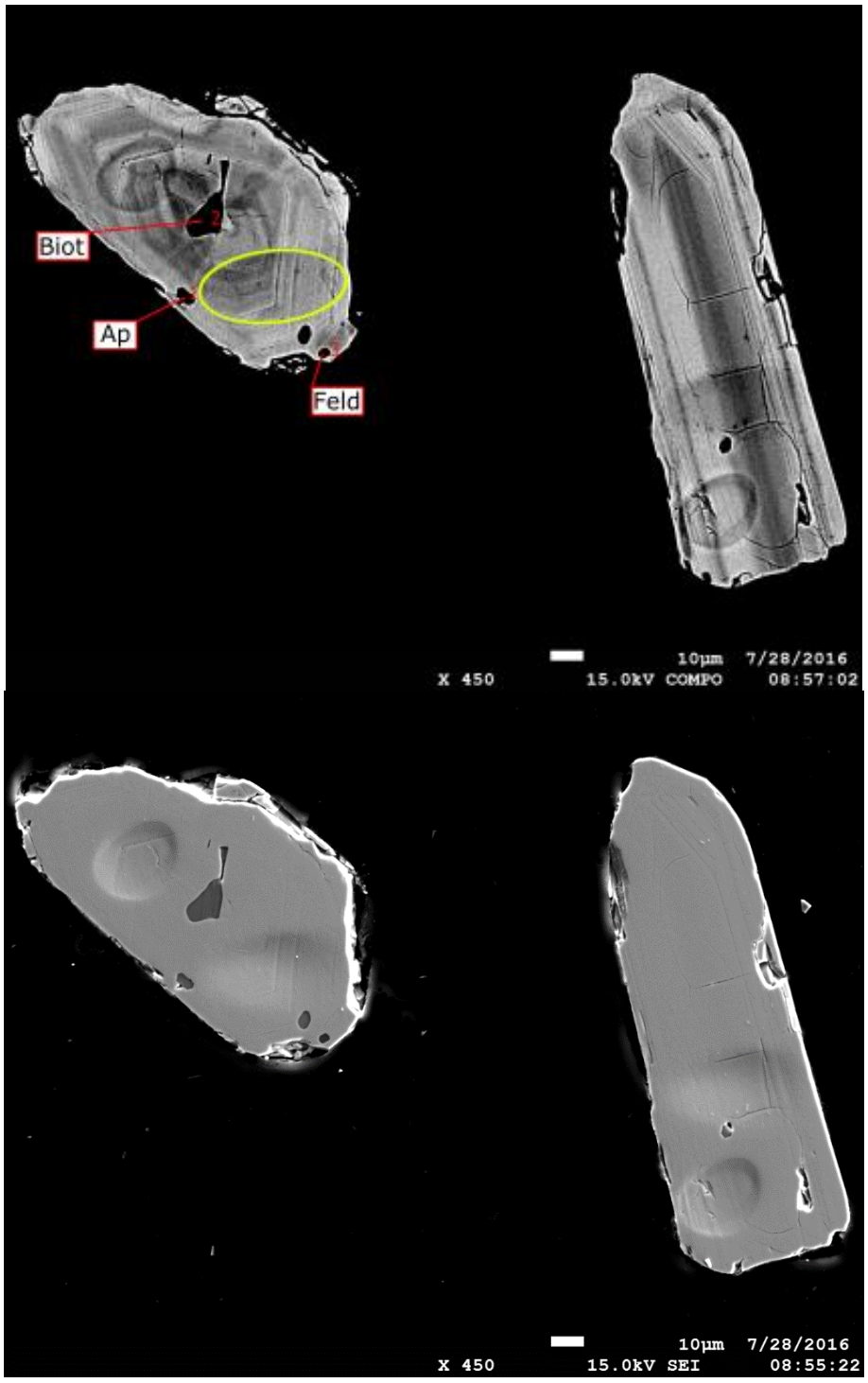
Biot
Ap
Feld
X 450
10µm
15.0kV COMPO
7/28/2016
08:57:02
X 450
10µm
15.0kV SEI
7/28/2016
08:55:22

1

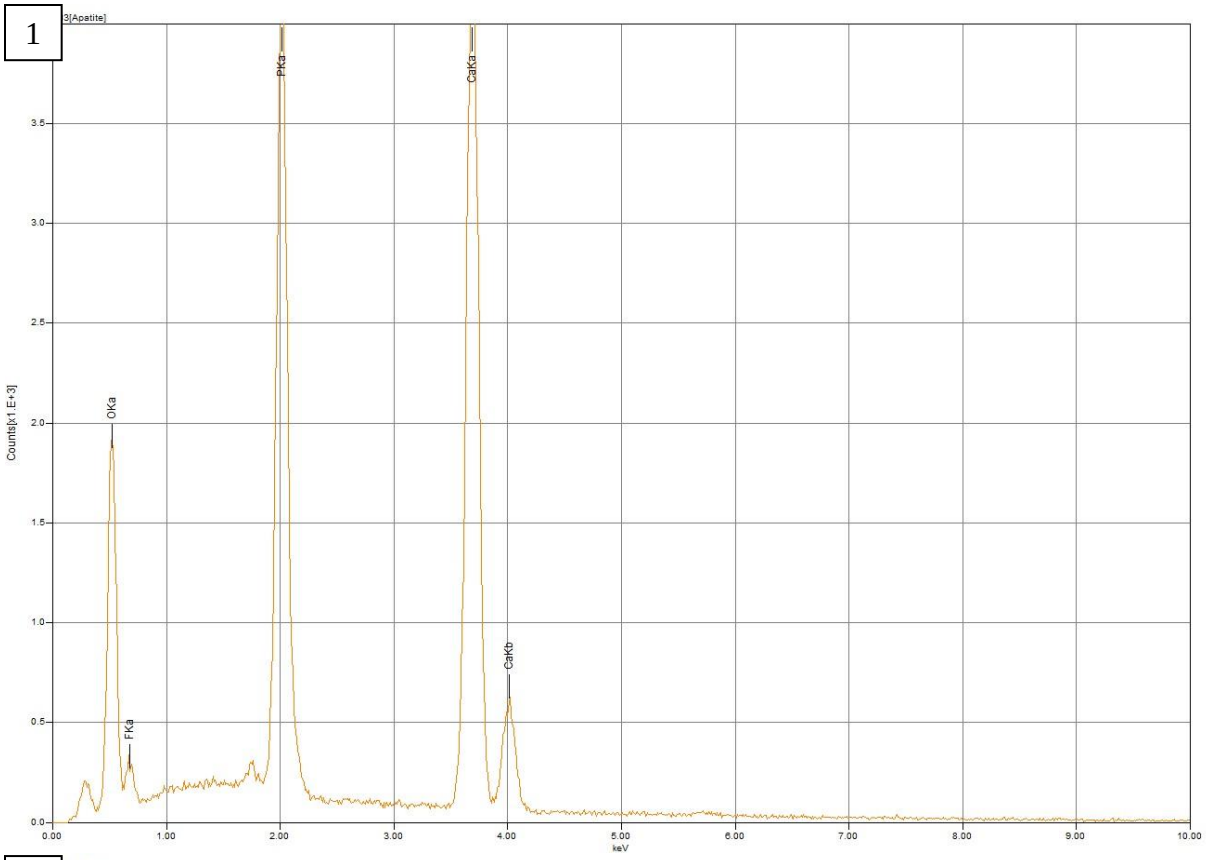
3[Apatite]
PKa
CaKa
OKa
CaKb
FKa
Counts[x1 E+3]
keV

2

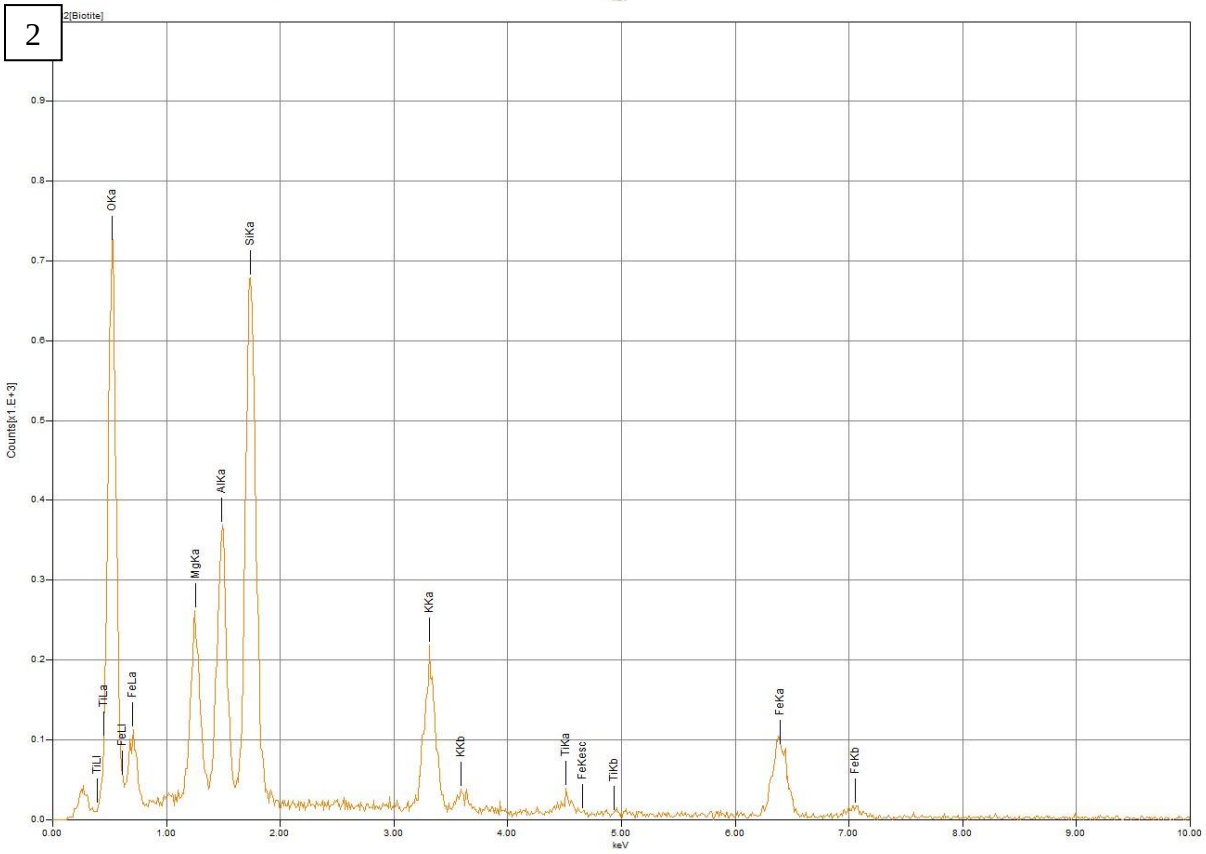
2[Biotite]
OKa
SiKa
AlKa
MgKa
KKa
TiLa
FeLa
TiLl
FeLl
KKb
TiKa
FeKesc
TiKb
FeKa
FeKb
Counts[x1 E+3]
keV

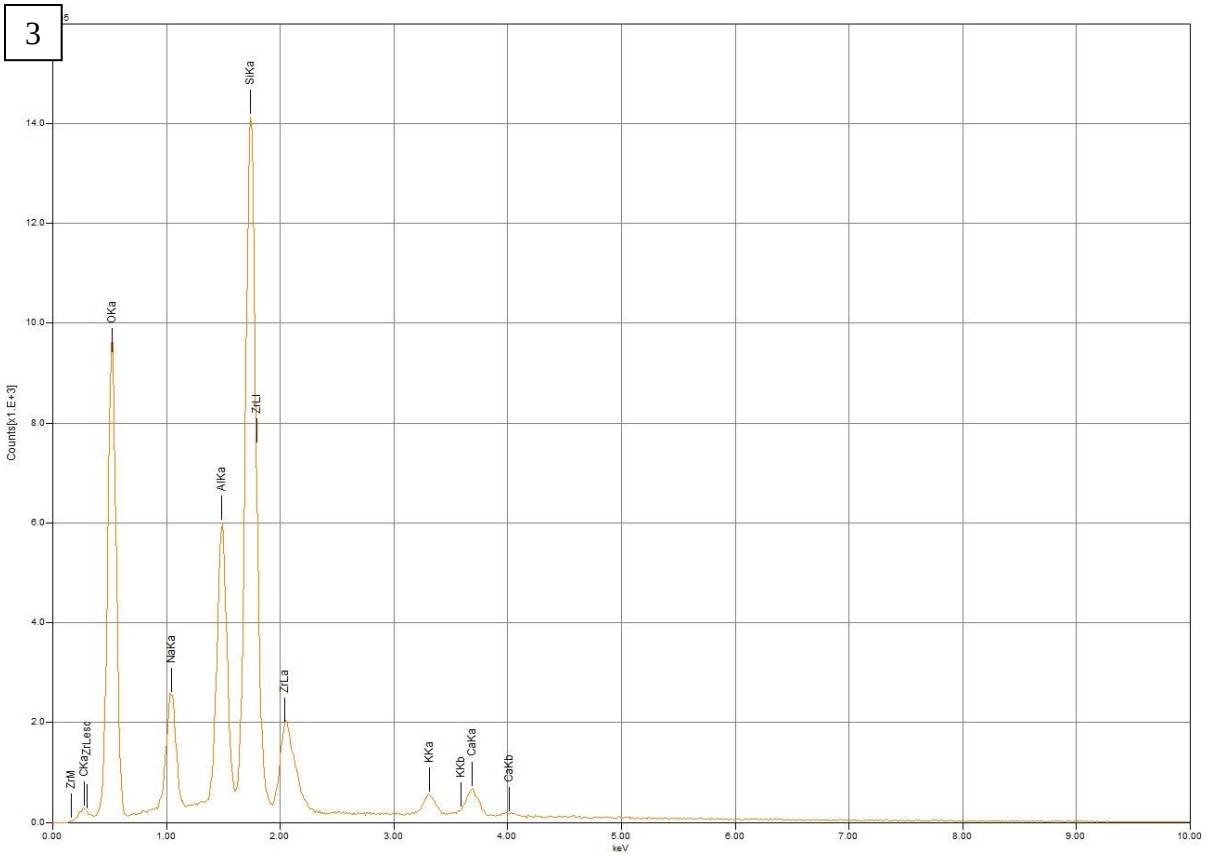
3
SiKa
OKa
ZrLl
AlKa
NaKa
ZrLa
KKa
KKb
CaKa
CaKb
ZrM
CKa
ZrLesc
Counts[x1 E+3]
keV

Grain 7

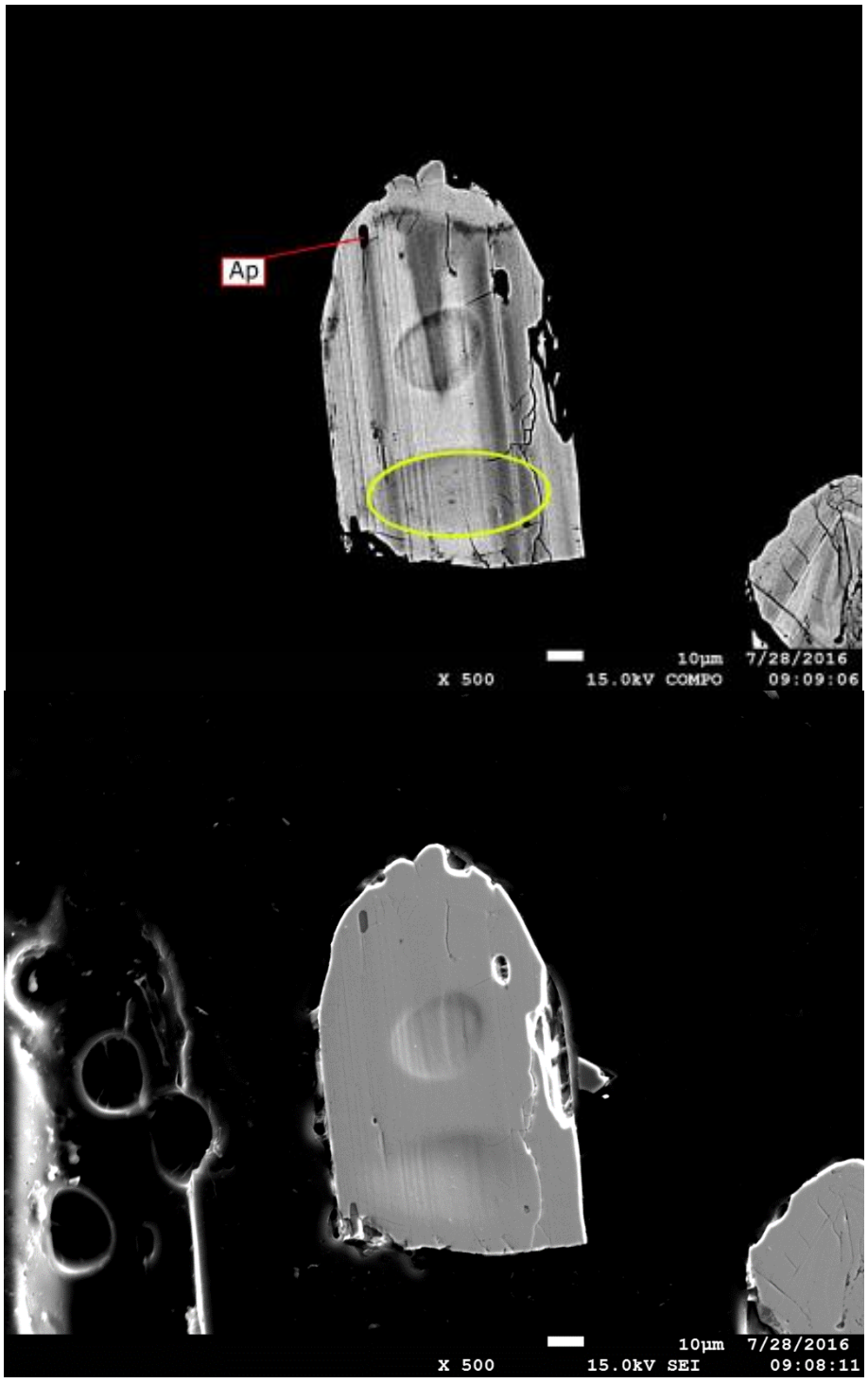
Ap
X 500
10µm
15.0kV COMPO
7/28/2016
09:09:06
X 500
10µm
15.0kV SEI
7/28/2016
09:08:11

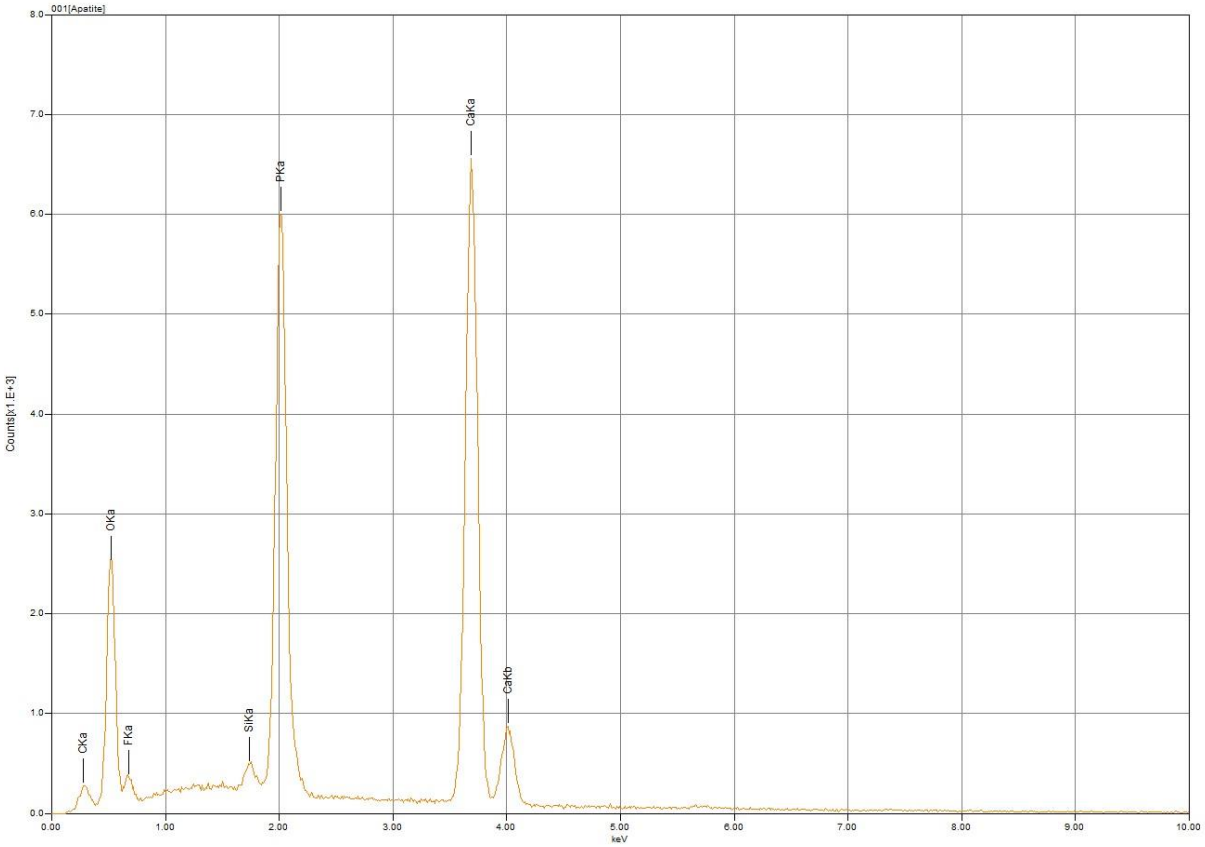
001[Apatite]
Counts[x1 E+3]
keV
CKa
OKa
FKa
SiKa
PKa
CaKa
CaKb

Grain 9

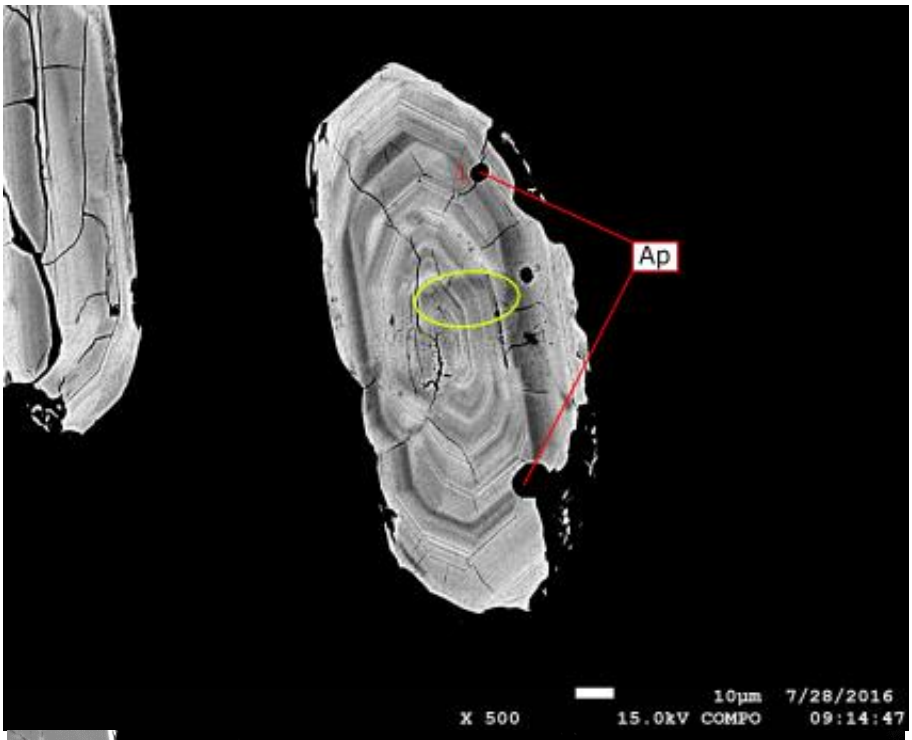
Ap
10µm 7/28/2016
X 500 15.0kV COMPO 09:14:47

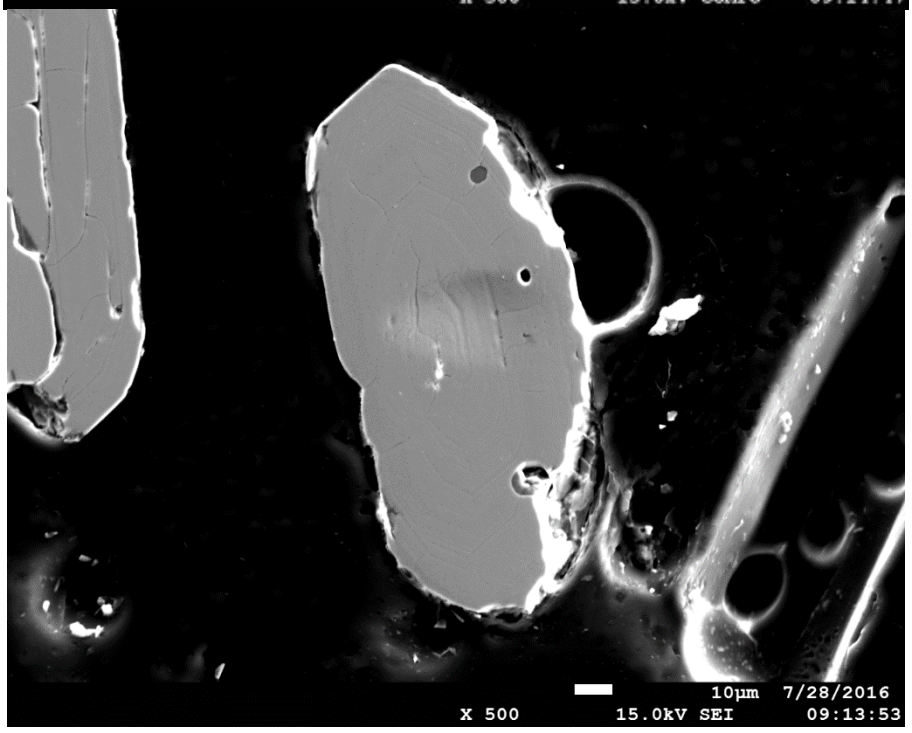
10µm 7/28/2016
X 500 15.0kV SEI 09:13:53

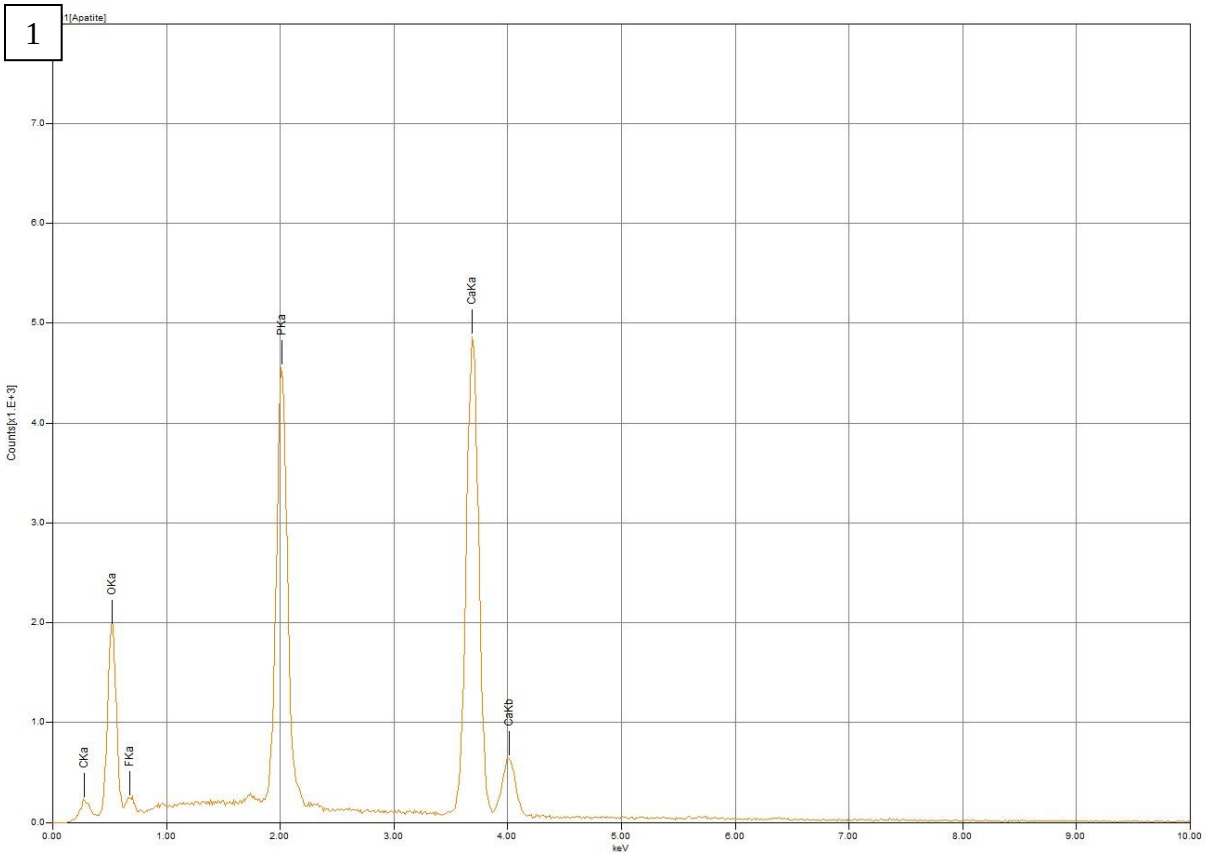
1
1[Apatite]
Counts[x1.E+3]
7.0
6.0
5.0
4.0
3.0
2.0
1.0
0.0
CKa
OKa
FKa
PKa
CaKa
CaKb
0.00
1.00
2.00
3.00
4.00
5.00
6.00
7.00
8.00
9.00
10.00
keV

Grain 13

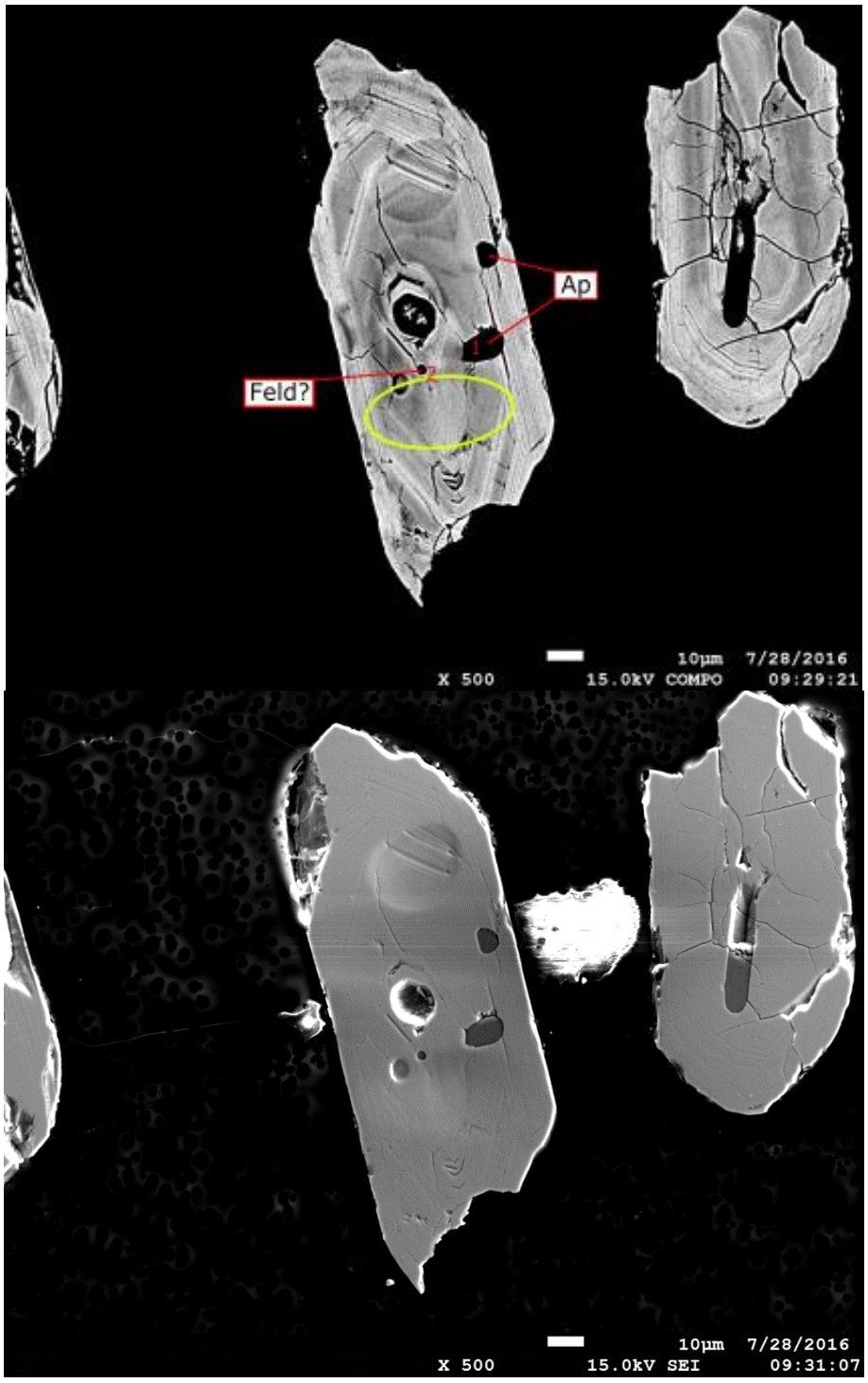
Ap
Feld?
X 500
10µm
15.0kV COMPO
7/28/2016
09:29:21
X 500
10µm
15.0kV SEI
7/28/2016
09:31:07

1

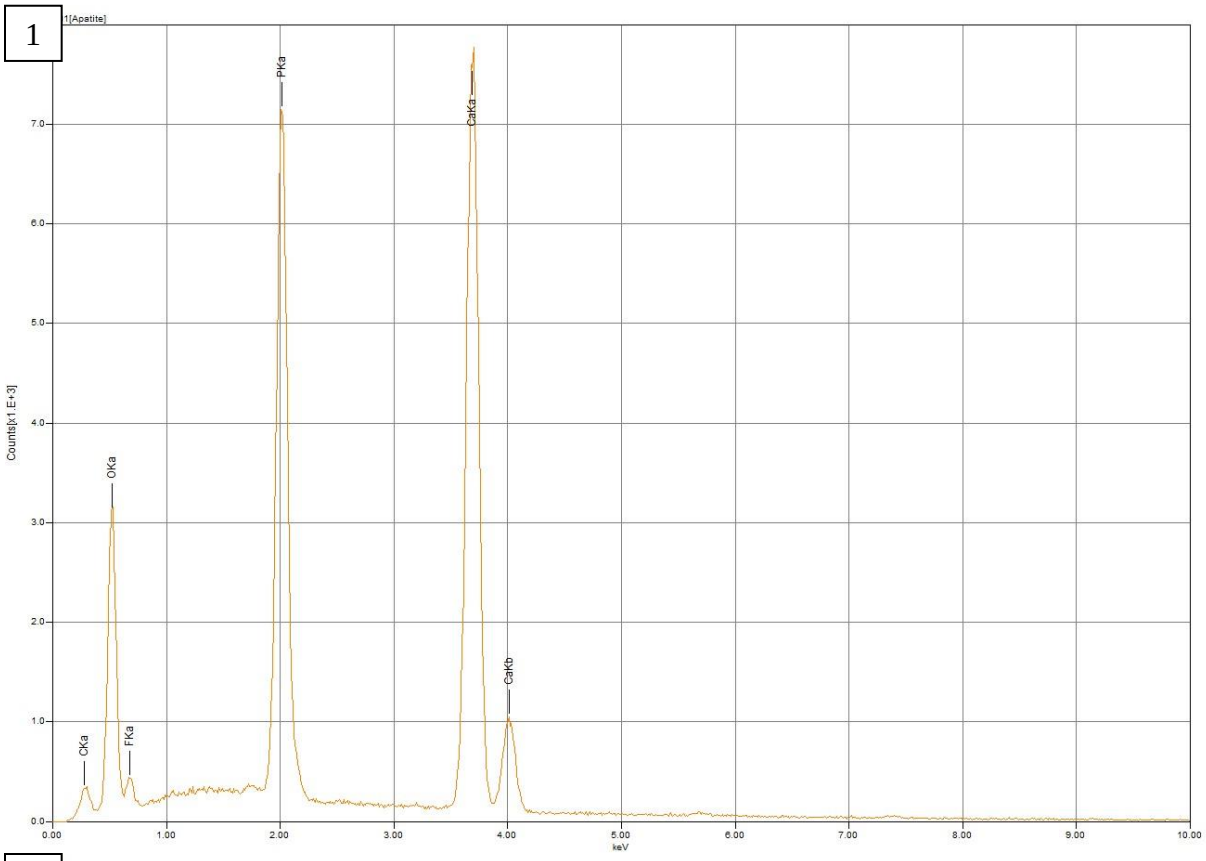
1[Apatite]
PKa
CaKa
OKa
CaKb
OKa
FKa
Counts[x1 E+3]
keV

2

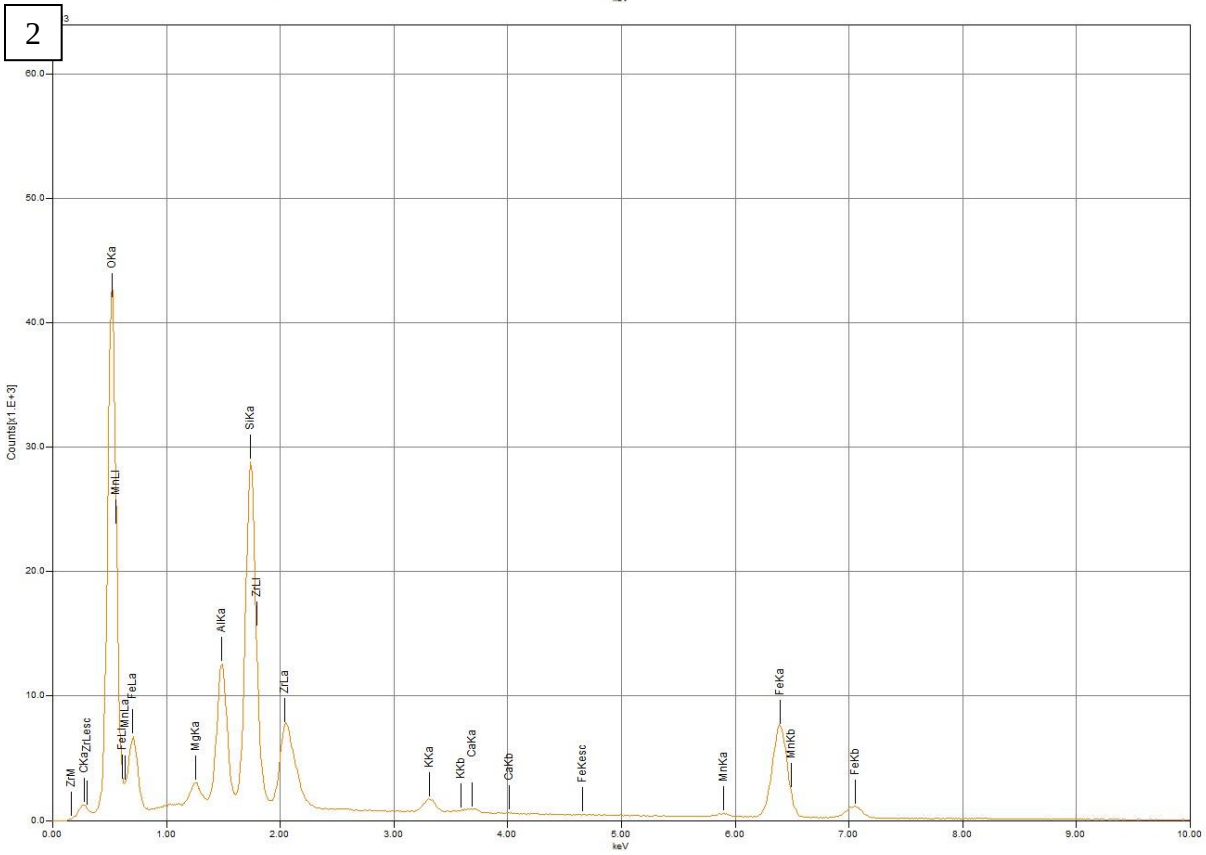
OKa
SiKa
MnLl
ZrLl
AlKa
FeLa
ZrLa
FeKa
MnKb
FeKb
MgKa
KKa
KKb
CaKa
CaKb
FeKesc
MnKa
ZrM
CKaZrLesc
FeLlMnLa
Counts[x1 E+3]
keV

Grain 15

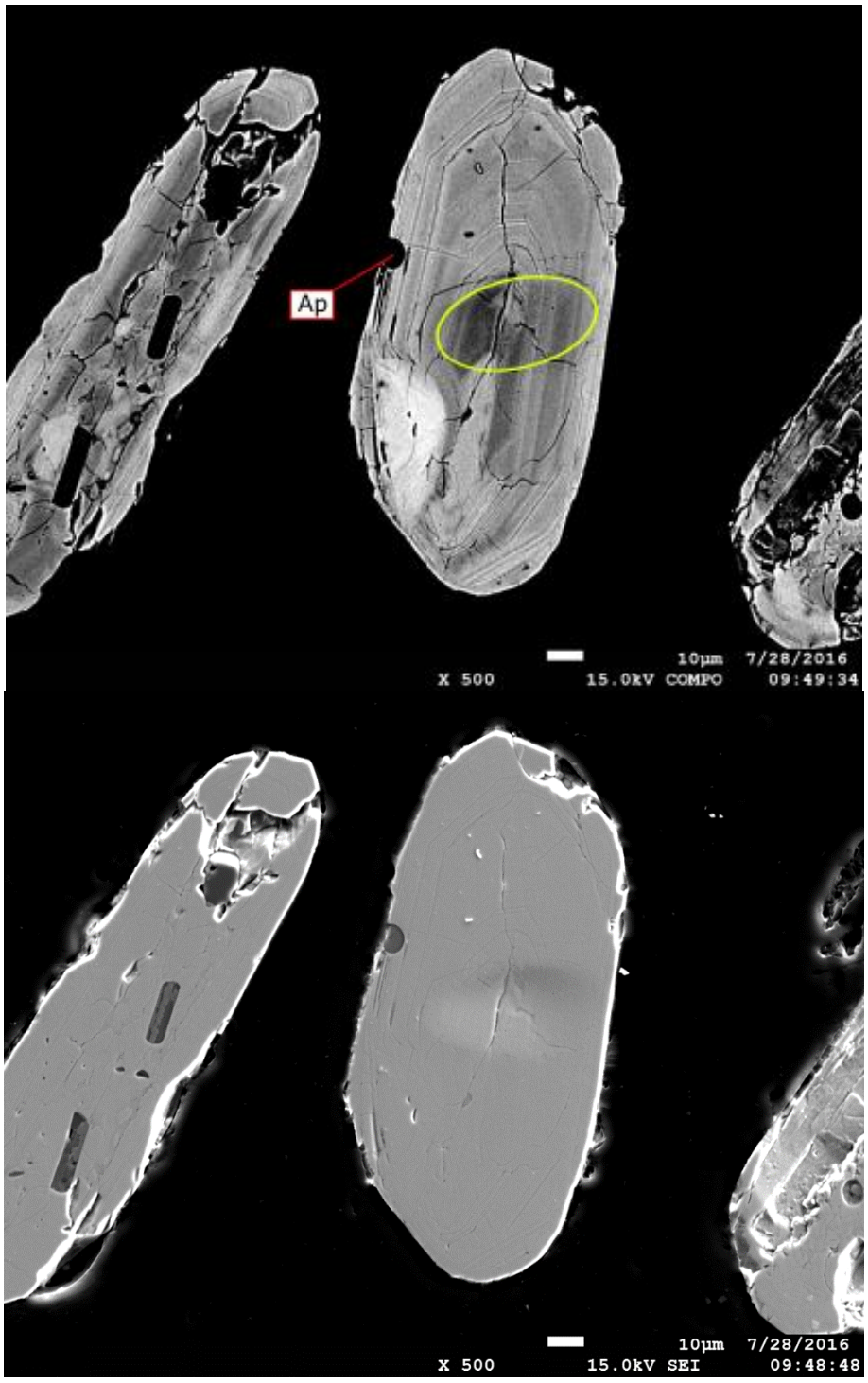
Ap
X 500
10µm
15.0kV COMPO
7/28/2016
09:49:34
X 500
10µm
15.0kV SEI
7/28/2016
09:48:48

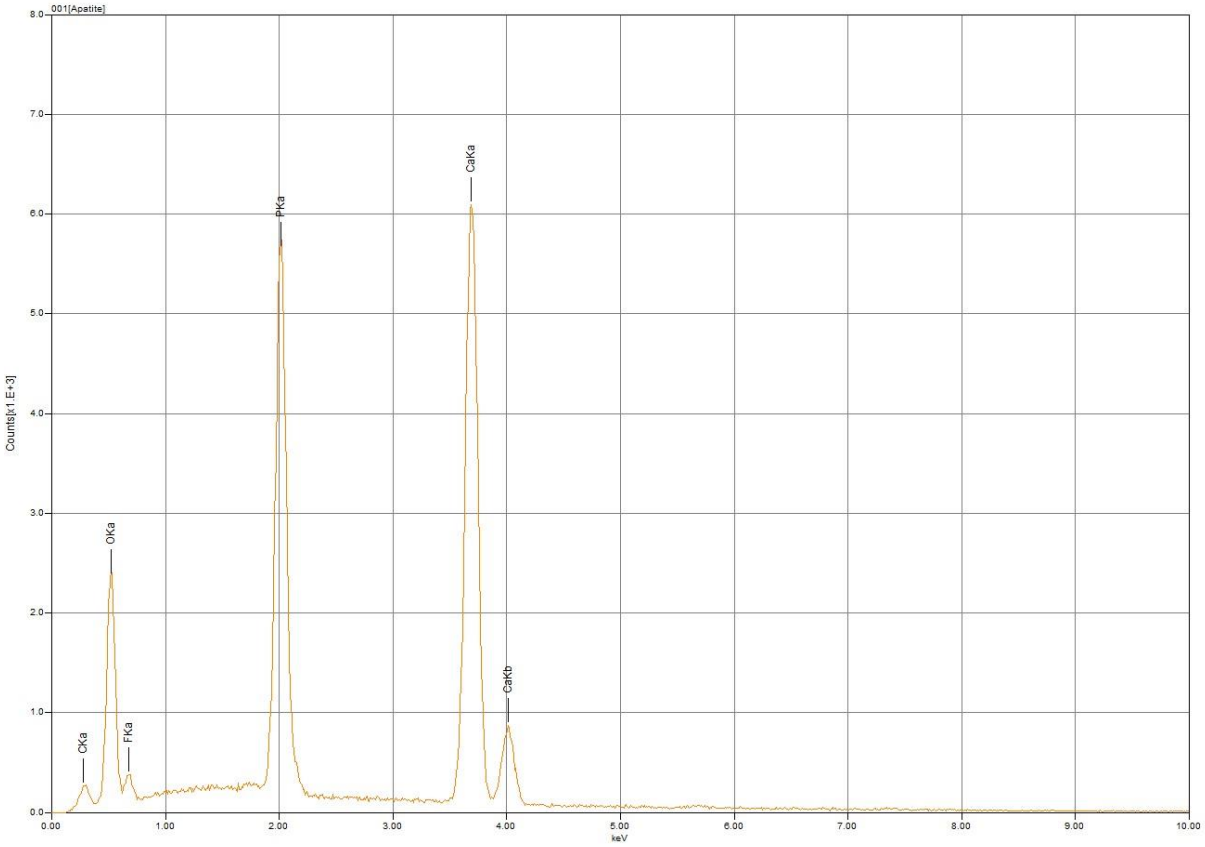
001[Apatite]
Counts[x1 E+3]
keV
CKa
OKa
FKa
PKa
CaKa
CaKb

Grain 25

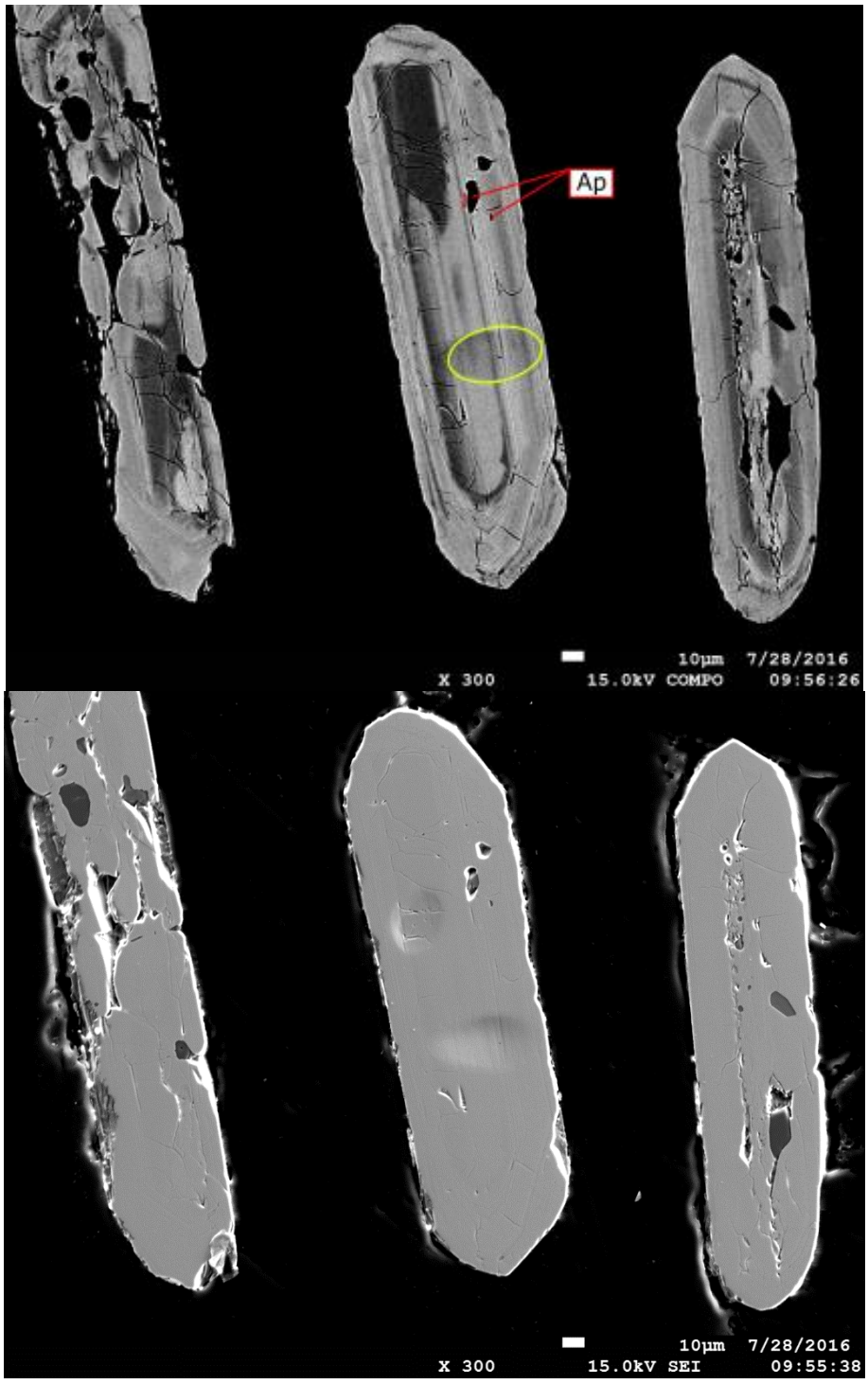
Ap
10µm 7/28/2016
X 300 15.0kV COMPO 09:56:26
10µm 7/28/2016
X 300 15.0kV SEI 09:55:38

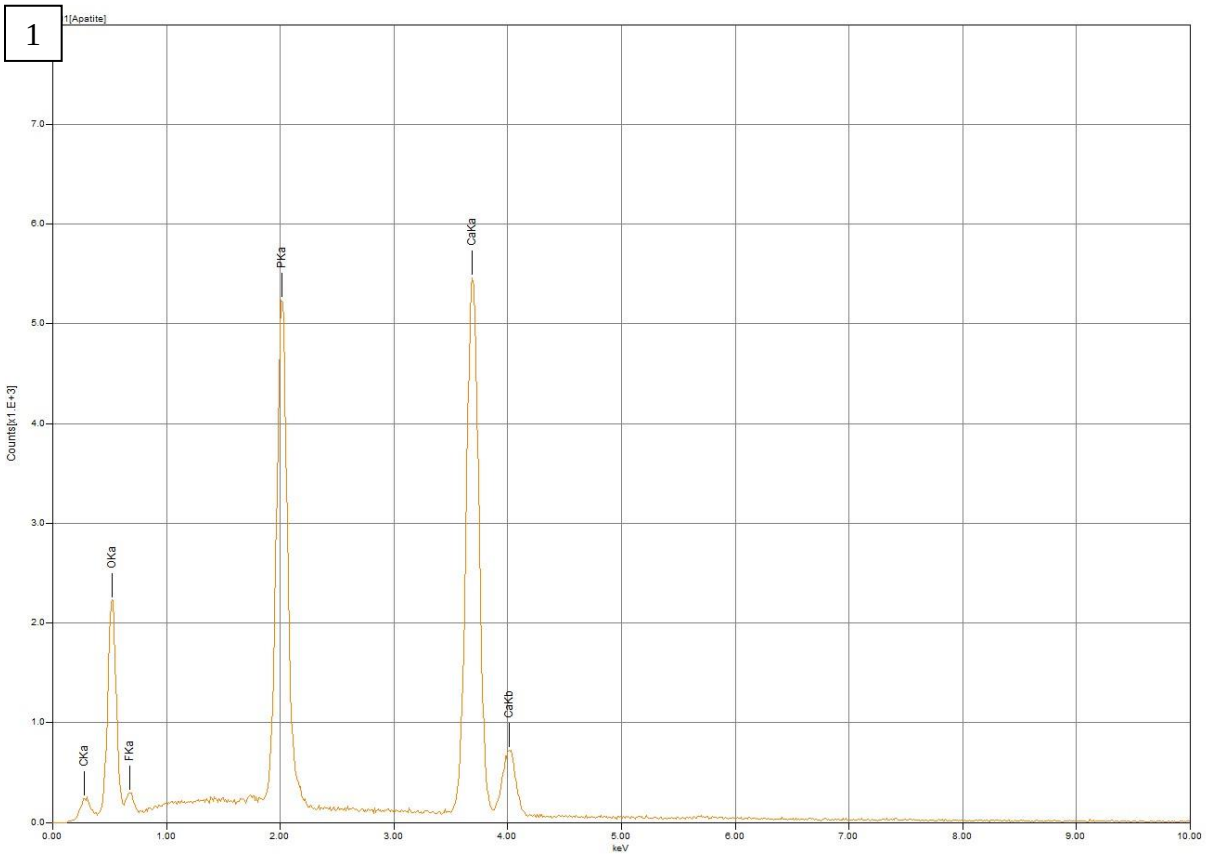
1
1[Apatite]
Counts[x1 E+3]
7.0
6.0
5.0
4.0
3.0
2.0
1.0
0.0
CKa
OKa
FKa
PKa
CaKa
CaKb
0.00
1.00
2.00
3.00
4.00
5.00
6.00
7.00
8.00
9.00
10.00
keV

Grain 30

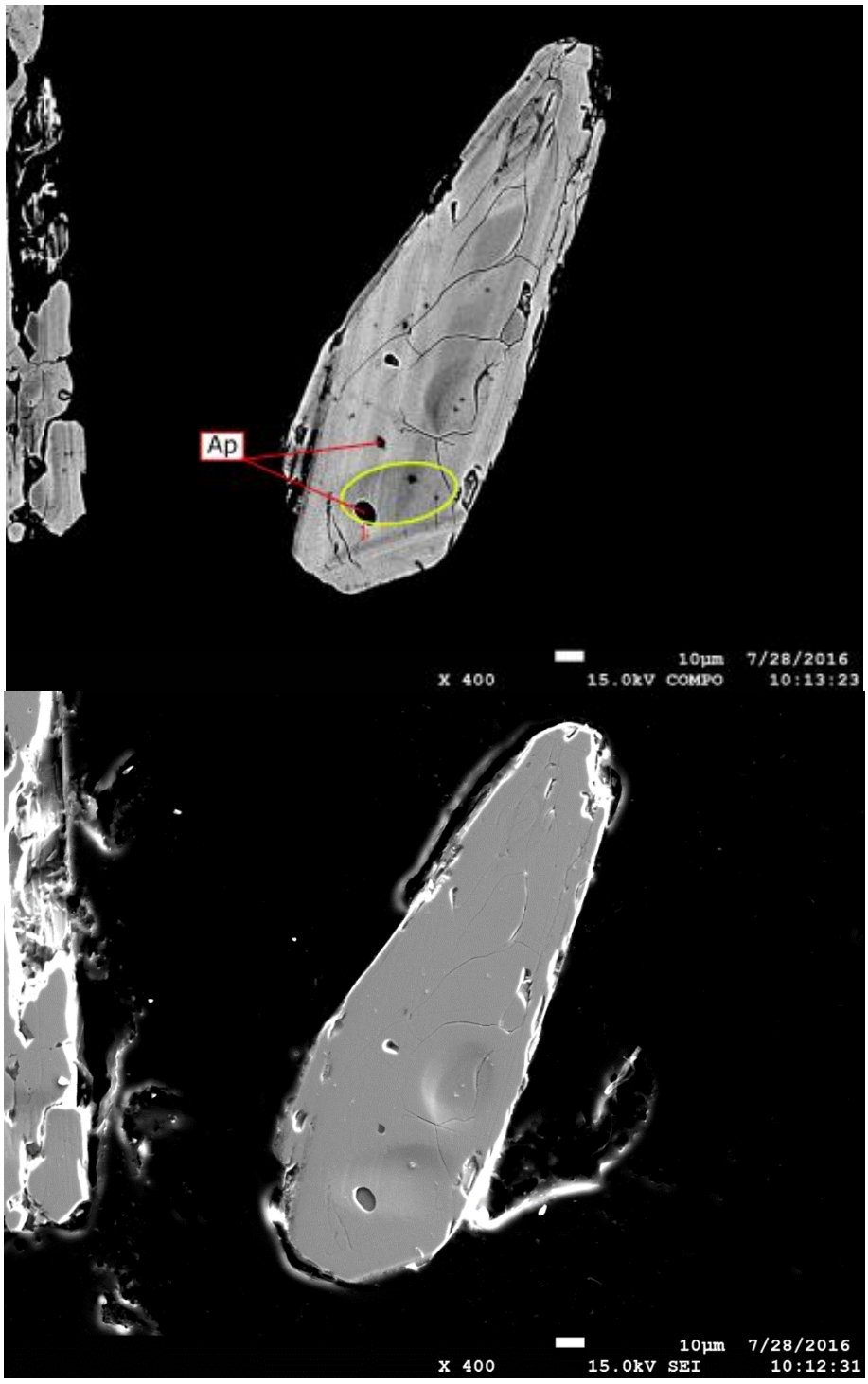
Ap
X 400
10µm
15.0kV COMPO
7/28/2016
10:13:23
X 400
10µm
15.0kV SEI
7/28/2016
10:12:31

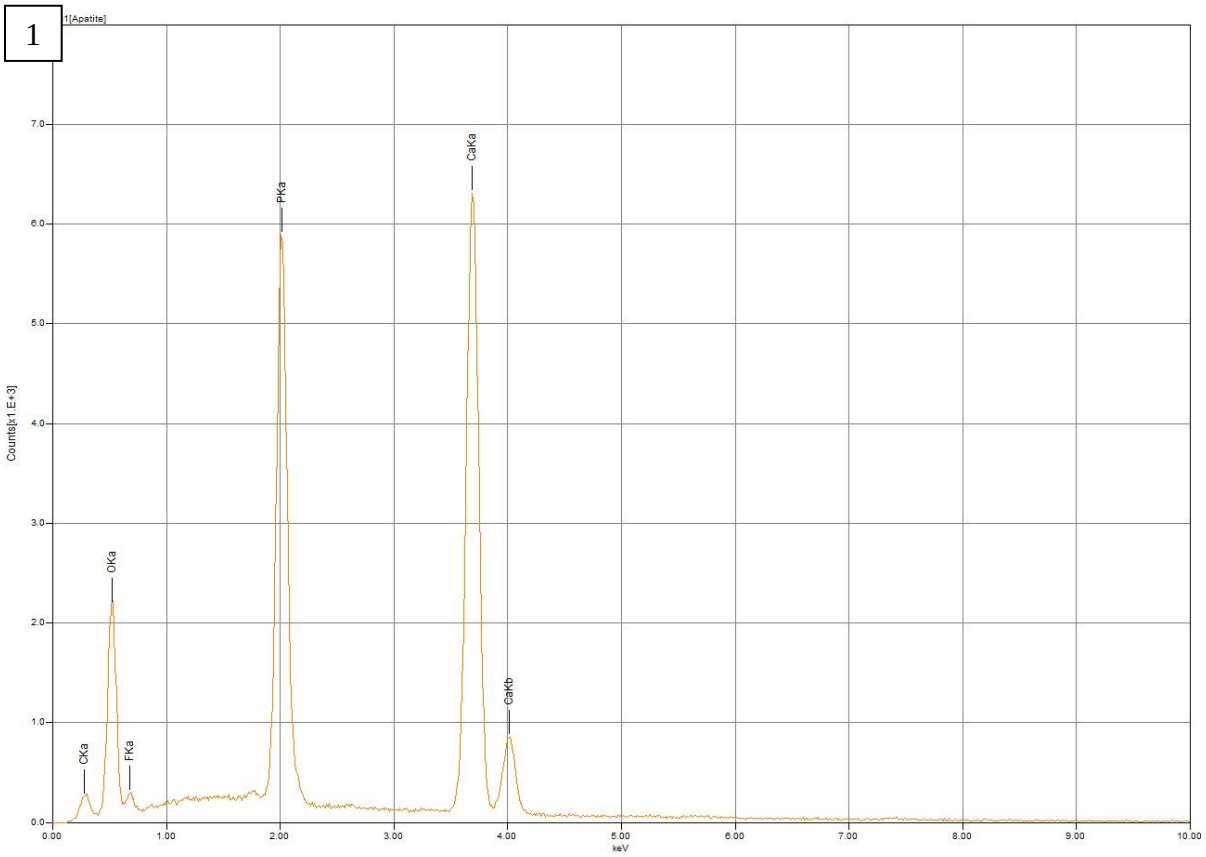
1
1[Apatite]
Counts[x1 E+3]
keV
CKa
OKa
FKa
PKa
CaKa
CaKb

Grain 33


Ap
Qtz
10µm 7/28/2016
X 450 15.0kV COMPO 10:05:50
10µm 7/28/2016
X 450 15.0kV SEI 10:05:01

1

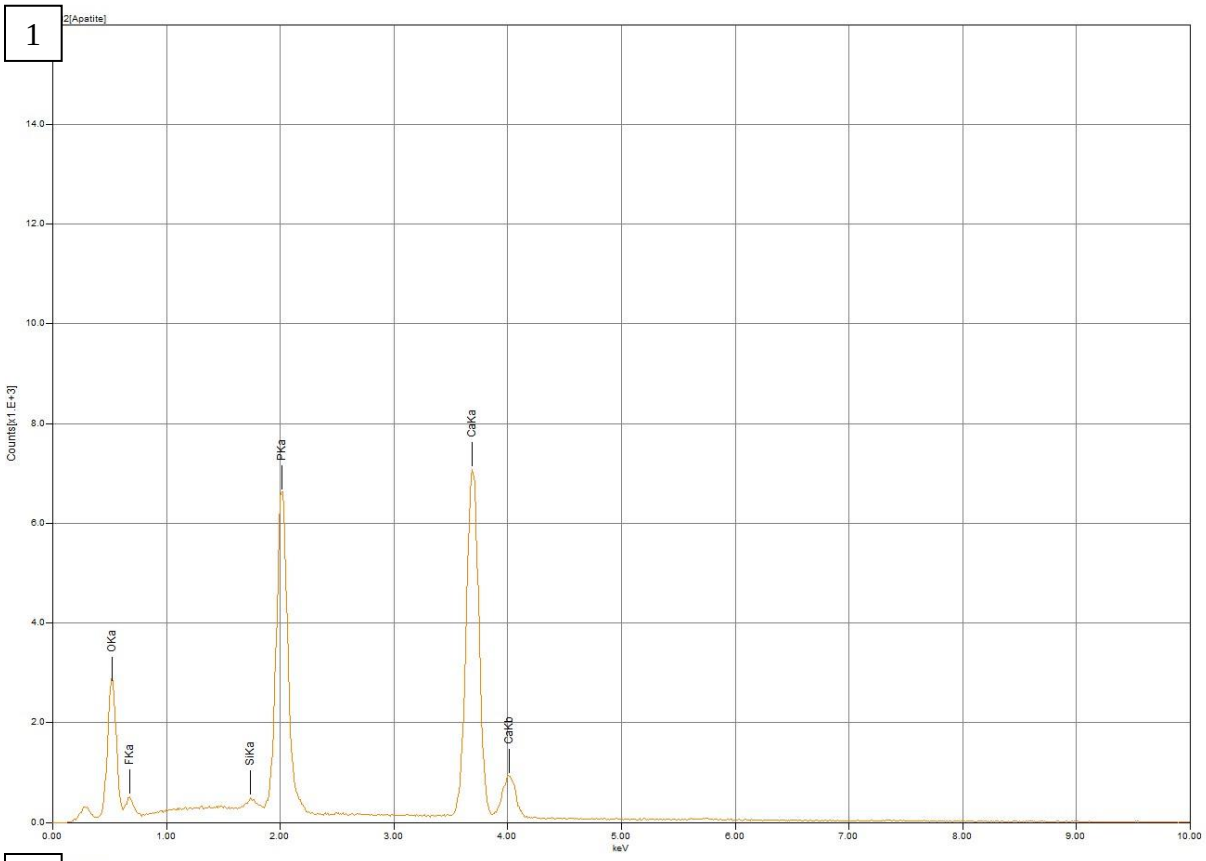
2[Apatite]
Counts[x1 E+3]
keV
OKa
FKa
SiKa
PKa
CaKa
CaKb

2

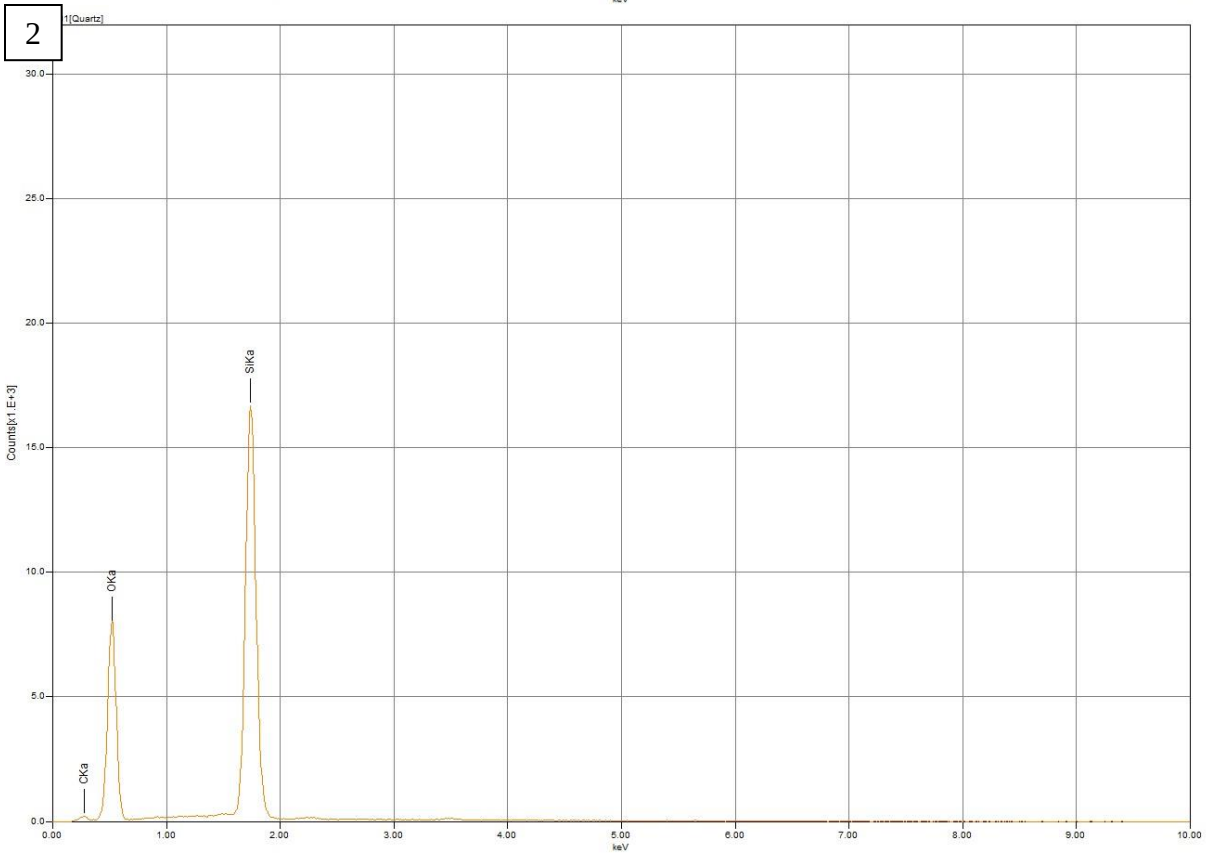
1[Quartz]
Counts[x1 E+3]
keV
CKa
OKa
SiKa

Grain 36

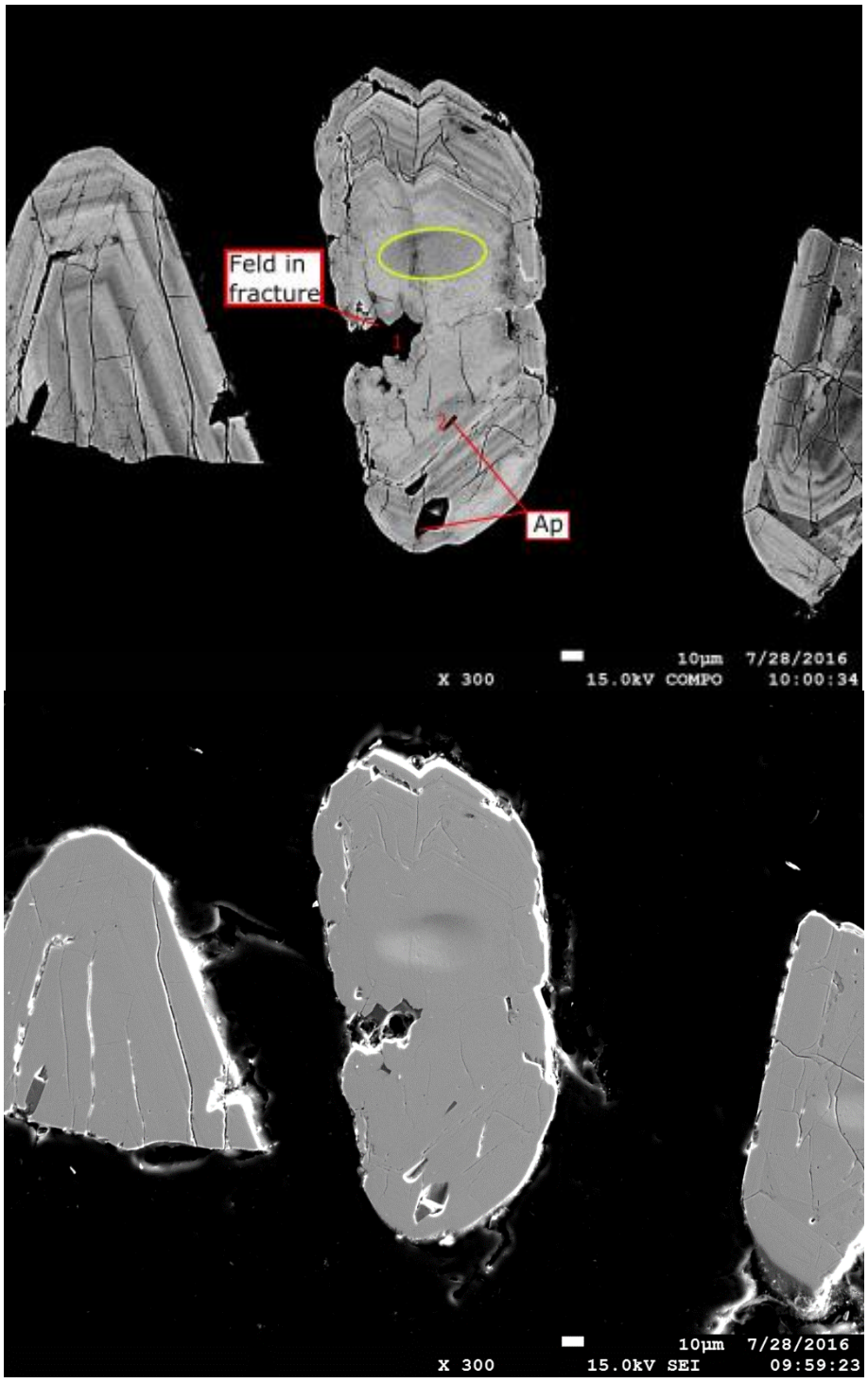
Feld in fracture
1
2
Ap
10µm 7/28/2016
X 300 15.0kV COMPO 10:00:34
10µm 7/28/2016
X 300 15.0kV SEI 09:59:23

1

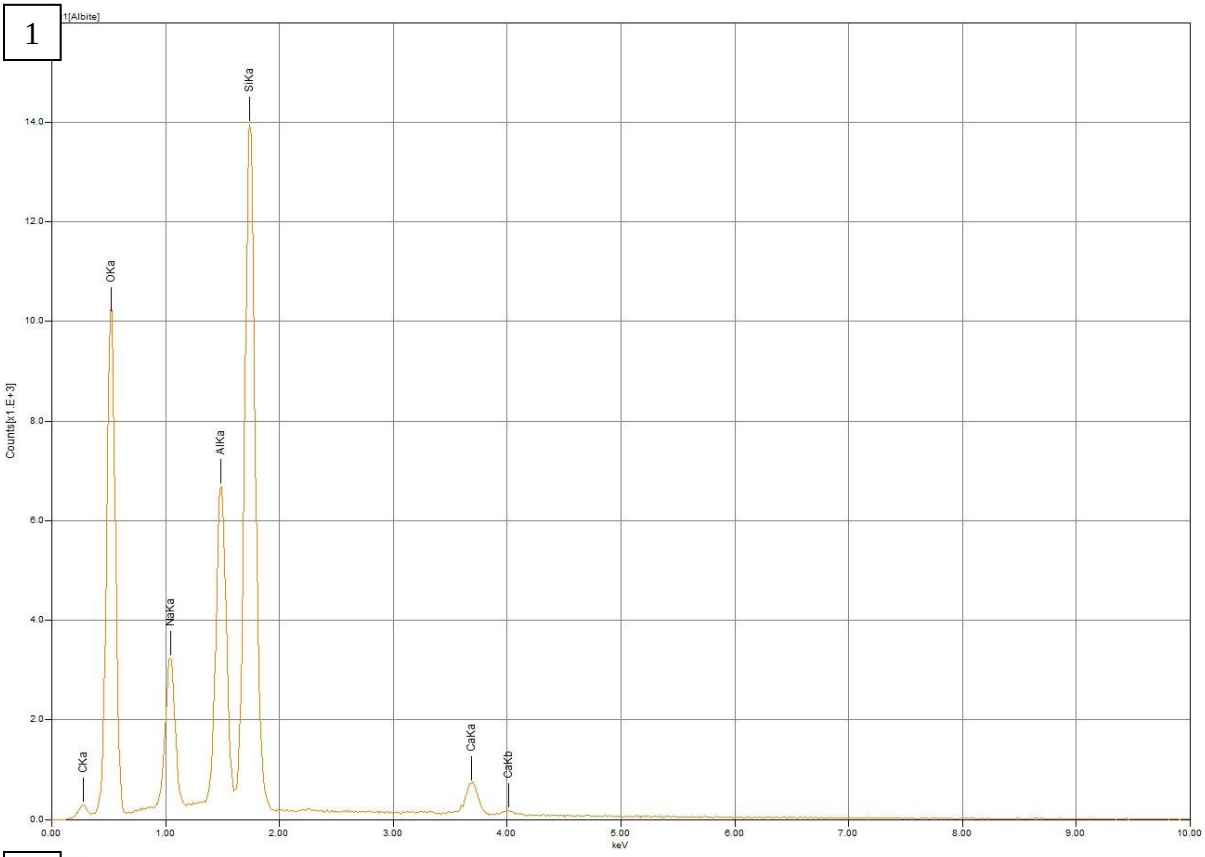
1[Albite]
Counts[x1 E+3]
keV
CKa
OKa
NaKa
AlKa
SiKa
CaKa
CaKb

2

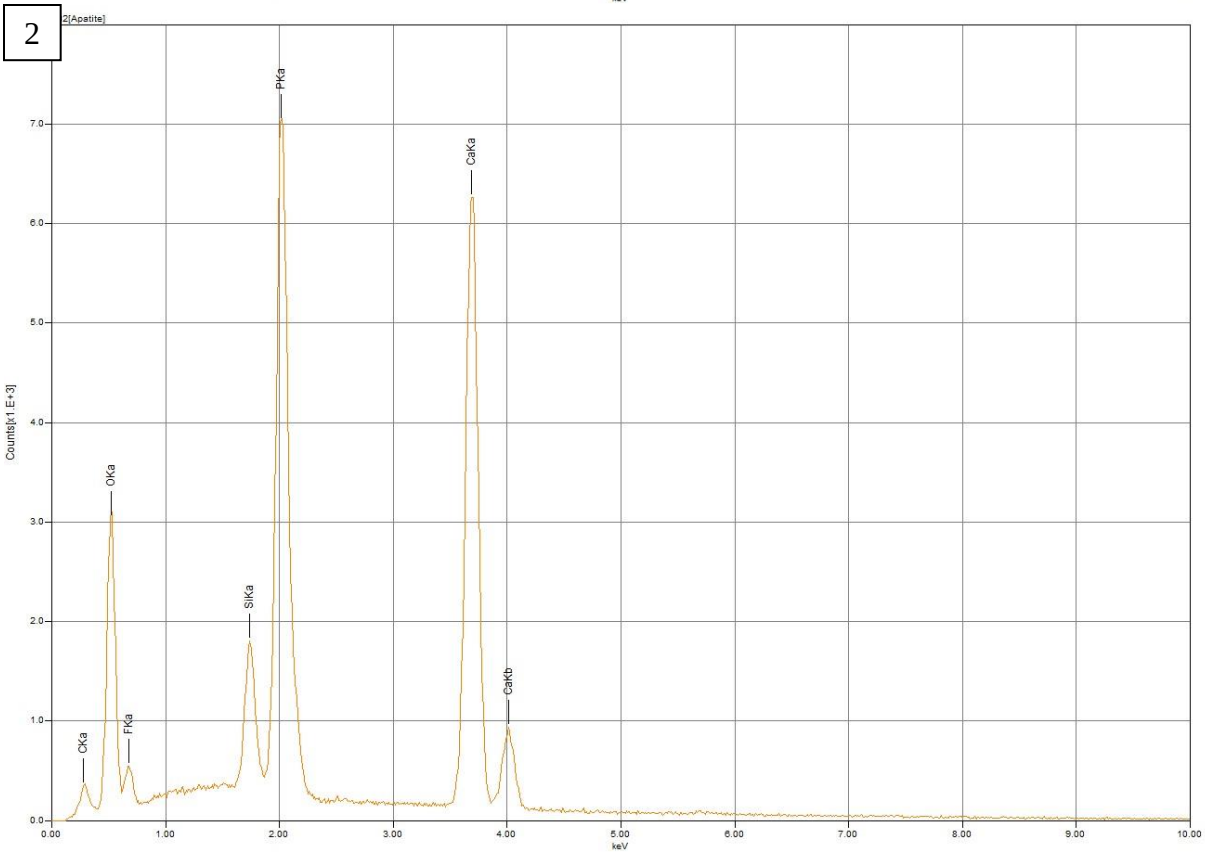
2[Apatite]
Counts[x1 E+3]
keV
CKa
OKa
FKa
SiKa
PKa
CaKa
CaKb

142981

Grain 6

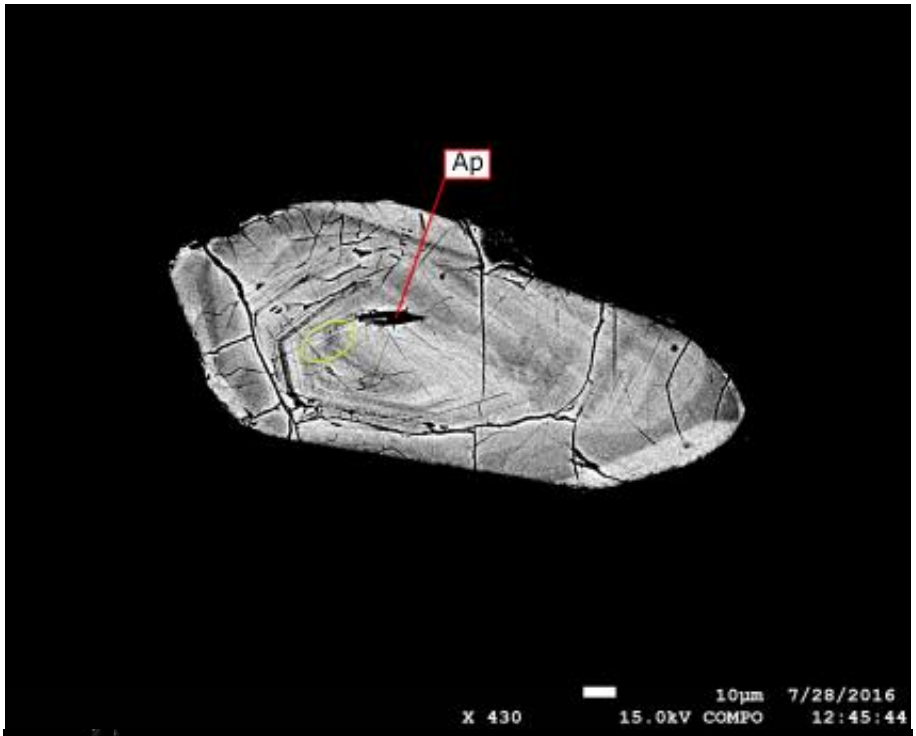

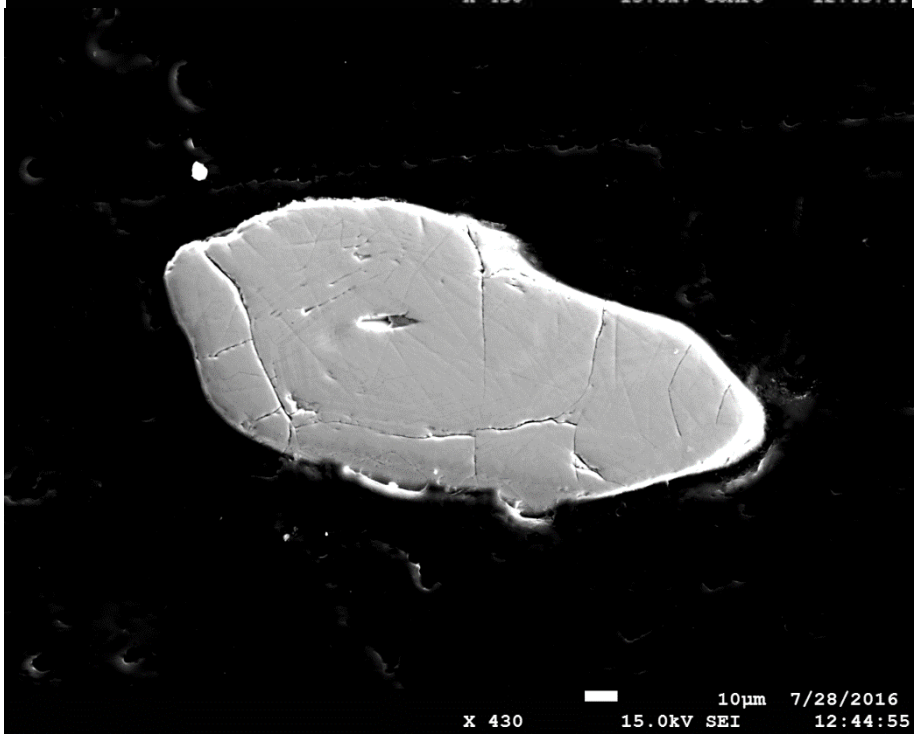

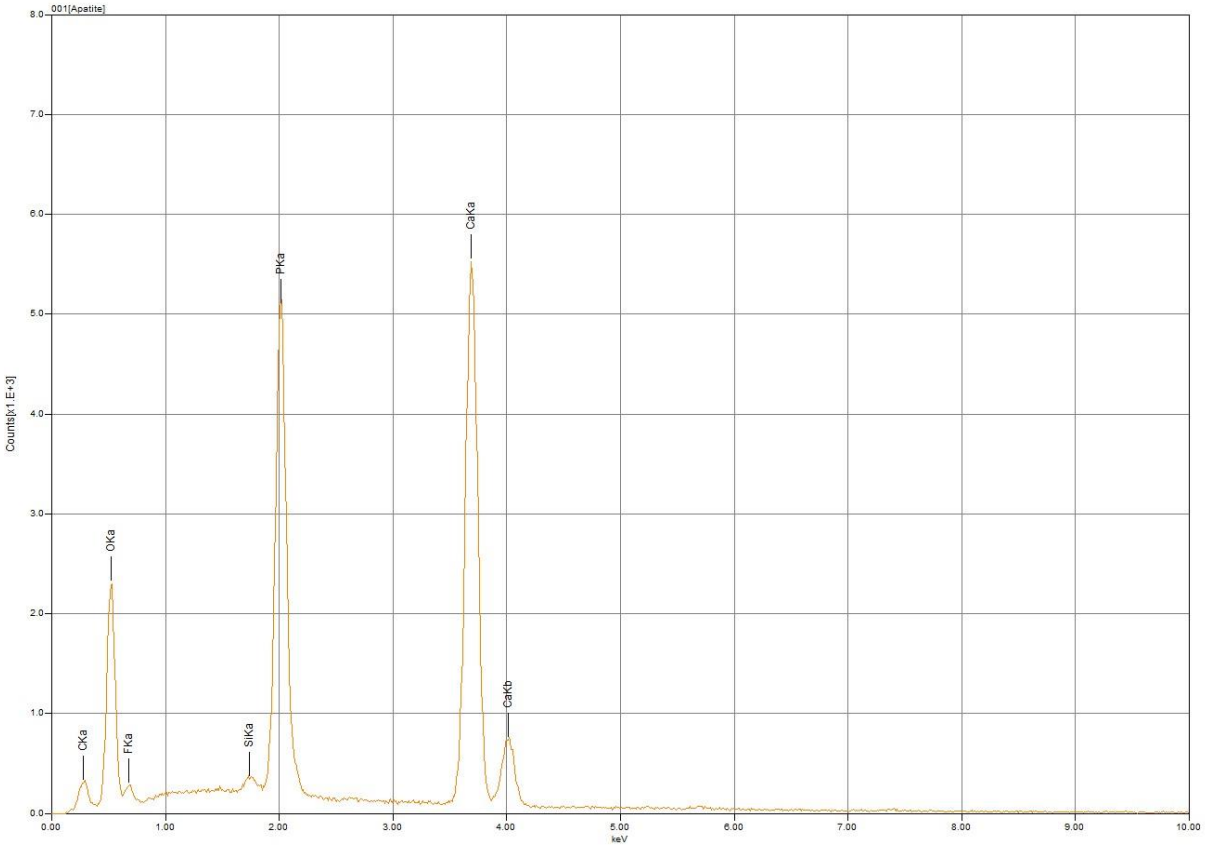
001[Apatite]
Counts[x1 E+3]
keV
CKa
OKa
FKa
SiKa
PKa
CaKa
CaKb

Grain 7

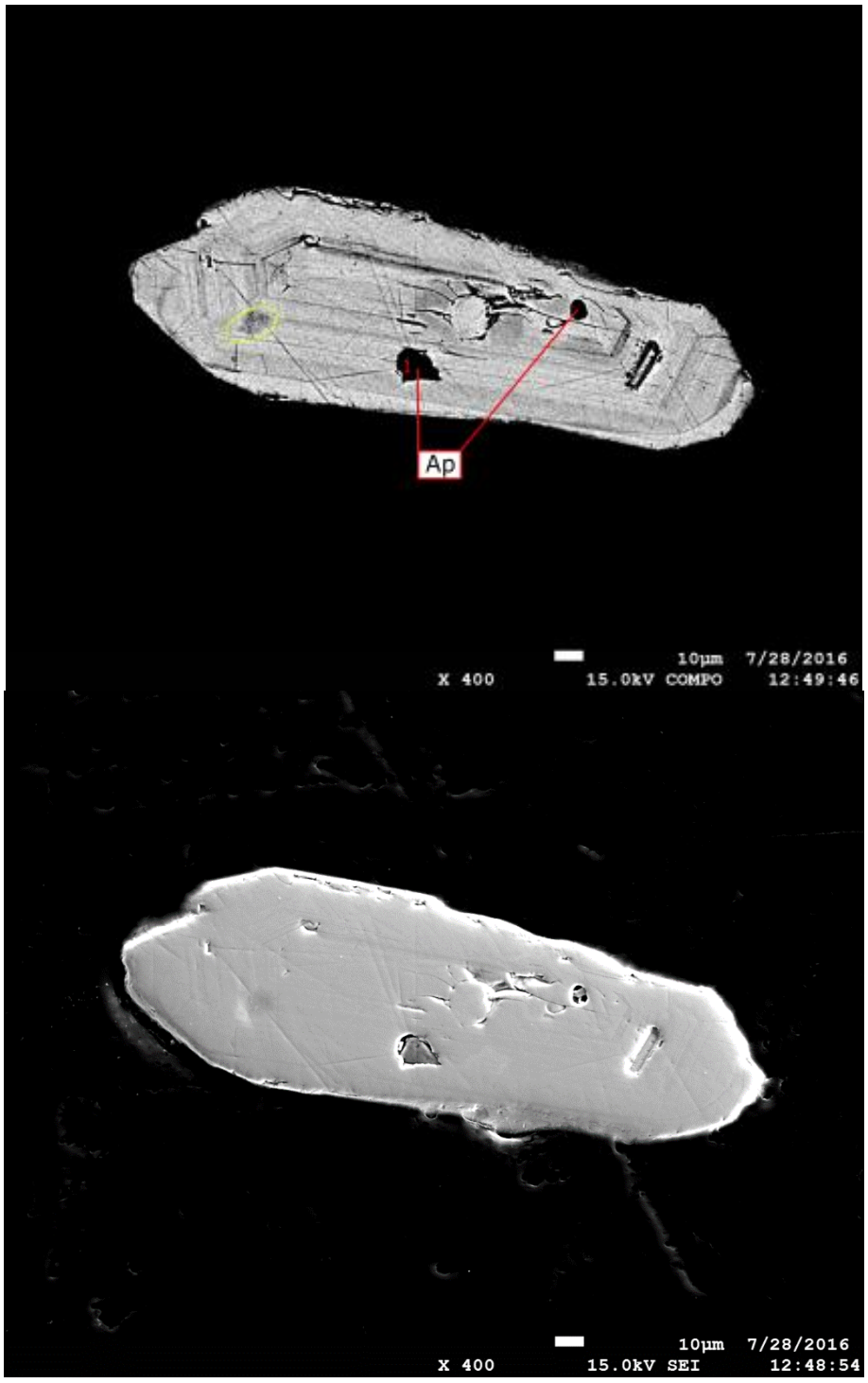
1
Ap
10µm 7/28/2016
X 400 15.0kV COMPO 12:49:46
10µm 7/28/2016
X 400 15.0kV SEI 12:48:54

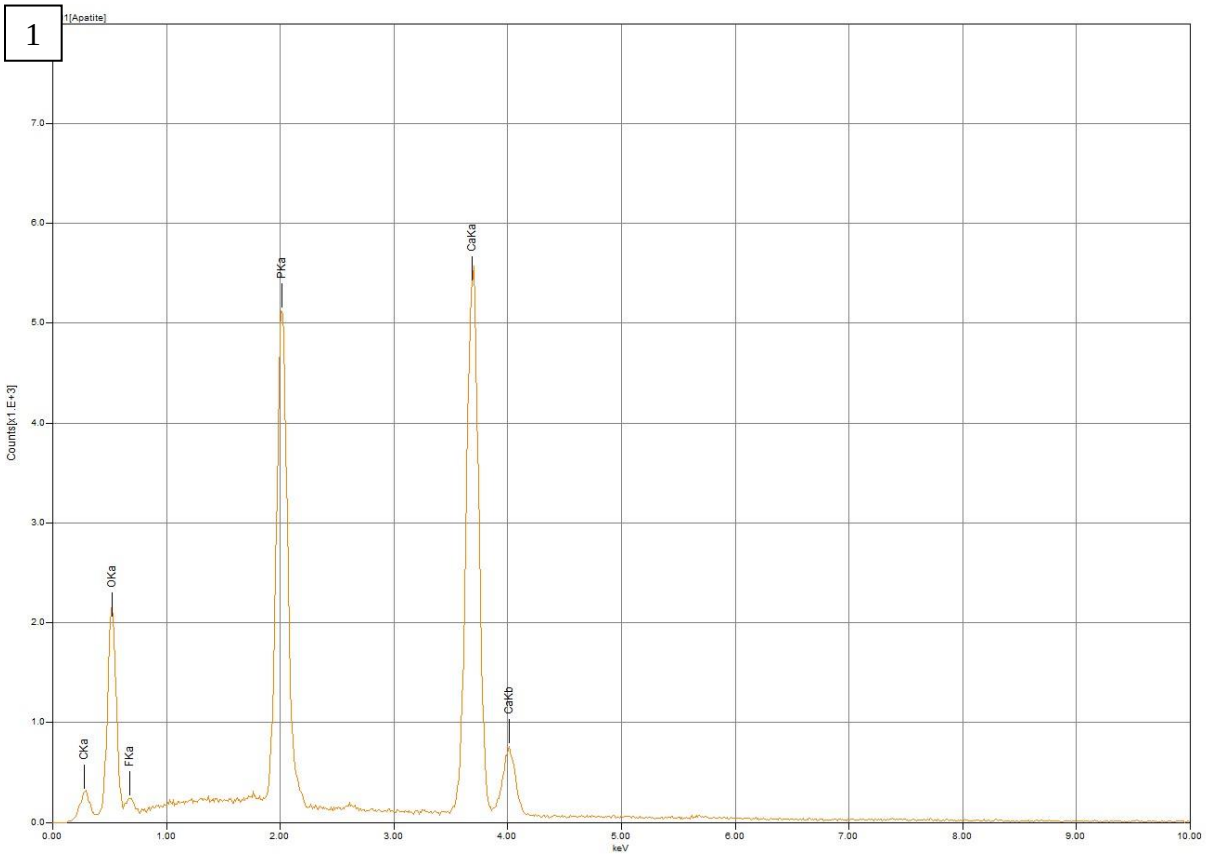
1
1[Apatite]
Counts[x1 E+3]
7.0
6.0
5.0
4.0
3.0
2.0
1.0
0.0
CKa
OKa
FKa
PKa
CaKa
CaKb
0.00
1.00
2.00
3.00
4.00
5.00
6.00
7.00
8.00
9.00
10.00
keV

Grain 9

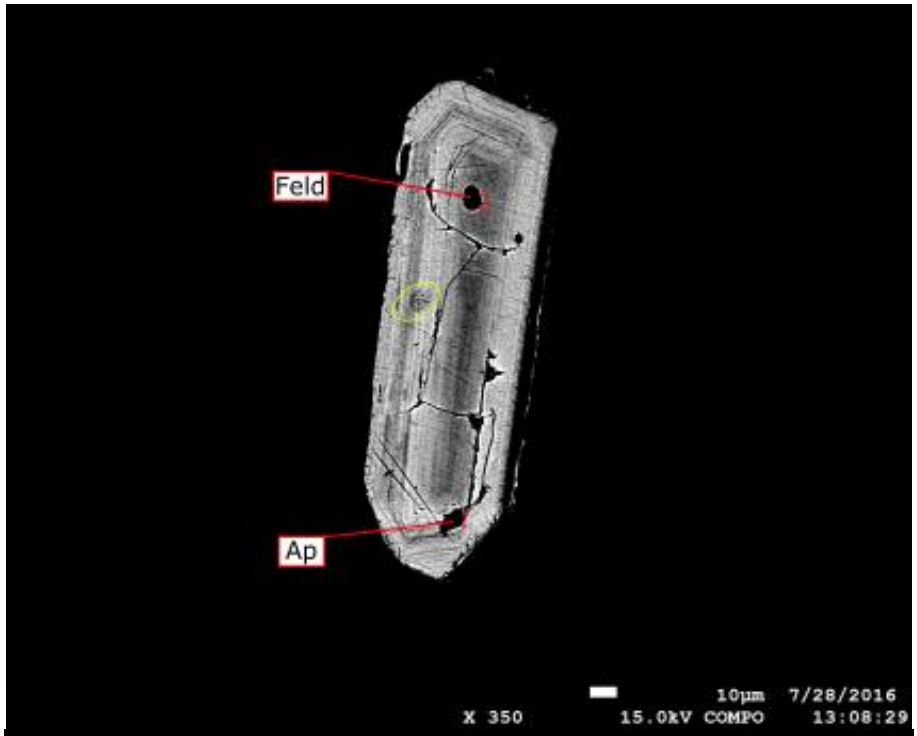
Feld
Ap
X 350
10µm 7/28/2016
15.0kV COMPO 13:08:29

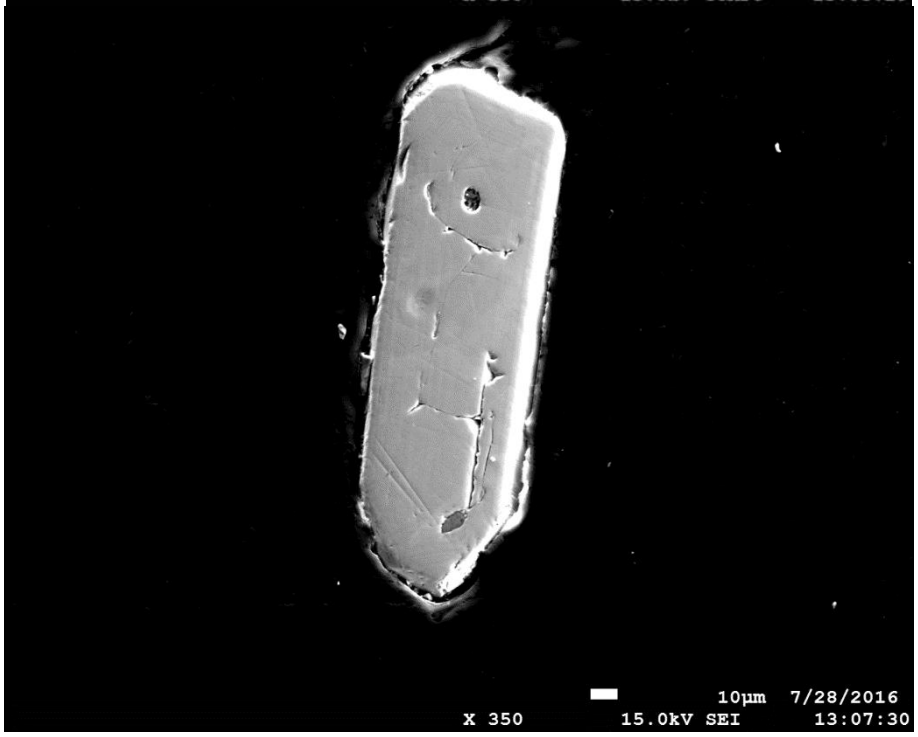
X 350
10µm 7/28/2016
15.0kV SEI 13:07:30

1

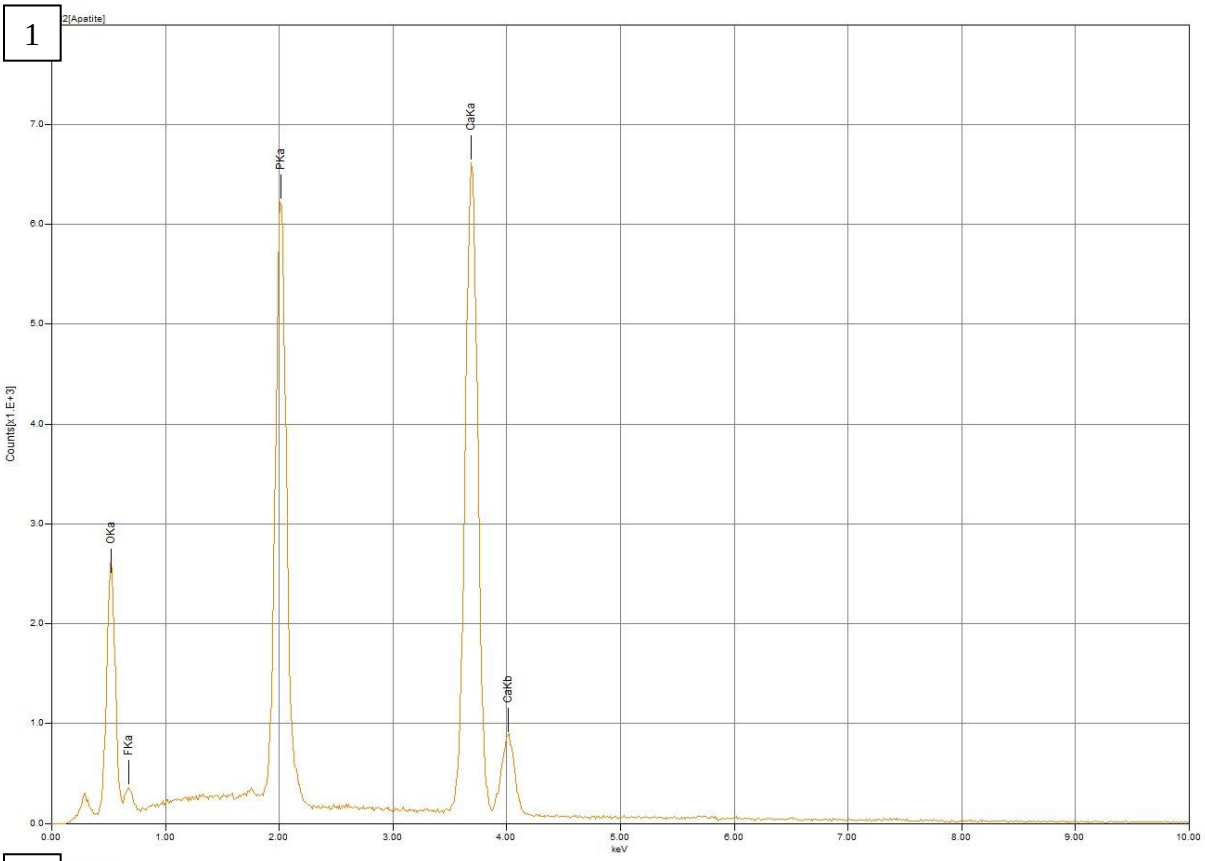
2[Apatite]
Counts[x1 E+3]
keV
OKa
FKa
FKa
CaKa
CaKb

2

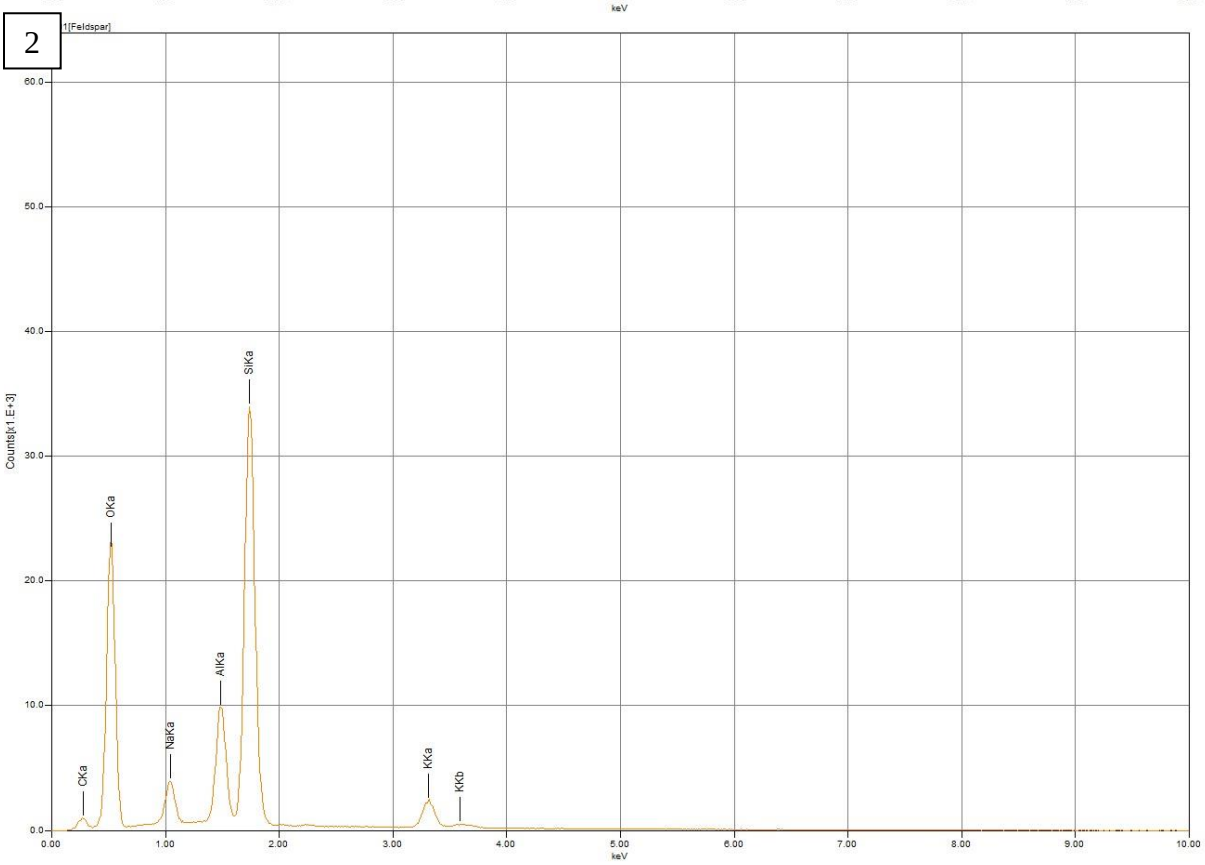
1[Feldspar]
Counts[x1 E+3]
keV
CKa
OKa
NaKa
AlKa
SiKa
KKa
KKb

Grain 10

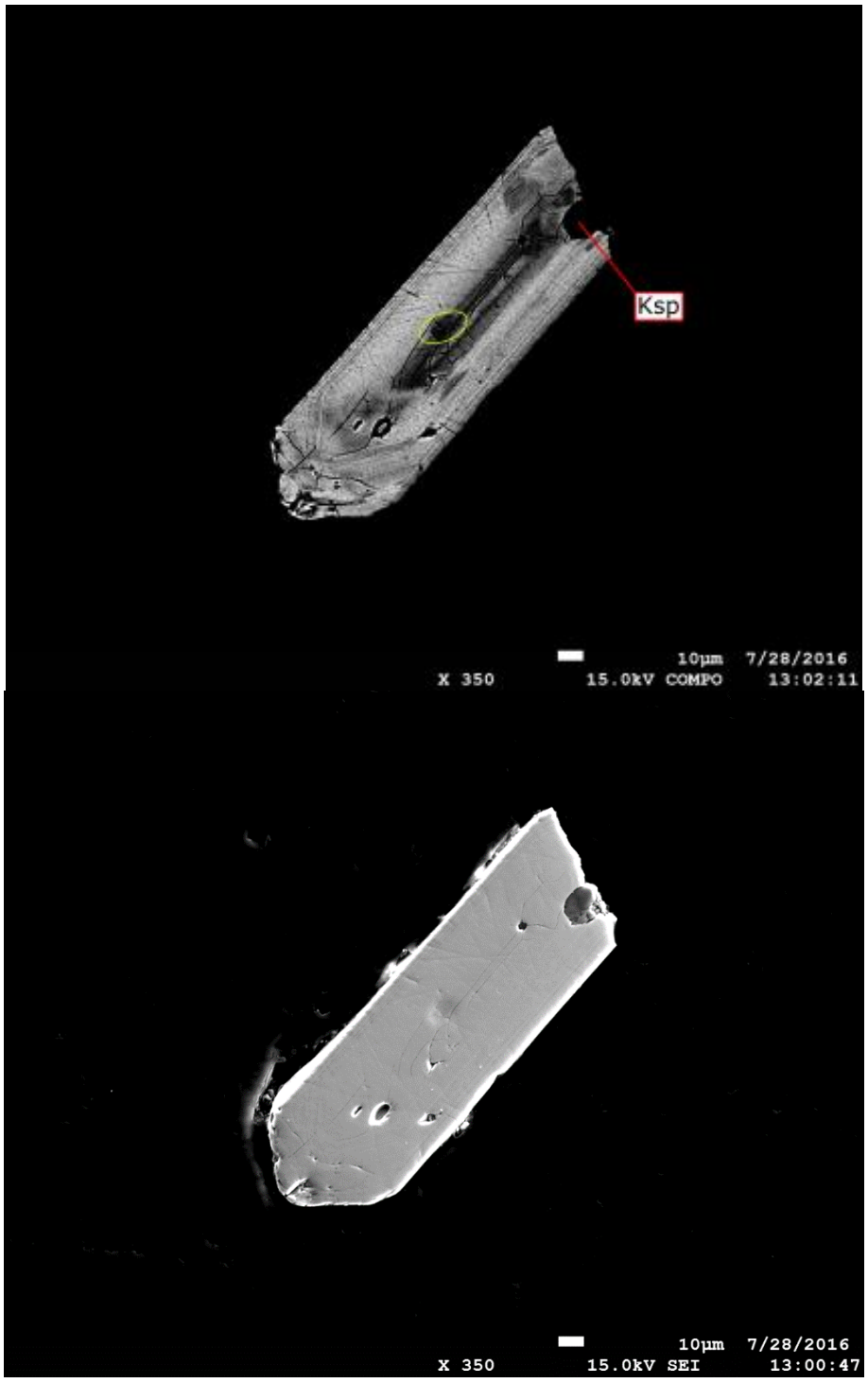
Ksp
10µm 7/28/2016
X 350 15.0kV COMPO 13:02:11
10µm 7/28/2016
X 350 15.0kV SEI 13:00:47

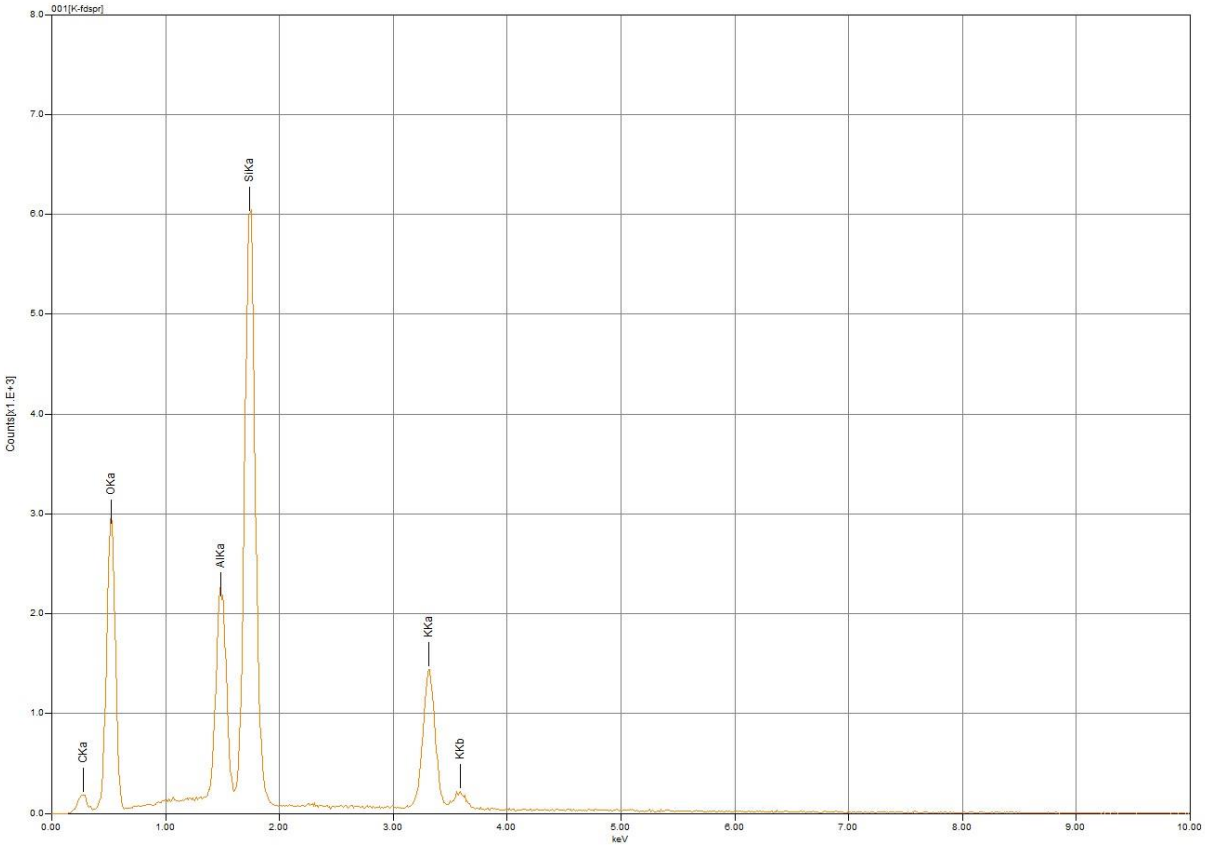
001[K-fdspr]
Counts[x1 E+3]
keV
CKa
OKa
AlKa
SiKa
KKa
KKb

Grain 11


Ap
10µm 7/28/2016
X 350 15.0kV COMPO 12:57:15
10µm 7/28/2016
X 350 15.0kV SEI 12:56:10

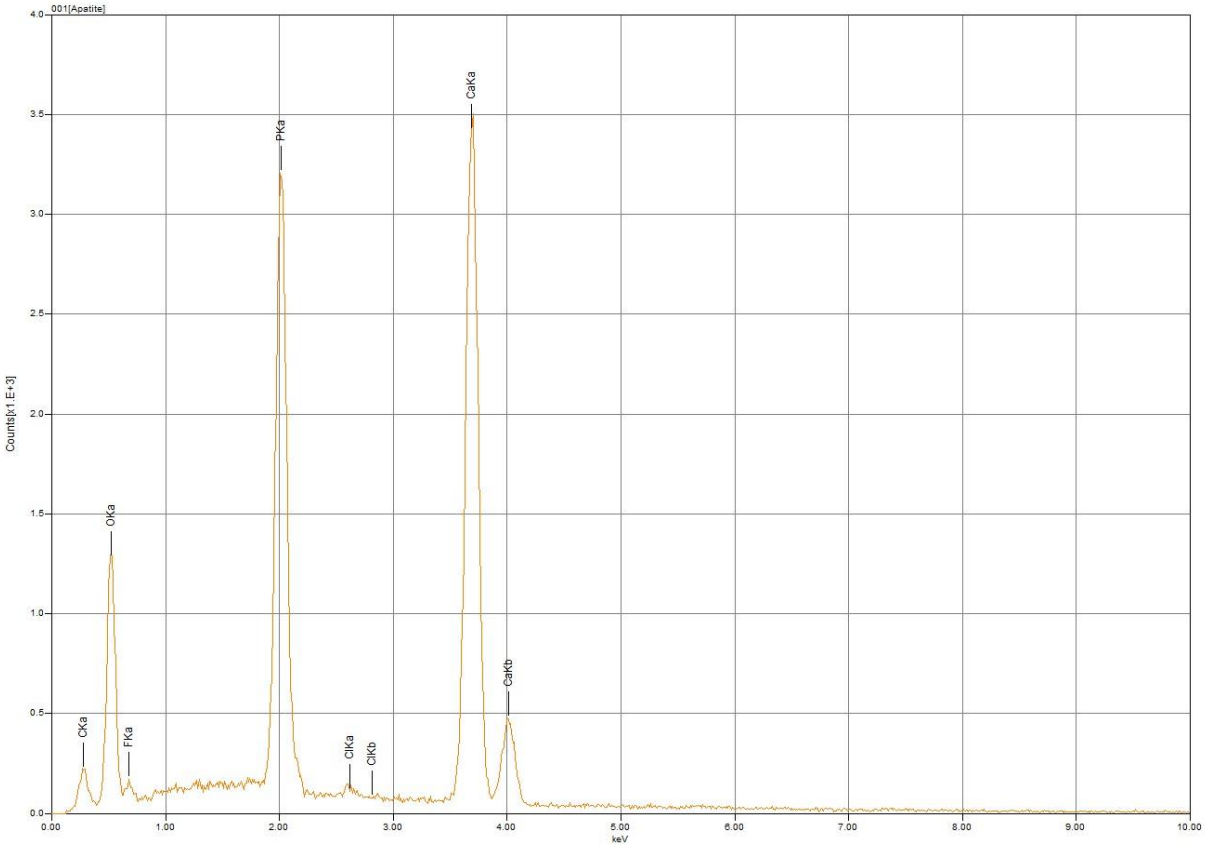
001[Apatite]
Counts[x1 E+3]
keV
CKa
OKa
FKa
PKa
ClKa
ClKb
CaKa
CaKb

169038

Mount A
Grain 9

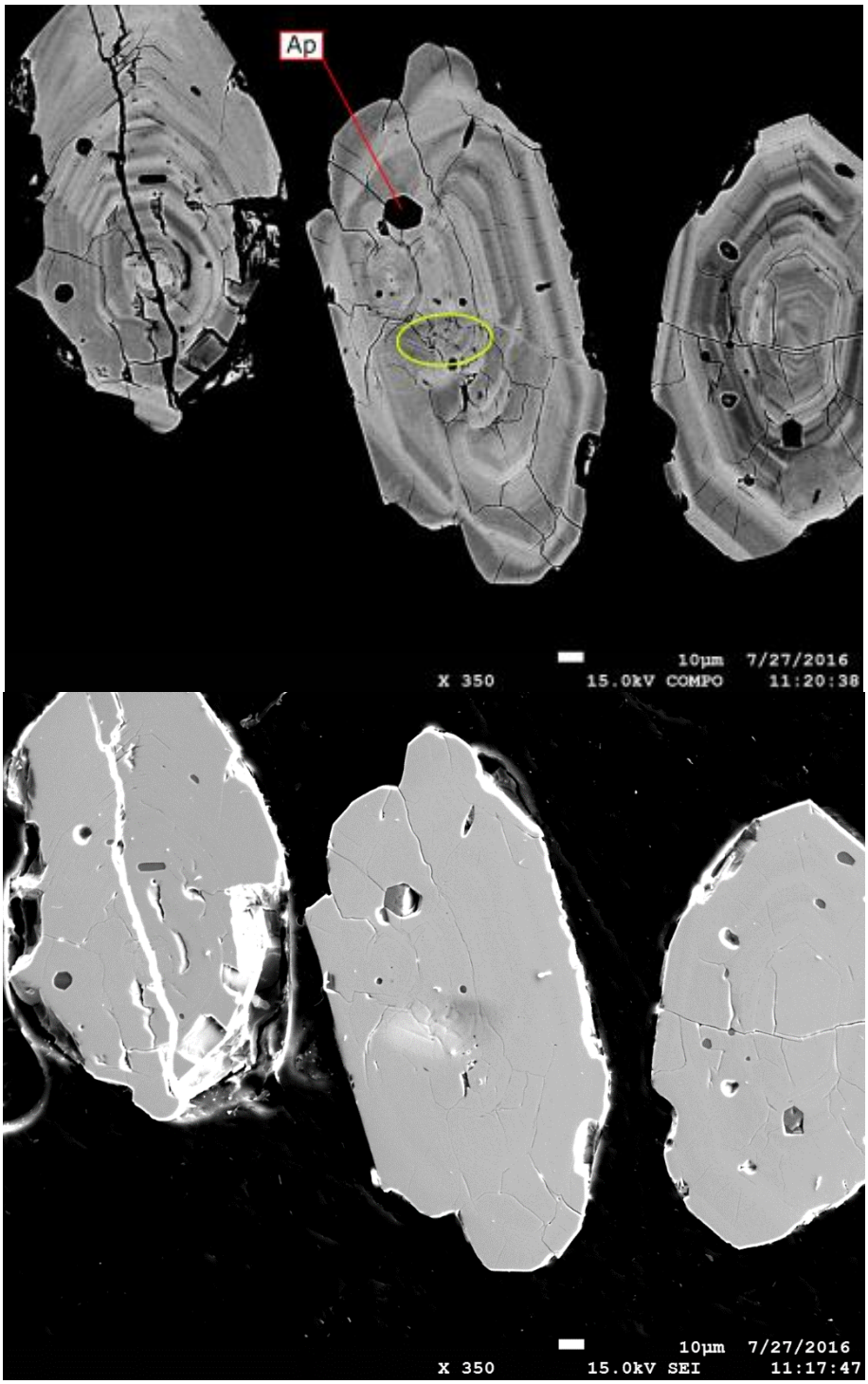

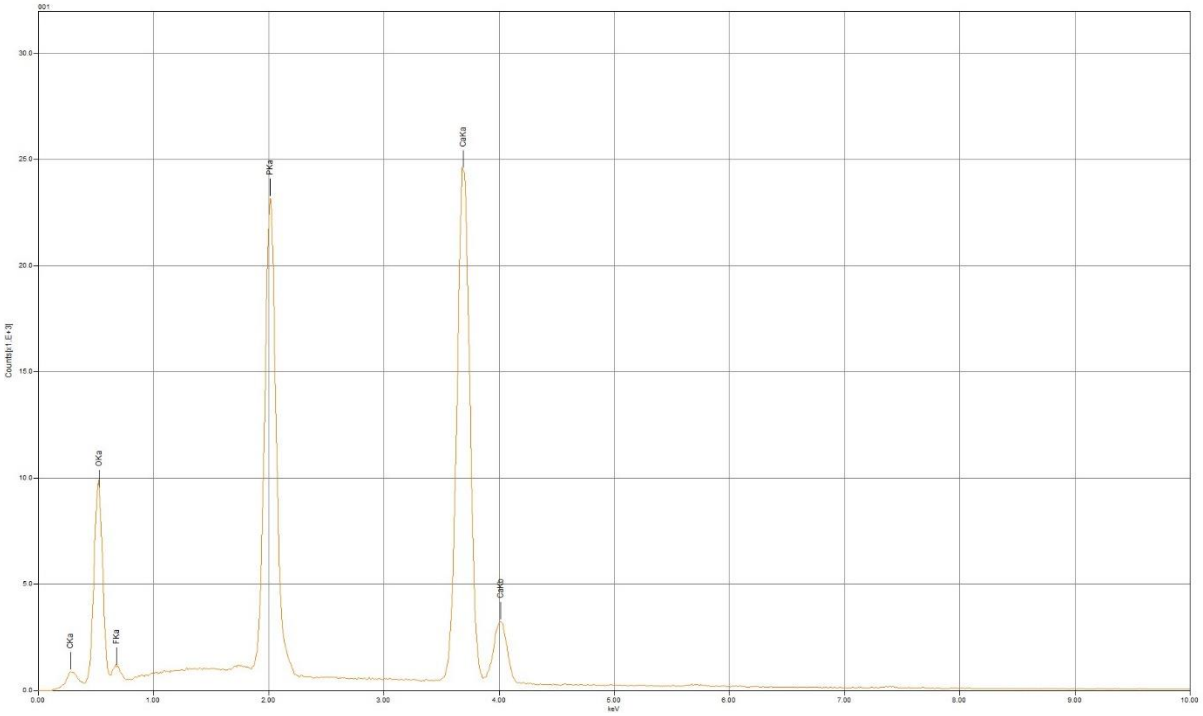
901
30.0
25.0
20.0
15.0
10.0
5.0
0.0
Counts[n.t.e.s]
OKa
FKa
PKa
CaKa
CaKb
0.00
1.00
2.00
3.00
4.00
5.00
6.00
7.00
8.00
9.00
10.00
keV

Grain 10


Ap
X 350
10µm 7/27/2016
15.0kV COMPO 11:27:11
X 350
10µm 7/27/2016
15.0kV SEI 11:25:52

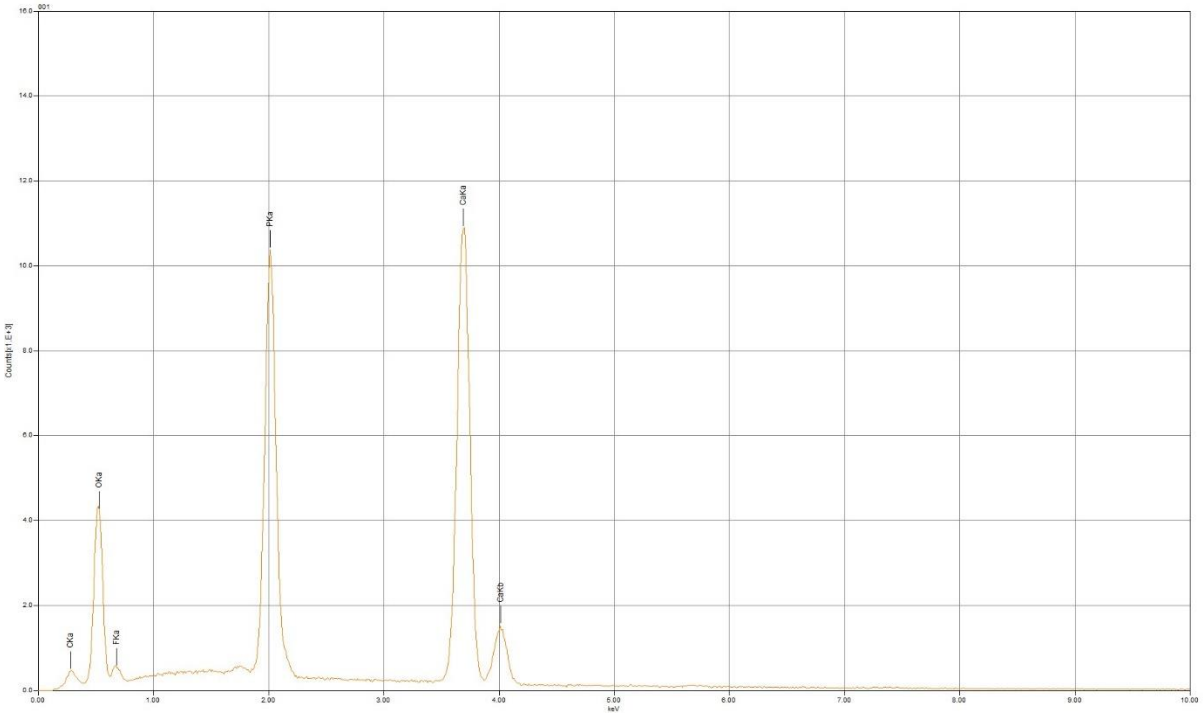
901
16.0
14.0
12.0
10.0
8.0
6.0
4.0
2.0
0.0
Counts[n.Ex3]
CKa
OKa
FKa
PKa
CaKa
CaKb
0.00
1.00
2.00
3.00
4.00
5.00
6.00
7.00
8.00
9.00
10.00
keV

Grain 12

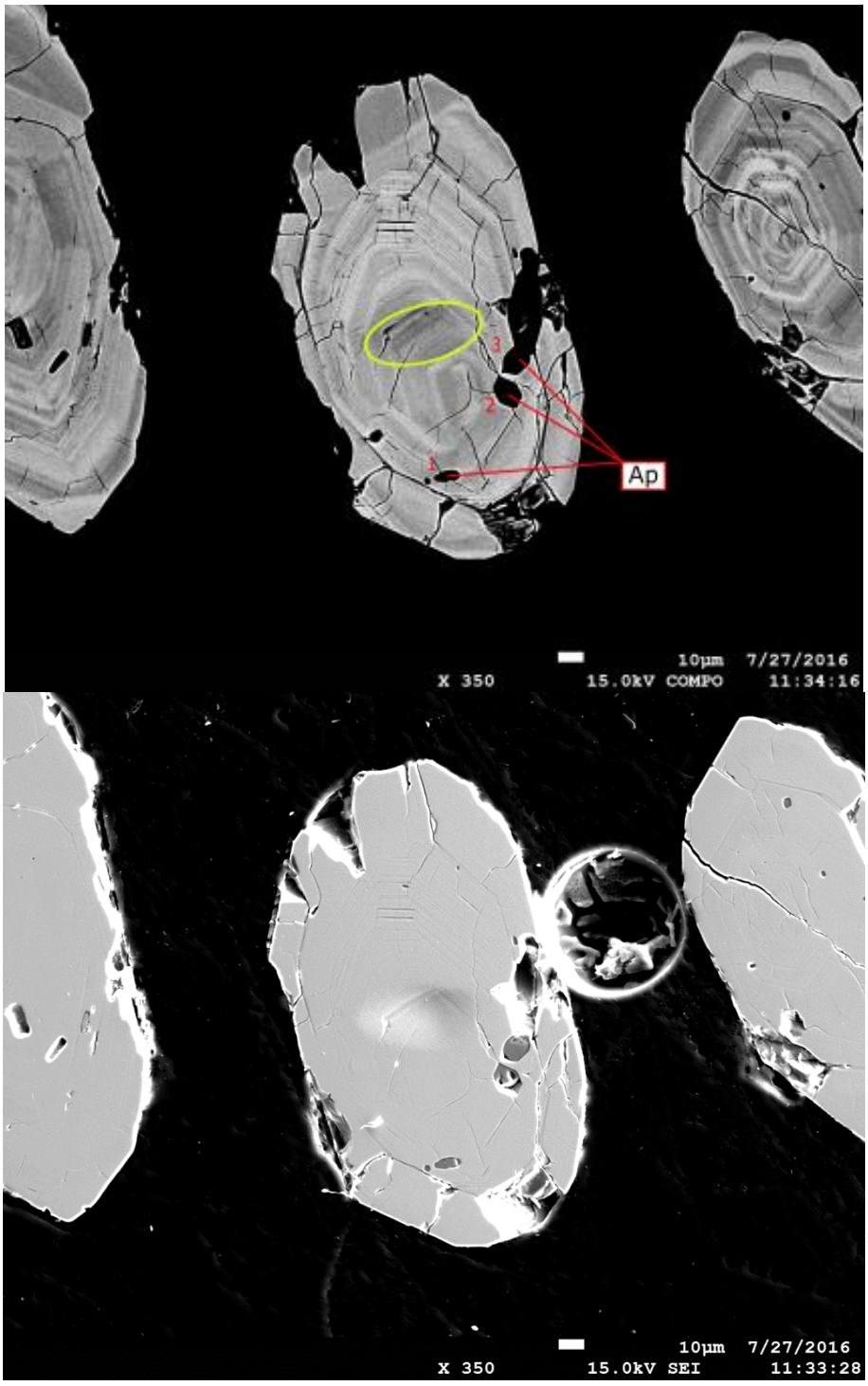
3
2
1
Ap
10µm 7/27/2016
X 350 15.0kV COMPO 11:34:16
10µm 7/27/2016
X 350 15.0kV SEI 11:33:28

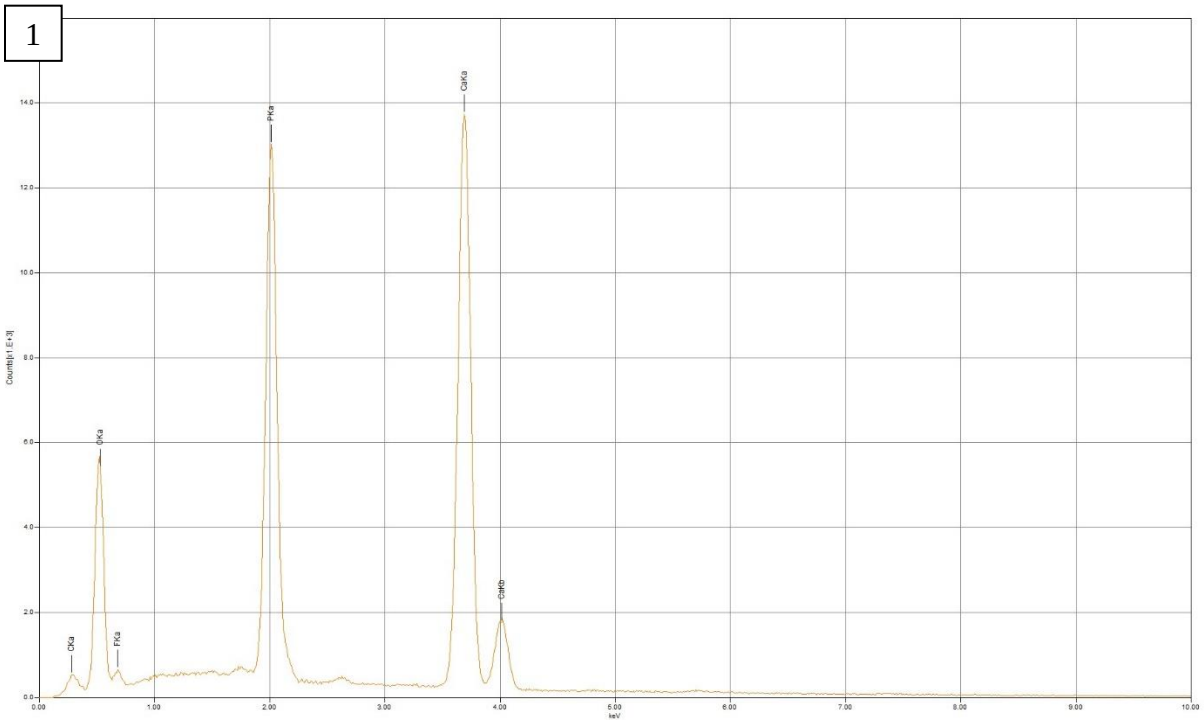
1
OKa
CKa
FKa
PKa
CaKa
CaKb
Counts[1.E+3]
keV

2

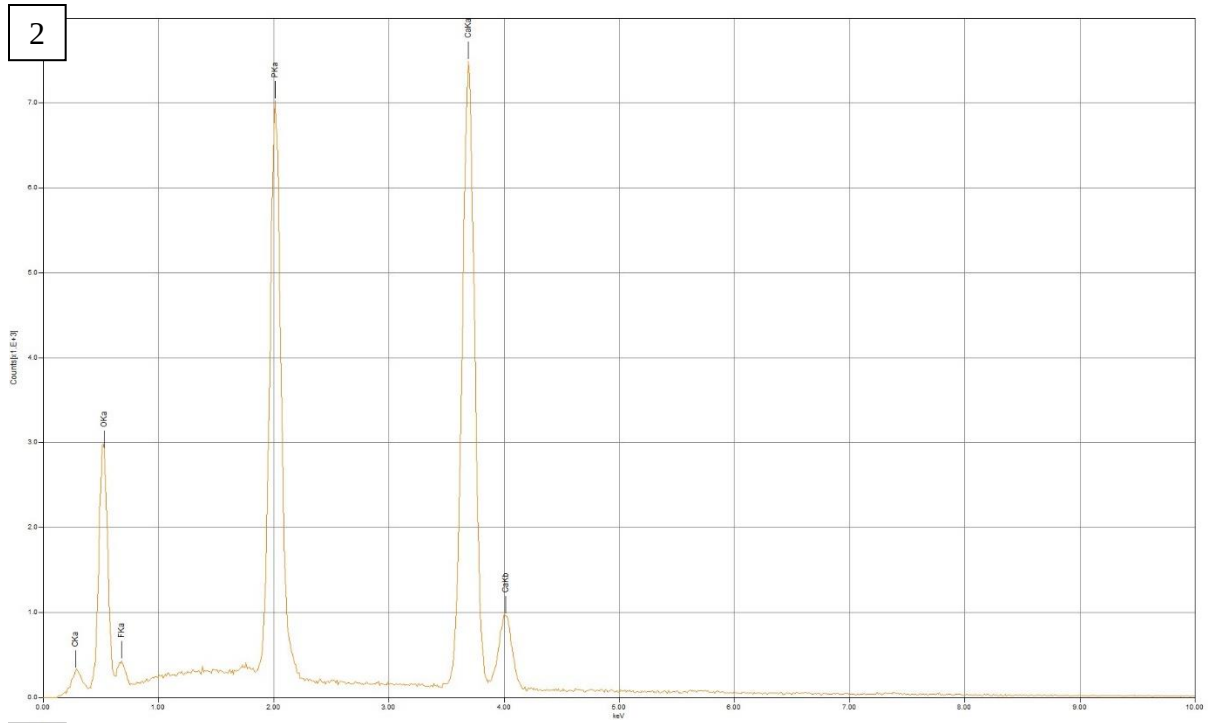
CaKa
PKa
OKa
CaKb
OKa
PKa
Counts[x1 E+3]
keV

3

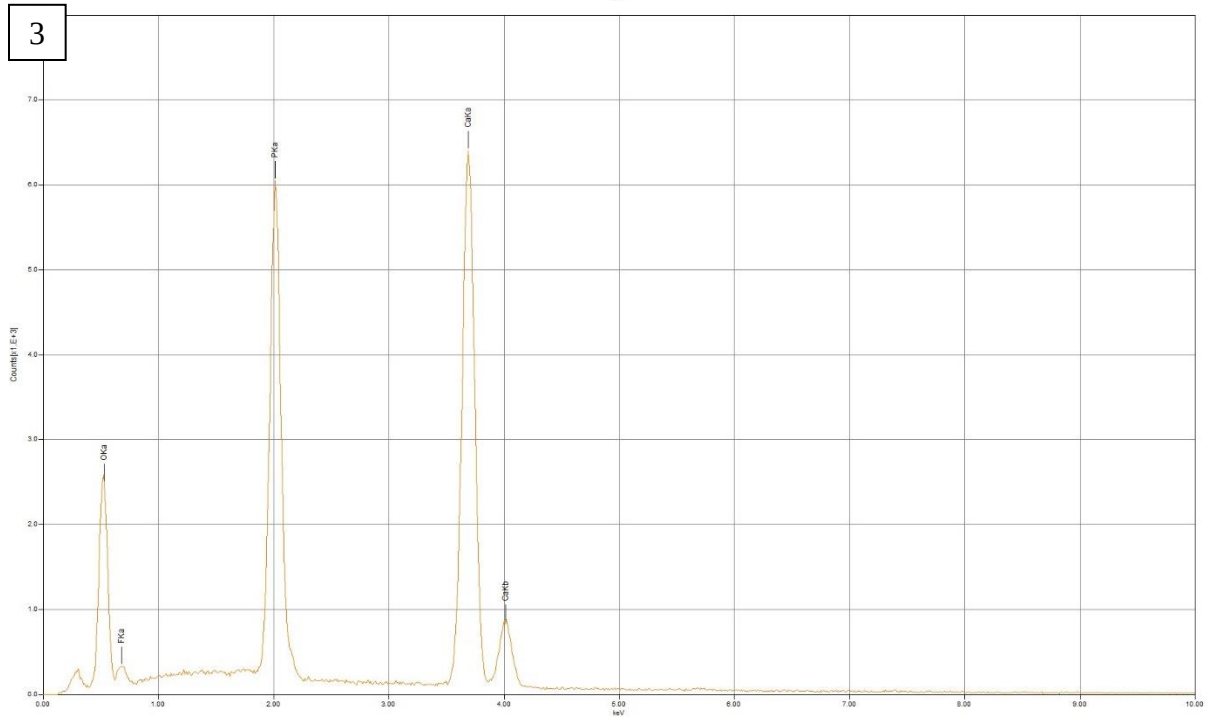
CaKa
PKa
OKa
CaKb
OKa
PKa
Counts[x1 E+3]
keV

Grain 15

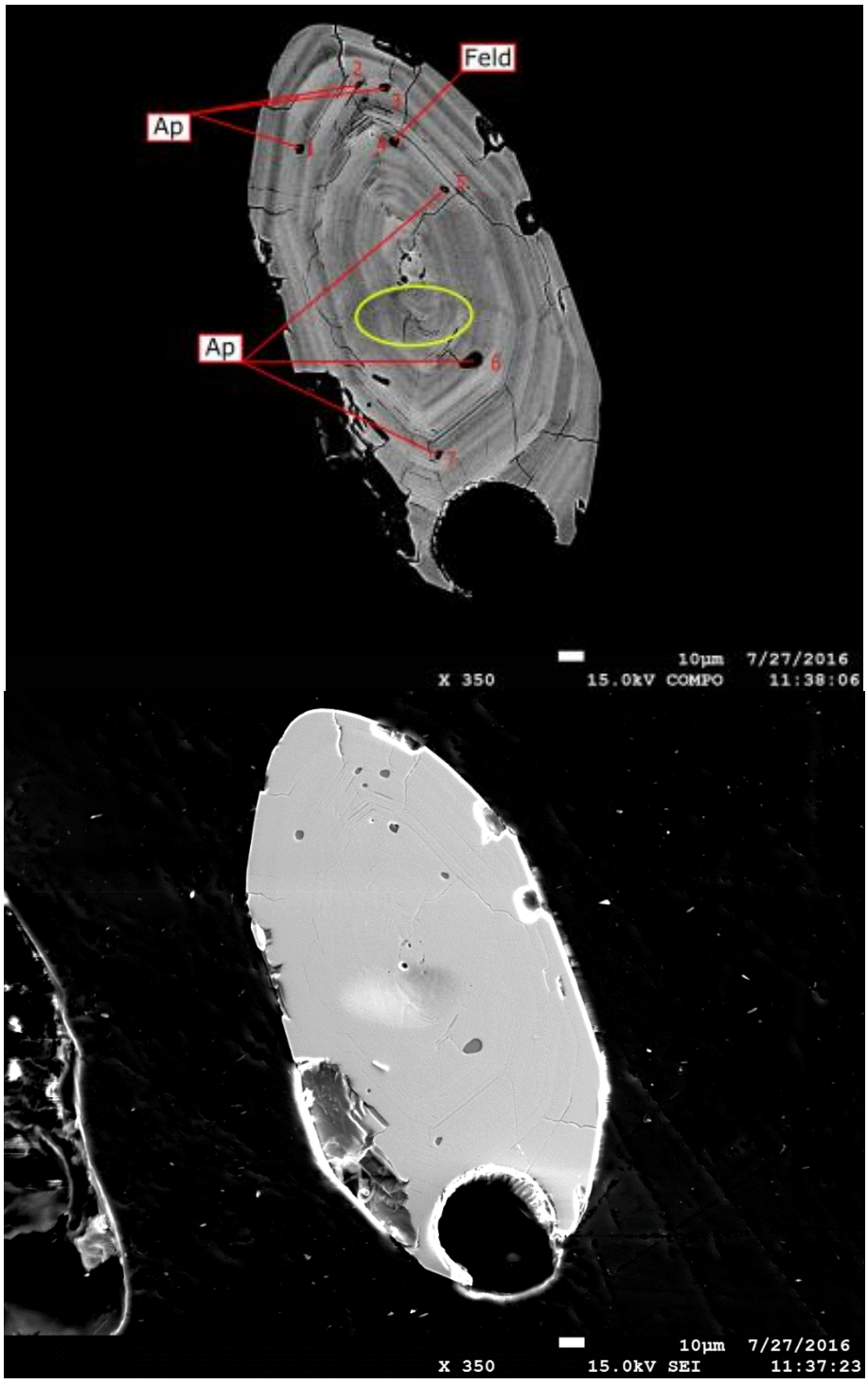
Feld
Ap
Ap
1
2
3
4
5
6
7
X 350
10µm 7/27/2016
15.0kV COMPO 11:38:06
X 350
10µm 7/27/2016
15.0kV SEI 11:37:23

1

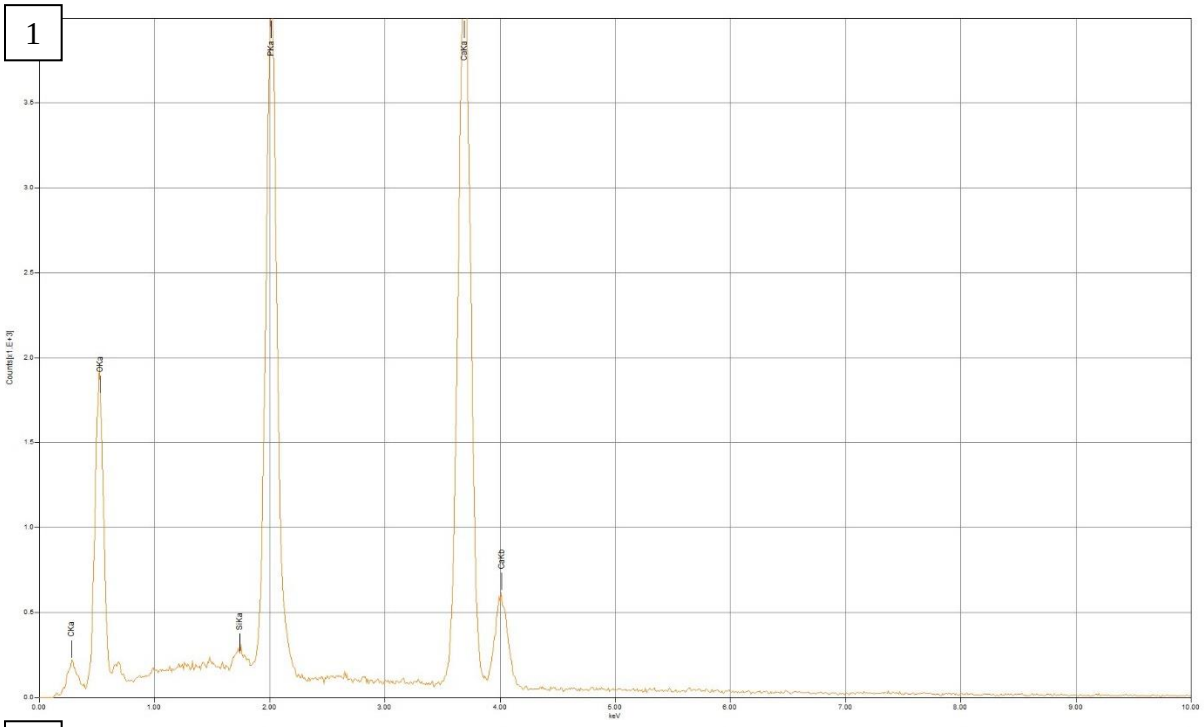
PKa
CaKa
OKa
CaKb
CKa
SiKa
Counts[x1 E+3]
keV

2

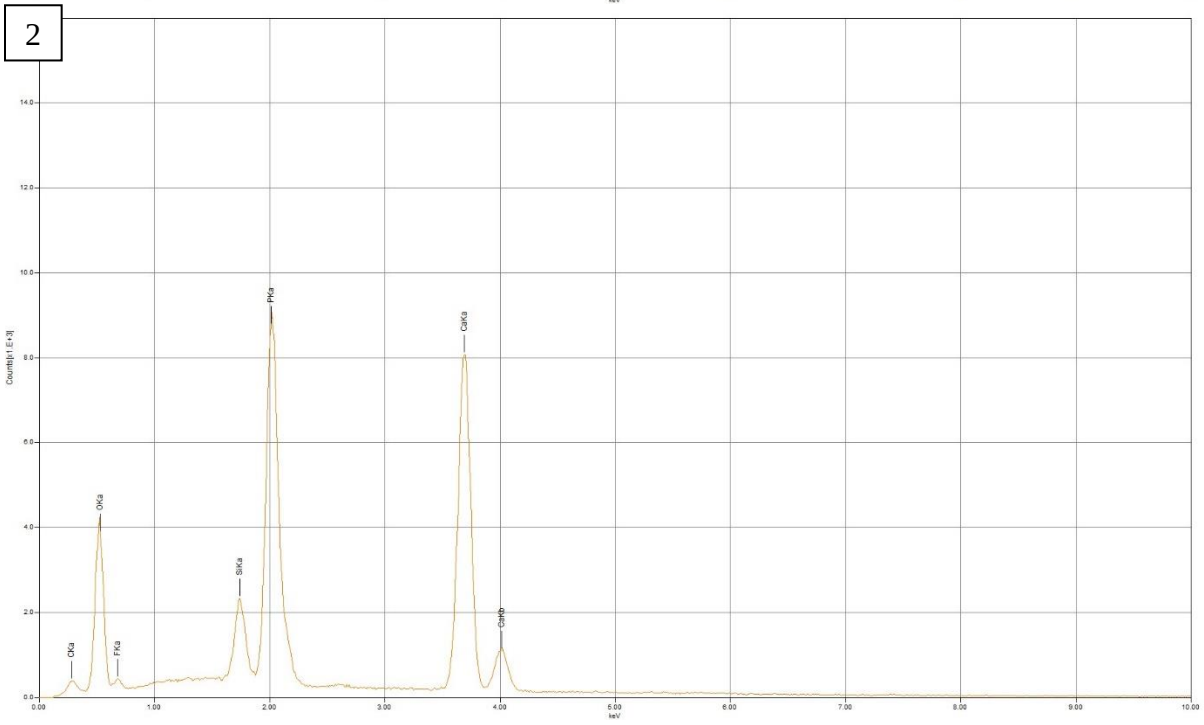
PKa
CaKa
OKa
SiKa
CaKb
CKa
FKa
Counts[x1 E+3]
keV

3

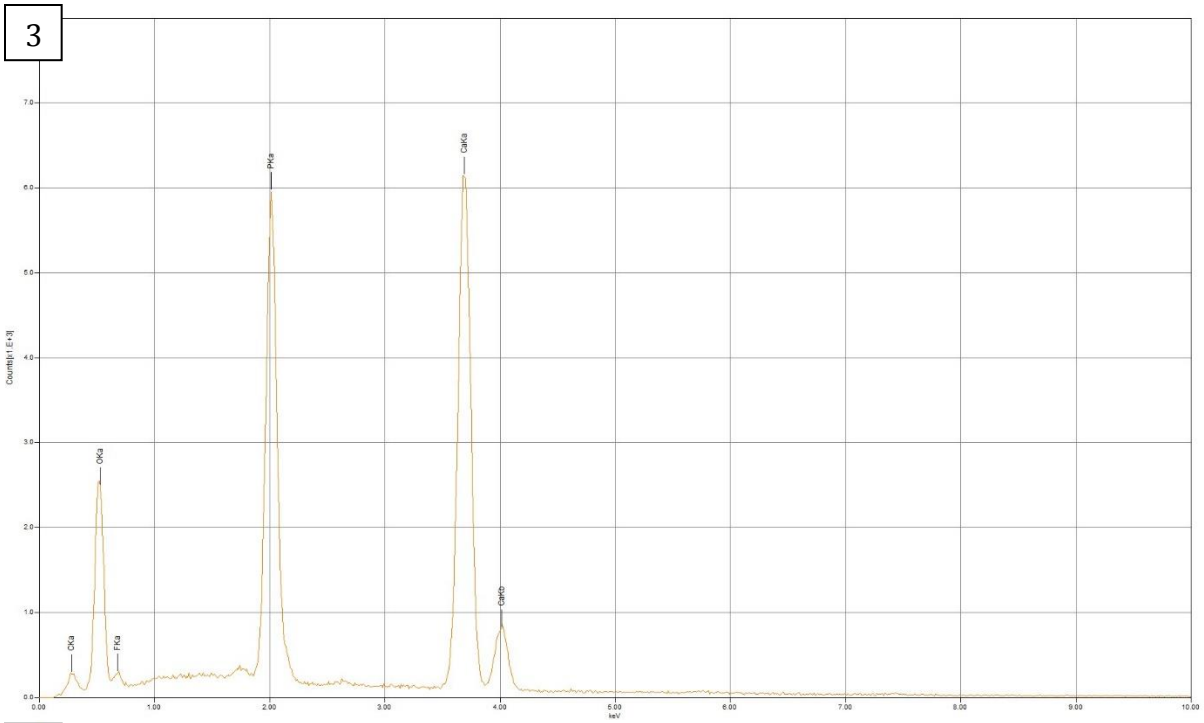
PKa
CaKa
OKa
CKa
FKa
CaKb
Counts[x1 E+3]
keV

4

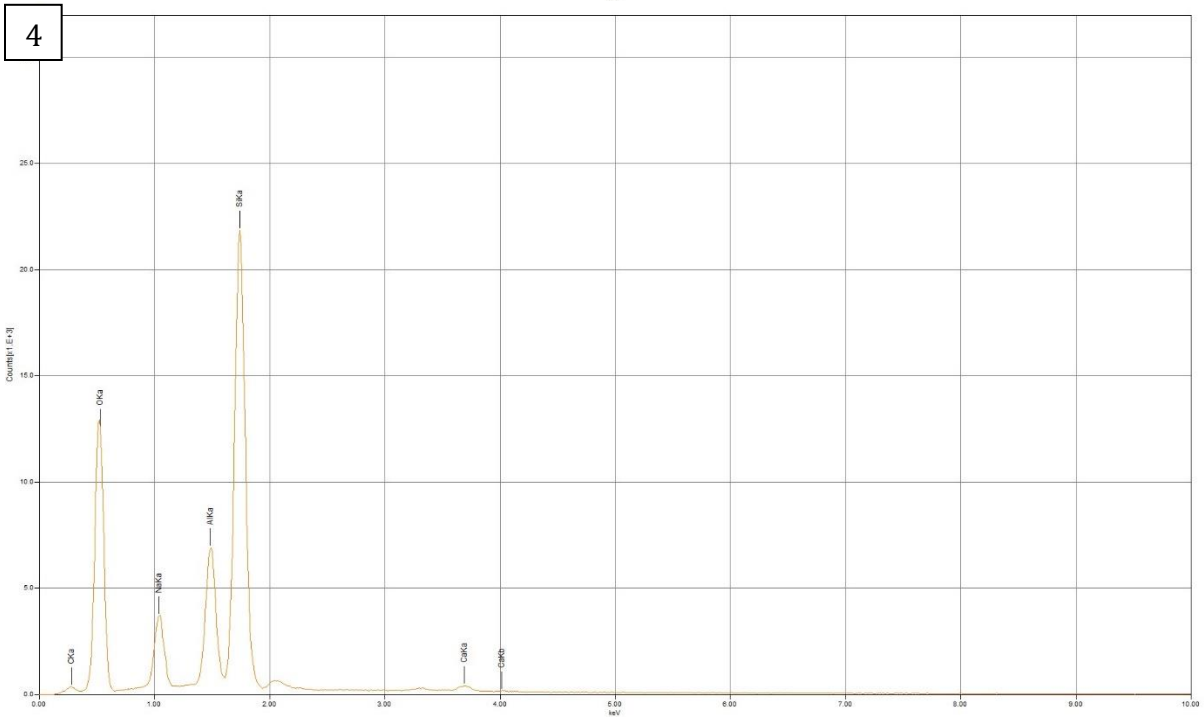
SiKa
OKa
AlKa
NaKa
CKa
CaKa
CaKb
Counts[x1 E+3]
keV

5

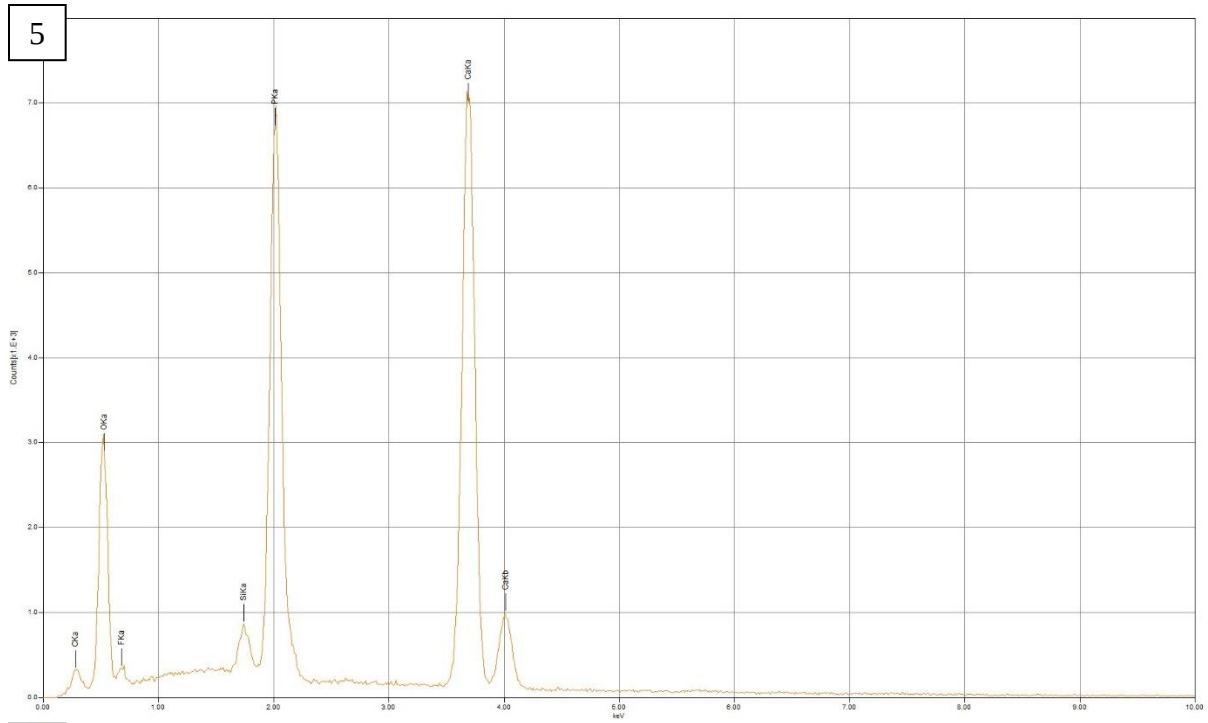
OKa
FKa
SiKa
PKa
CaKa
CaKb
Counts[x1 E+3]
keV

6

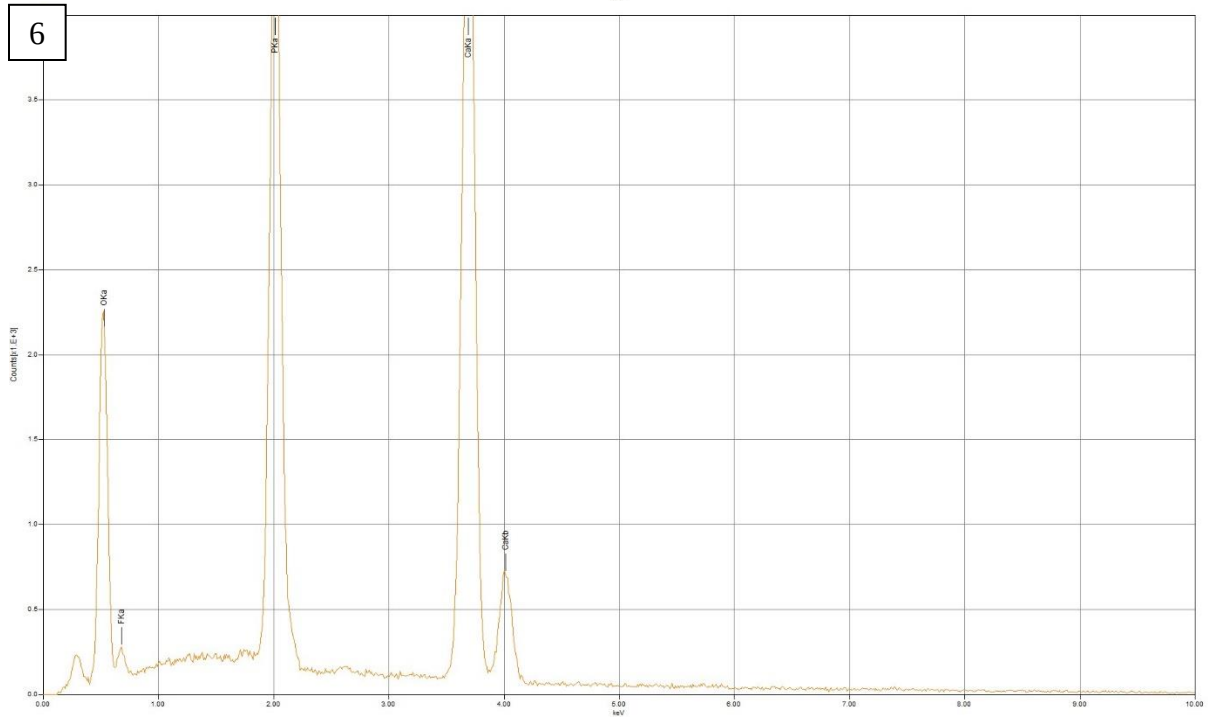
OKa
FKa
PKa
CaKa
CaKb
Counts[x1 E+3]
keV

7

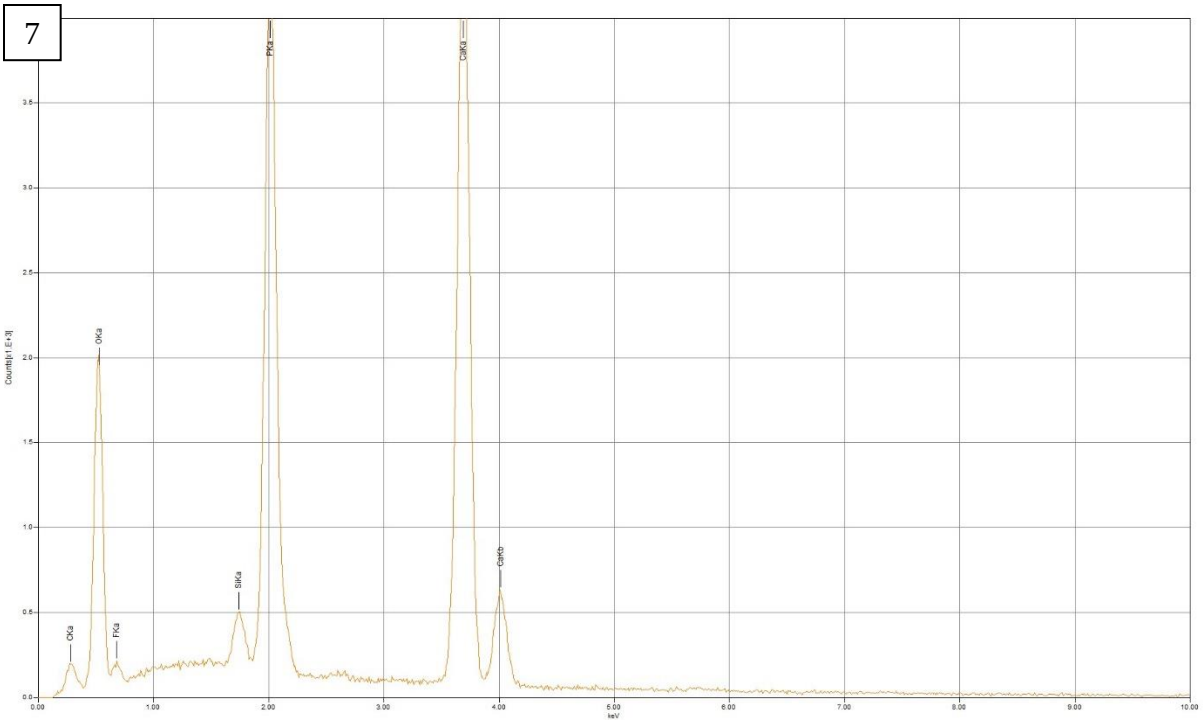

Grain 16

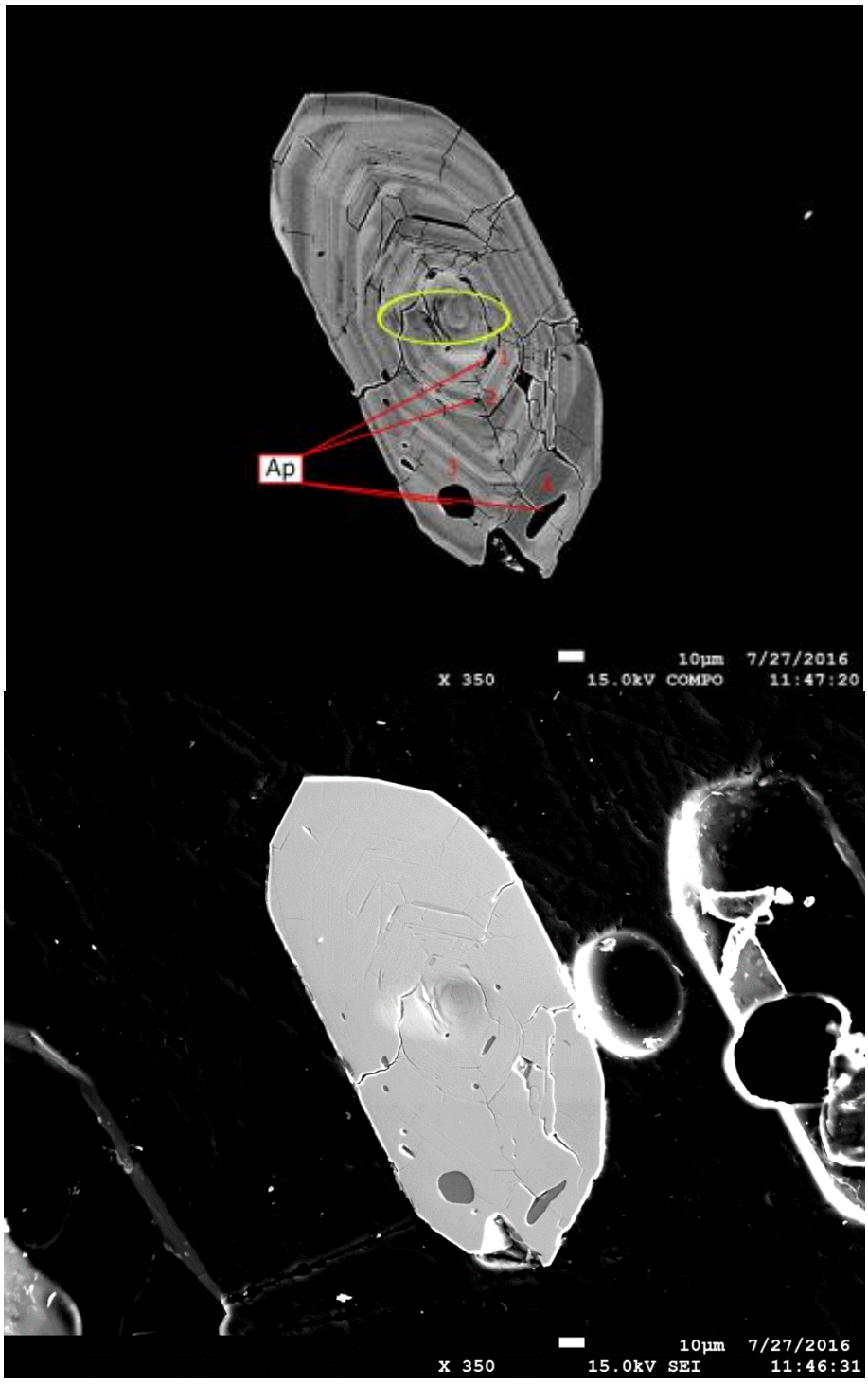
Ap
1
2
3
4
X 350
10µm
15.0kV COMPO
7/27/2016
11:47:20
X 350
10µm
15.0kV SEI
7/27/2016
11:46:31

1

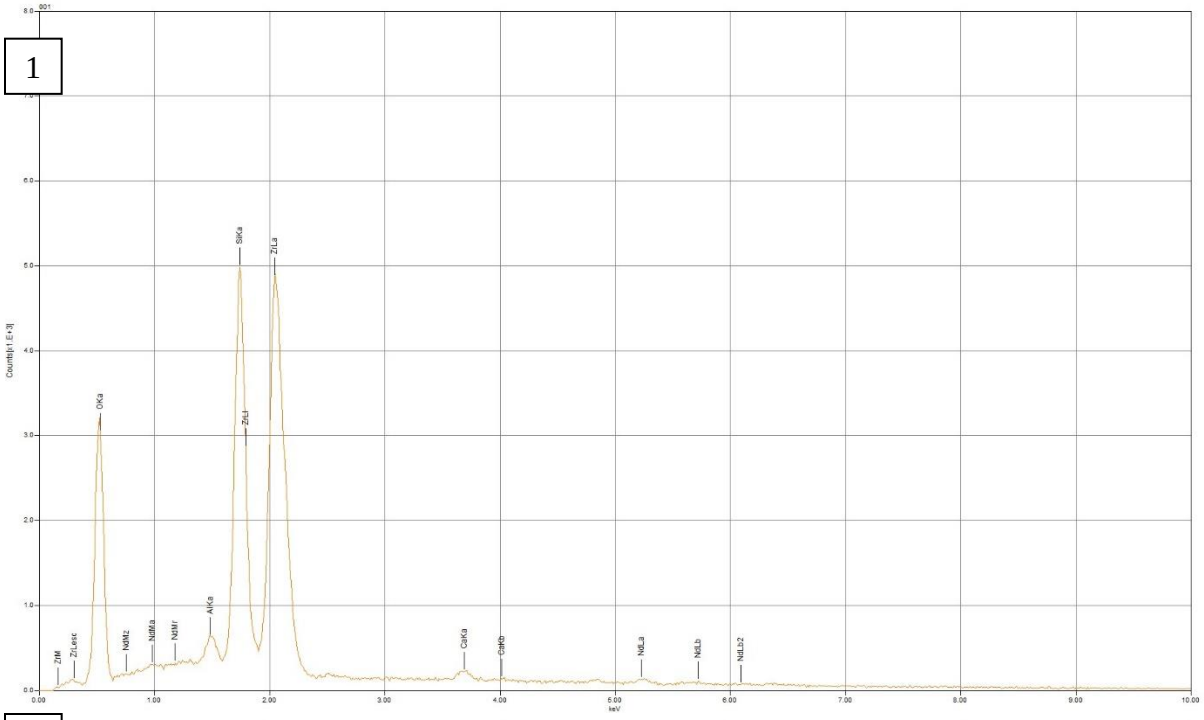
Counts[x1 E+3]
keV
ZrM
ZrLeac
OKa
NdMz
NdMa
NdMr
AlKa
SiKa
ZrLl
ZrLa
CaKa
CaKb
NdLa
NdLb
NdLb2

2

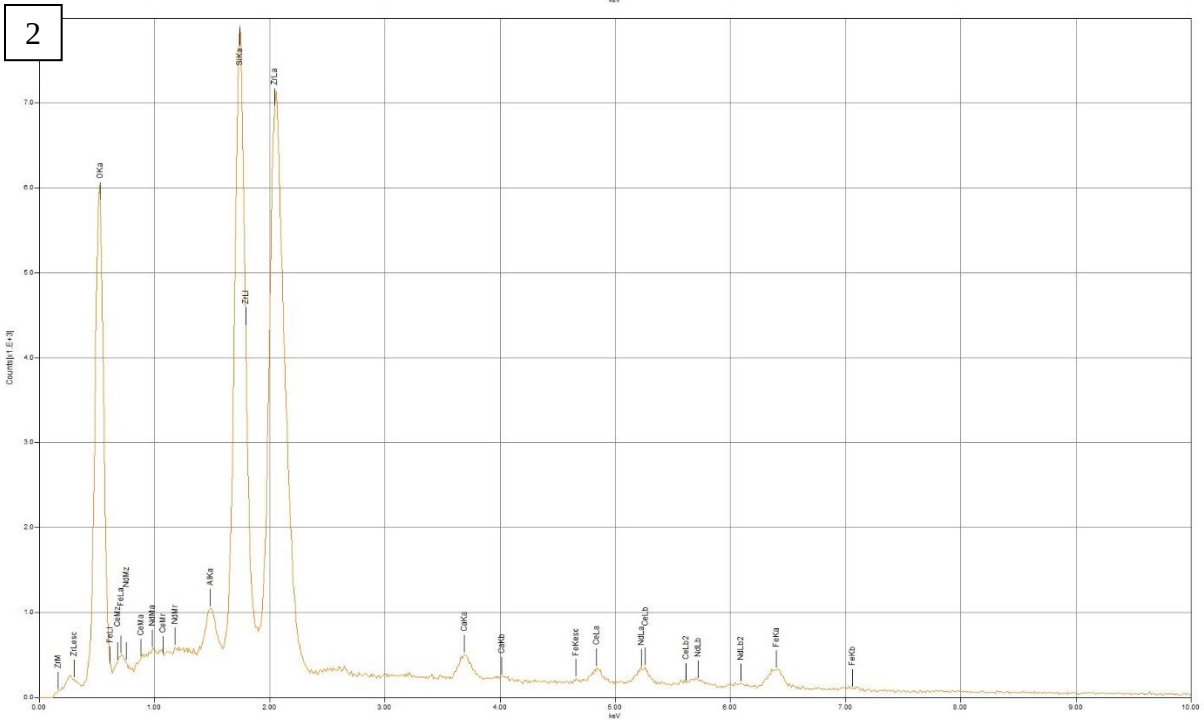
Counts[x1 E+3]
keV
ZrM
ZrLeac
FeLl
CeMz
FeLa
NdMz
CeMa
NdMa
CeMr
NdMr
AlKa
OKa
SiKa
ZrLl
ZrLa
CaKa
CaKb
FeKeac
CeLa
NdLa
CeLb
CeLb2
NdLb
NdLb2
FeKa
FeKb

4

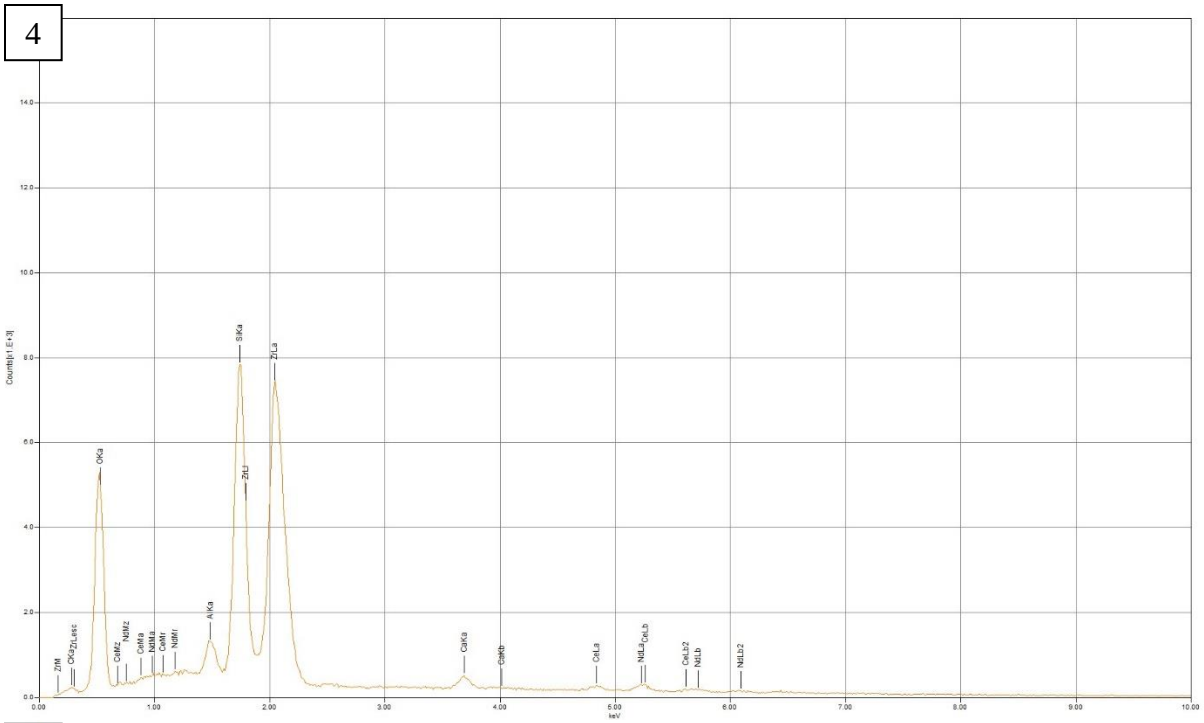
Counts[x1 E+3]
OKa
ZnM
OKa2ZnLess
CeM2
NdM2
CeMa
NdMa
CeMr
NdMr
AlKa
SiKa
ZnLl
ZnLa
CaKa
CaKb
CeLa
NdLa_CeLb
CeLb2
NdLb
NdLb2
keV

3

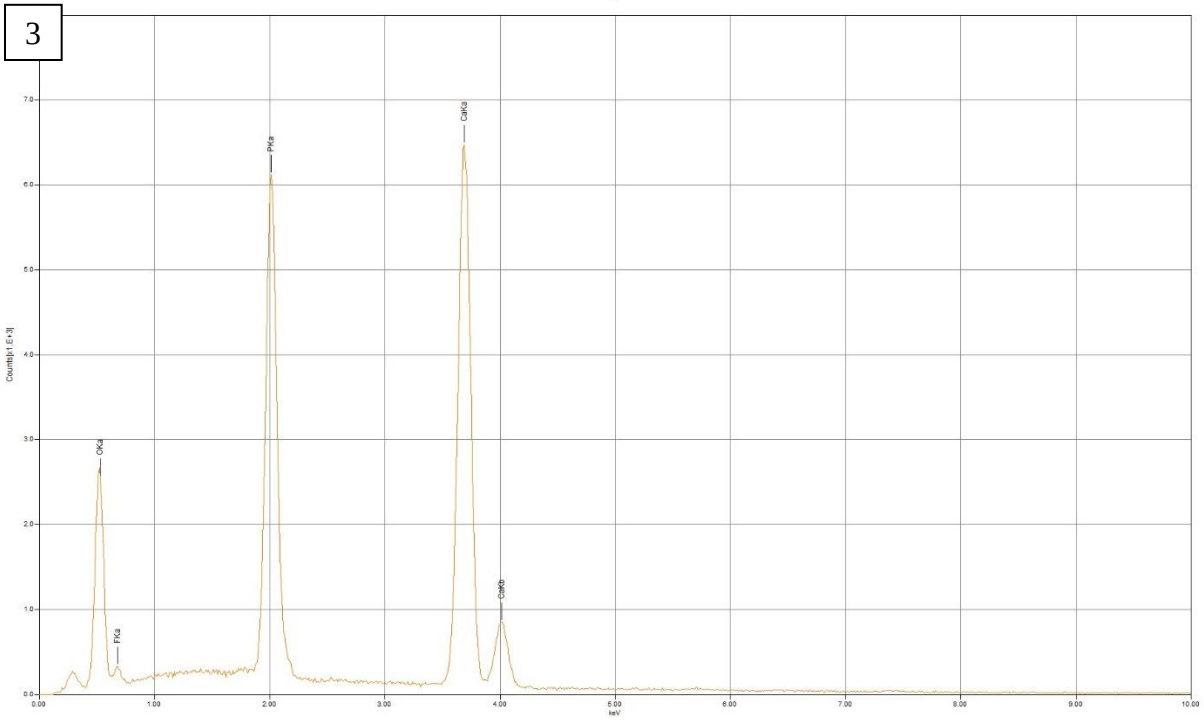
Counts[x1 E+3]
OKa
FKa
PKa
CaKa
CaKb
keV

Grain 17

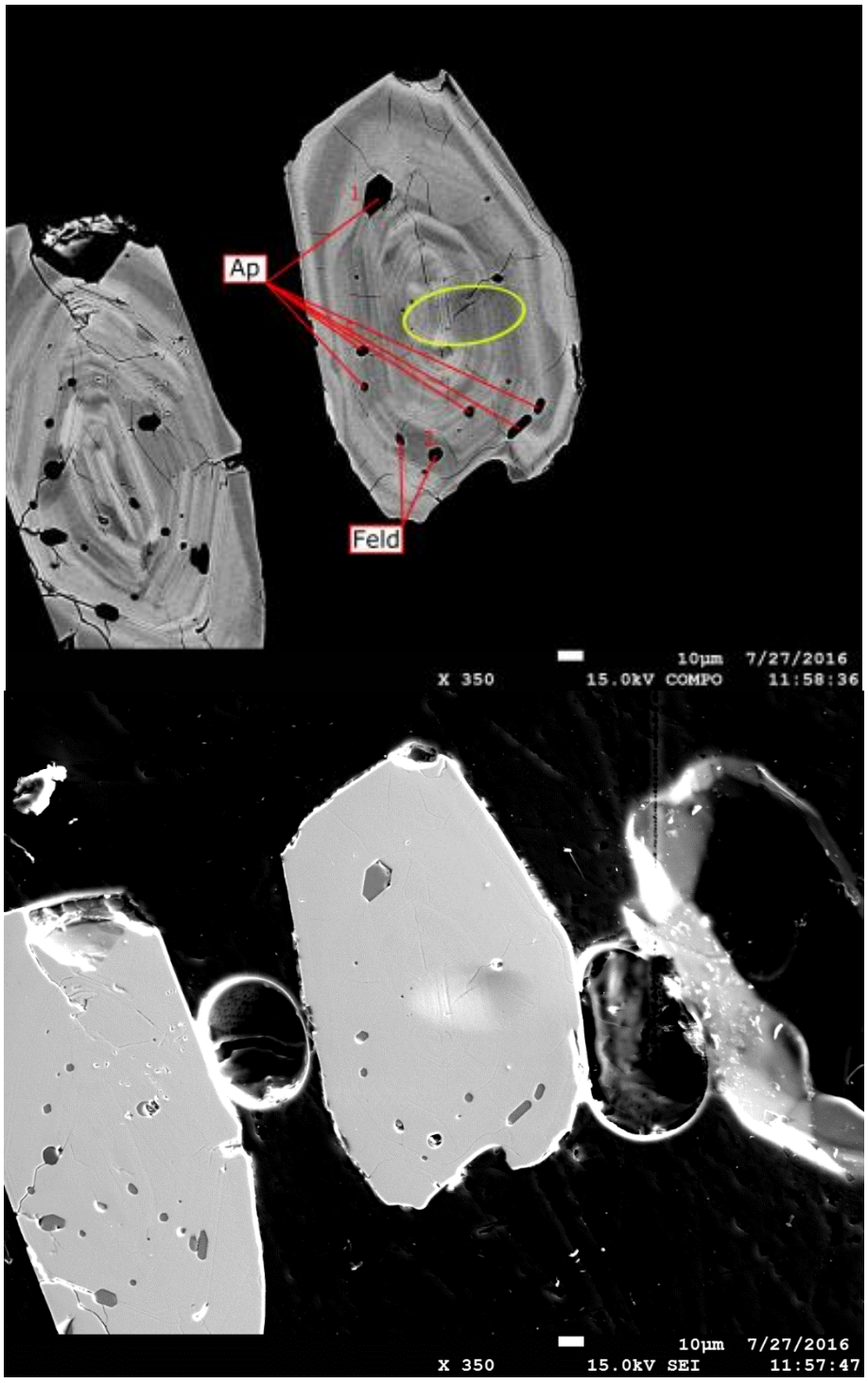
Ap
Feld
10µm 7/27/2016
X 350 15.0kV COMPO 11:58:36
10µm 7/27/2016
X 350 15.0kV SEI 11:57:47

1

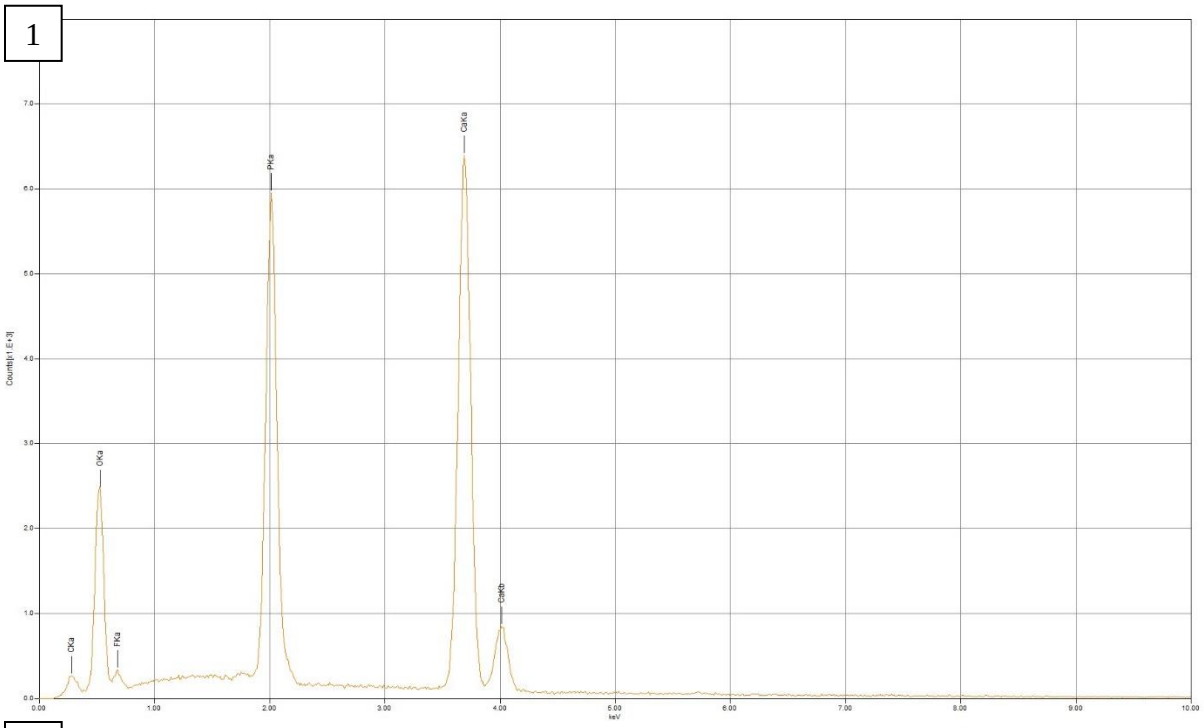

2

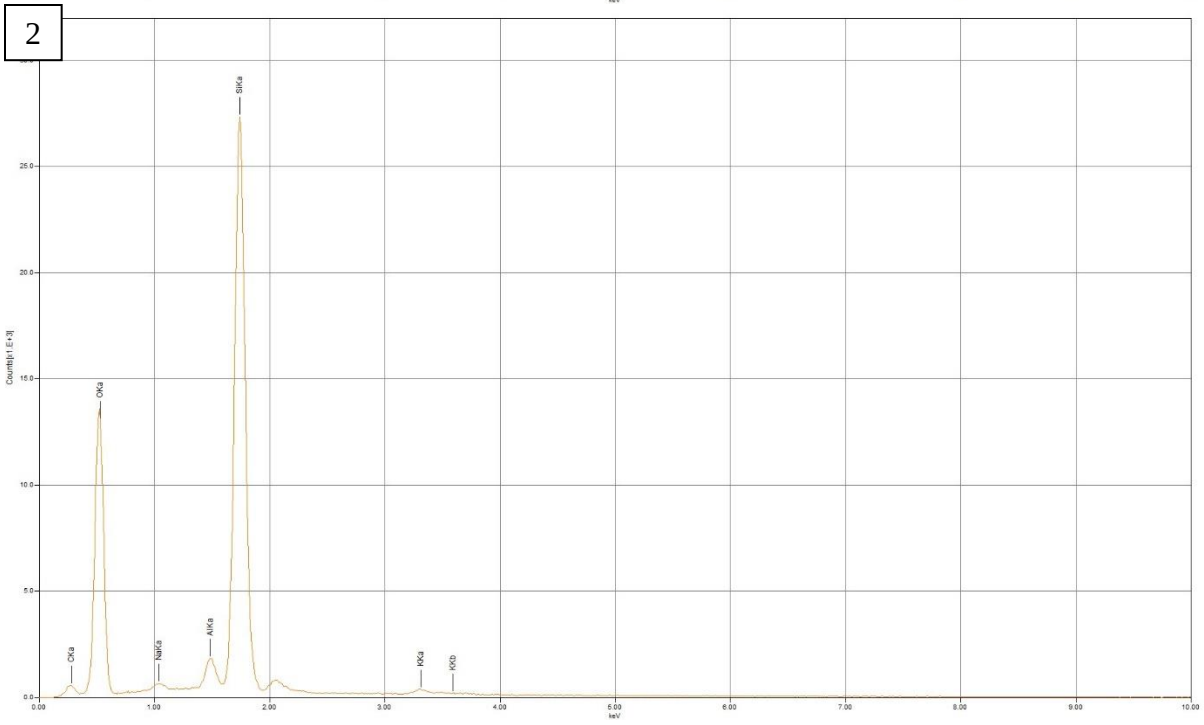

Grain 19

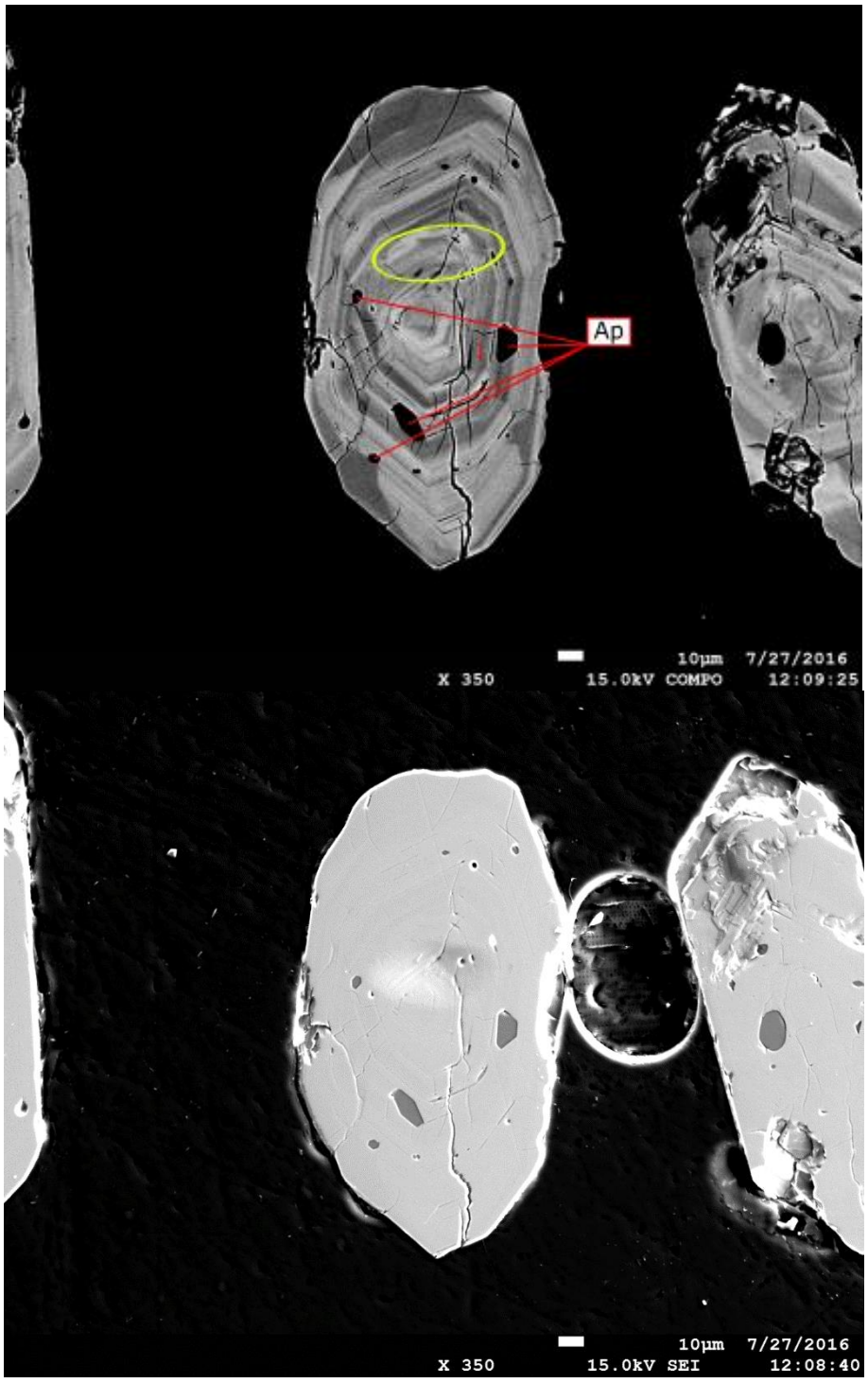
Ap
X 350
10µm 7/27/2016
15.0kV COMPO 12:09:25
X 350
10µm 7/27/2016
15.0kV SEI 12:08:40

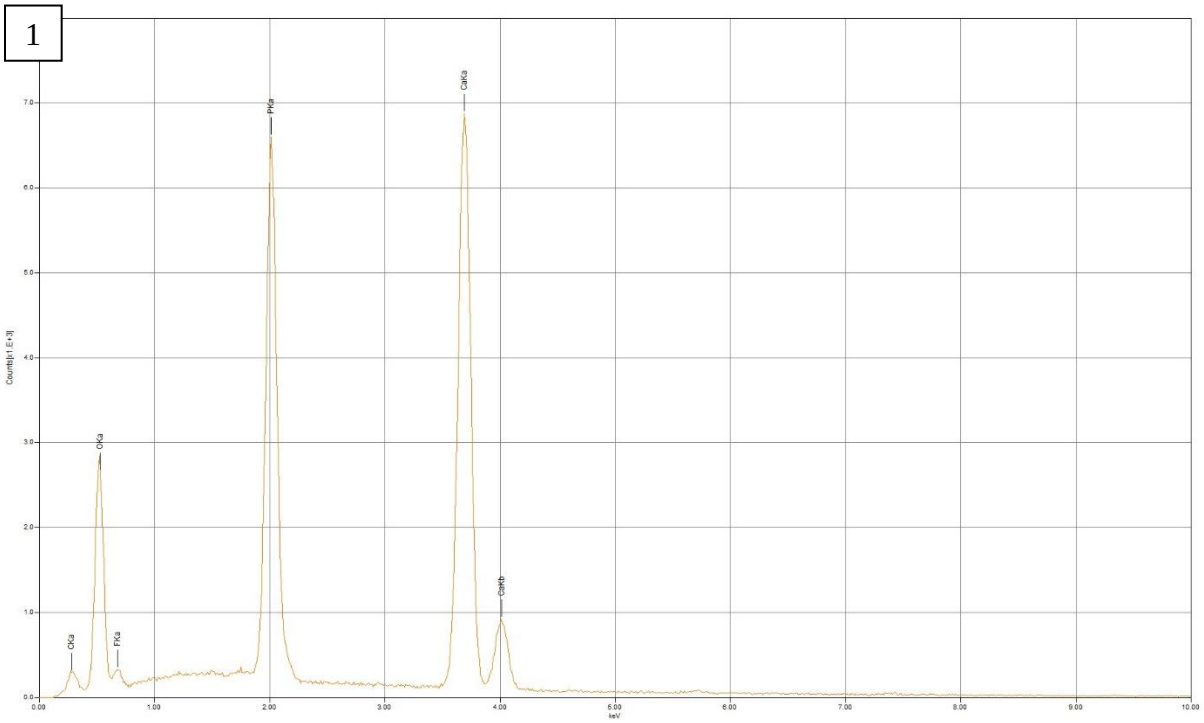
1
PKa
CaKa
OKa
CaKb
OKa
FKa
Counts[n.Ex3]
keV

Grain 23

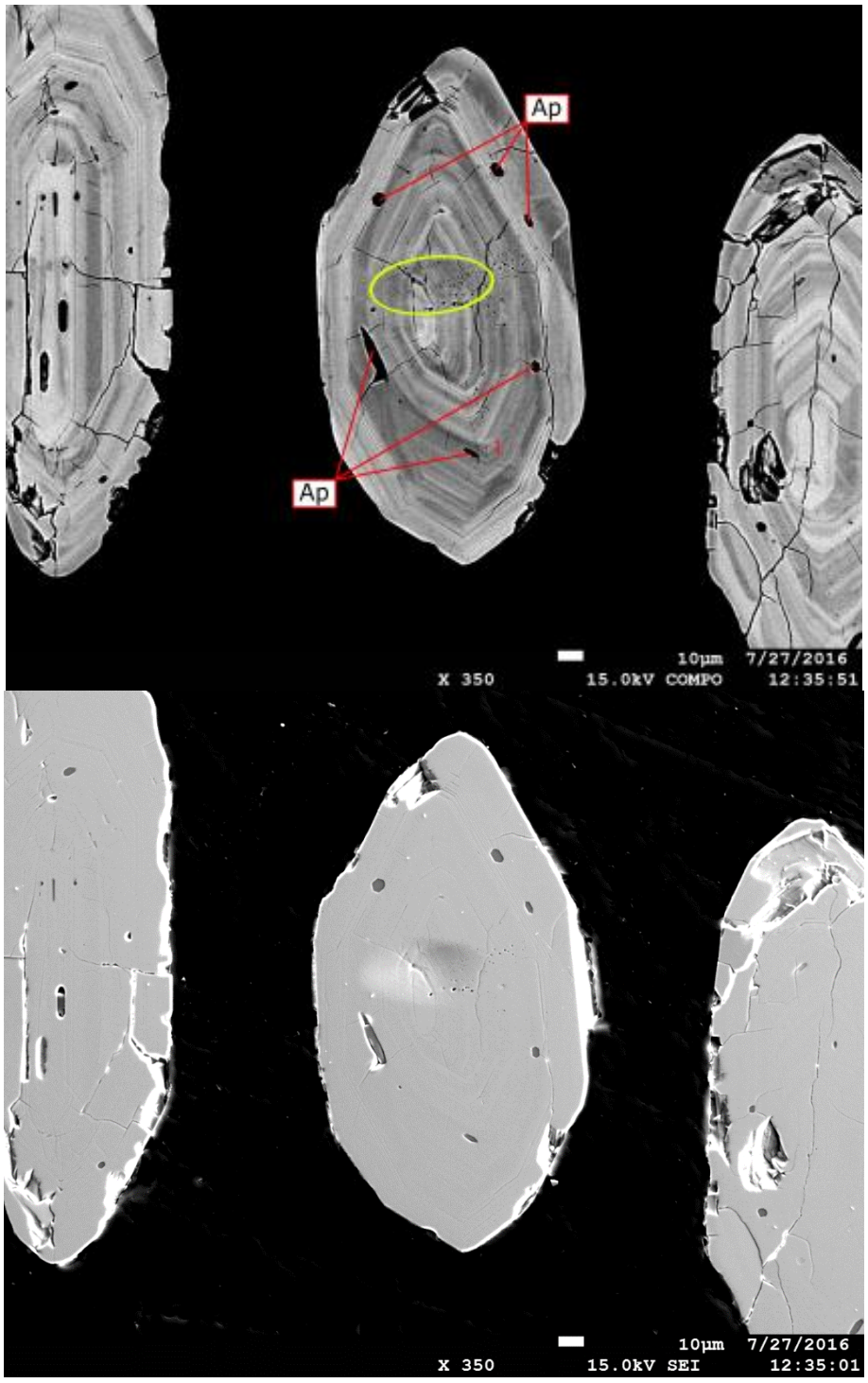
Ap
Ap
X 350
10µm
15.0kV COMPO
7/27/2016
12:35:51
X 350
10µm
15.0kV SEI
7/27/2016
12:35:01

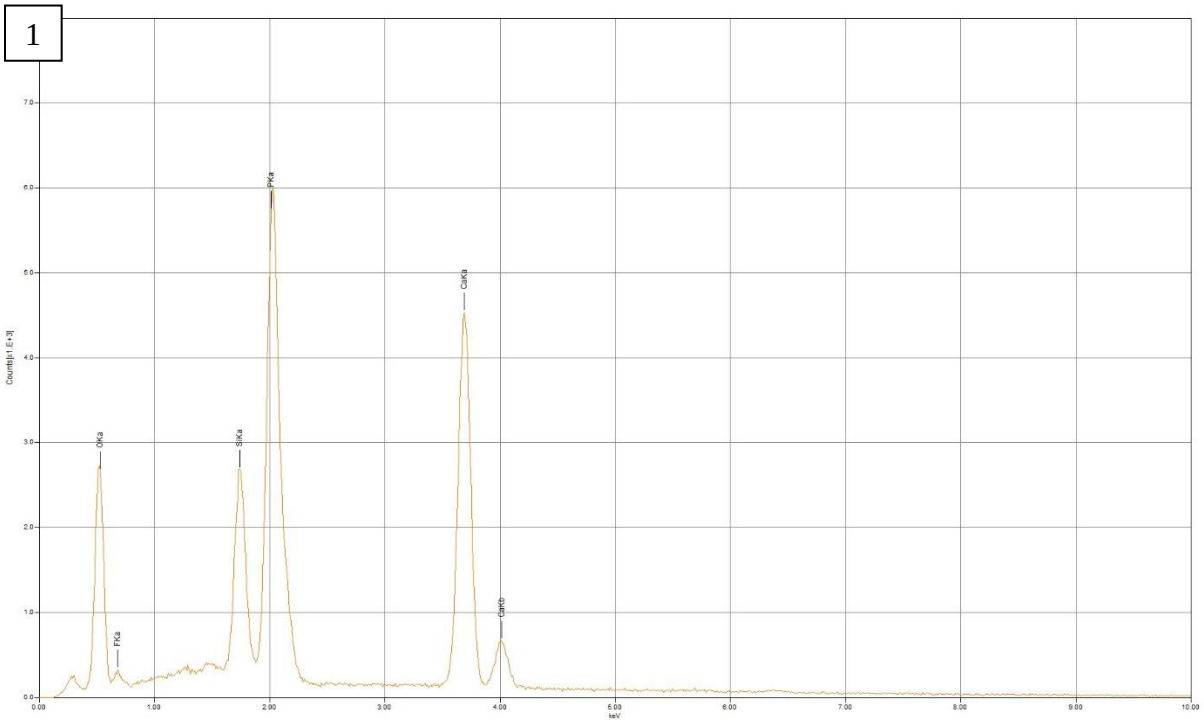
1
OKa
FKa
SiKa
PKa
CaKa
CaKb
Counts[n.Ex3]
keV

Grain 24

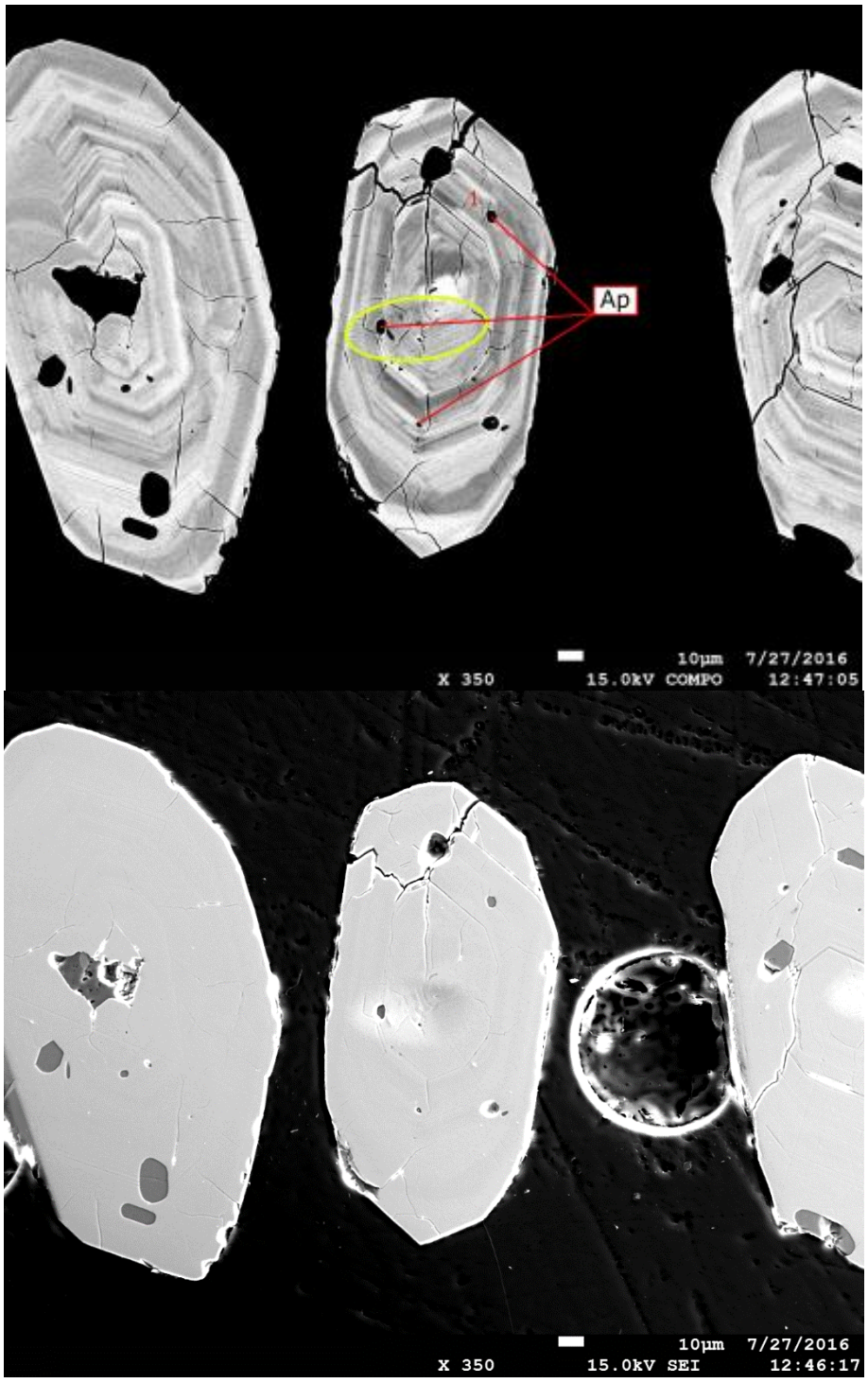
Ap
10µm 7/27/2016
X 350 15.0kV COMPO 12:47:05
10µm 7/27/2016
X 350 15.0kV SEI 12:46:17

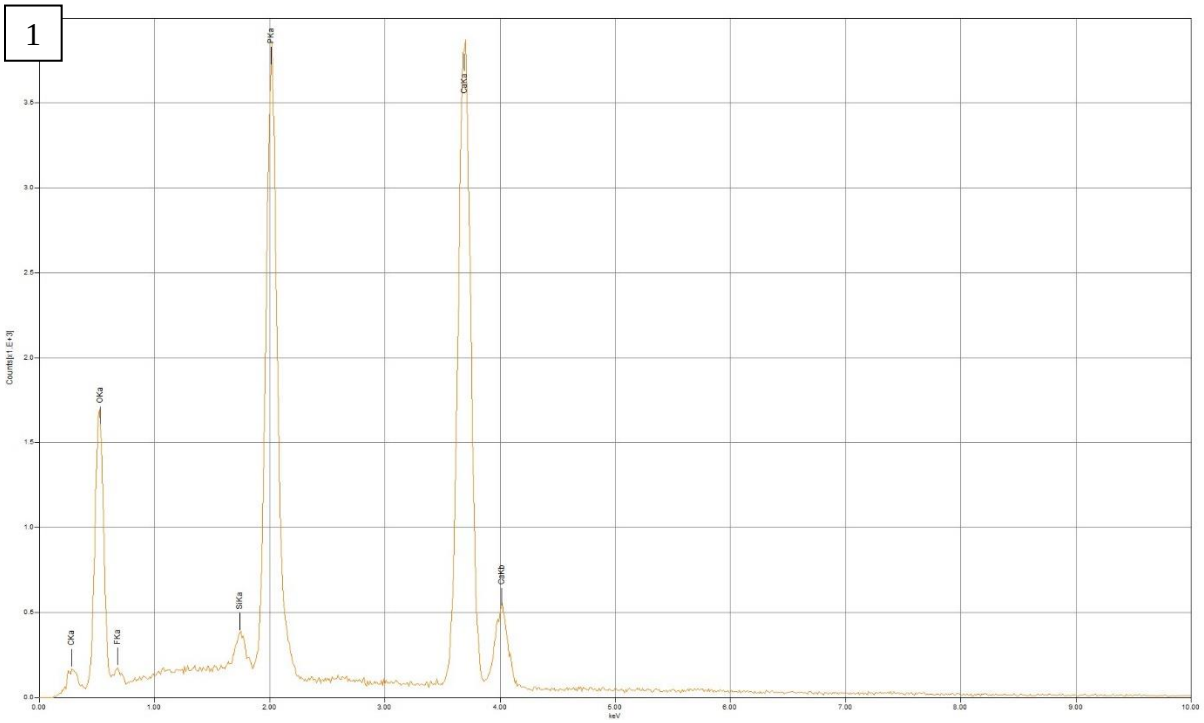
1
OKa
FKa
SiKa
PKa
CaKa
CaKb
Counts[n.f.x.]
keV

Grain 27


Ap, Feld
Ap
Ap
1
3 4
2
10µm 7/27/2016
X 350 15.0kV COMPO 12:52:57
10µm 7/27/2016
X 350 15.0kV SEI 12:51:59

1

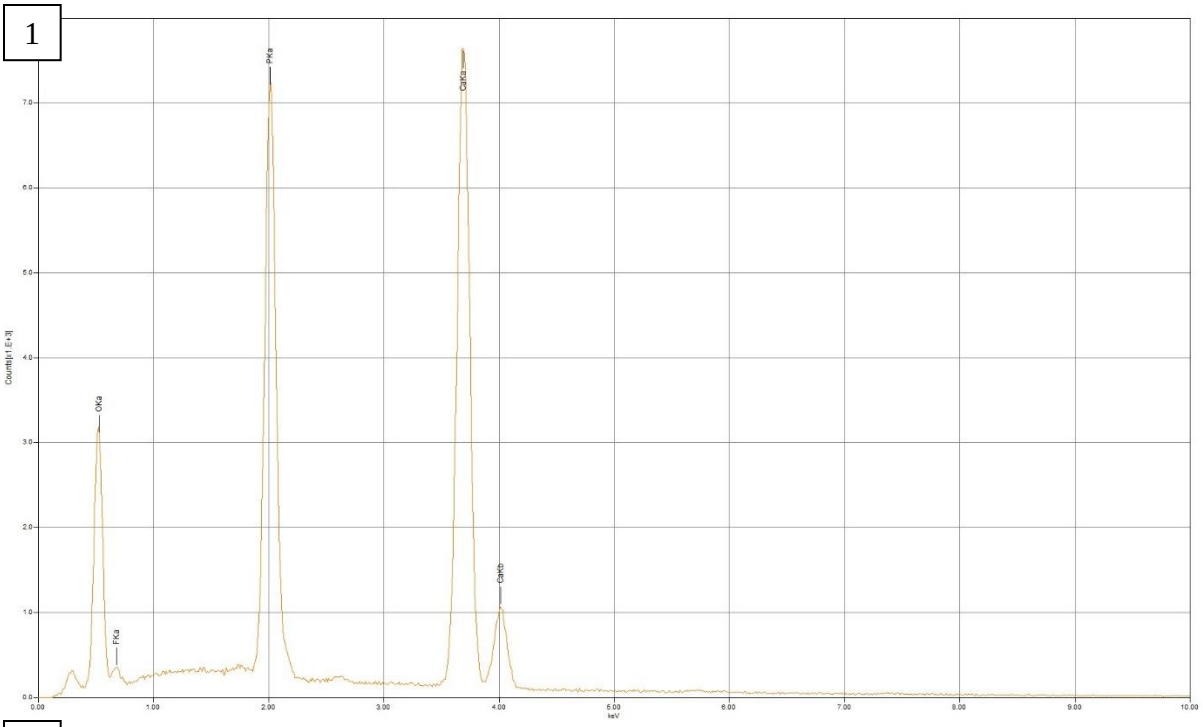
PKa
CaKa
OKa
FKa
CaKb
Counts[x1 E+3]
keV

2

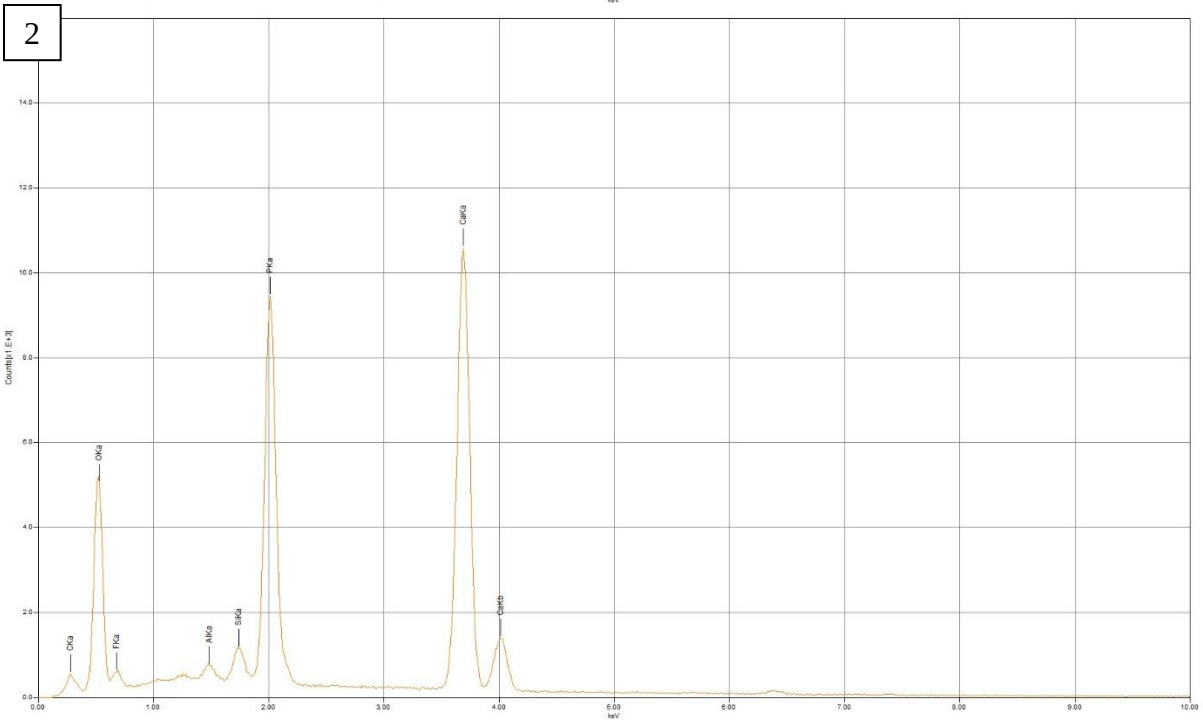
CaKa
PKa
OKa
CKa
FKa
AlKa
SiKa
CaKb
Counts[x1 E+3]
keV

4

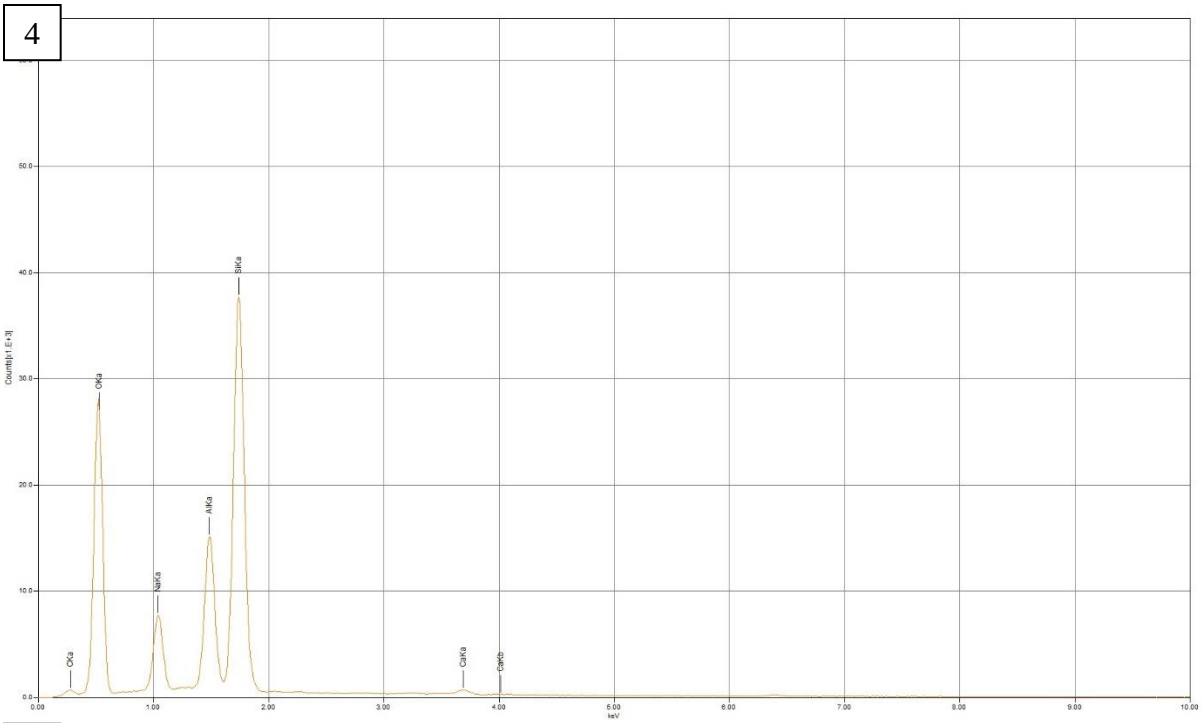
OKa
CKa
NKa
AlKa
SiKa
CaKa
CaKb
Counts[x1 E+3]
keV

3

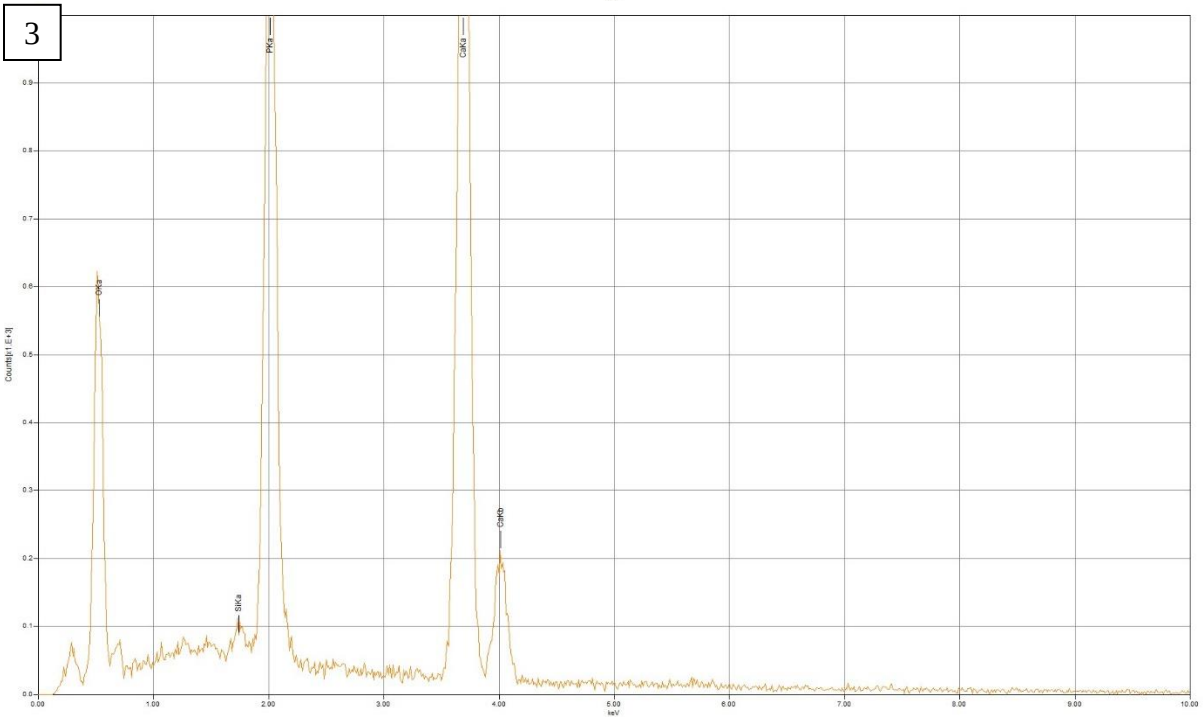
OKa
SiKa
PKa
CaKa
CaKb
Counts[x1 E+3]
keV

Grain 29

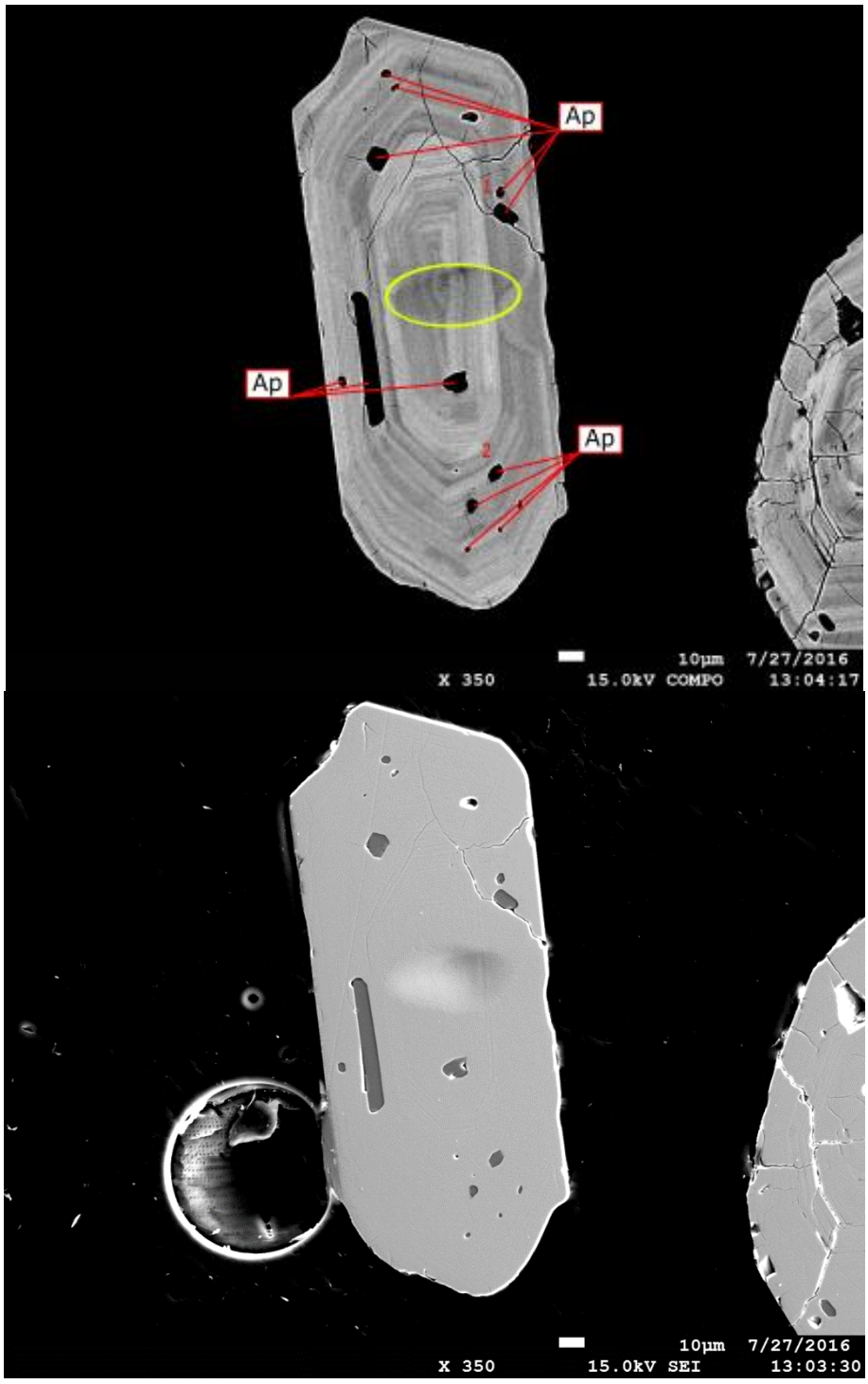
Ap
Ap
Ap
1
2
X 350
10µm 7/27/2016
15.0kV COMPO 13:04:17
X 350
10µm 7/27/2016
15.0kV SEI 13:03:30

1

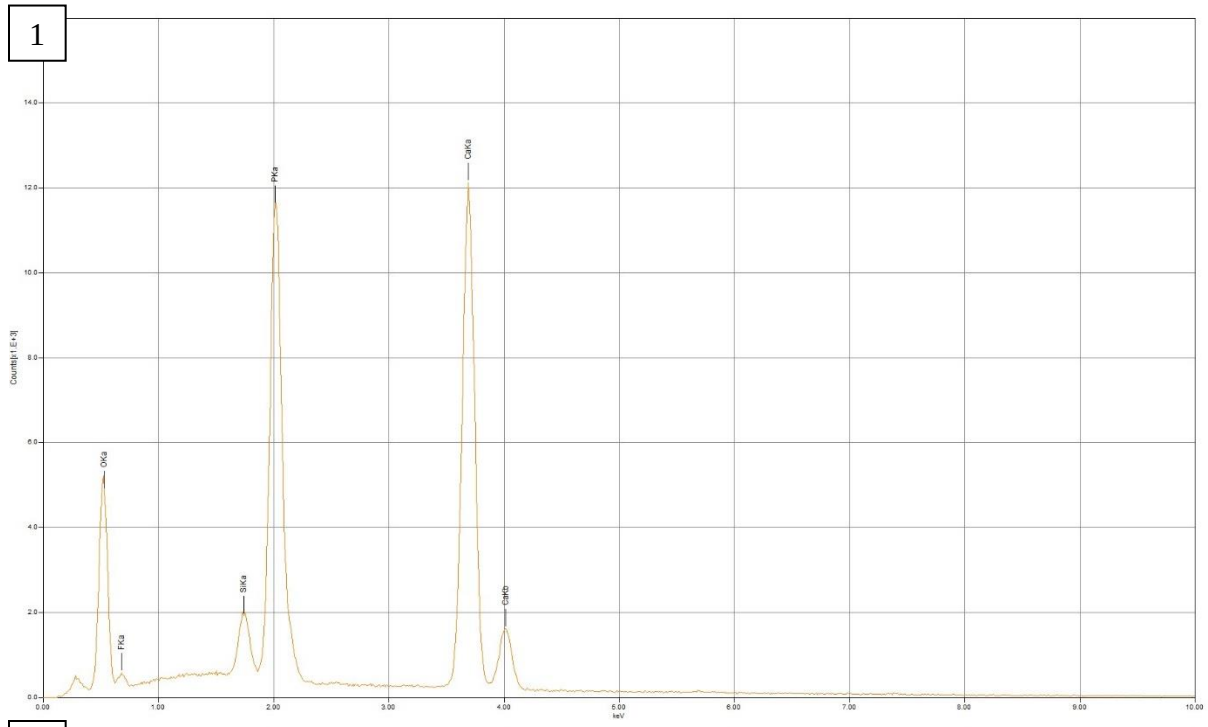
OKa
FKa
SiKa
PKa
CaKa
CaKb
keV

2

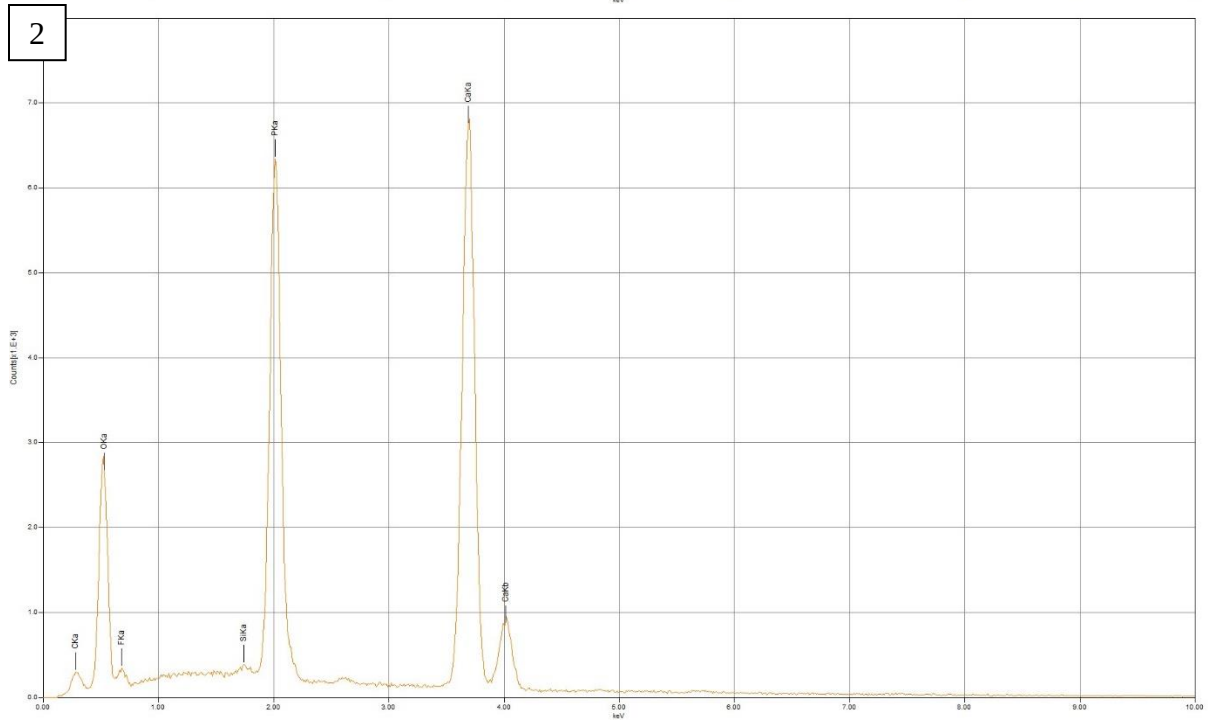
CKa
OKa
FKa
SiKa
PKa
CaKa
CaKb
keV

Grain 30

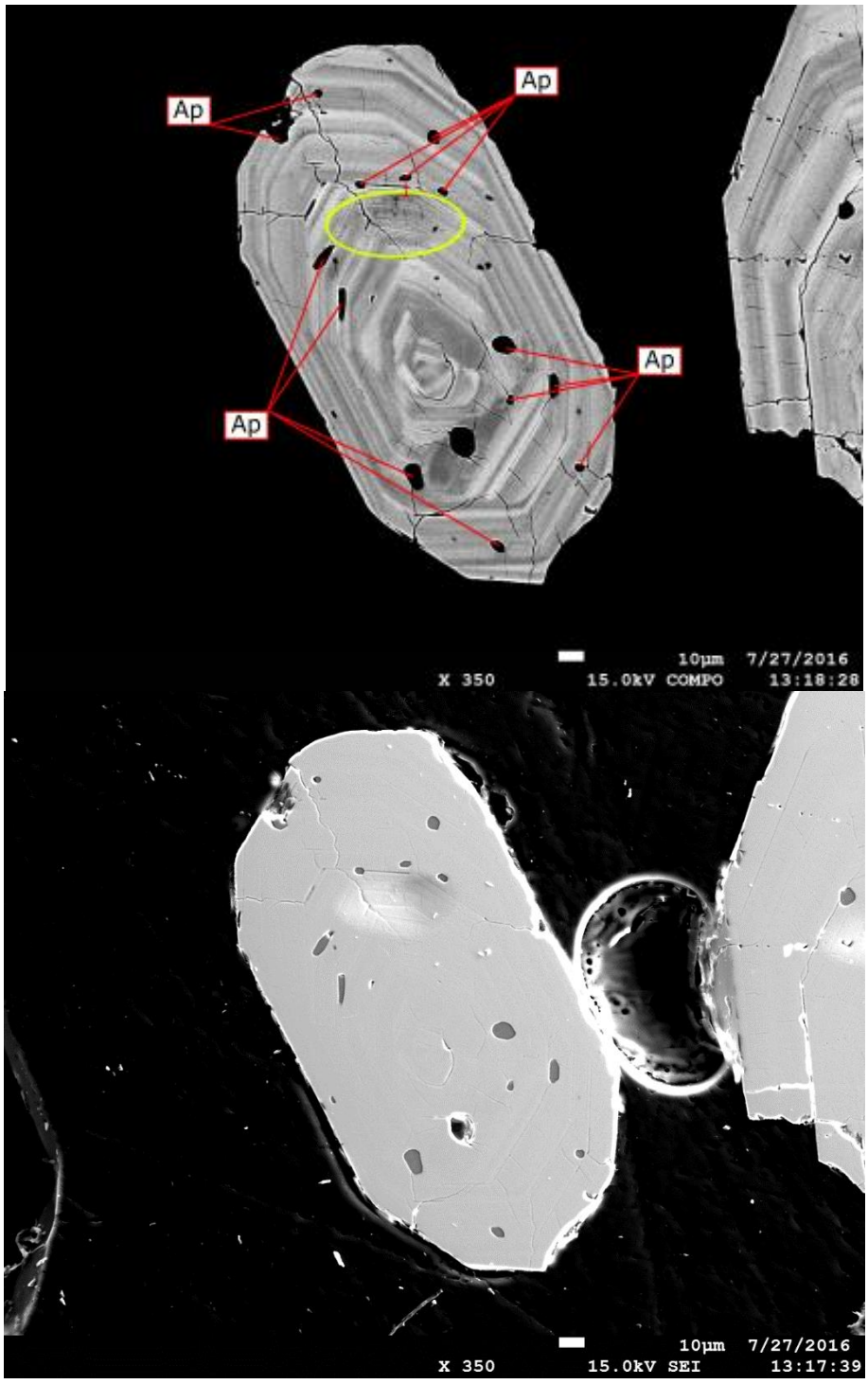
Ap
Ap
Ap
Ap
X 350
10µm
15.0kV COMPO
7/27/2016
13:16:28
X 350
10µm
15.0kV SEI
7/27/2016
13:17:39

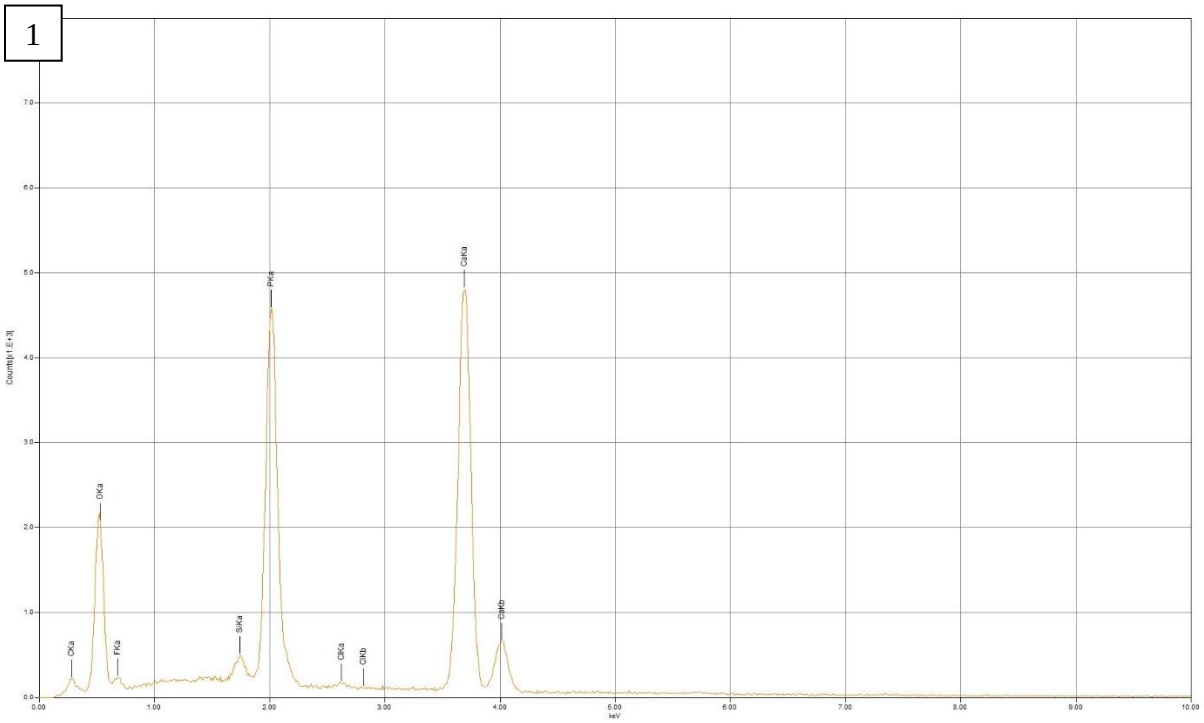
1
Counts[n.f.x.]
OKa
FKa
SiKa
PKa
CaKa
ClKb
keV

Grain 32

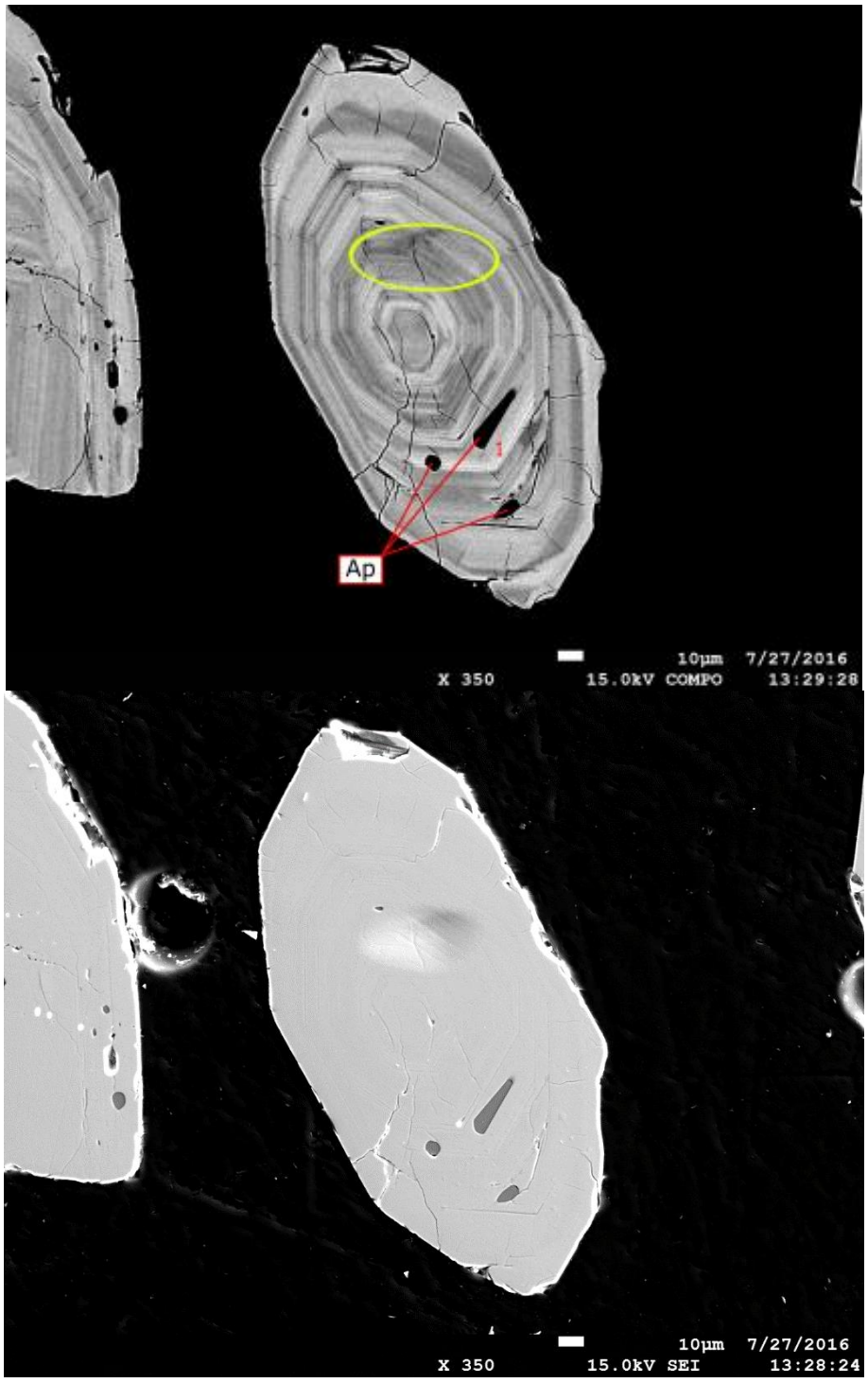
1
Ap
10µm 7/27/2016
X 350 15.0kV COMPO 13:29:28
10µm 7/27/2016
X 350 15.0kV SEI 13:28:24

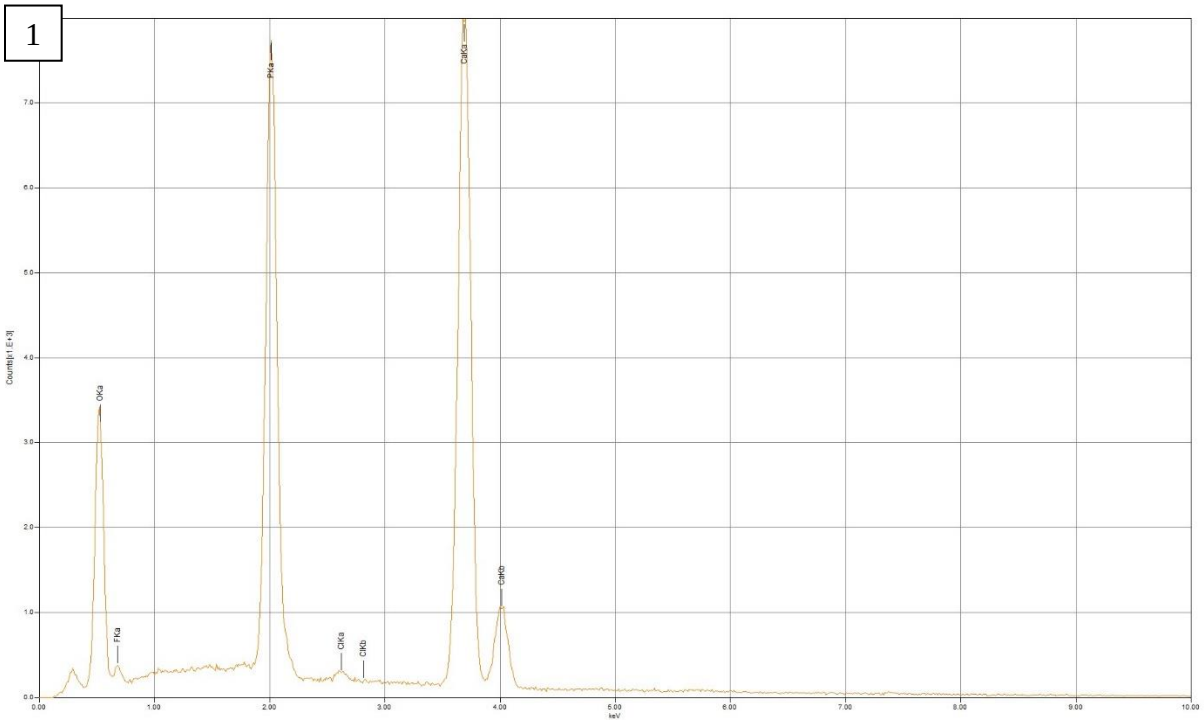
1
OKa
FKa
PKa
CaKa
ClKa
ClKb
CaKb
Counts[n.t.e.s]
keV

Grain 33


Ap
Ap
1
2
X 300
10µm 7/27/2016
15.0kV COMPO 13:34:06
X 300
10µm 7/27/2016
15.0kV SEI 13:33:15

1

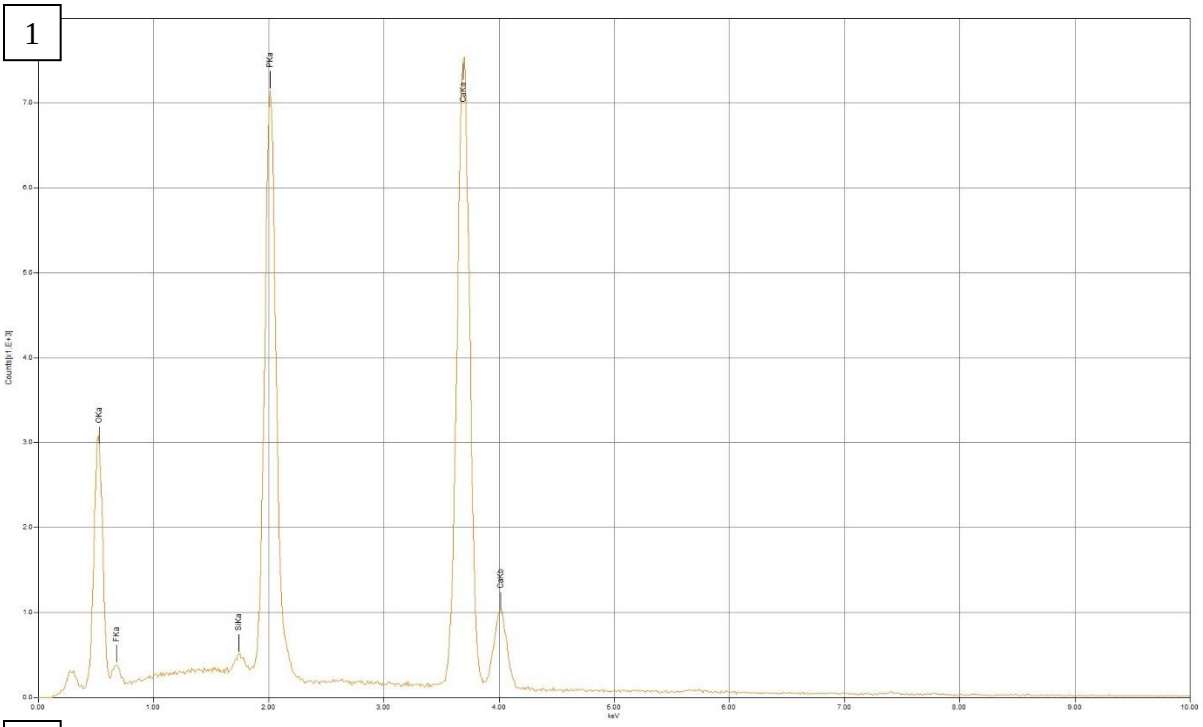
PKa
CaKa
OKa
FKa
SiKa
CaKb
Counts[x1 E+3]
keV

2

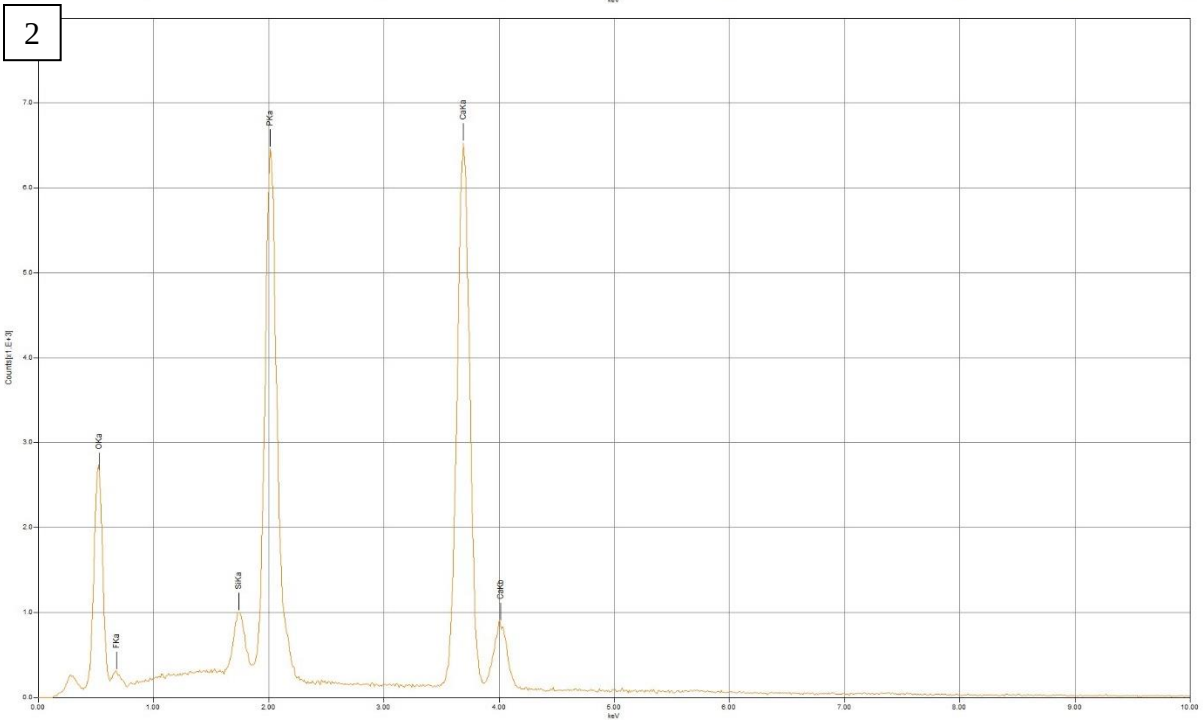
PKa
CaKa
OKa
FKa
SiKa
CaKb
Counts[x1 E+3]
keV

Grain 34

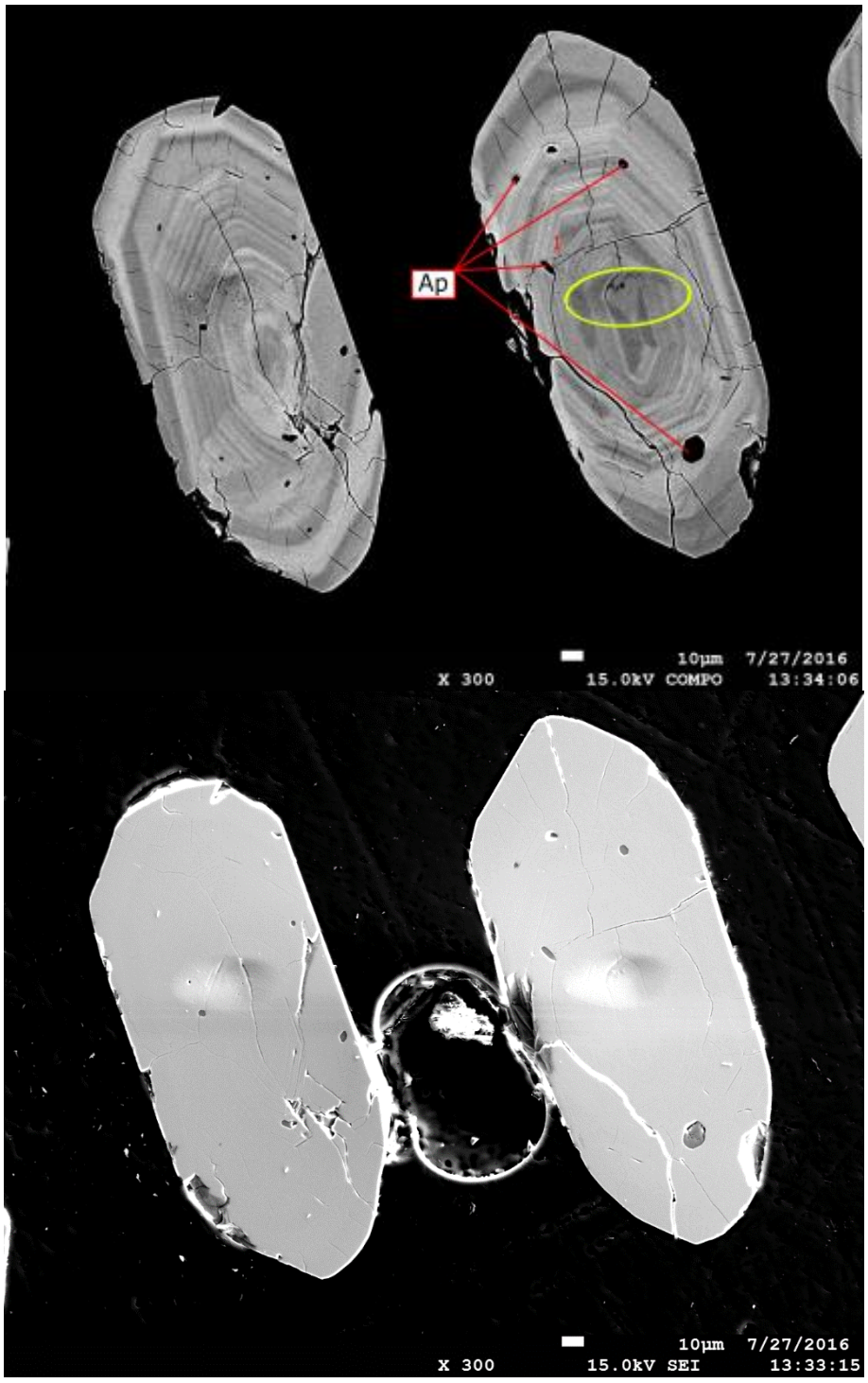
Ap
X 300
10µm 7/27/2016
15.0kV COMPO 13:34:06
X 300
10µm 7/27/2016
15.0kV SEI 13:33:15

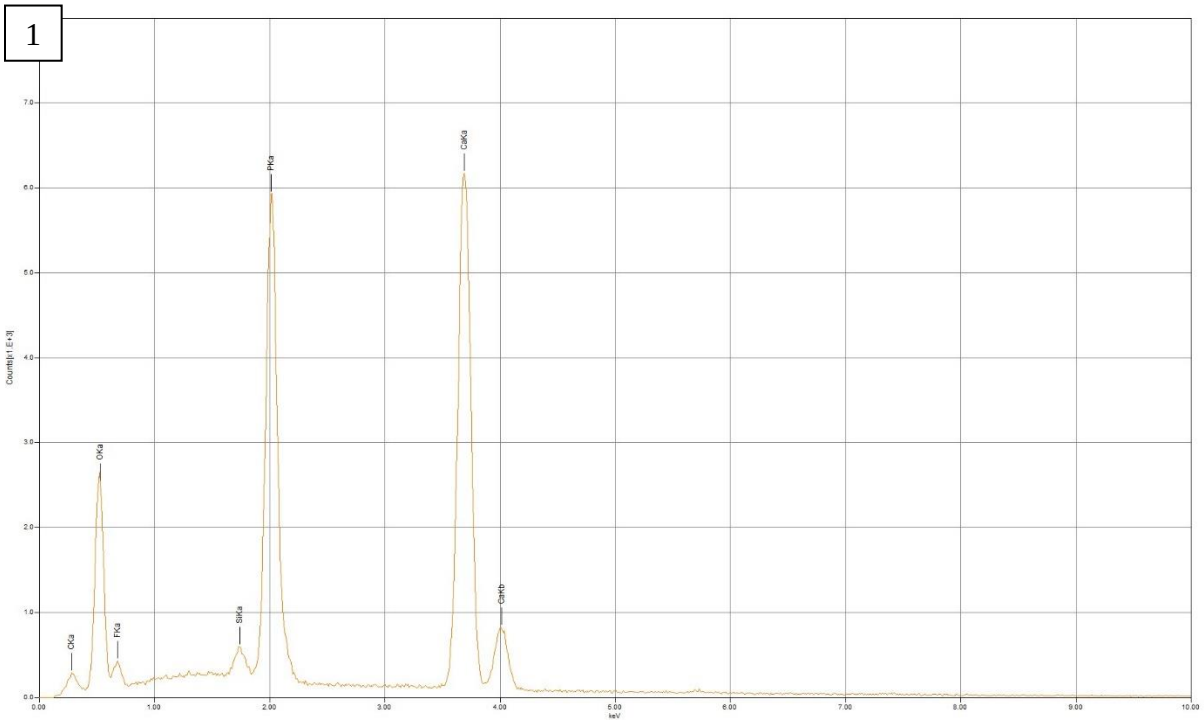
1
CKa
OKa
FKa
SiKa
PKa
CaKa
CaKb
Counts[n.Ex3]
keV

Grain 35

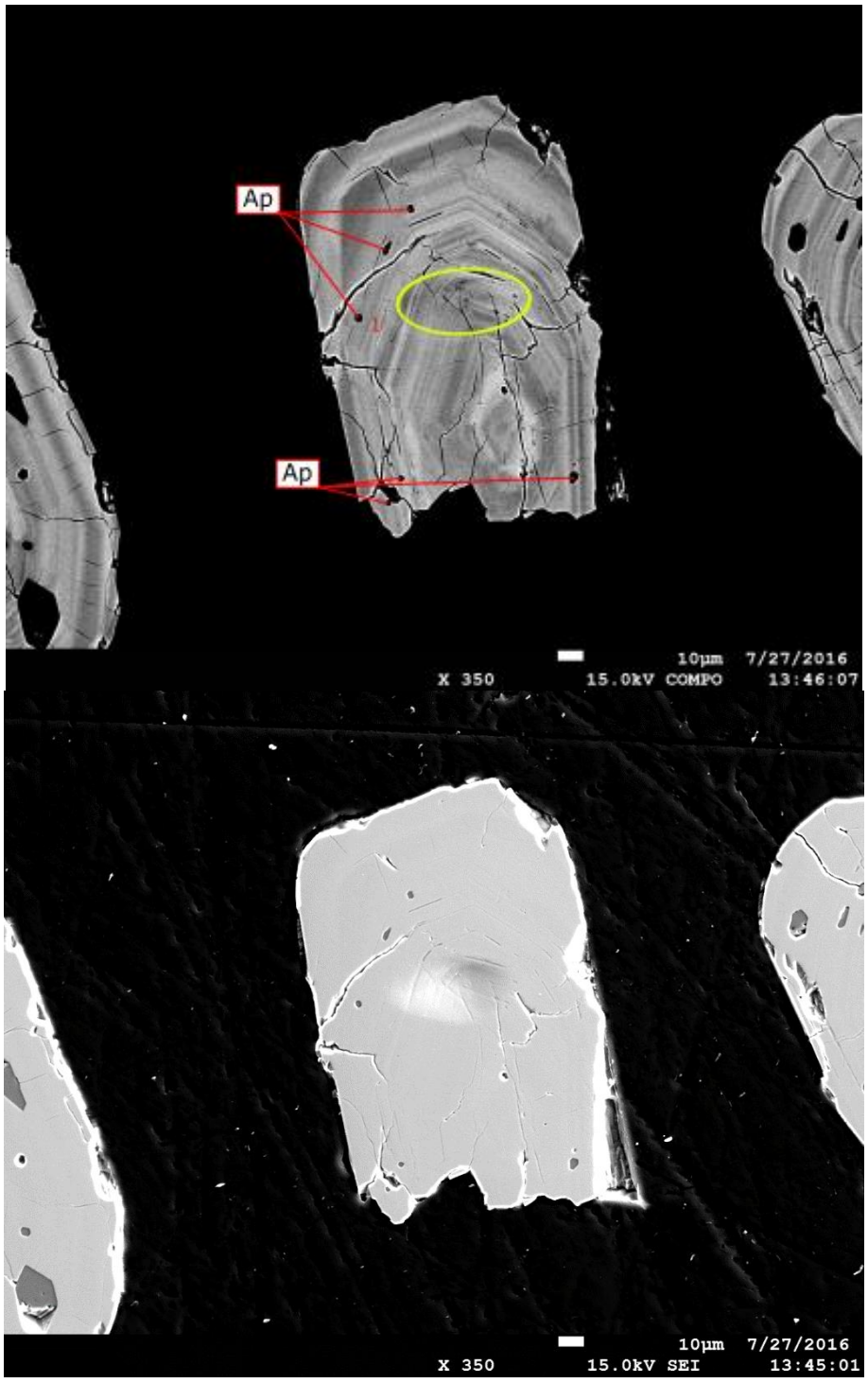
Ap
Ap
X 350
10µm
15.0kV COMPO
7/27/2016
13:46:07
X 350
10µm
15.0kV SEI
7/27/2016
13:45:01

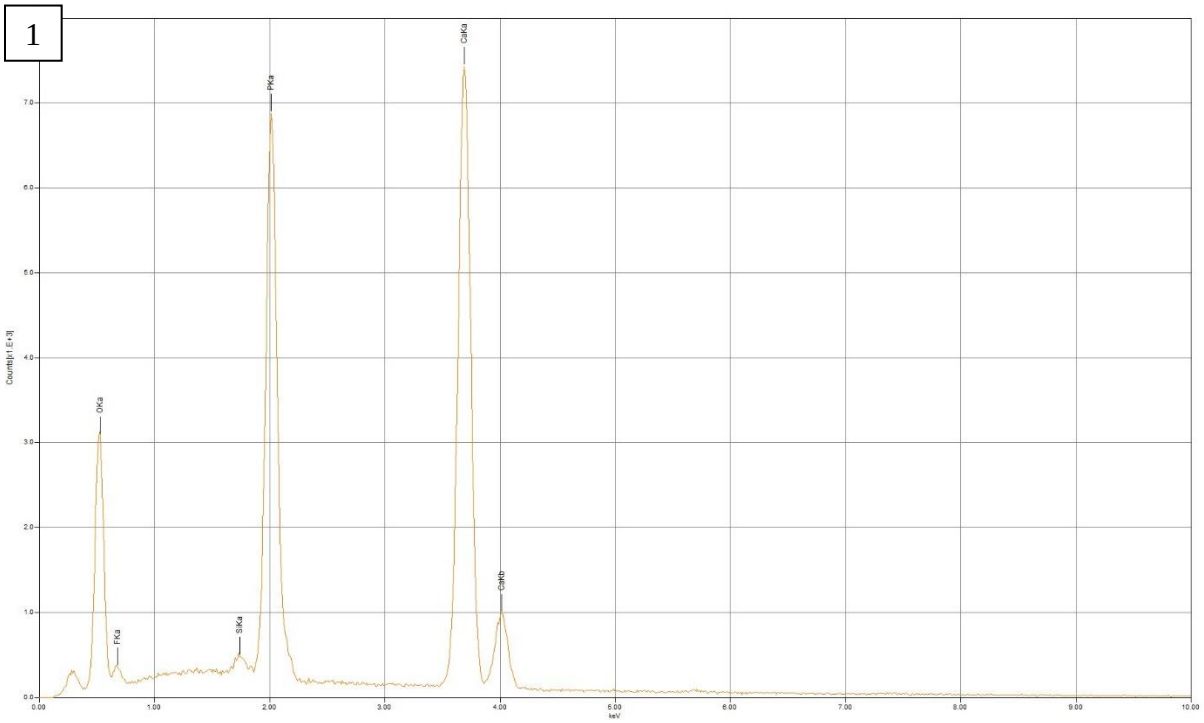
1
CaKa
PKa
OKa
FKa
SiKa
CaKb
Counts[n.f.x.]
keV

Grain 37

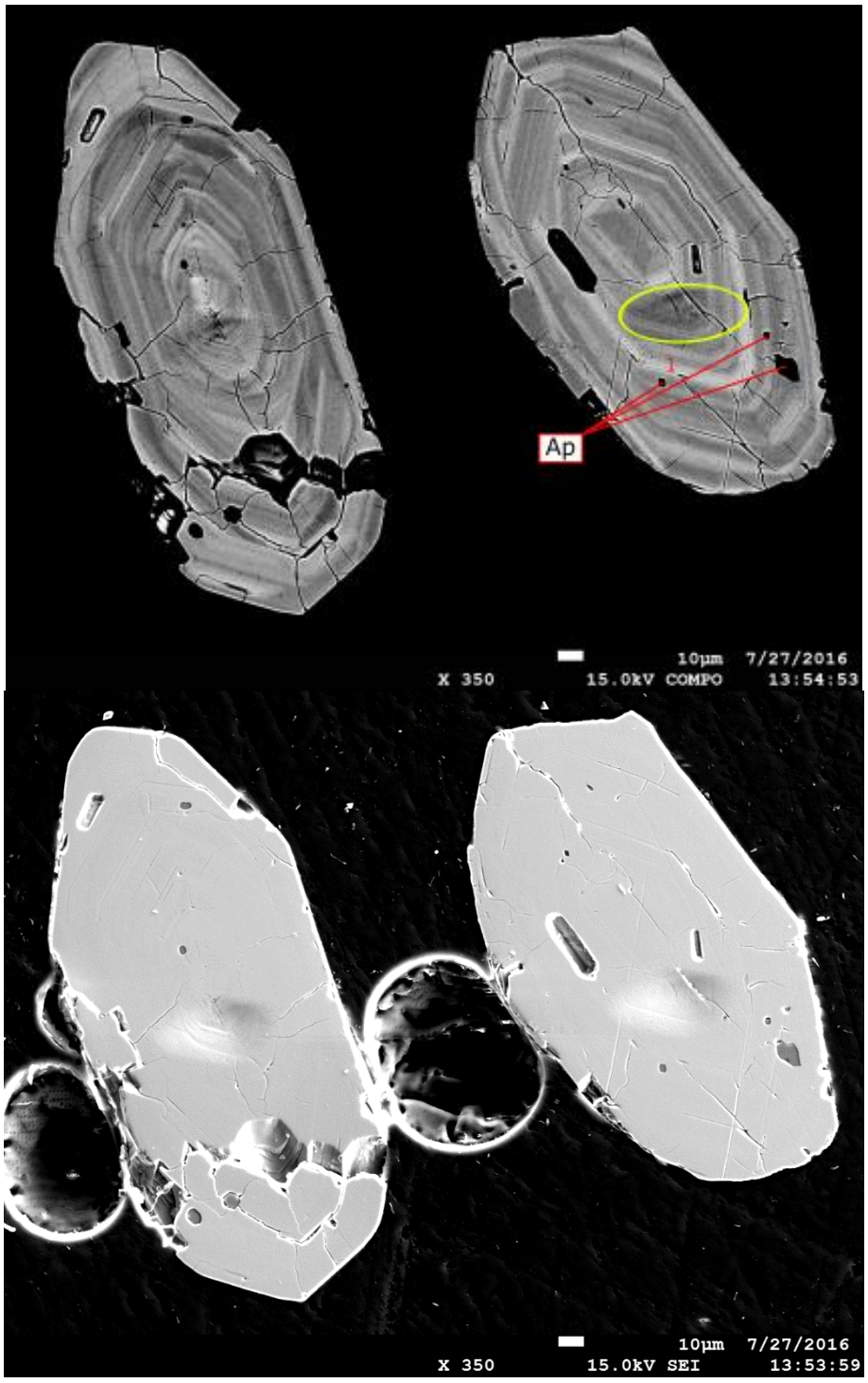
Ap
X 350
10µm 7/27/2016
15.0kV COMPO 13:54:53
X 350
10µm 7/27/2016
15.0kV SEI 13:53:59

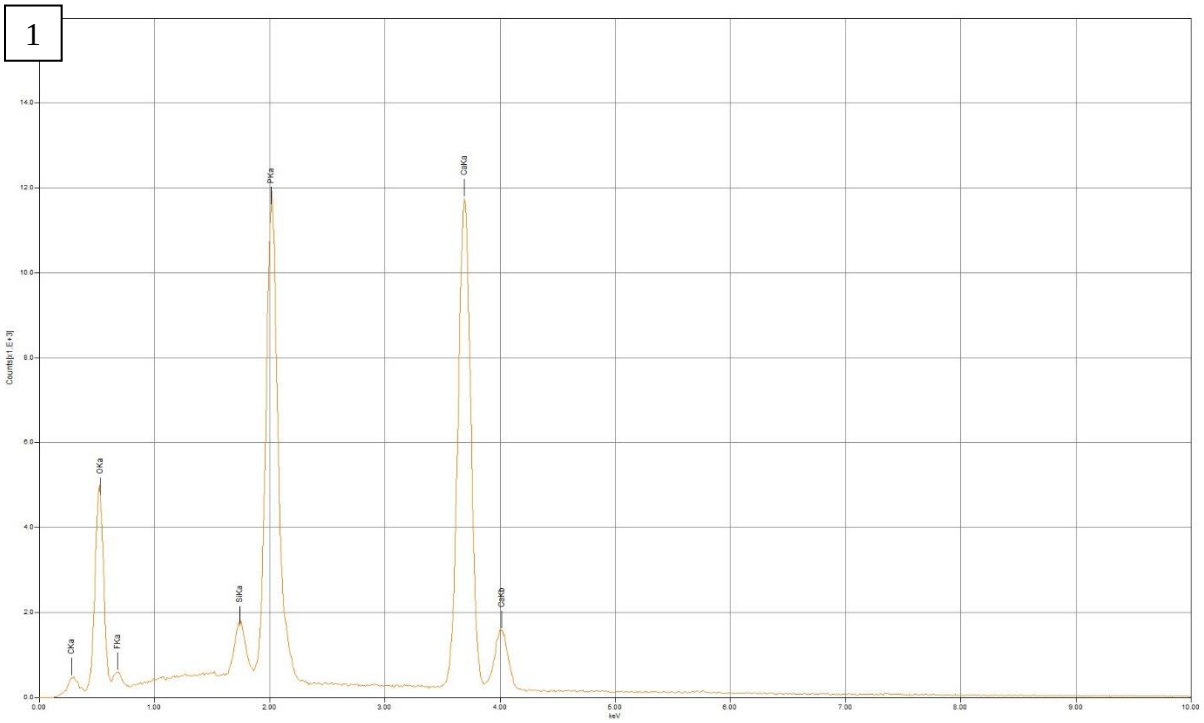
1
CKa
OKa
FKa
SiKa
PKa
CaKa
CaKb
keV

Grain 38

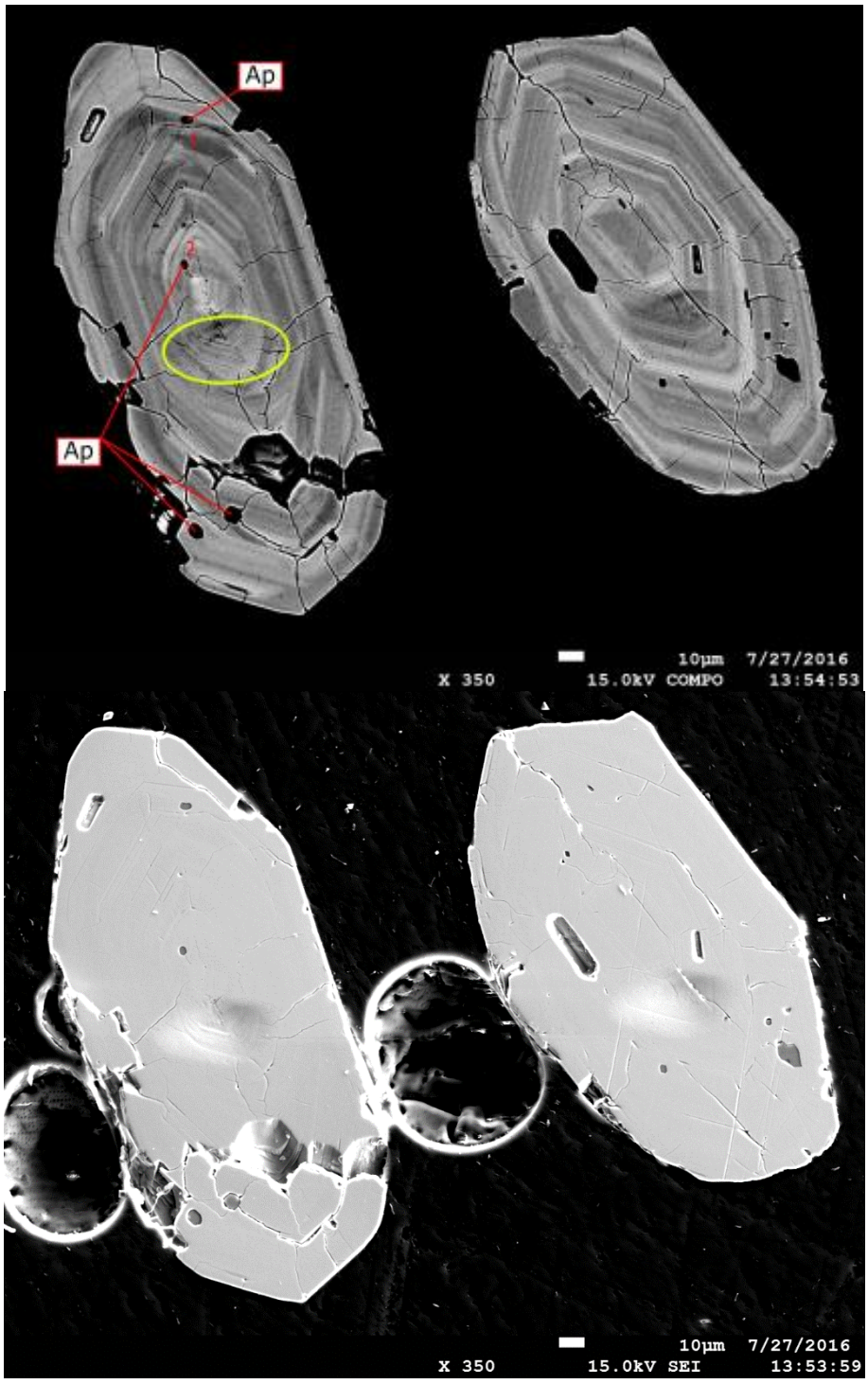
Ap
Ap
X 350
10µm 7/27/2016
15.0kV COMPO 13:54:53
X 350
10µm 7/27/2016
15.0kV SEI 13:53:59

1

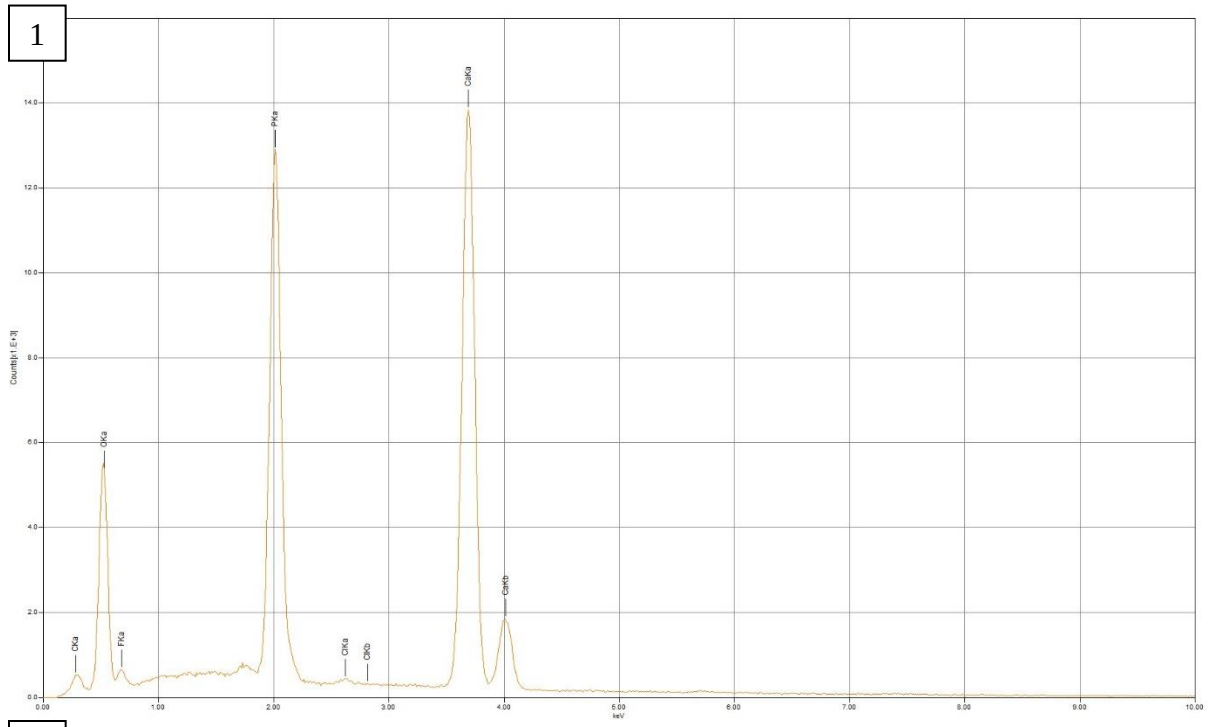
CaKa
PKa
OKa
CKa
CaKb
OKb
FKa
Counts[x1 E+3]
keV

2

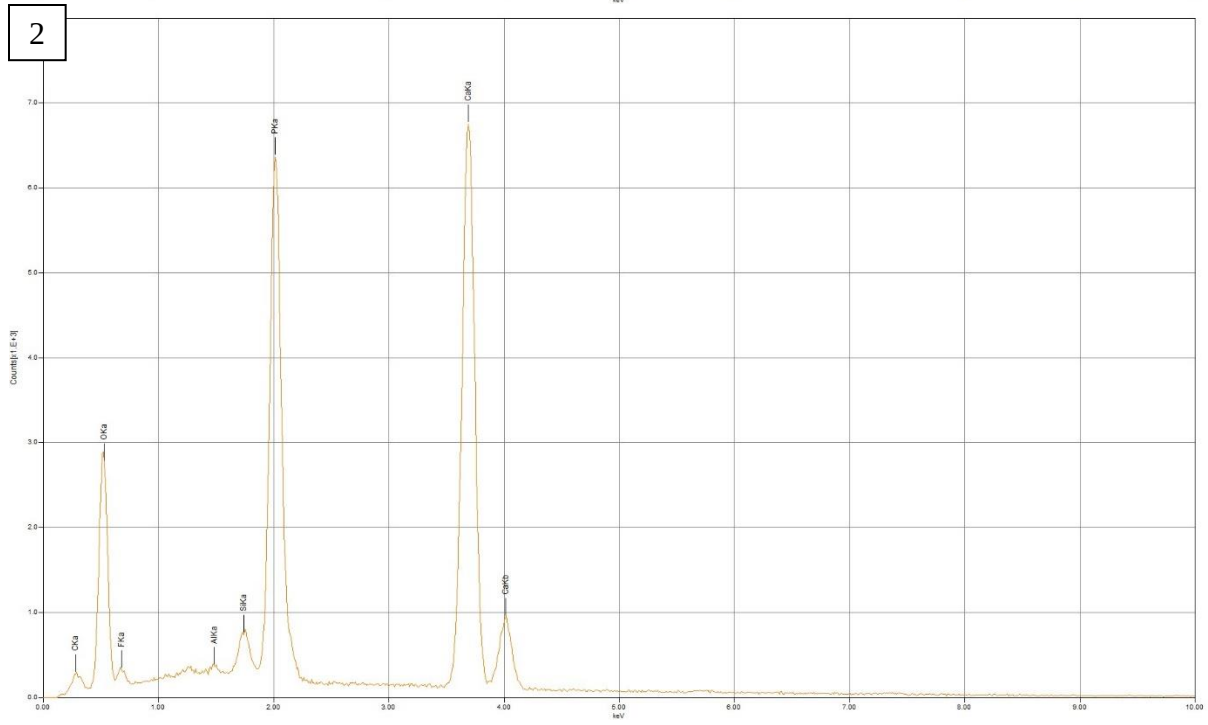
CaKa
PKa
OKa
SiKa
CaKb
AlKa
FKa
CKa
Counts[x1 E+3]
keV

Grain 39

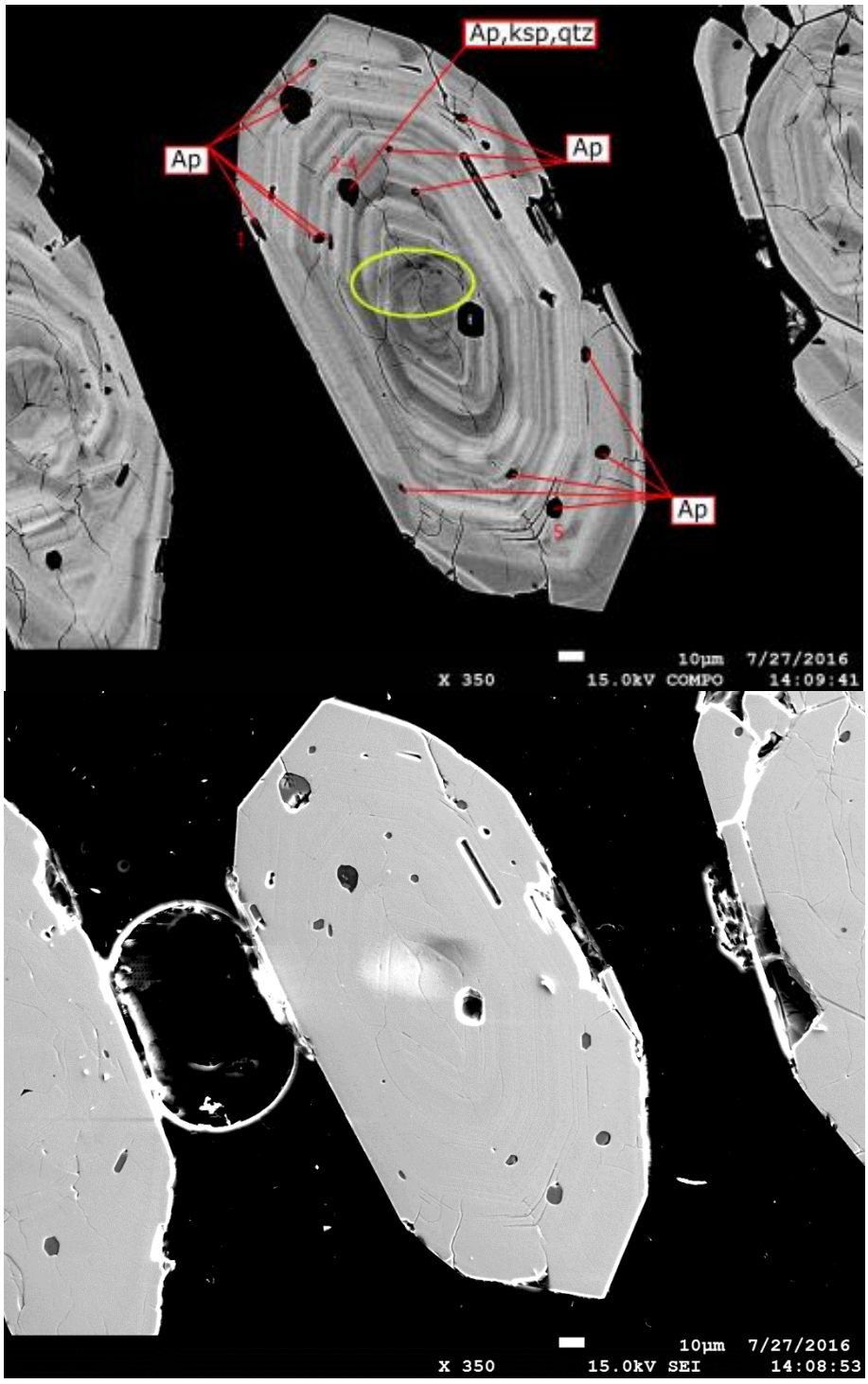
Ap,ksp,qtz
Ap
Ap
Ap
1
2
5
X 350
10µm
15.0kV COMPO
7/27/2016
14:09:41
X 350
10µm
15.0kV SEI
7/27/2016
14:08:53

1

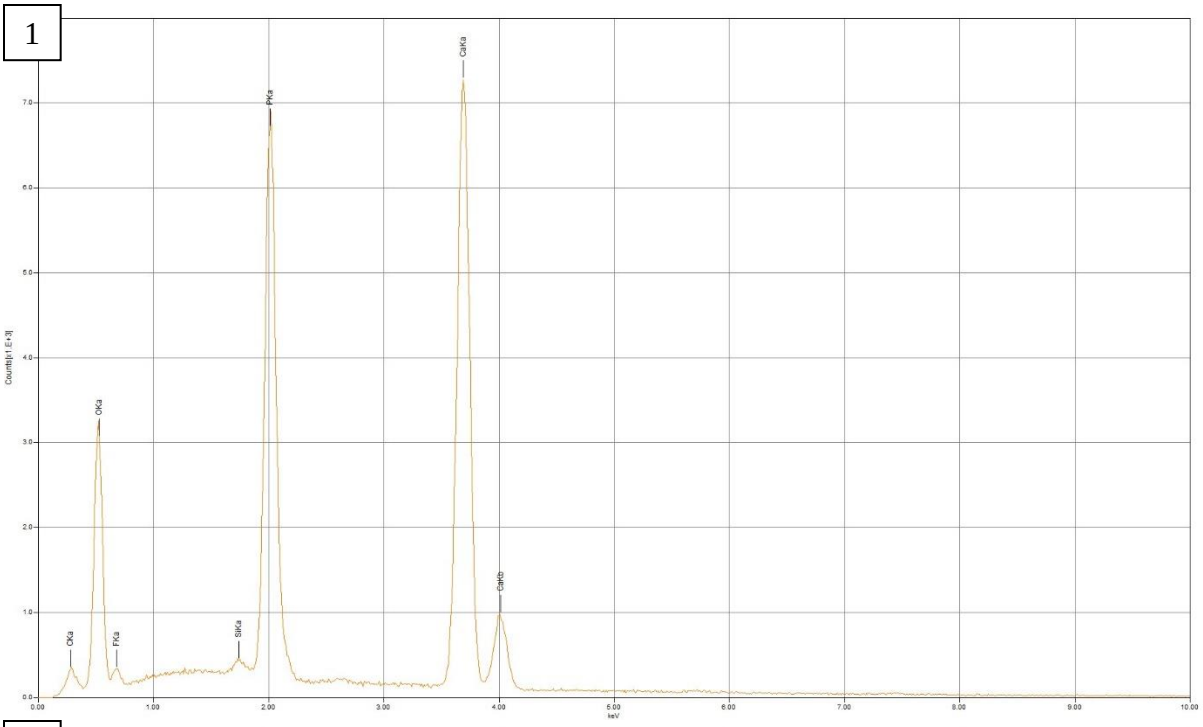
CaKa
PKa
OKa
CaKb
OKa
FKa
SiKa
keV

2

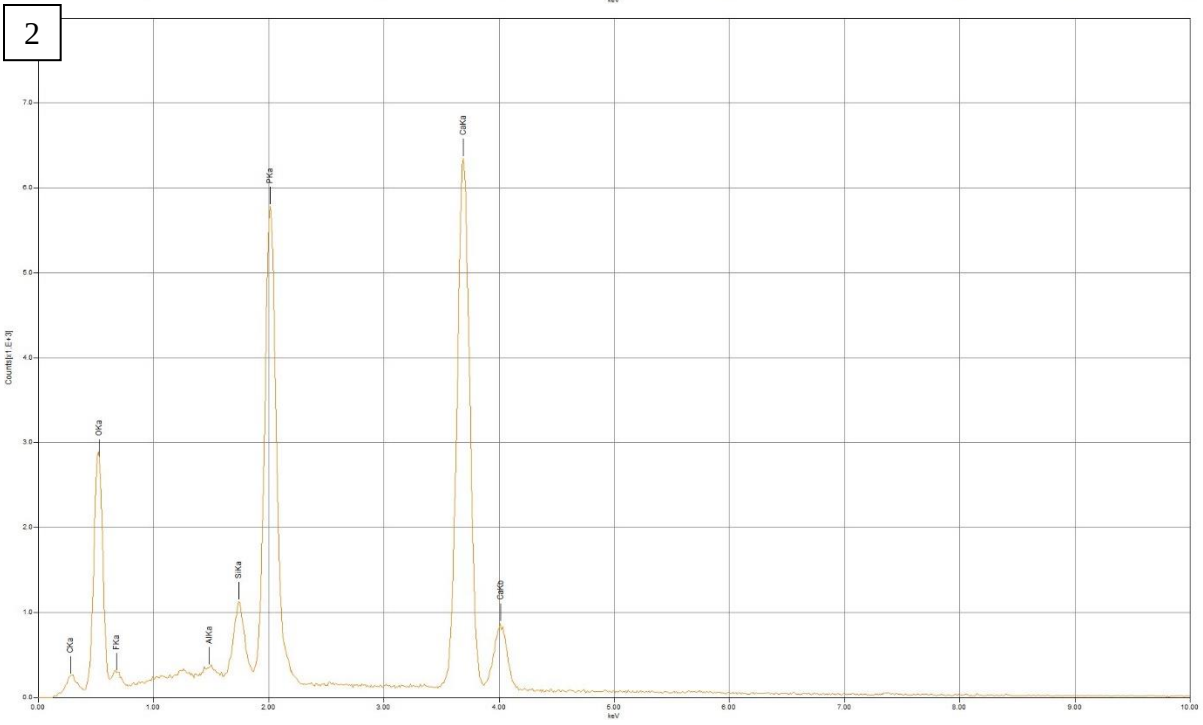
CaKa
PKa
OKa
SiKa
CaKb
OKa
FKa
AlKa
keV

3

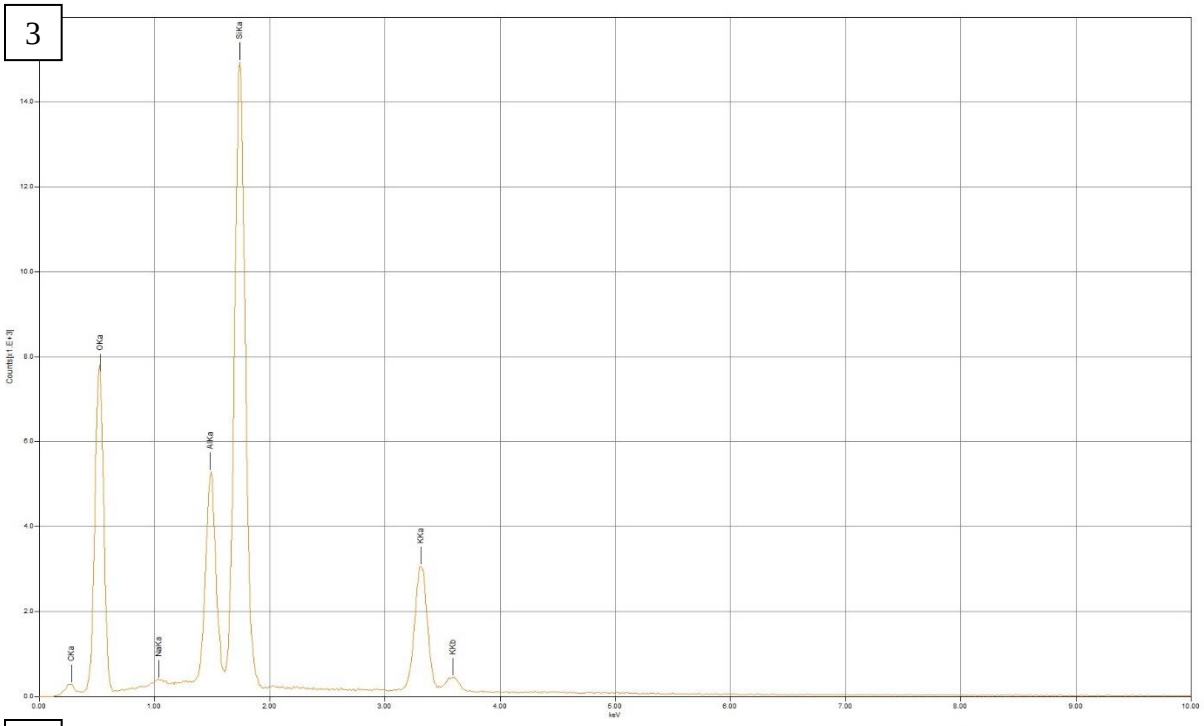
SiKa
OKa
AlKa
KKa
CKa
NaKa
KKb
Counts[x1 E+3]
keV

4

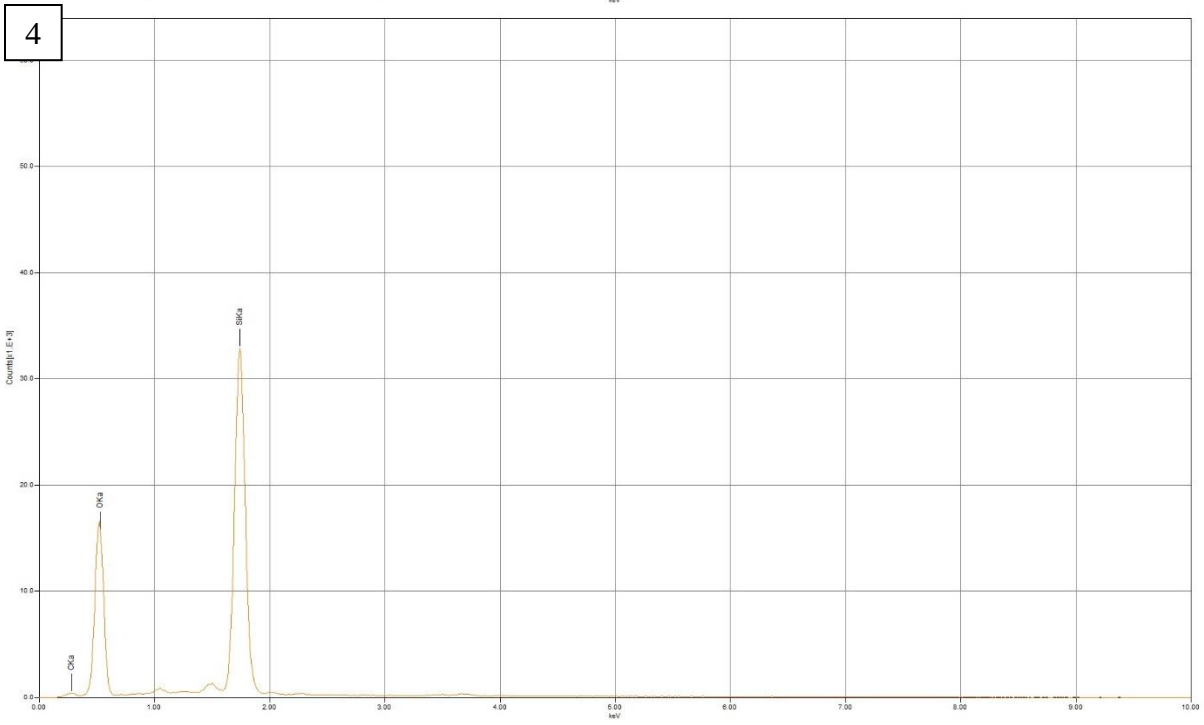
SiKa
OKa
CKa
Counts[x1 E+3]
keV

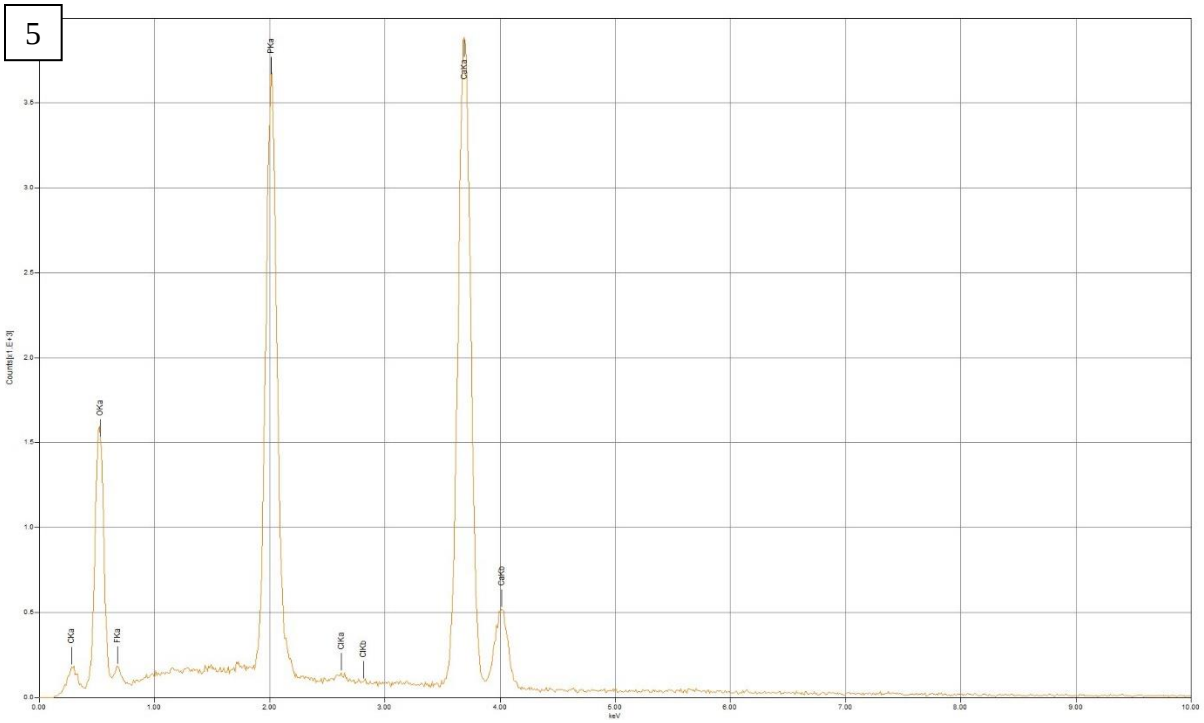
5
PKa
CaKa
OKa
CKa
FKa
CKb
CaKb
Counts[n.E.x]
keV

Grain 41


2-4
Fe-Ti,Ap
1
Ap
Ap
10µm 7/27/2016
X 300 15.0kV COMPO 14:26:31
10µm 7/27/2016
X 300 15.0kV SEI 14:25:43

1

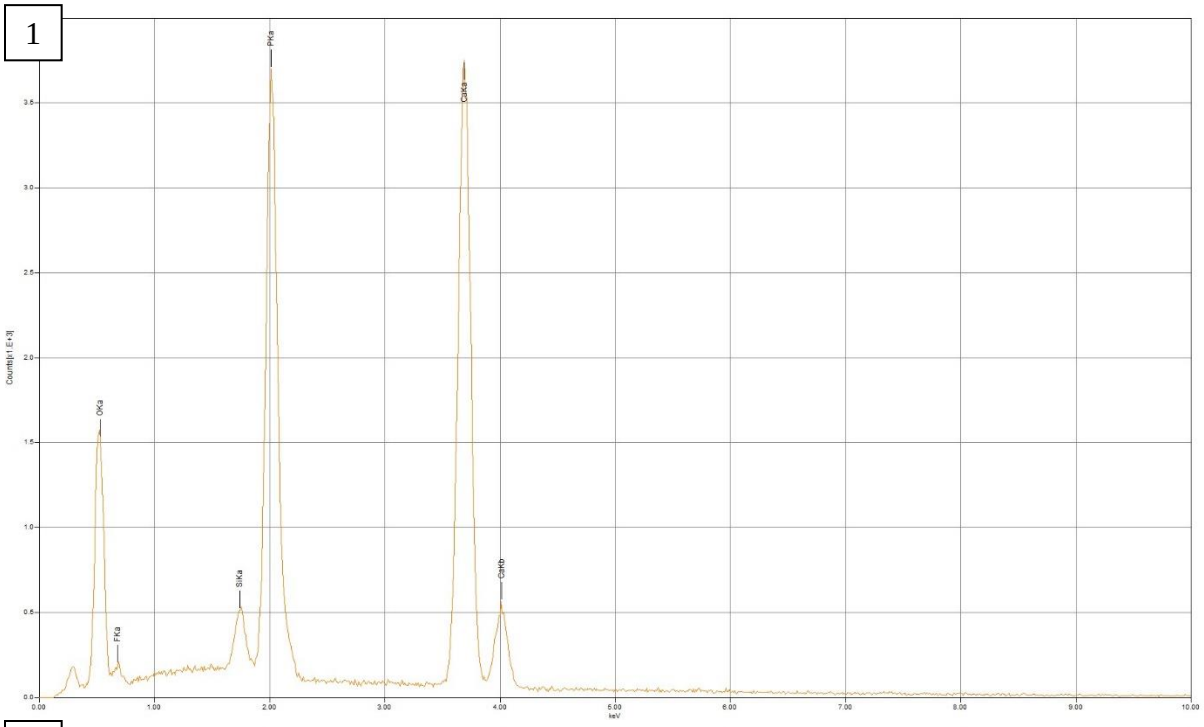
PKa
CaKa
OKa
SiKa
CaKb
FKa
Counts[x1 E+3]
keV

2

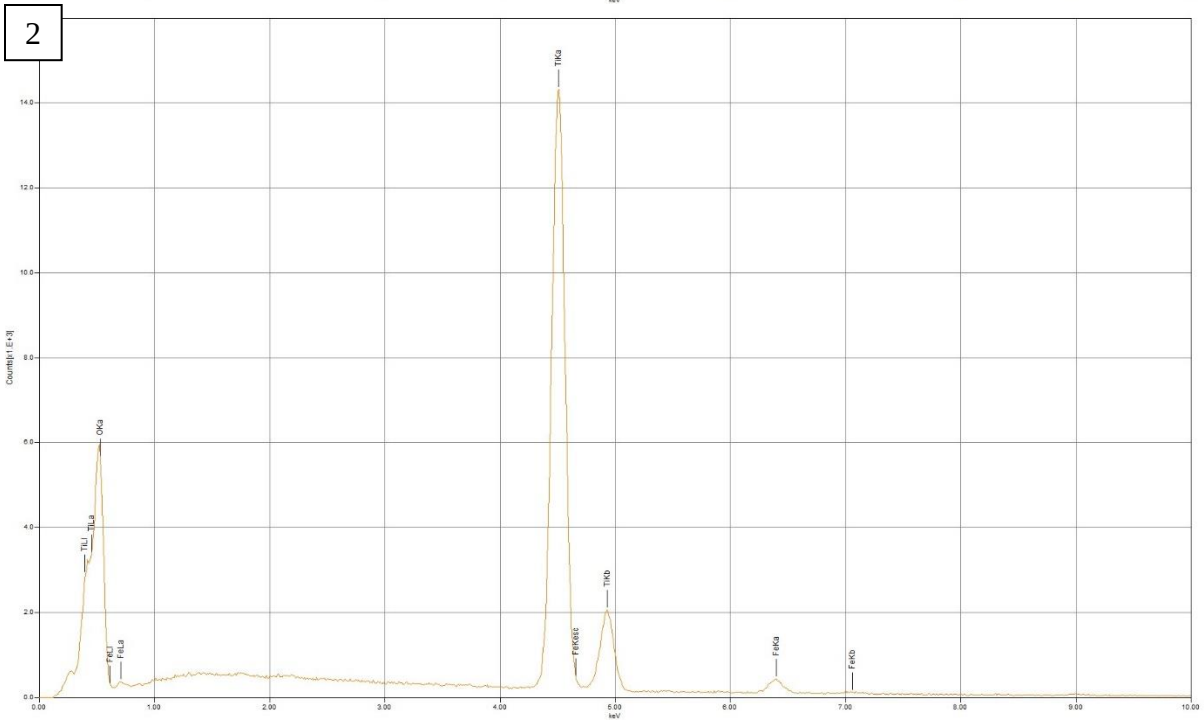
TiKa
OKa
TiLa
TiLl
FeLl
FeLa
TiKb
FeKa
FeKb
Counts[x1 E+3]
keV

4

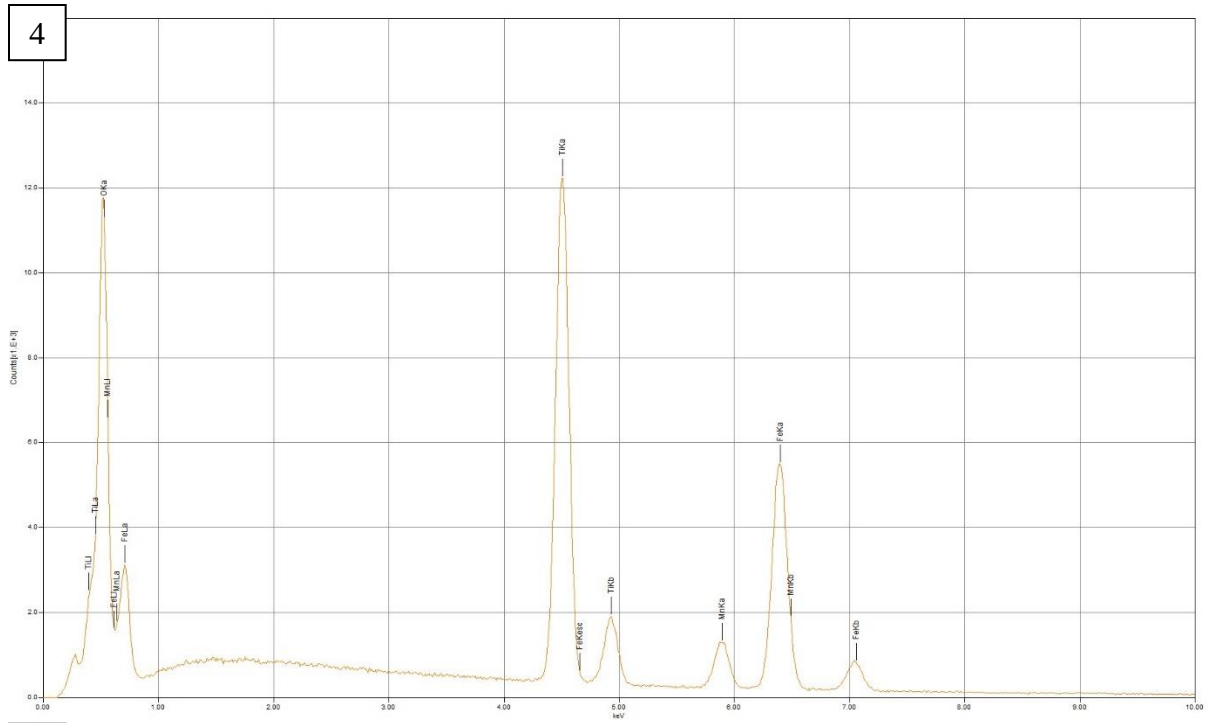
OKa
MnLl
TiLa
TiLl
FeLa
FeLl
MnLa
TiKa
FeKbSat
TiKb
MnKa
FeKa
MnKb
FeKb
Counts[n1 E+3]
keV

3

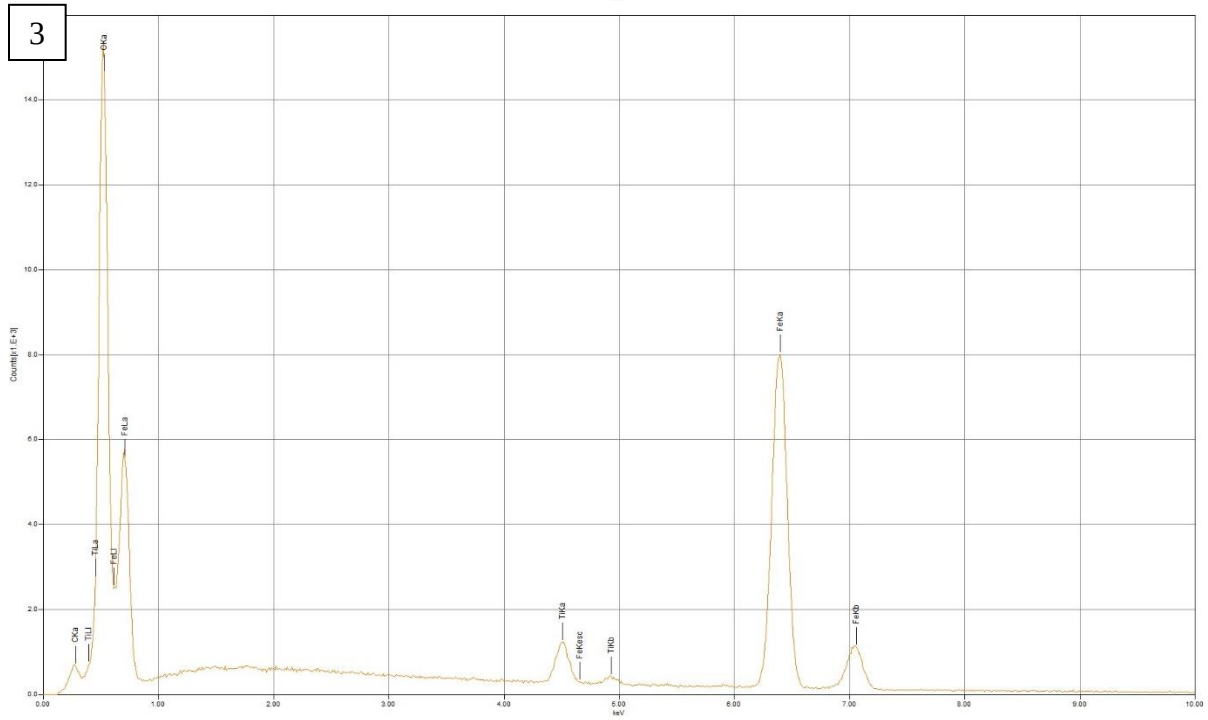
OKa
MnLl
TiLa
TiLl
FeLa
FeLl
OKa
TiLl
TiLa
FeLl
FeLa
TiKa
FeKbsc
TiKb
FeKa
FeKb
Counts[n1 E+3]
keV

Grain 42


Ap
Ap
X 300
10µm 7/27/2016
15.0kV COMPO 14:49:47
X 300
10µm 7/27/2016
15.0kV SEI 14:49:00

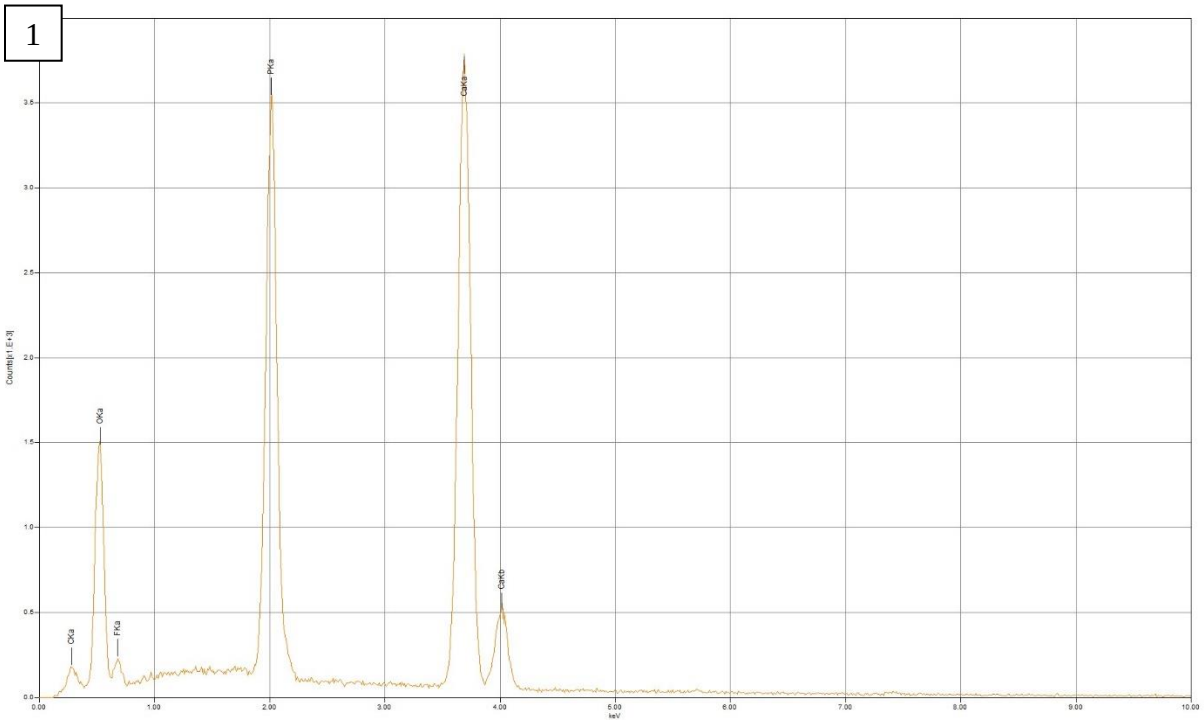
1
PKa
CaKa
OKa
FKa
CaKb
Counts[1.E+3]
keV

Grain 44


Ap
X 300
10µm 7/27/2016
15.0kV COMPO 14:59:50
X 300
10µm 7/27/2016
15.0kV SEI 14:59:00

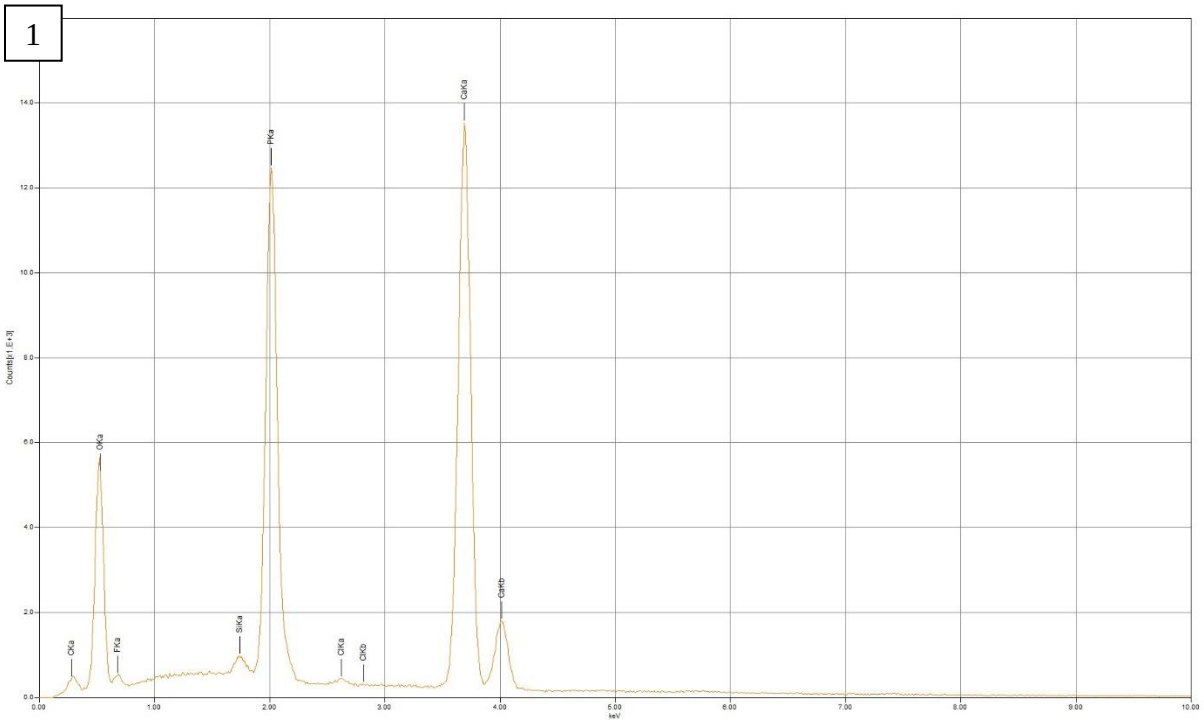
1
CKa
OKa
FKa
SiKa
PKa
ClKa
CaKa
CaKb
Counts[1 Ex:1]
keV

Grain 46

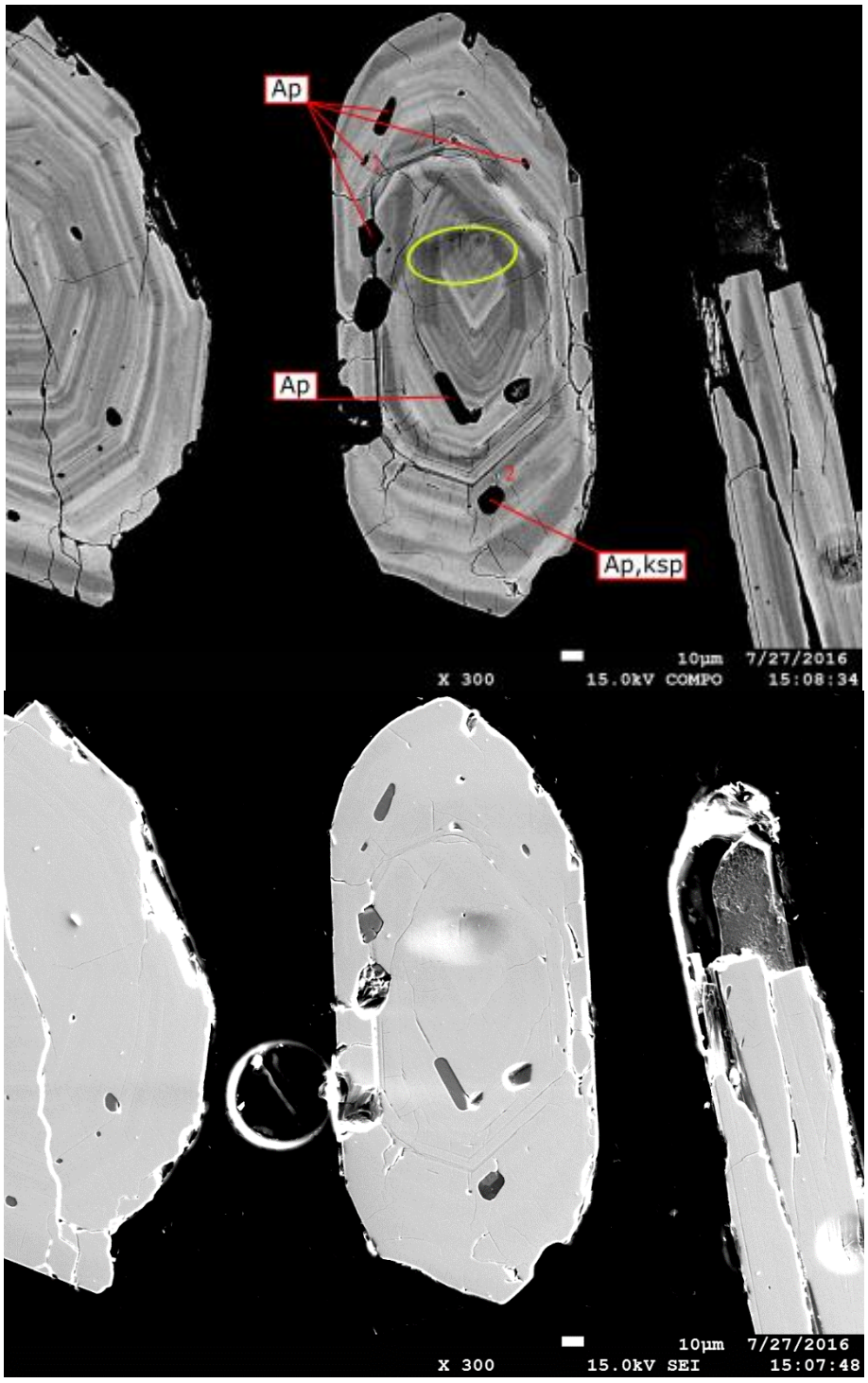
Ap
Ap
Ap,ksp
10µm 7/27/2016
X 300 15.0kV COMPO 15:08:34
10µm 7/27/2016
X 300 15.0kV SEI 15:07:48

1

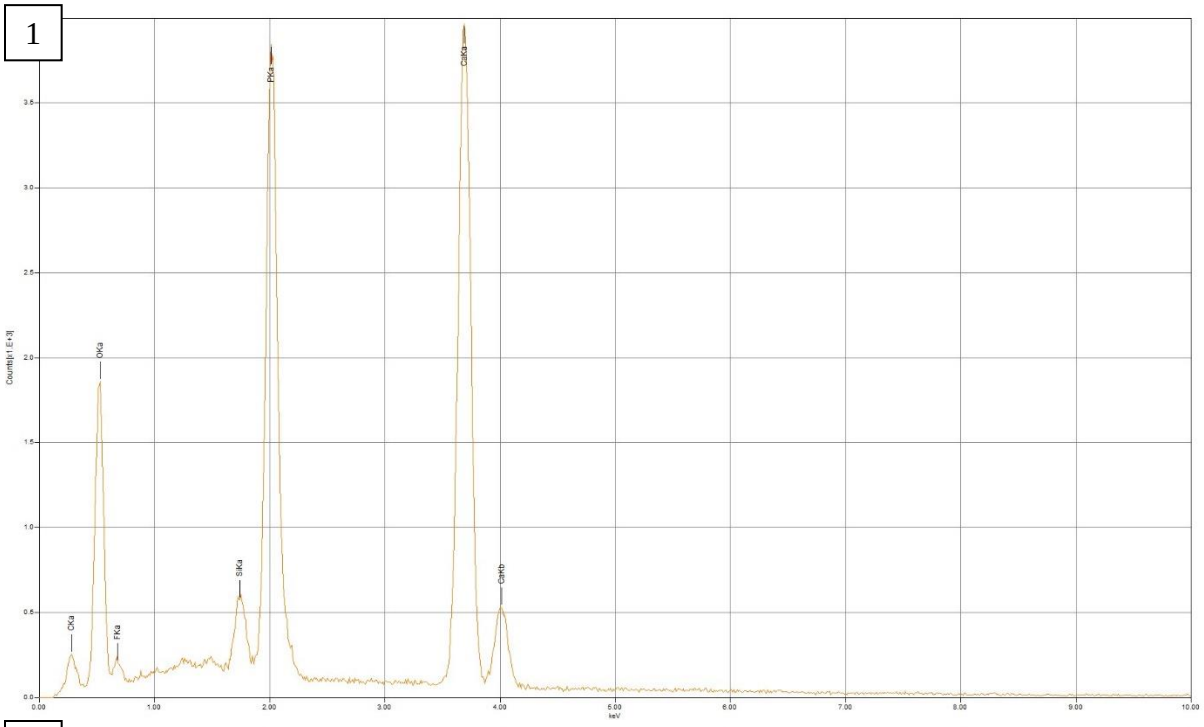
PKa
CaKa
OKa
SiKa
CaKb
CKa
FKa
Counts[x1 E+3]
keV

2

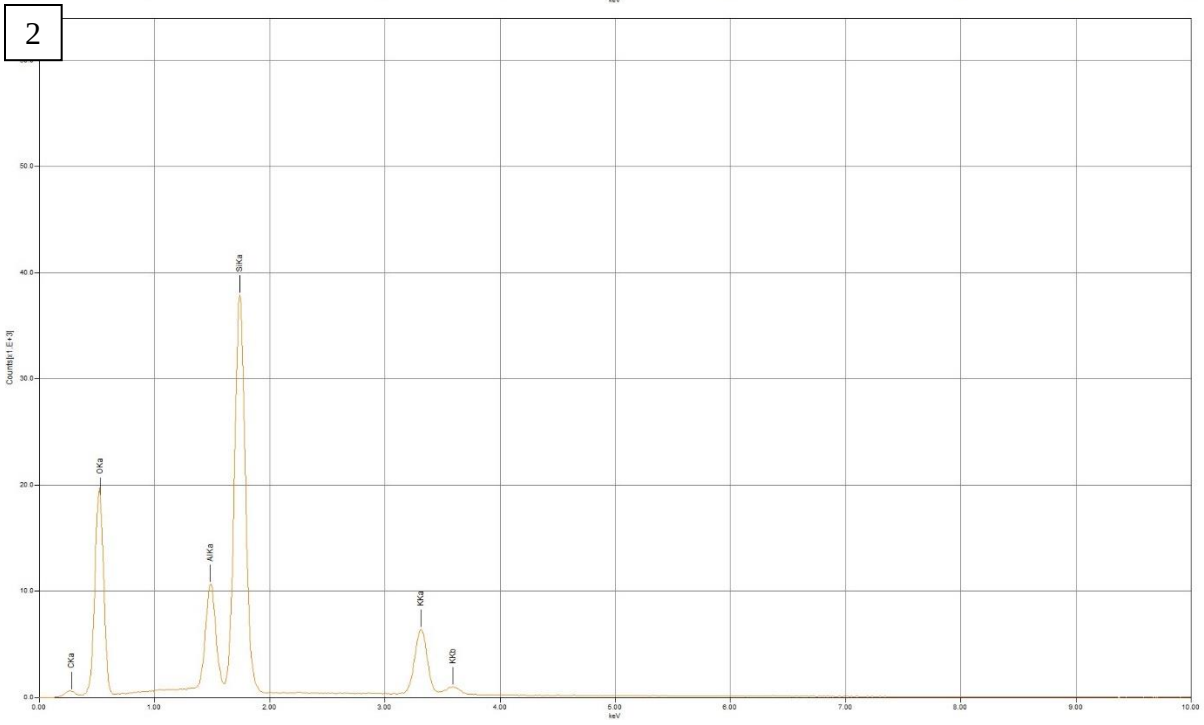
SiKa
OKa
AlKa
KKa
KKb
CKa
Counts[x1 E+3]
keV

Grain 48

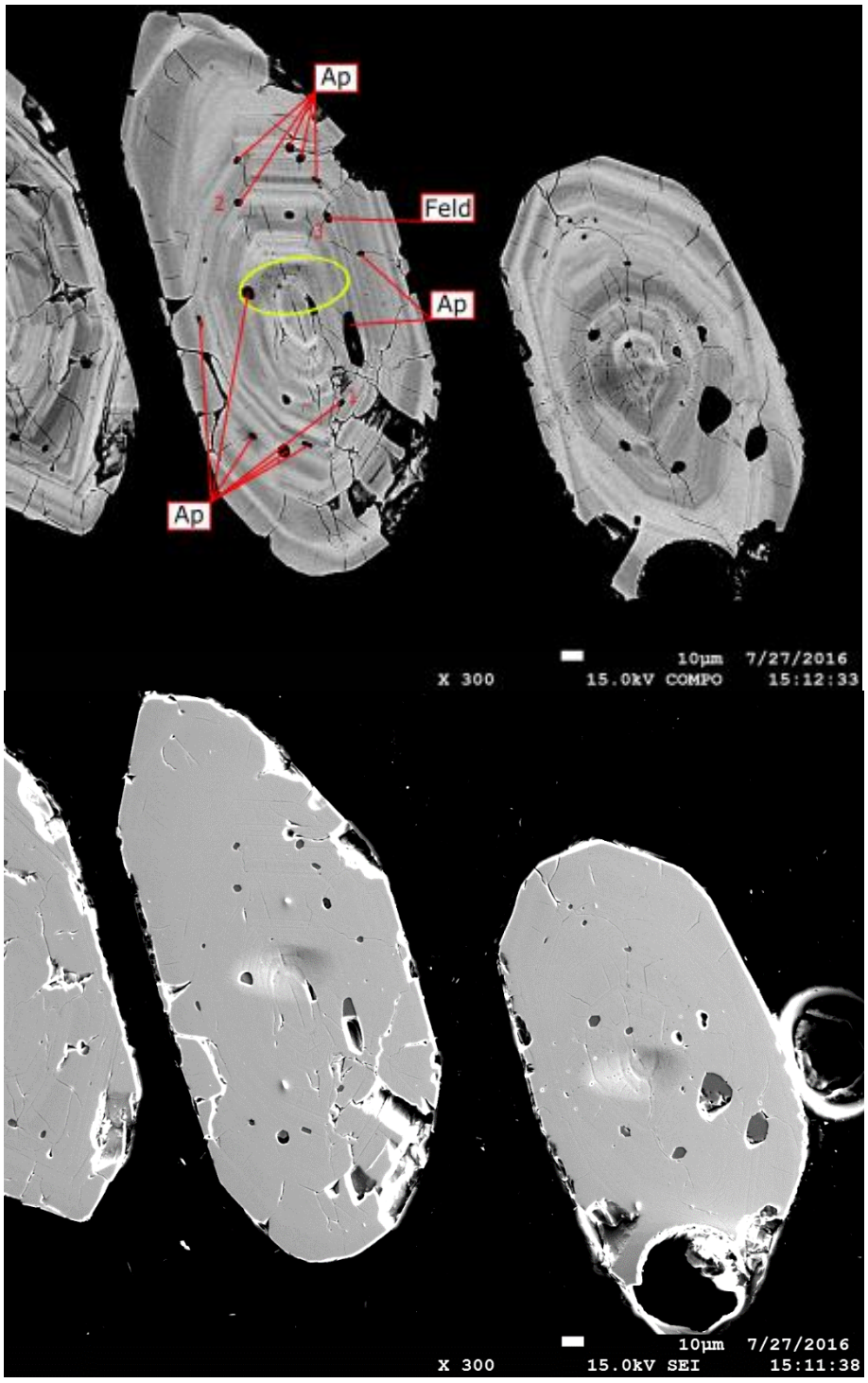
Ap
Feld
Ap
Ap
10µm 7/27/2016
X 300 15.0kV COMPO 15:12:33
10µm 7/27/2016
X 300 15.0kV SEI 15:11:38

1

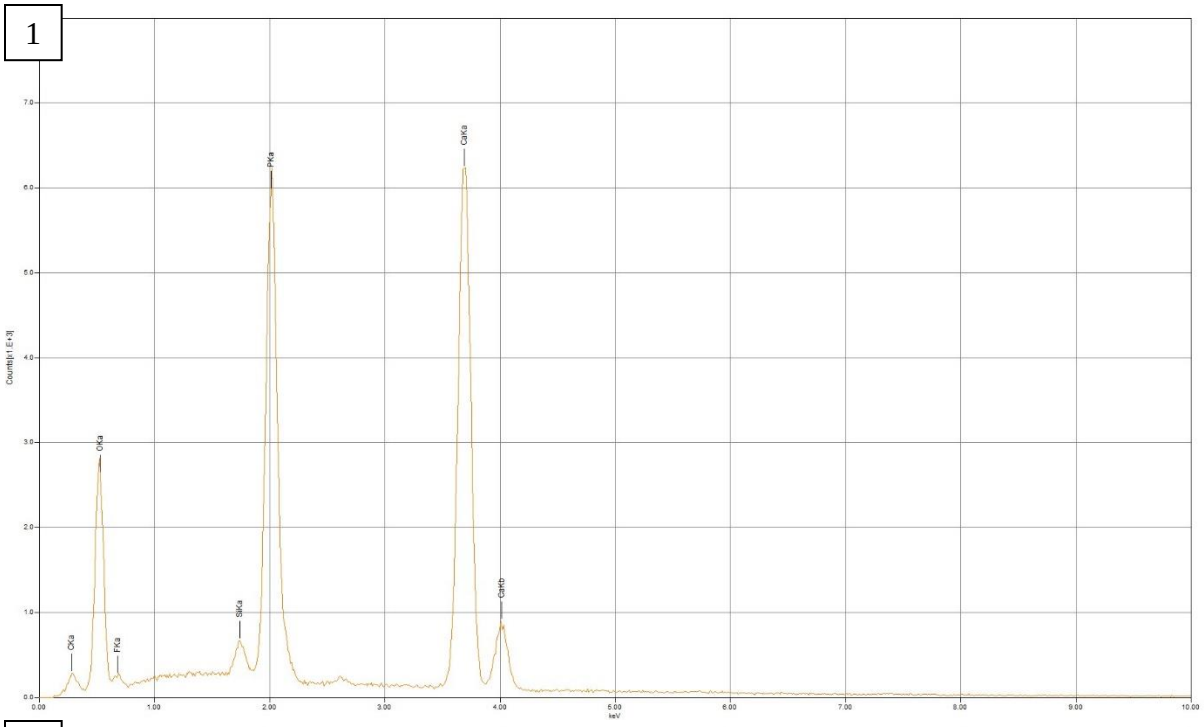
OKa
PKa
CaKa
CaKb
SiKa
FKa
CKa
Counts[x1 E+3]
keV

2

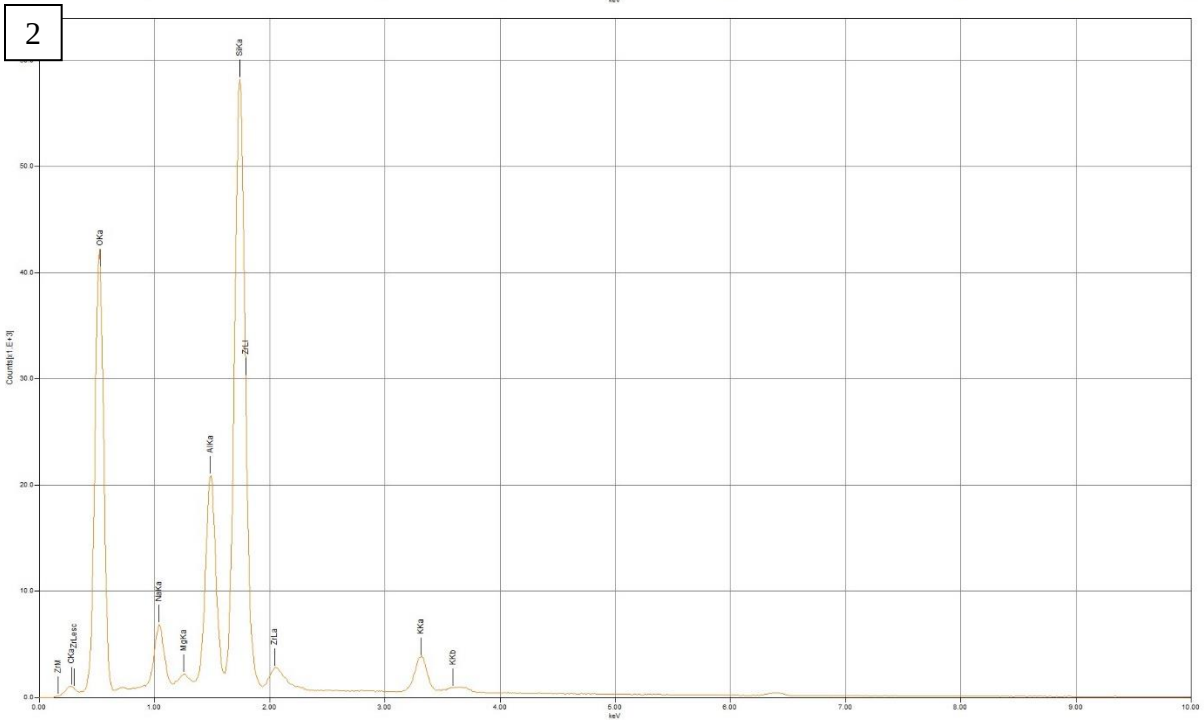
SiKa
OKa
ZrLl
AlKa
NaKa
ZrLa
KKa
MgKa
ZrM
CKa
ZrLssc
KKb
Counts[x1 E+3]
keV

3

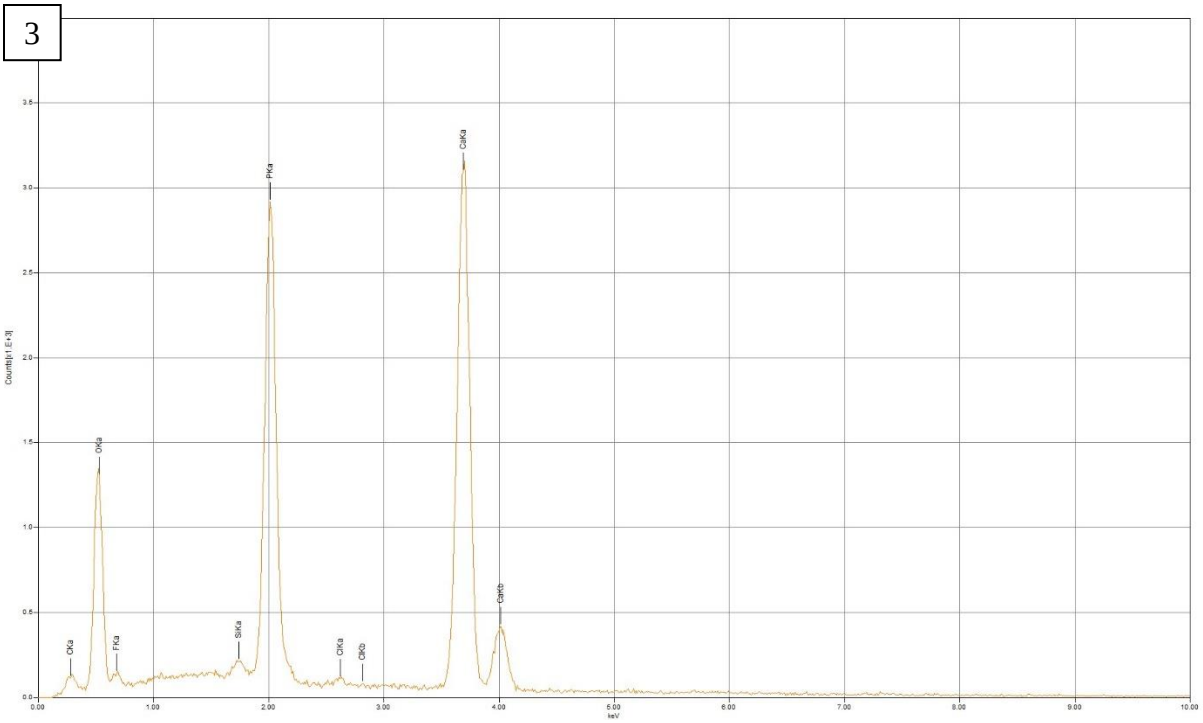

Grain 49

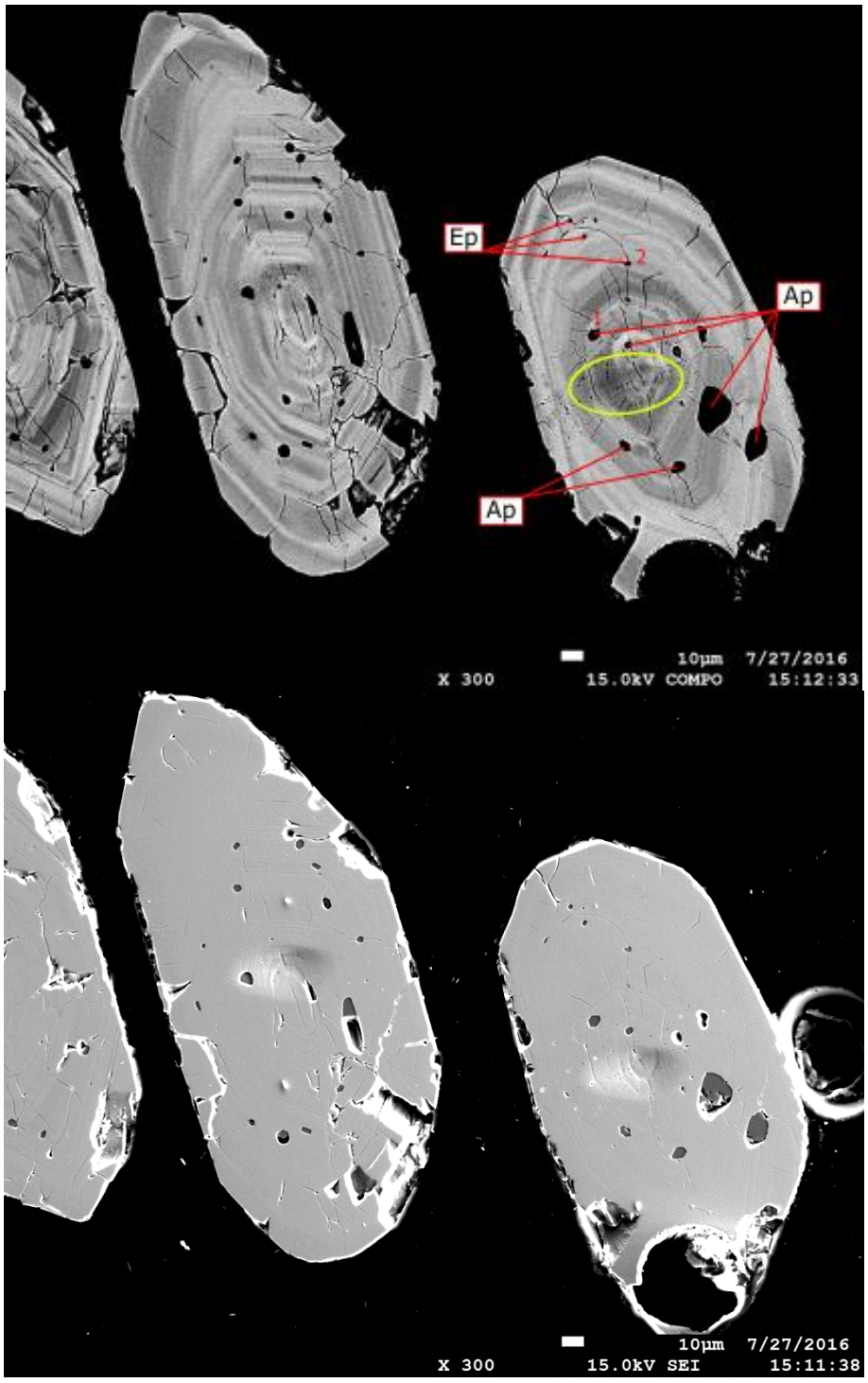
Ep
Ap
Ap
10µm 7/27/2016
X 300 15.0kV COMPO 15:12:33
10µm 7/27/2016
X 300 15.0kV SEI 15:11:38

1

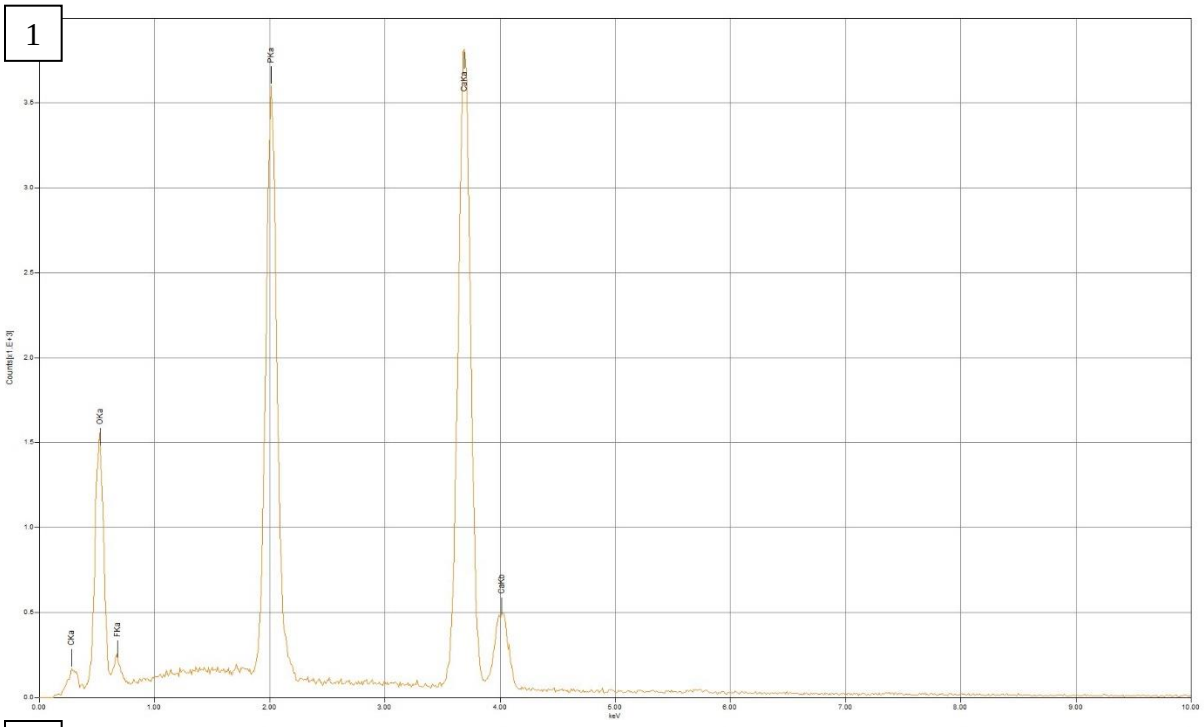
PKa
CaKa
OKa
CaKb
CKa
FKa
Counts[n1 E+3]
keV

2

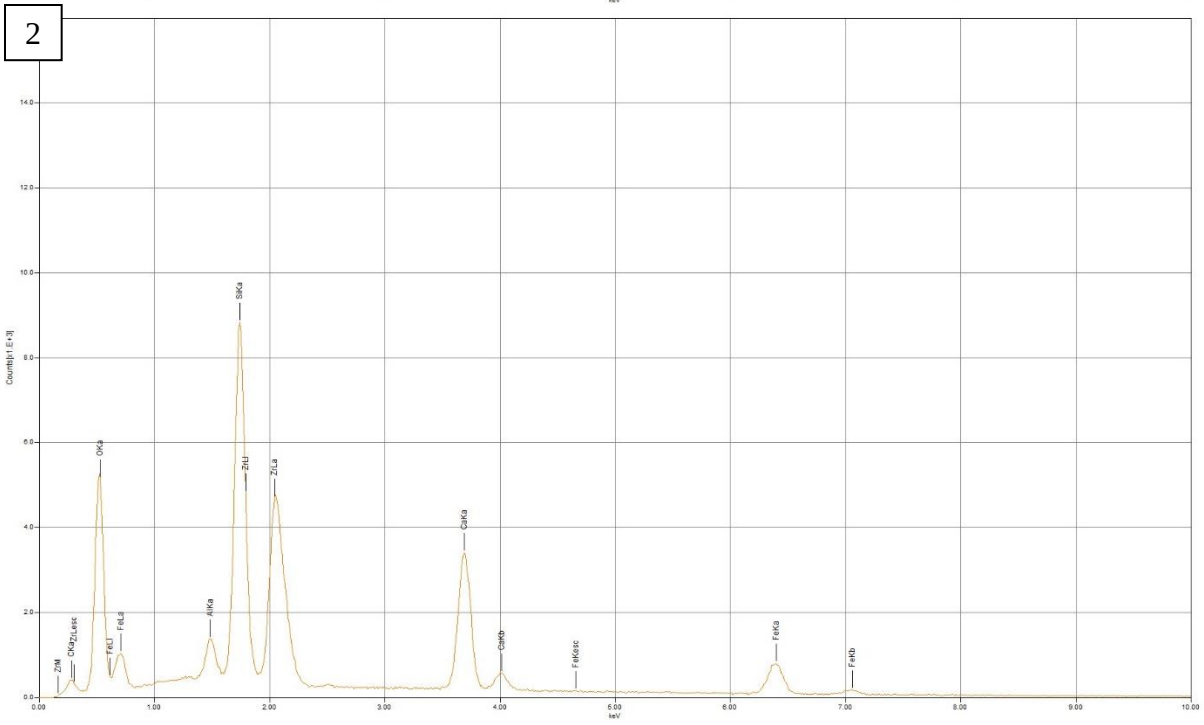
SiKa
OKa
ZnJ
ZnLa
CaKa
AlKa
ZnM
CKa
ZnLesc
FeLl
FeLa
CaKb
FeKesc
FeKa
FeKb
Counts[n1 E+3]
keV

Grain 51


Ap
1
Ap
100µm 7/27/2016
X 250 15.0kV COMPO 15:59:52
100µm 7/27/2016
X 250 15.0kV SEI 15:58:55

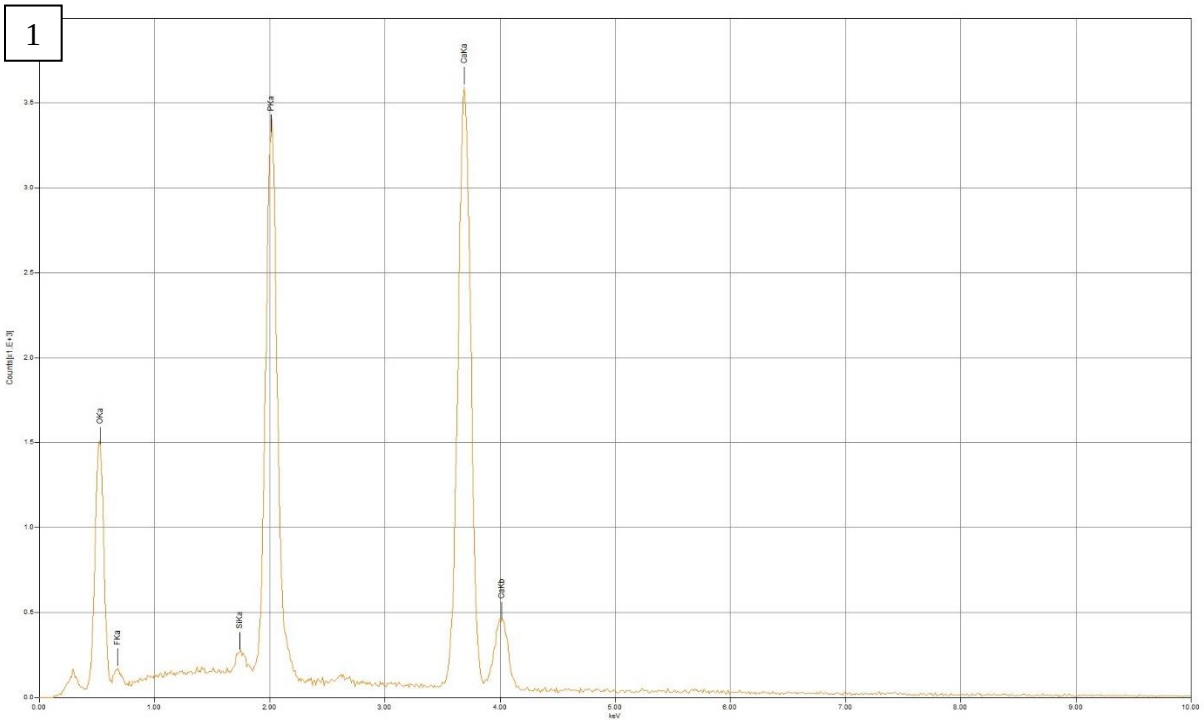
1
OKa
FKa
SiKa
PKa
CaKa
CaKb
Counts[1.E+3]
keV

Grain 52


Ap
Ap
100µm 7/27/2016
X 250 15.0kV COMPO 15:59:52
100µm 7/27/2016
X 250 15.0kV SEI 15:58:55

1

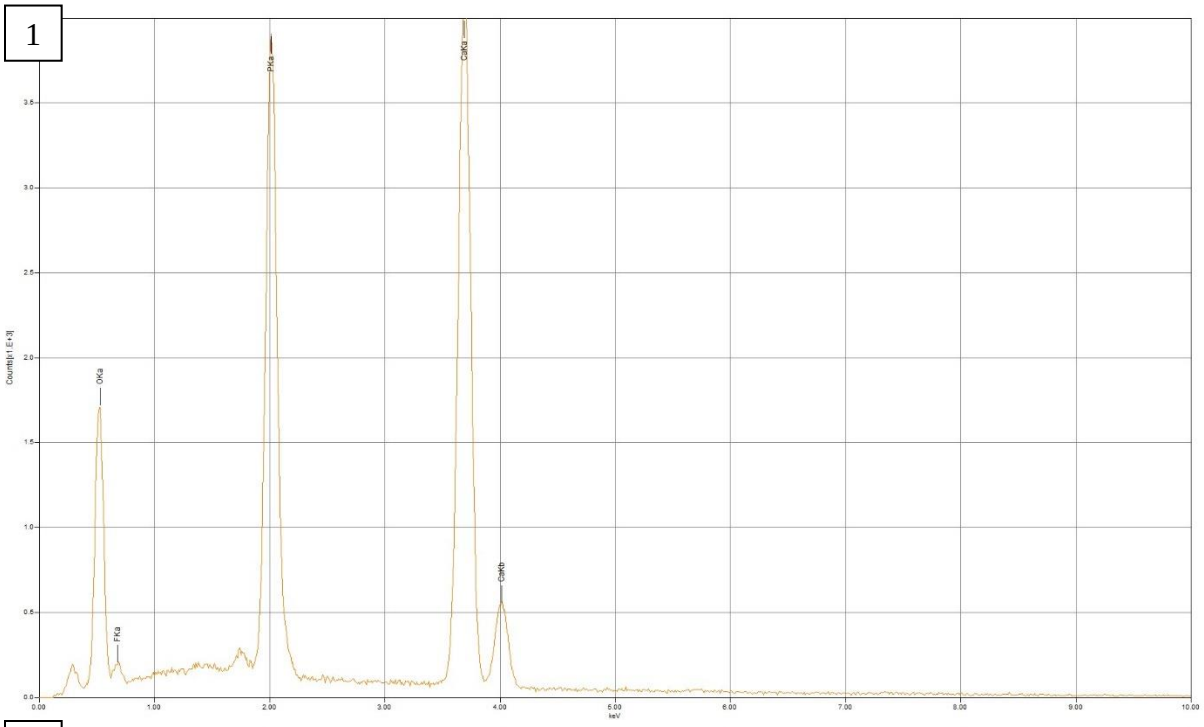
OKa
FKa
PKa
CaKa
CaKb
Counts[x1 E+3]
keV

2

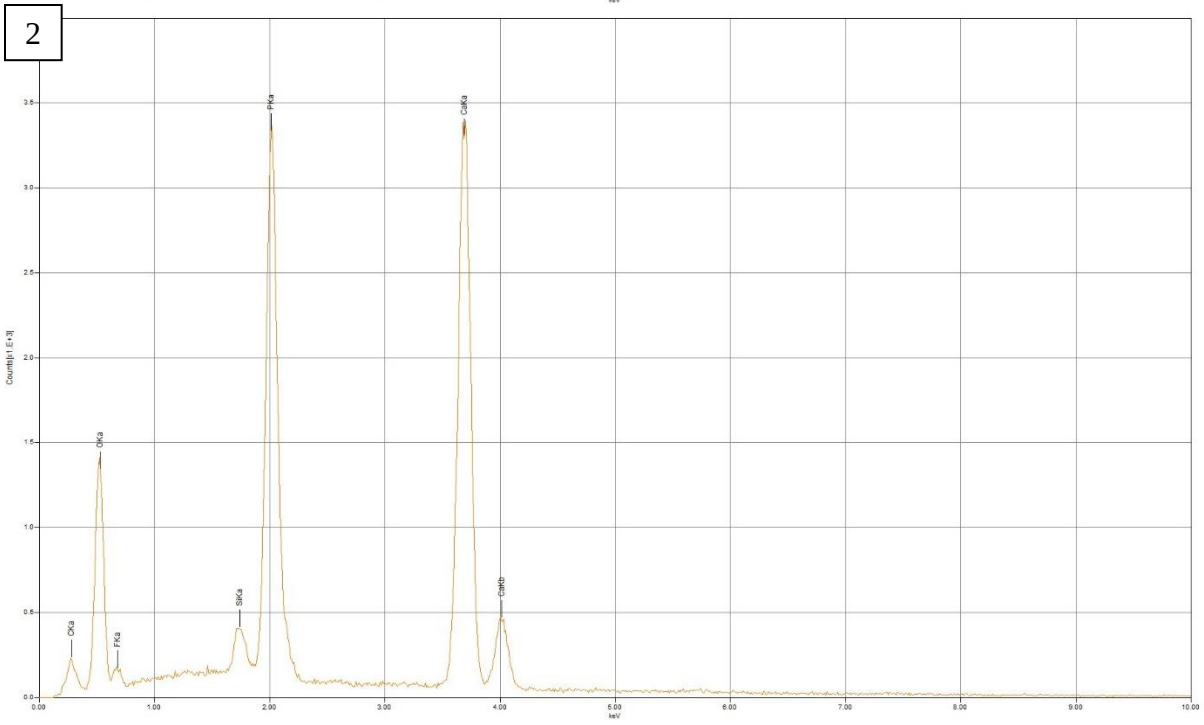
CKa
OKa
FKa
SiKa
PKa
CaKa
CaKb
Counts[x1 E+3]
keV

Grain 54

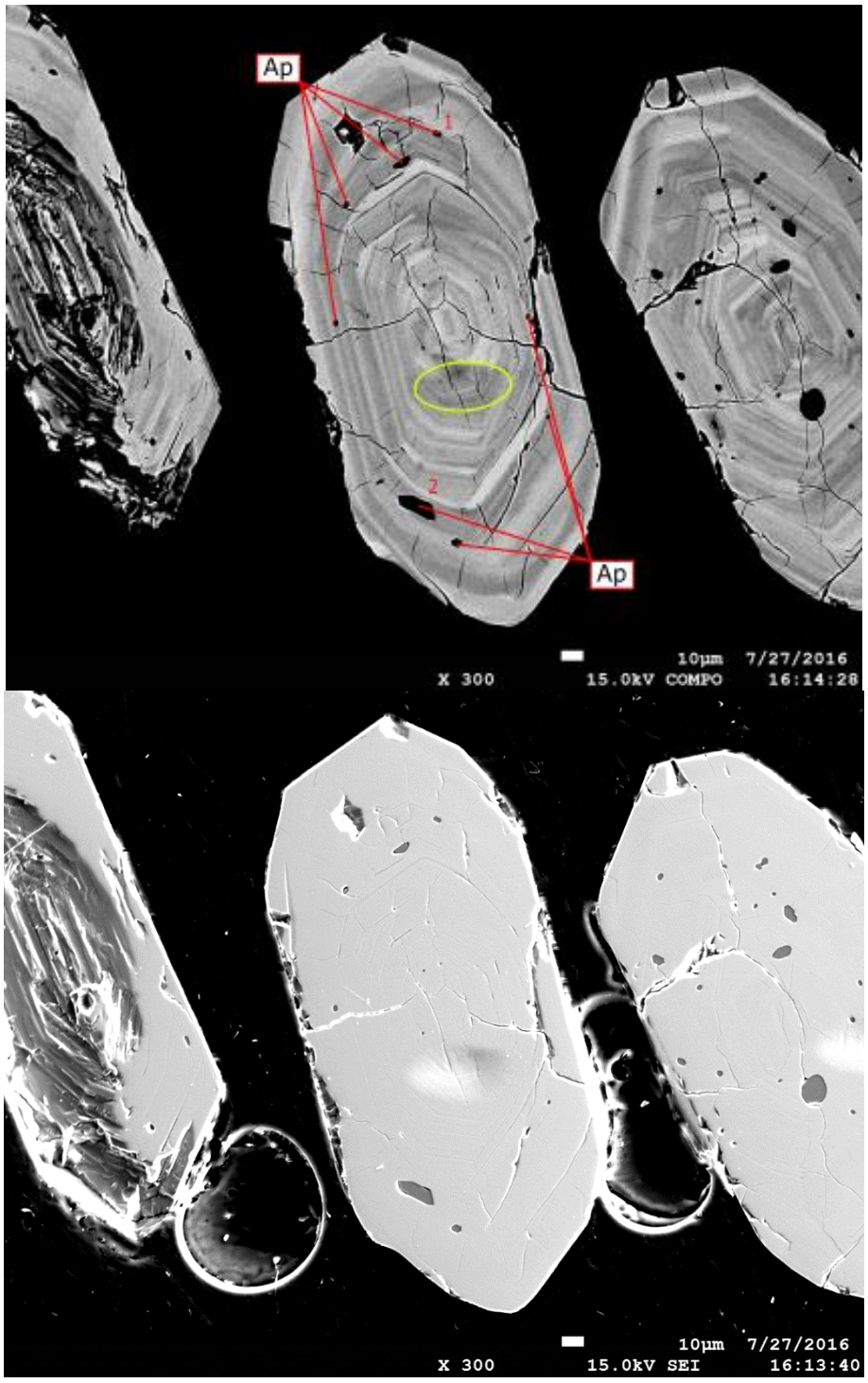
Ap
1
2
Ap
10µm 7/27/2016
X 300 15.0kV COMPO 16:14:28
10µm 7/27/2016
X 300 15.0kV SEI 16:13:40

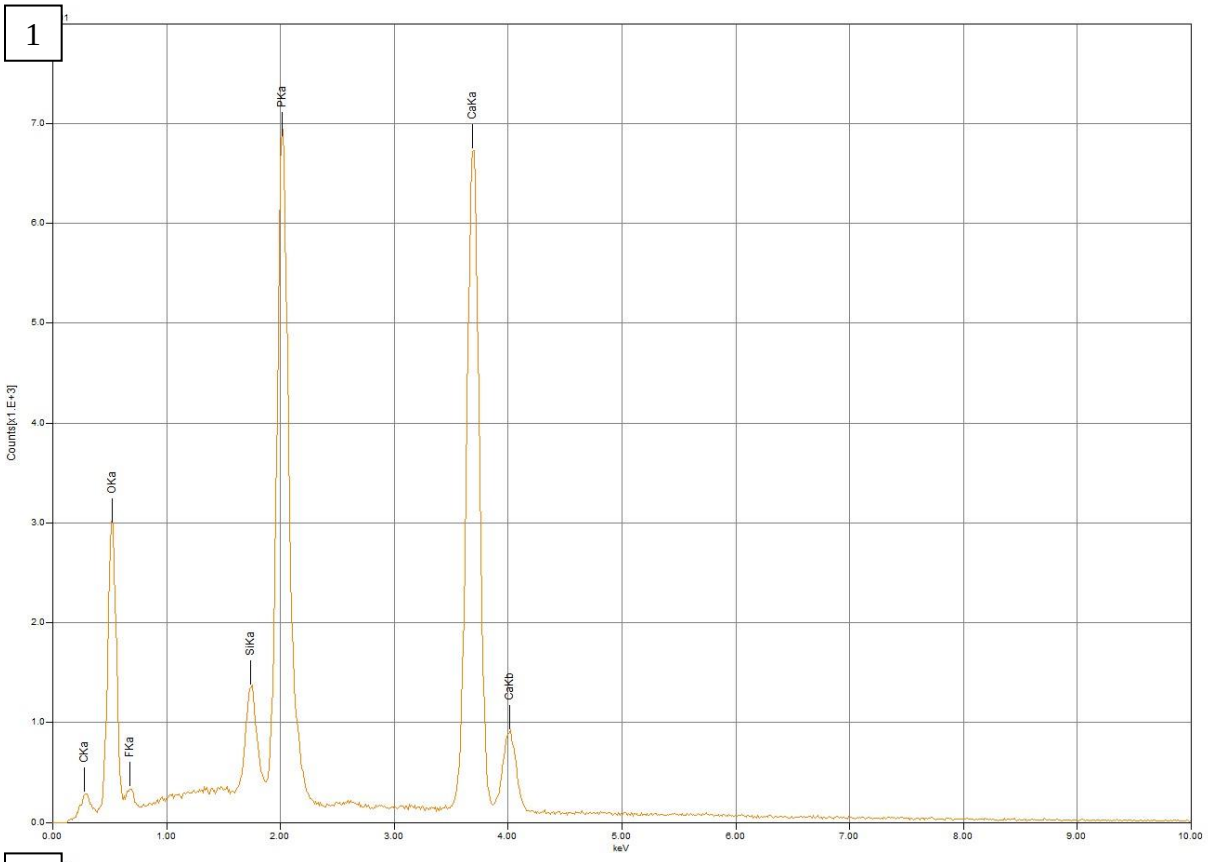
1
PKa
CaKa
OKa
SiKa
CaKb
CKa
FKa
Counts[x1 E+3]
keV

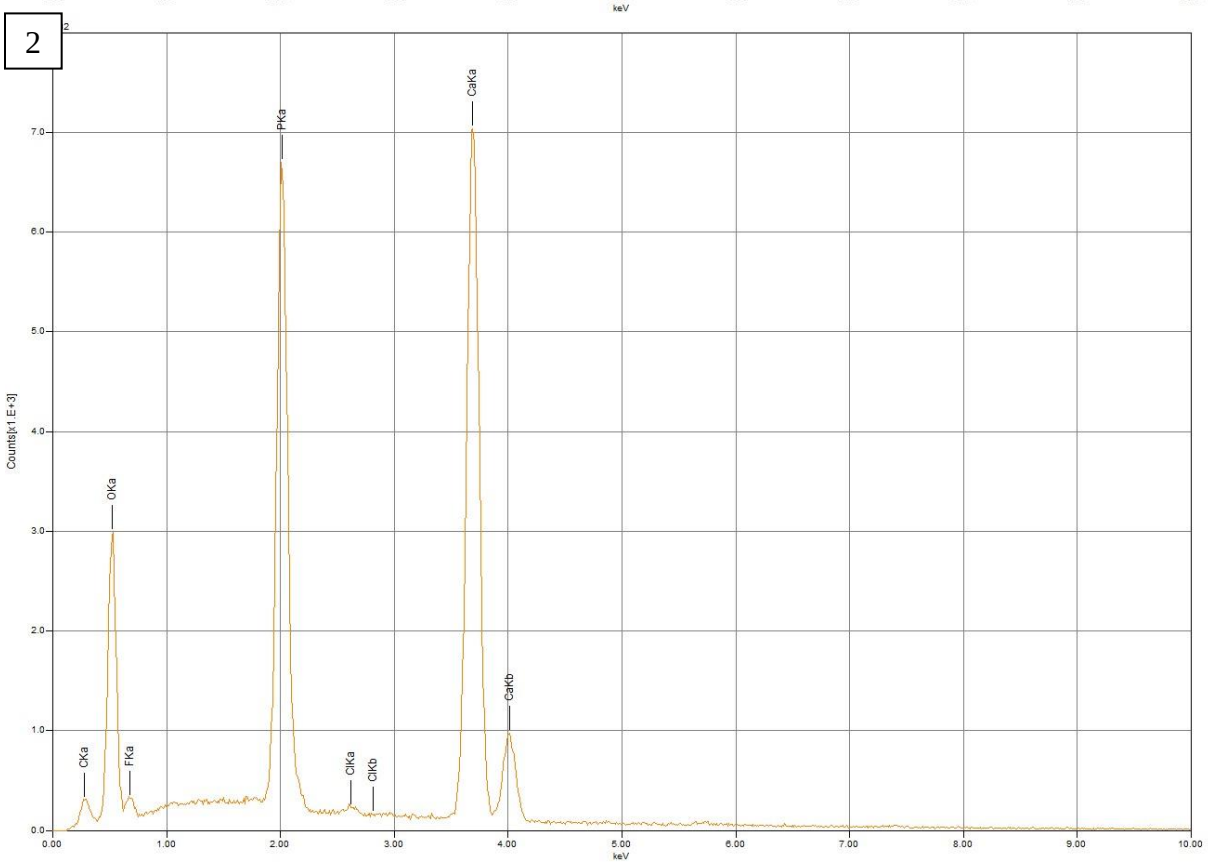
2
PKa
CaKa
OKa
CaKb
CKa
FKa
ClKa
ClKb
Counts[x1 E+3]
keV

Grain 57

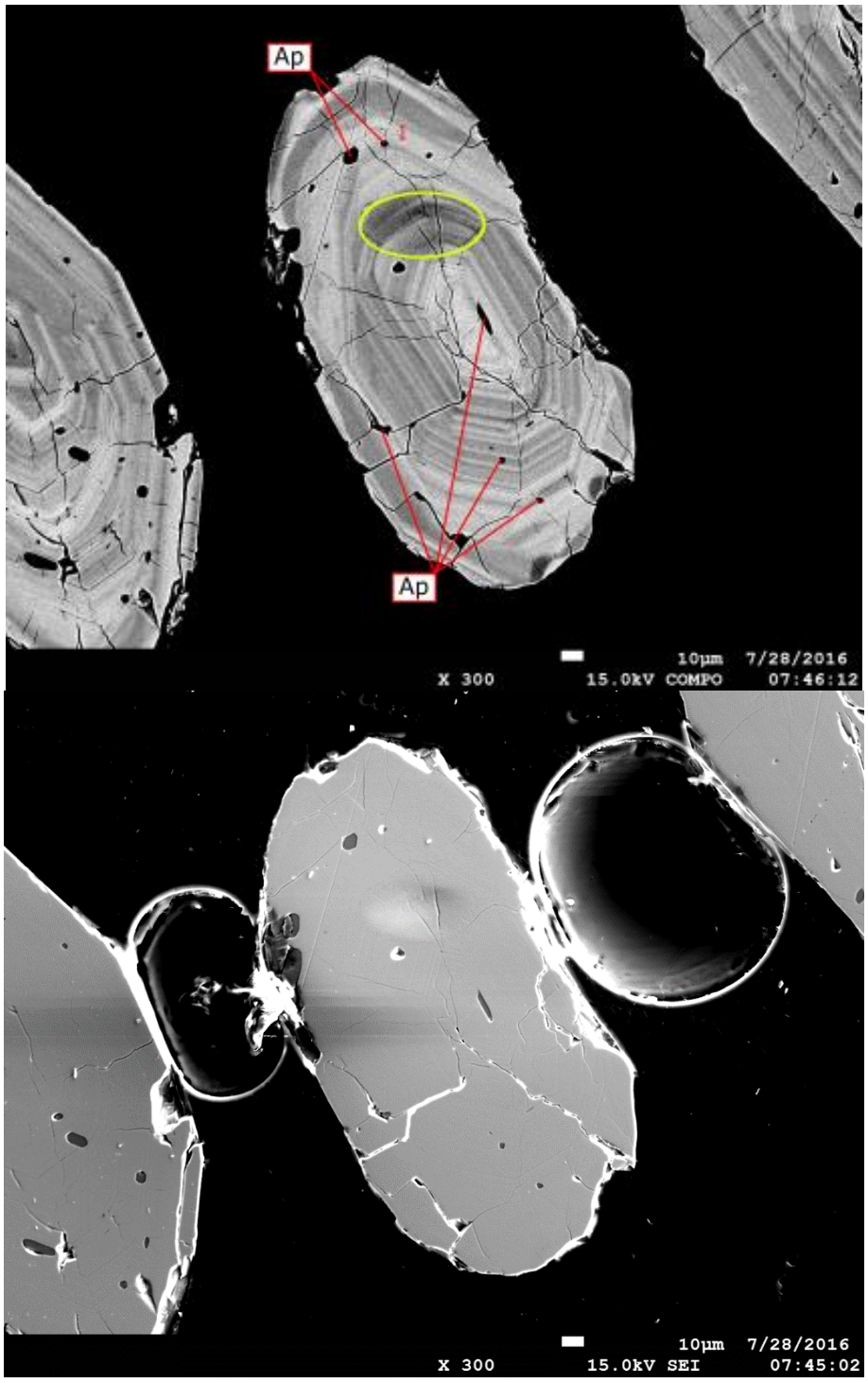
Ap
Ap
X 300
10µm 7/28/2016
15.0kV COMPO 07:46:12
X 300
10µm 7/28/2016
15.0kV SEI 07:45:02

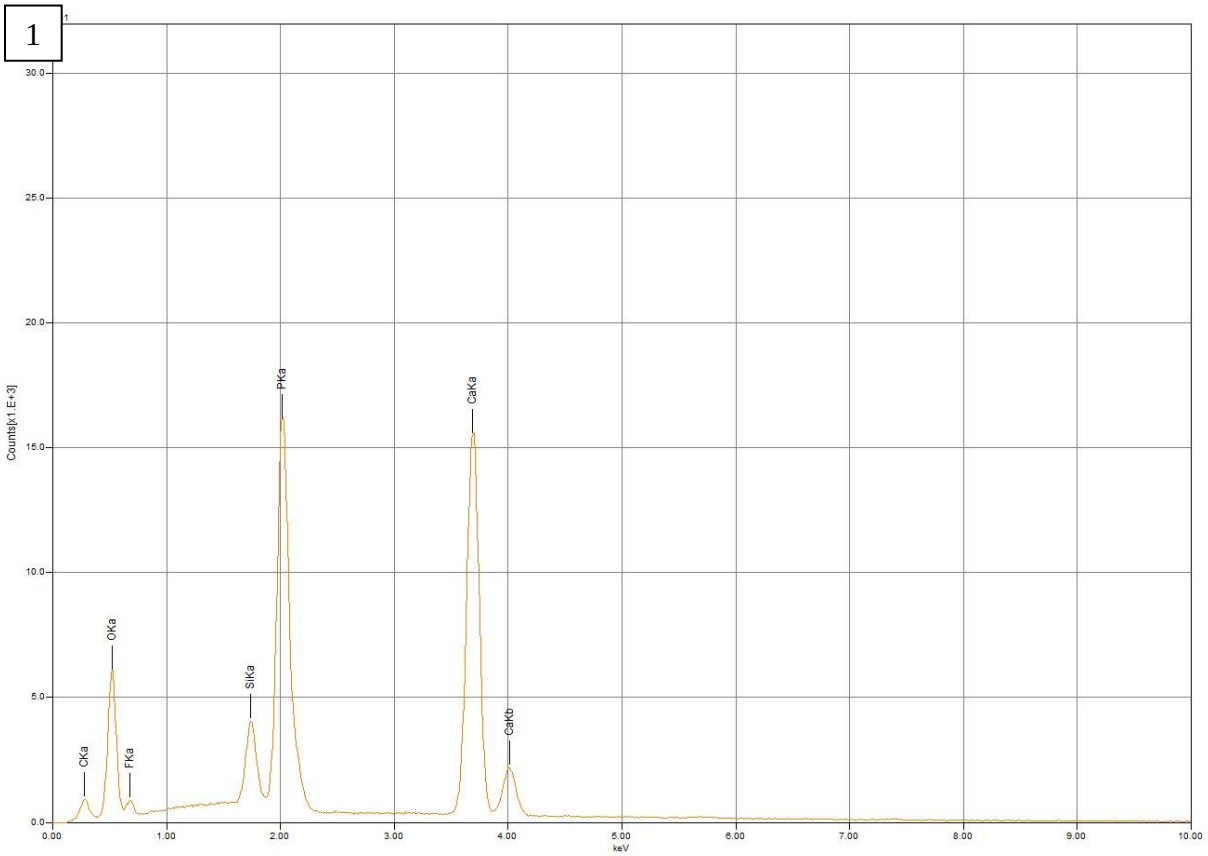
1
Counts[x1 E+3]
30.0
25.0
20.0
15.0
10.0
5.0
0.0
CKa
OKa
FKa
SiKa
PKa
CaKa
CaKb
0.00
1.00
2.00
3.00
4.00
5.00
6.00
7.00
8.00
9.00
10.00
keV

Grain 58

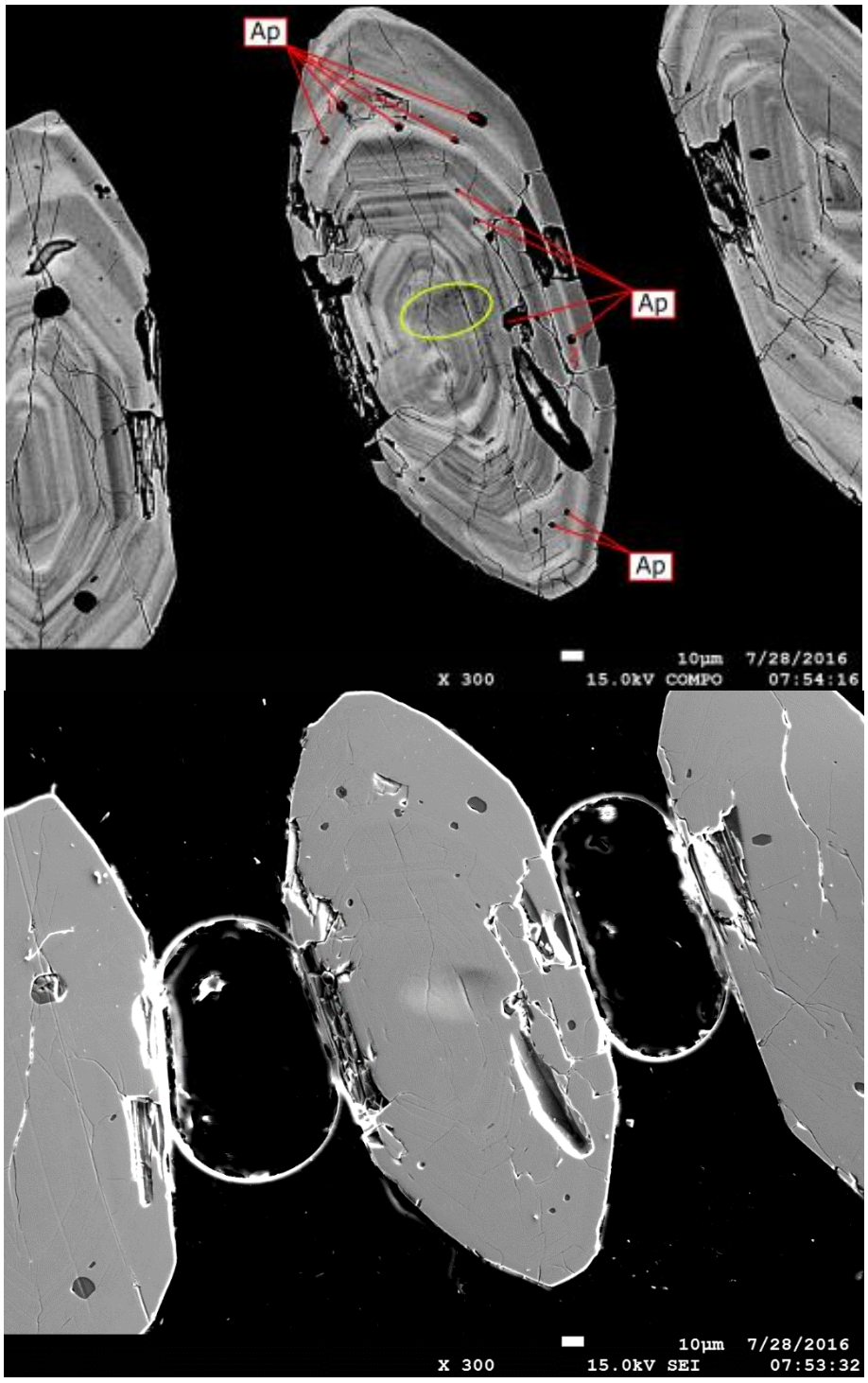
Ap
Ap
Ap
X 300
10µm 7/28/2016
15.0kV COMPO 07:54:16
X 300
10µm 7/28/2016
15.0kV SEI 07:53:32

1

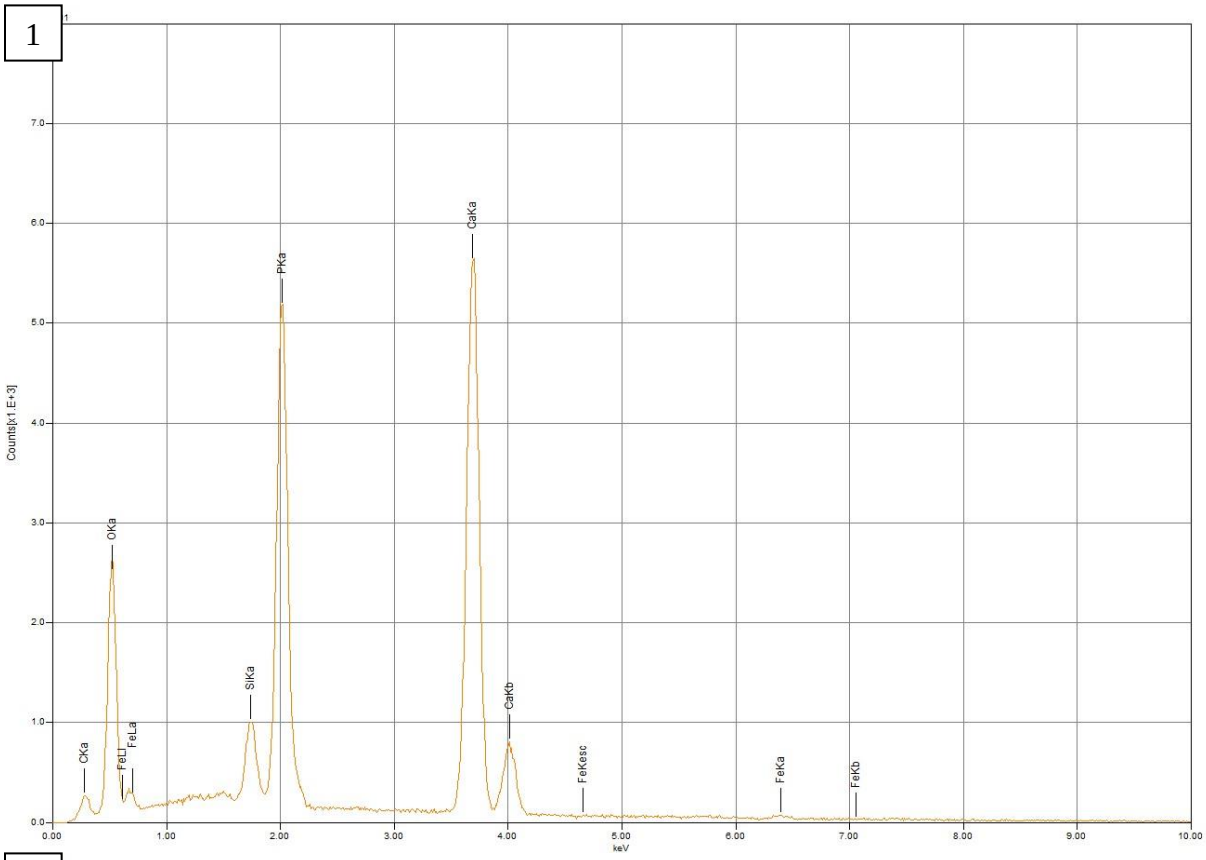
Counts[x1 E+3]
keV
CKa
OKa
FeLl
FeLa
SiKa
PKa
CaKa
CaKb
FeKesc
FeKa
FeKb

2

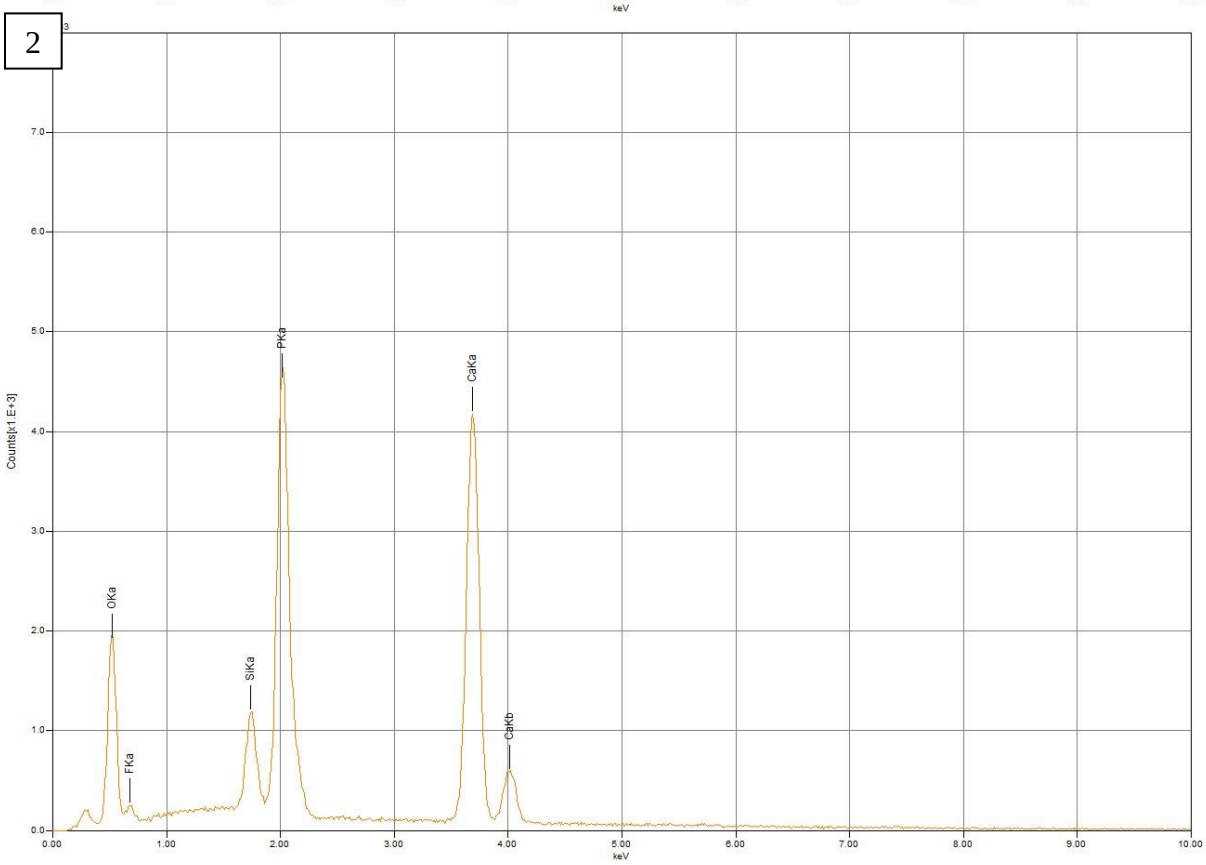
Counts[x1 E+3]
keV
OKa
FKa
SiKa
PKa
CaKa
CaKb

Grain 59

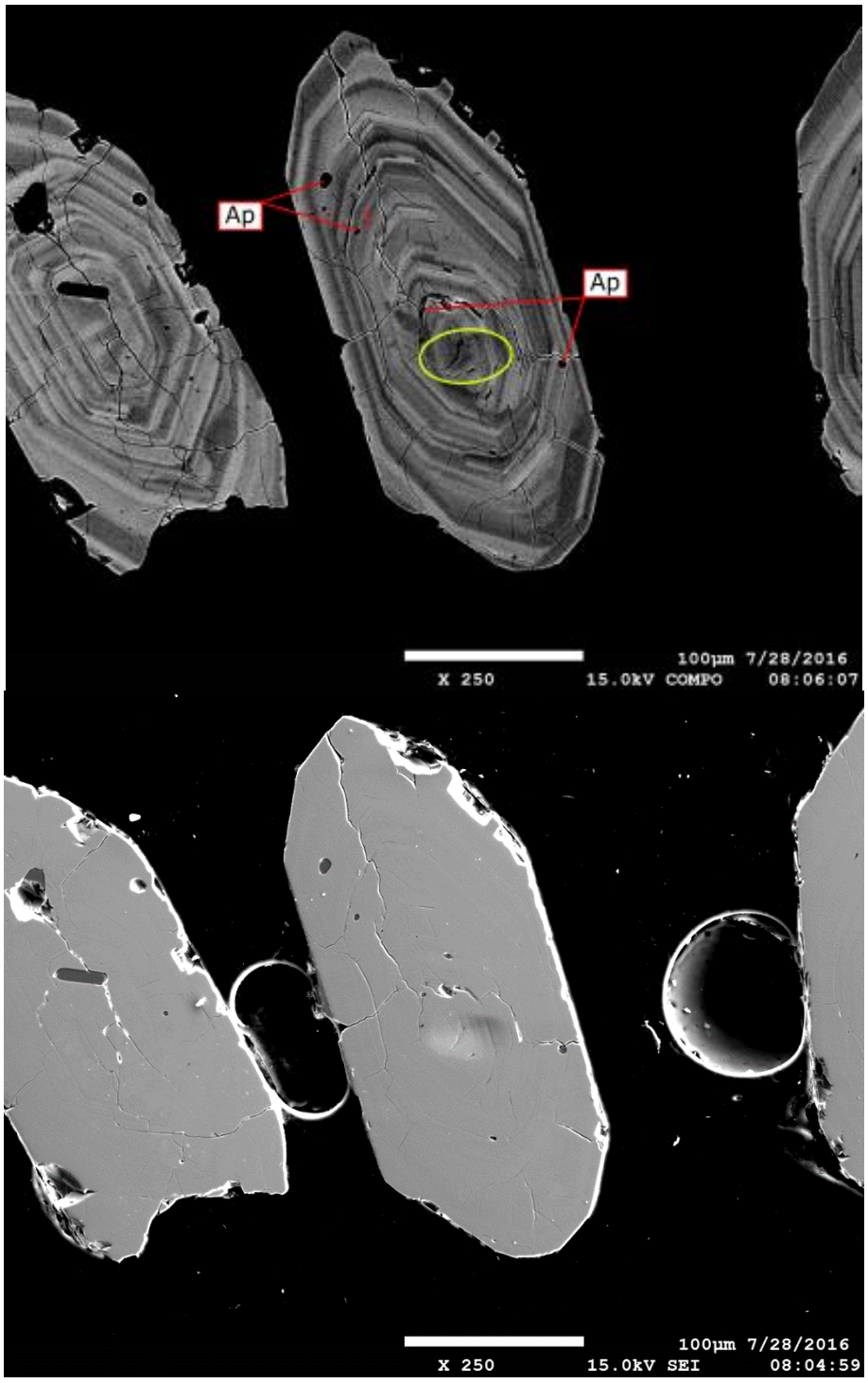
Ap
Ap
100µm 7/28/2016
X 250 15.0kV COMPO 08:06:07
100µm 7/28/2016
X 250 15.0kV SEI 08:04:59

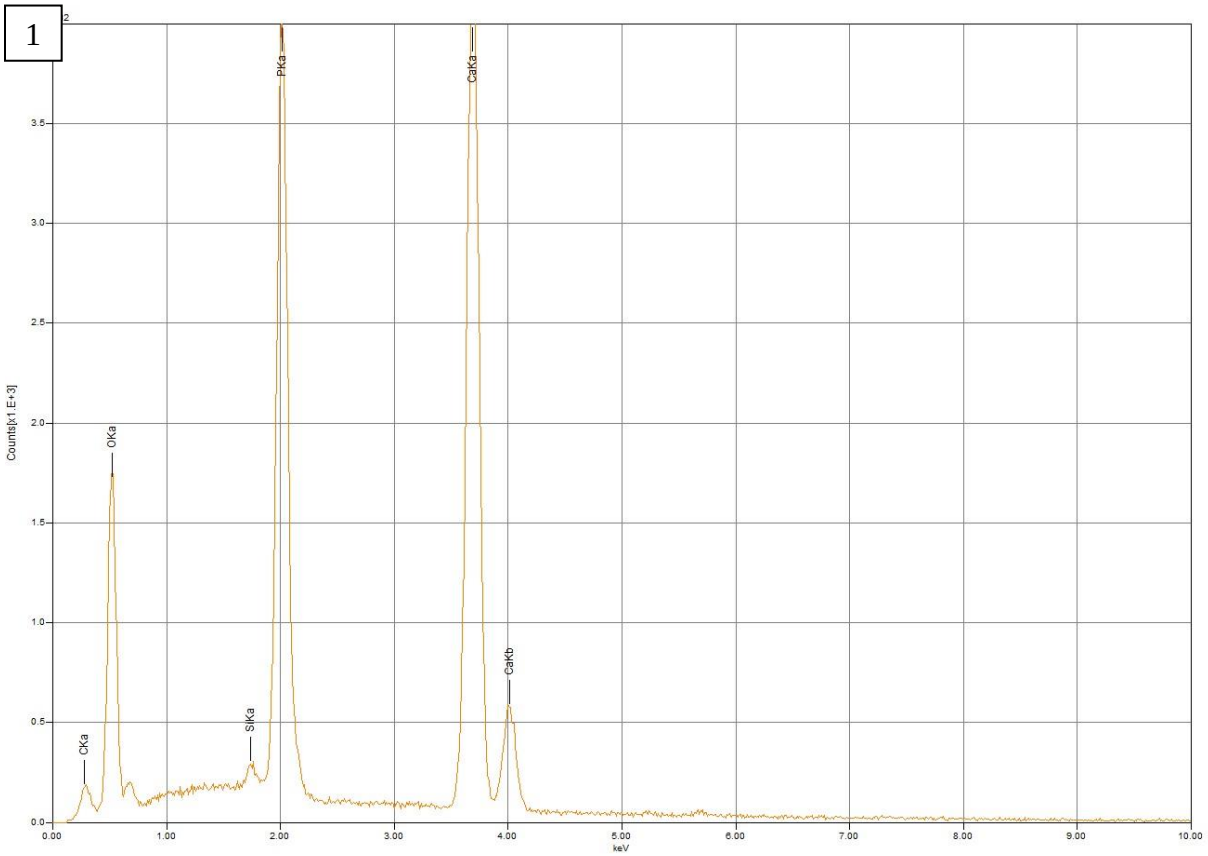
1
Counts[x1 E+3]
CKa
OKa
SiKa
PKa
CaKa
CaKb
keV

Grain 60

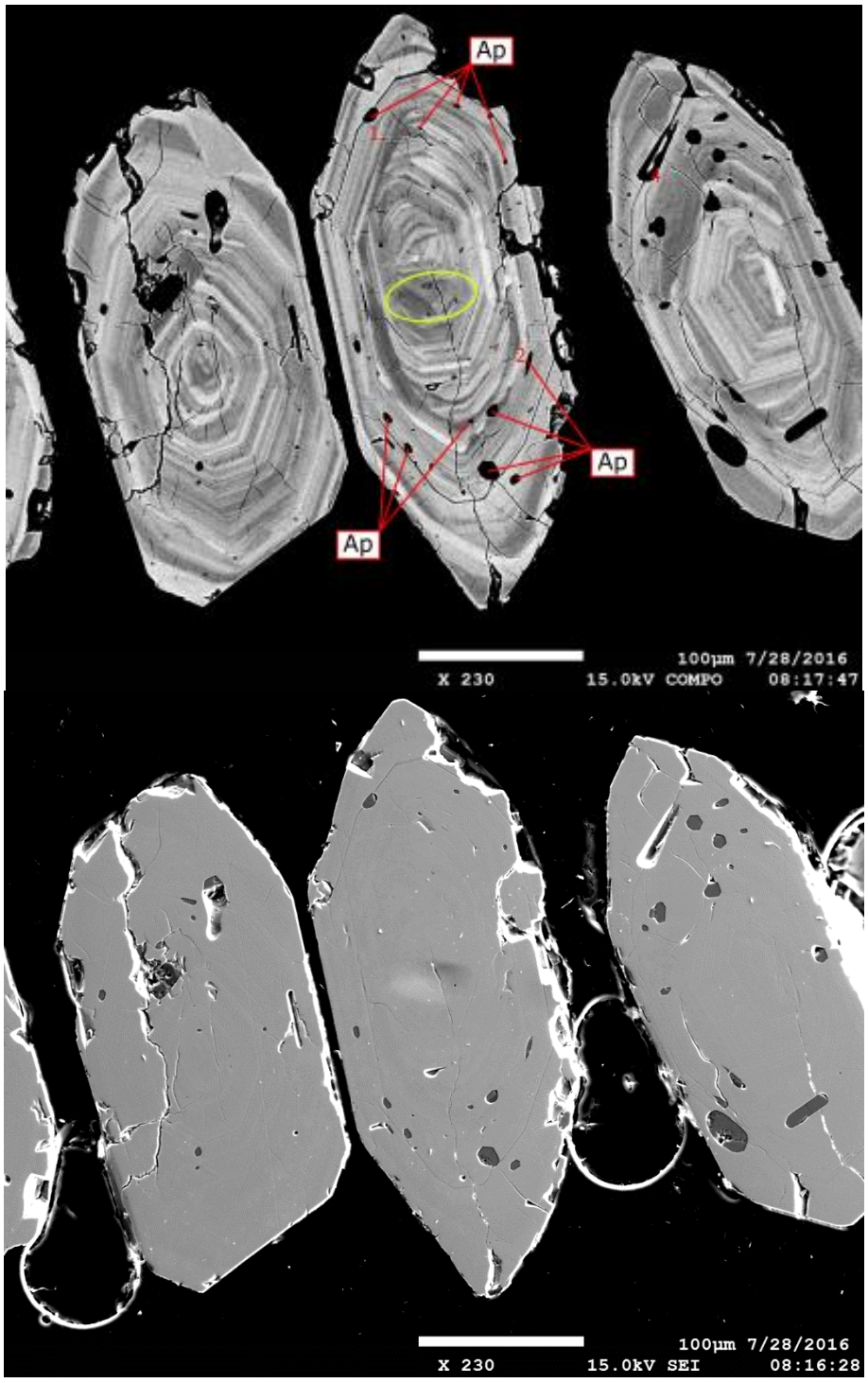
Ap
1
2
Ap
Ap
100µm 7/28/2016
X 230 15.0kV COMPO 08:17:47
100µm 7/28/2016
X 230 15.0kV SEI 08:16:28

1

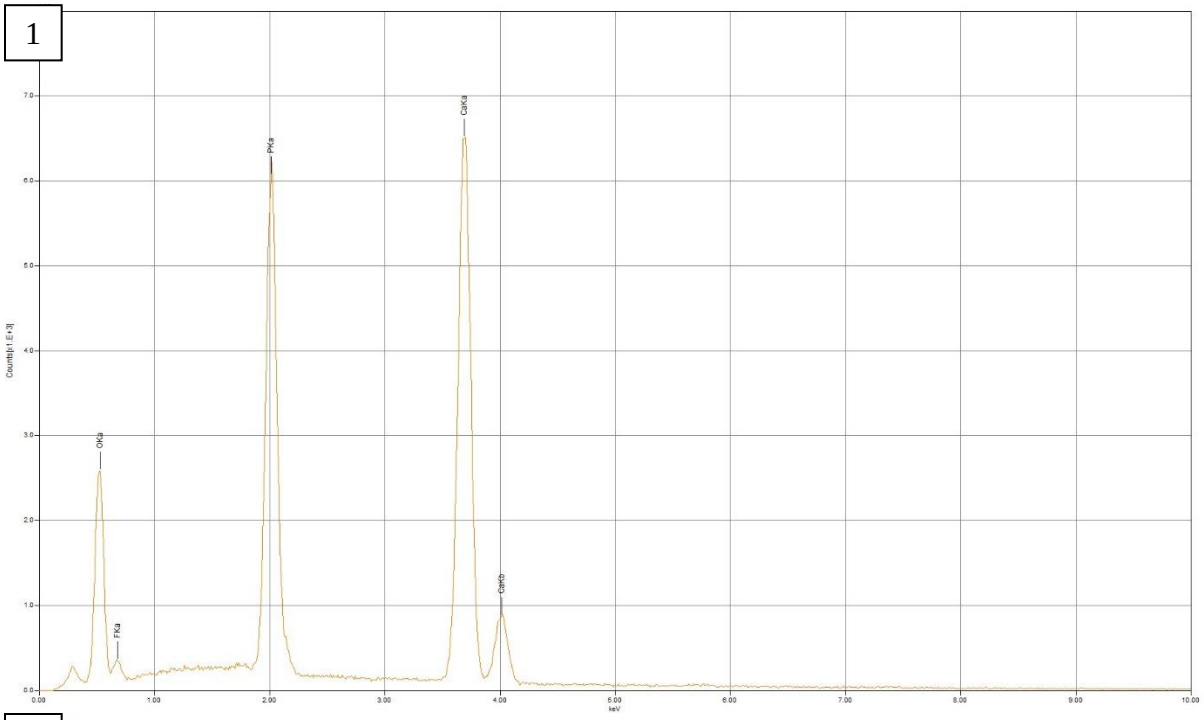
OKa
FKa
PKa
CaKa
CaKb
Counts[x1.E+3]
keV

2

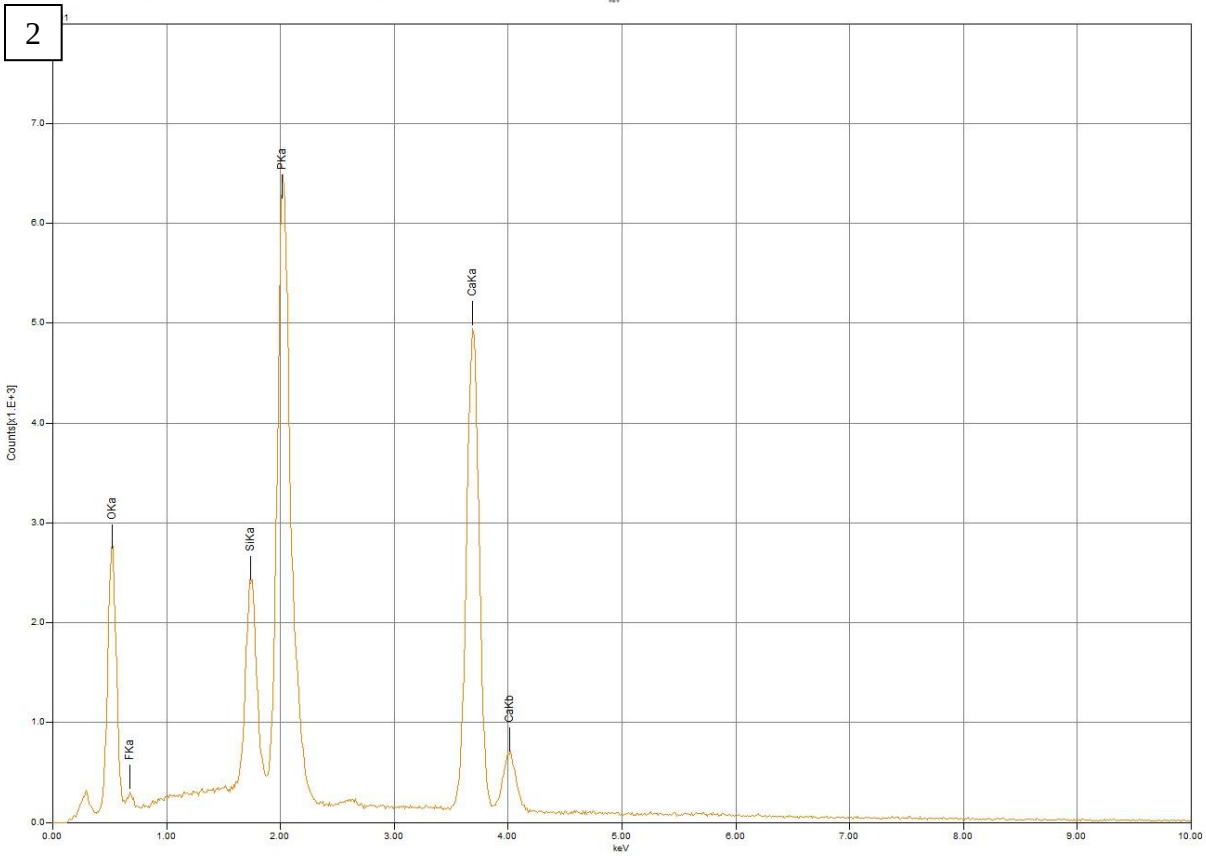
OKa
FKa
SiKa
PKa
CaKa
CaKb
Counts[x1.E+3]
keV

Grain 60

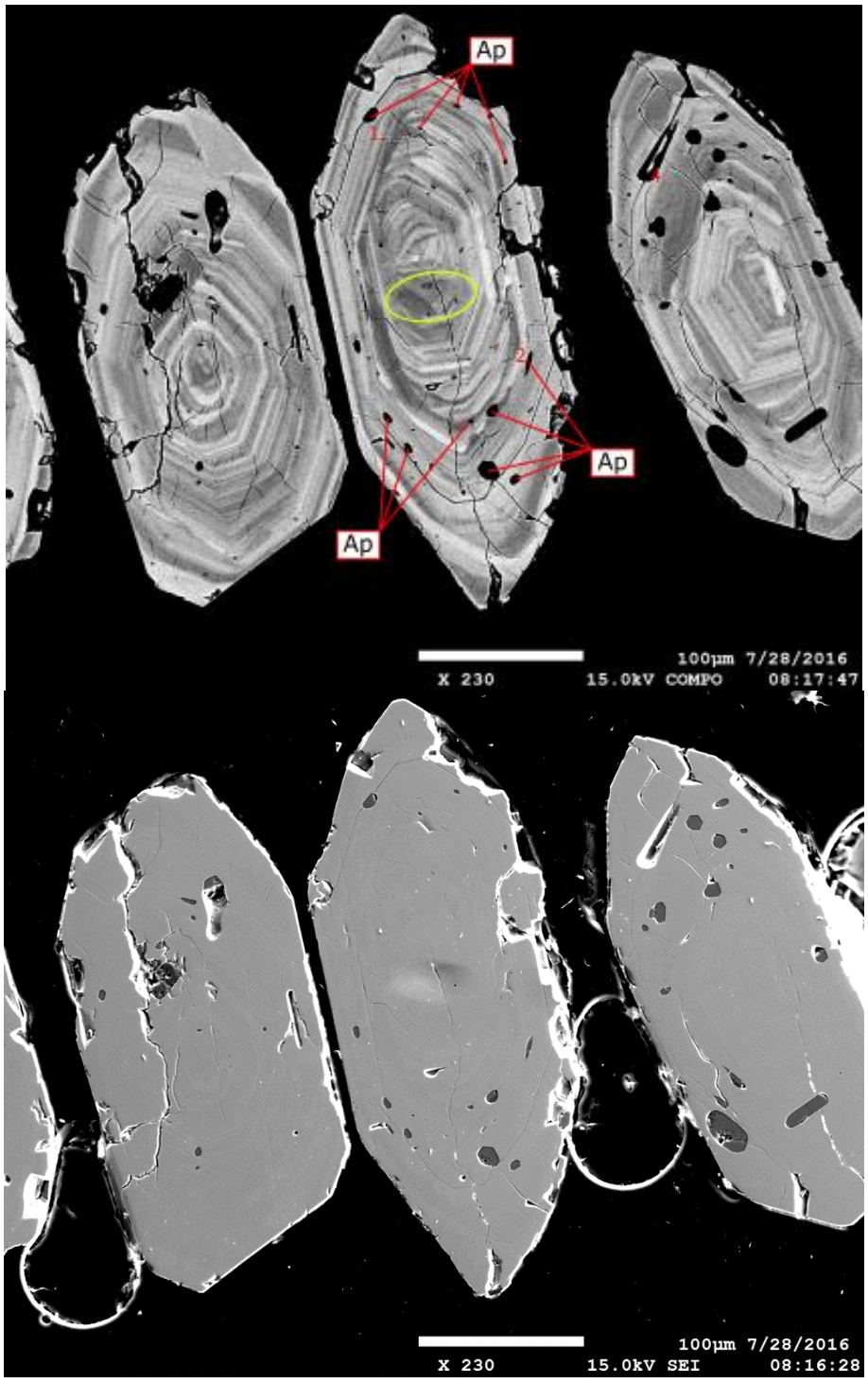
Ap
1
2
Ap
Ap
100µm 7/28/2016
X 230 15.0kV COMPO 08:17:47
100µm 7/28/2016
X 230 15.0kV SEI 08:16:28

1

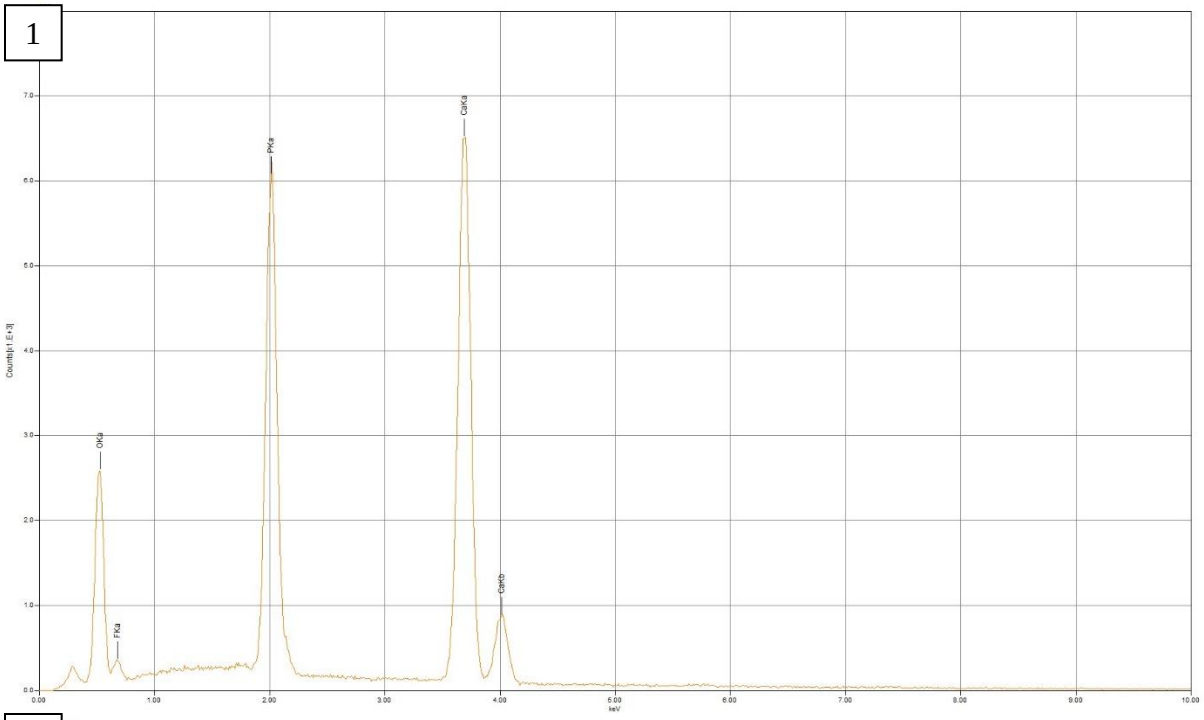
OKa
FKa
PKa
CaKa
CaKb
Counts[x1.E+3]
keV

2

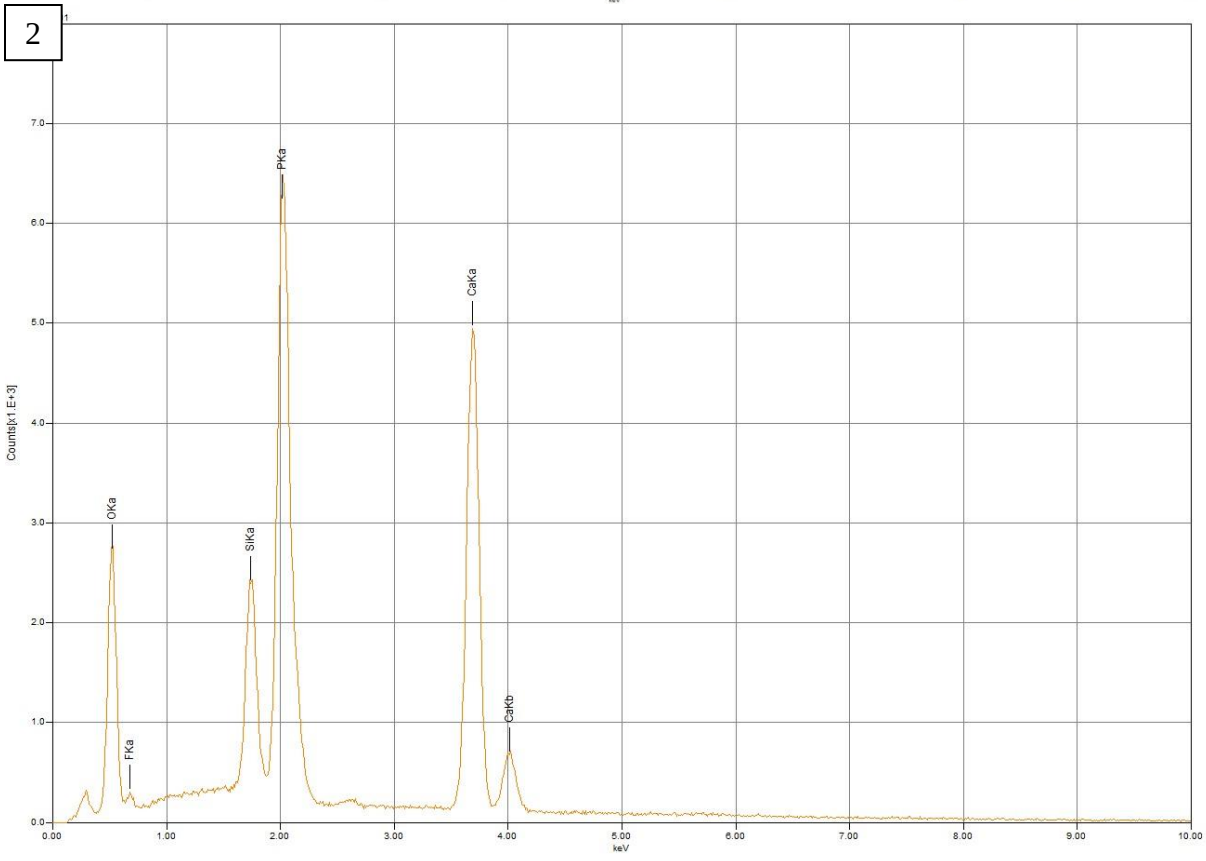
OKa
FKa
SiKa
PKa
CaKa
CaKb
Counts[x1.E+3]
keV

Mount B
Grain 1

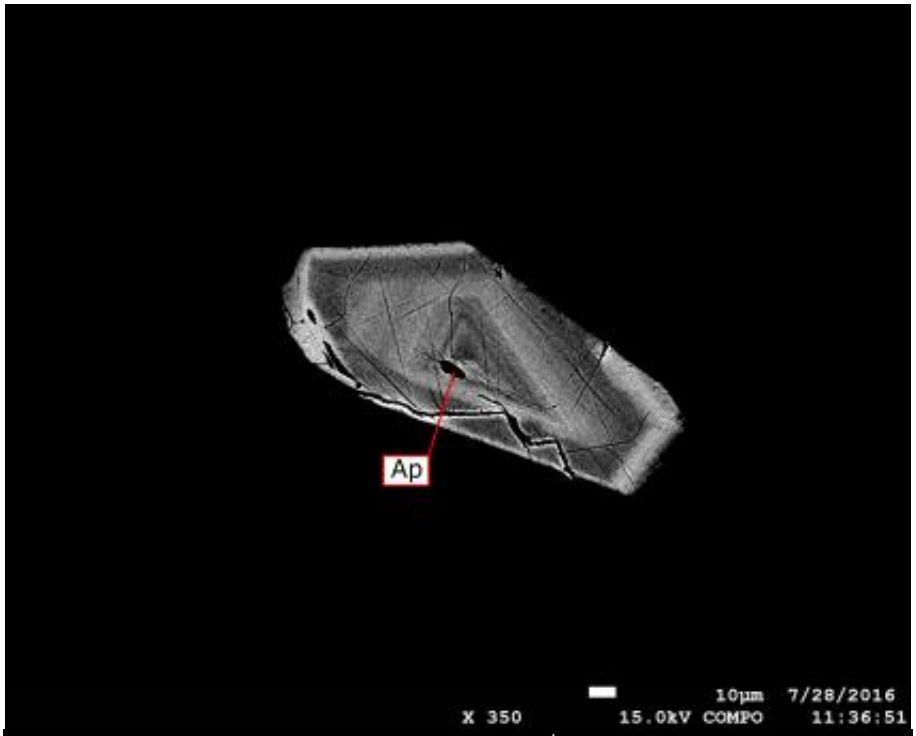

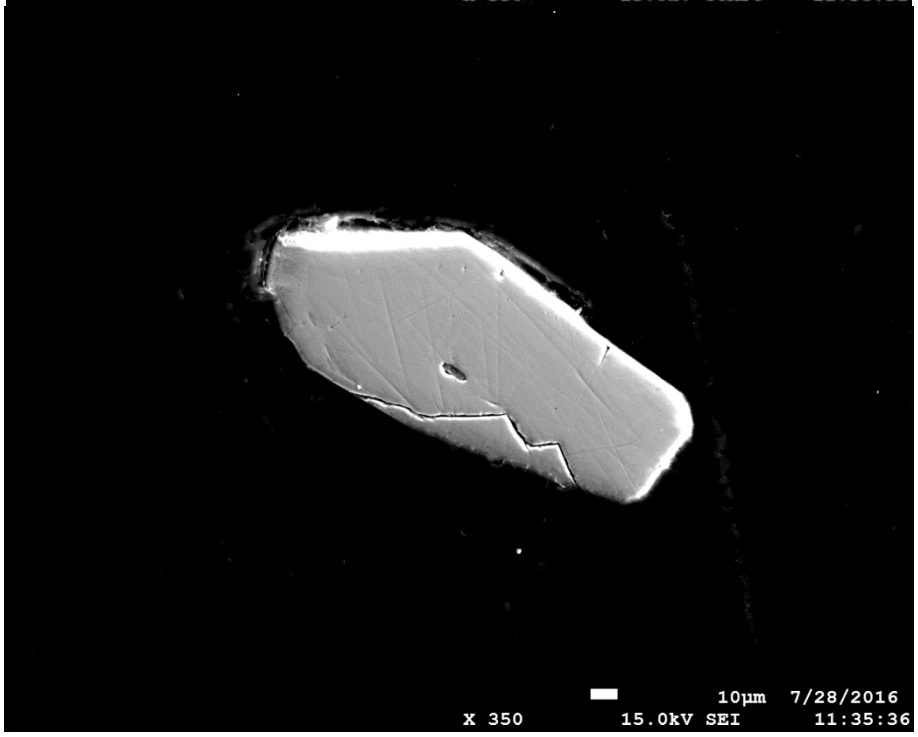

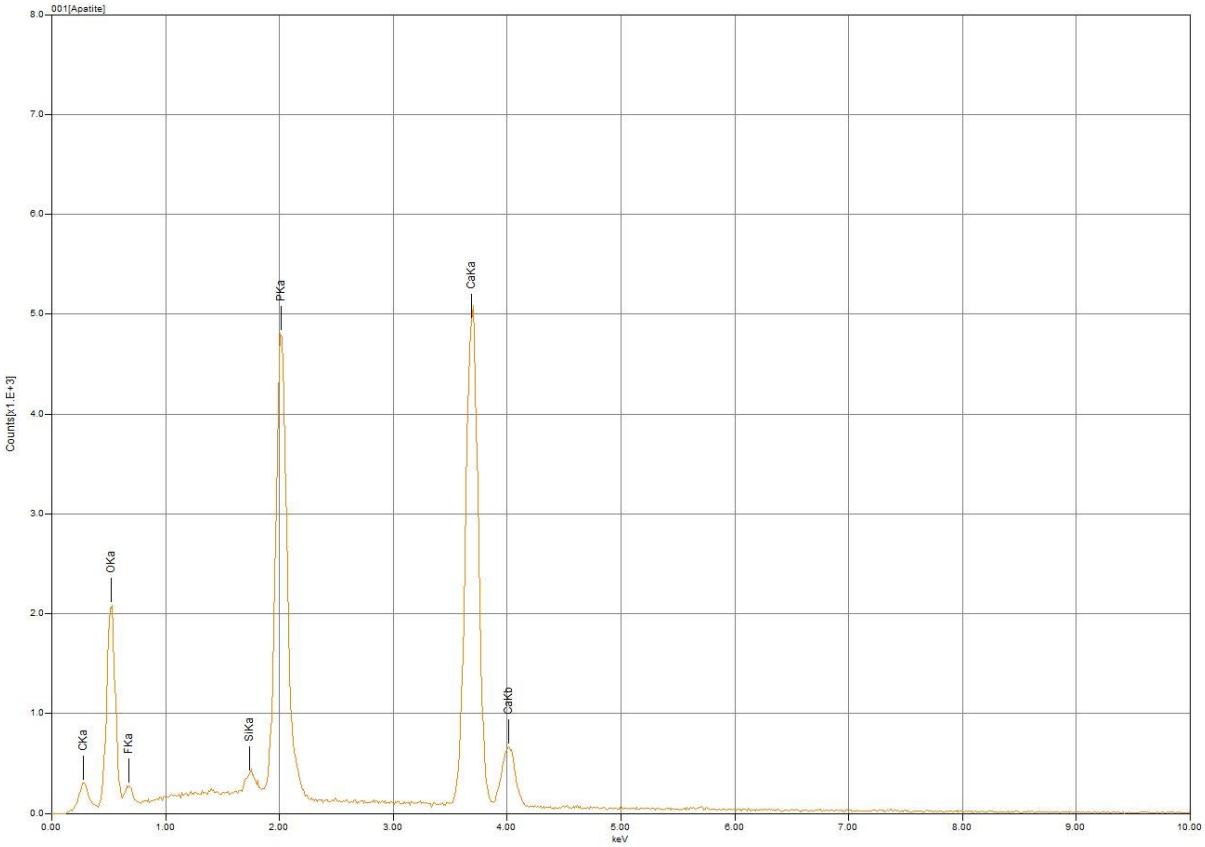
001[Apatite]
Counts[x1 E+3]
keV
CKa
OKa
FKa
SiKa
PKa
CaKa
CaKb

Grain 4

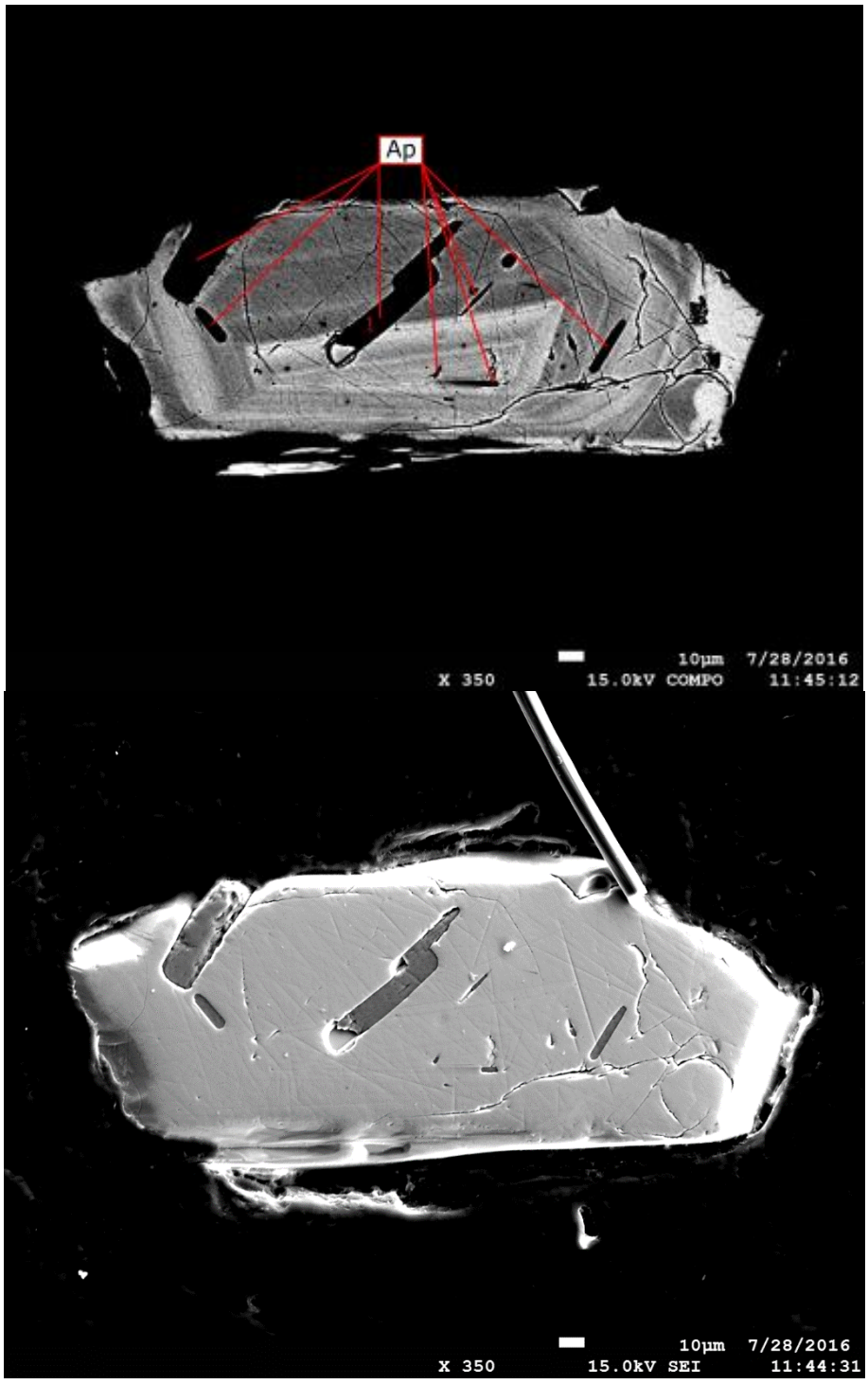
Ap
X 350
10µm 7/28/2016
15.0kV COMPO 11:45:12
X 350
10µm 7/28/2016
15.0kV SEI 11:44:31

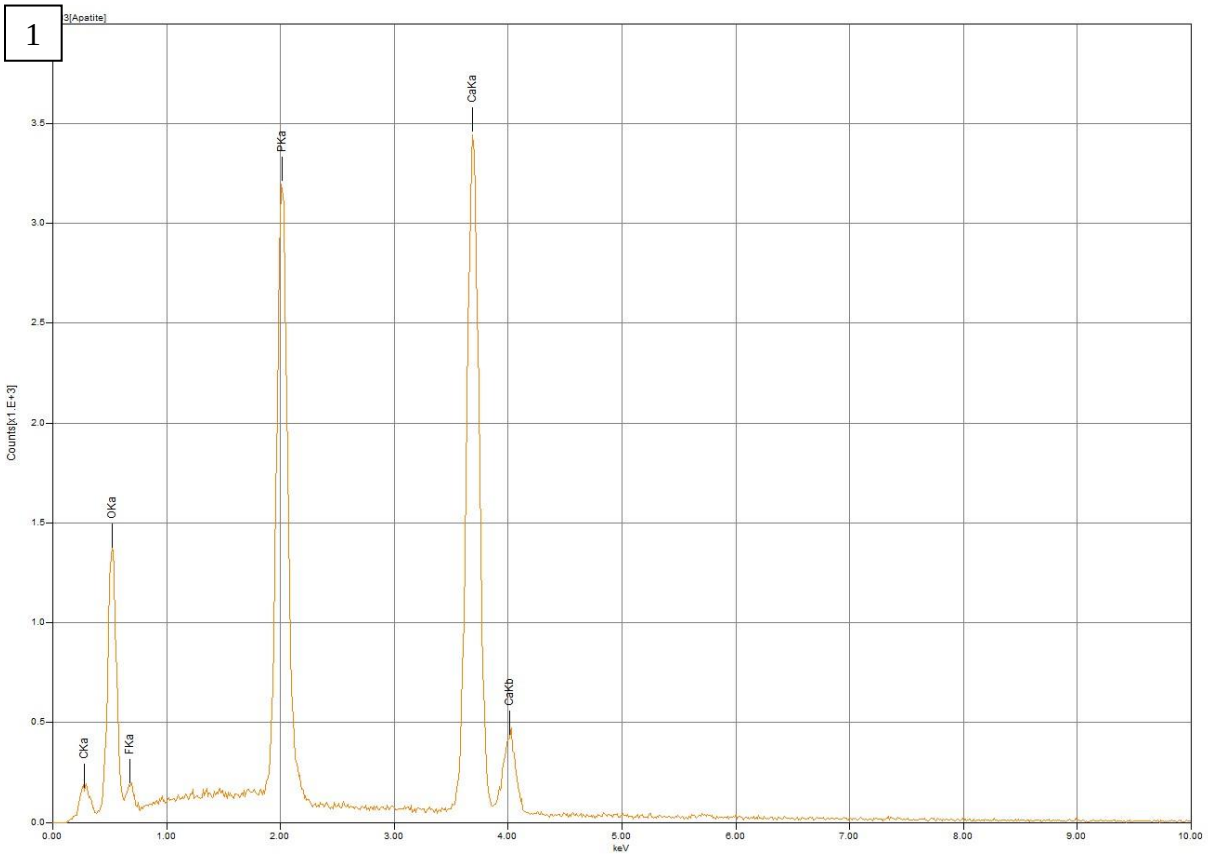
1
3[Apatite]
CaKa
PKa
OKa
CKa
FKa
CaKb
Counts[x1 E+3]
keV
0.00
1.00
2.00
3.00
4.00
5.00
6.00
7.00
8.00
9.00
10.00
0.0
0.5
1.0
1.5
2.0
2.5
3.0
3.5

Grain 5

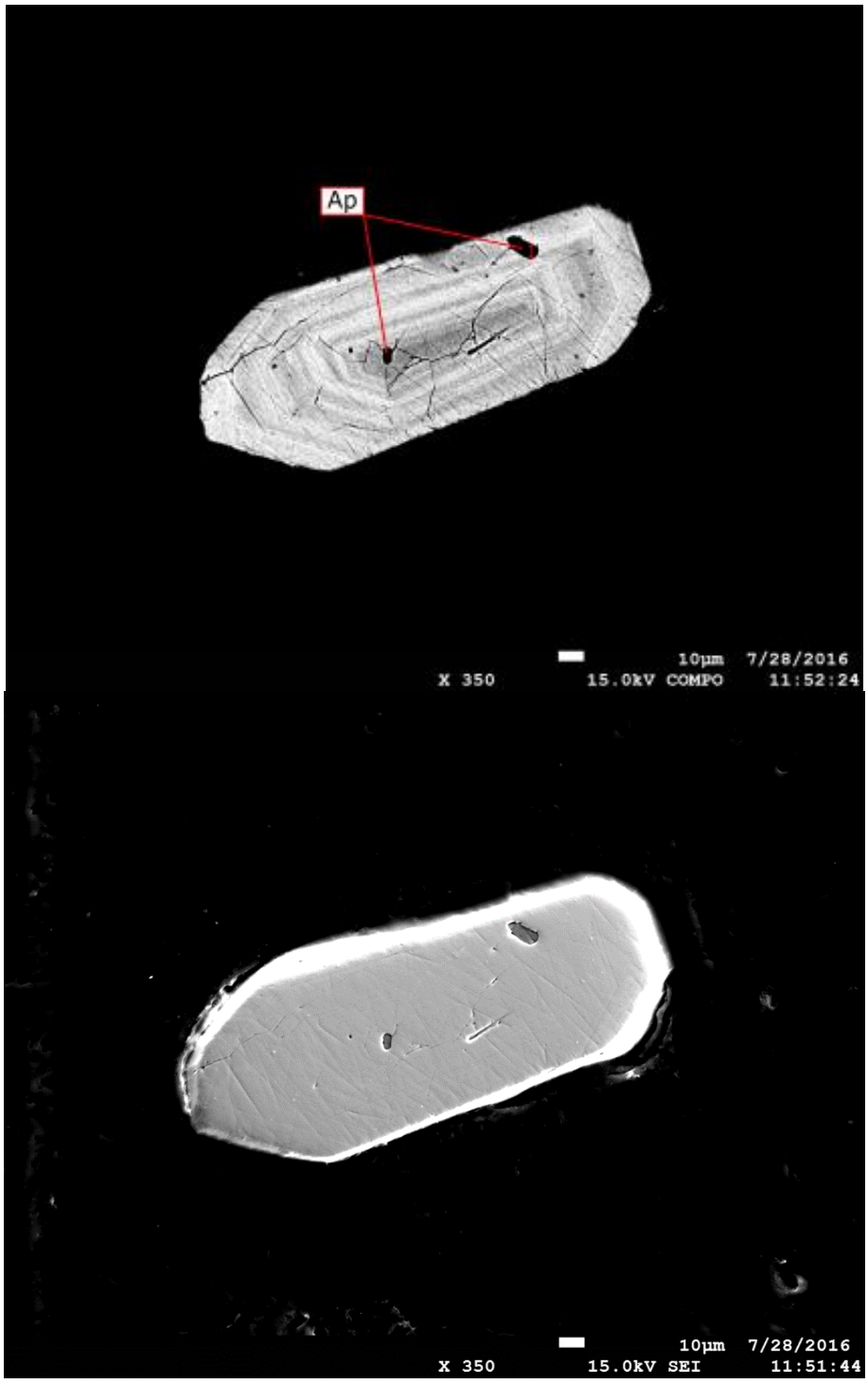
Ap
X 350
10µm
15.0kV COMPO
7/28/2016
11:52:24
X 350
10µm
15.0kV SEI
7/28/2016
11:51:44

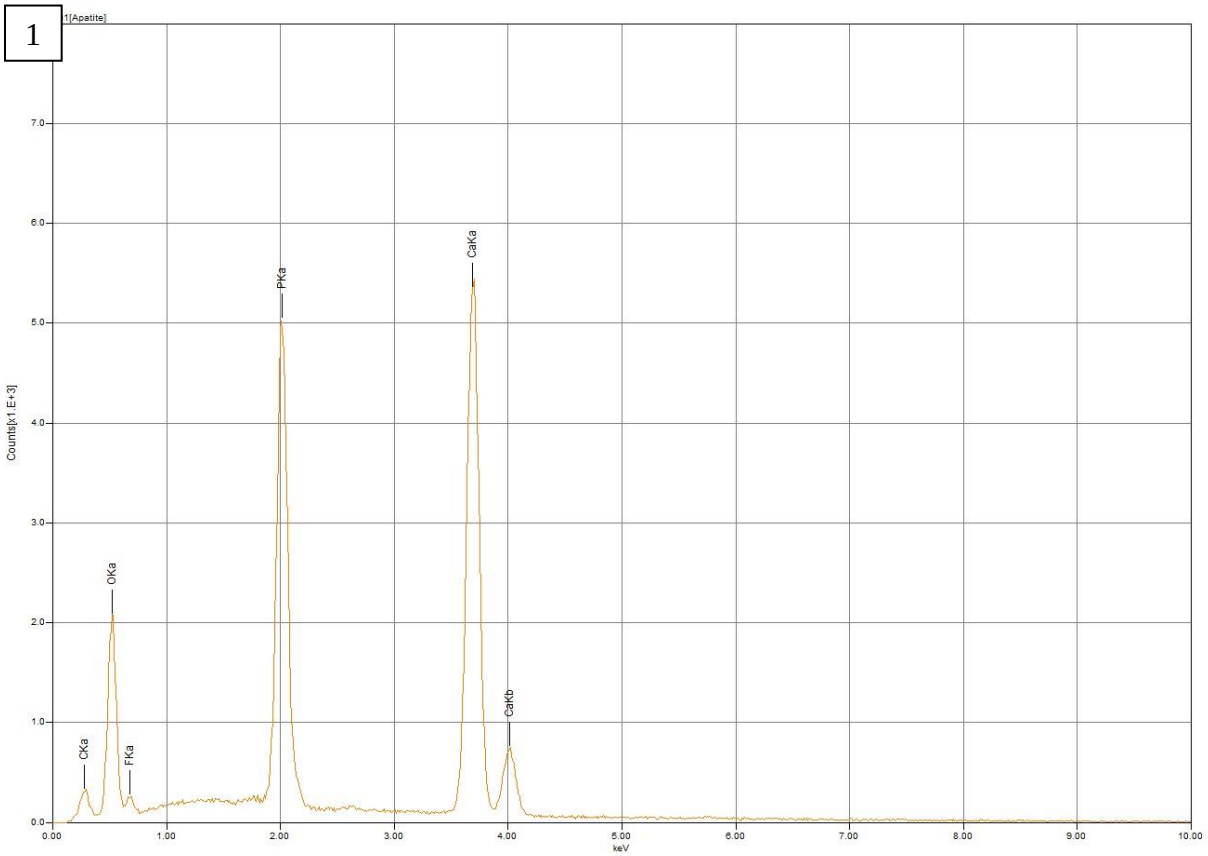
1
1[Apatite]
Counts[x1 E+3]
keV
CKa
OKa
FKa
PKa
CaKa
CaKb

Grain 8

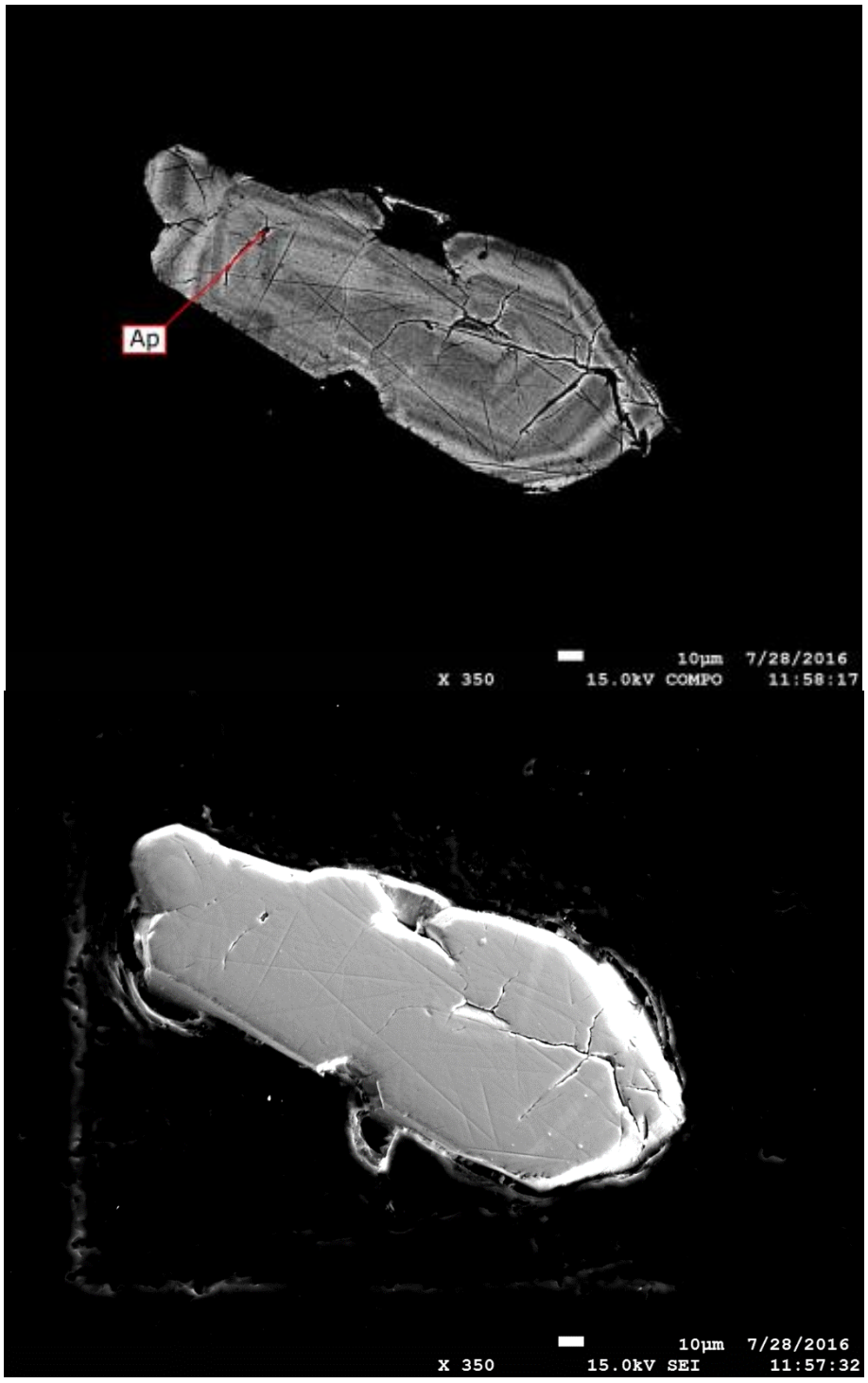
Ap
10µm 7/28/2016
X 350 15.0kV COMPO 11:58:17
10µm 7/28/2016
X 350 15.0kV SEI 11:57:32

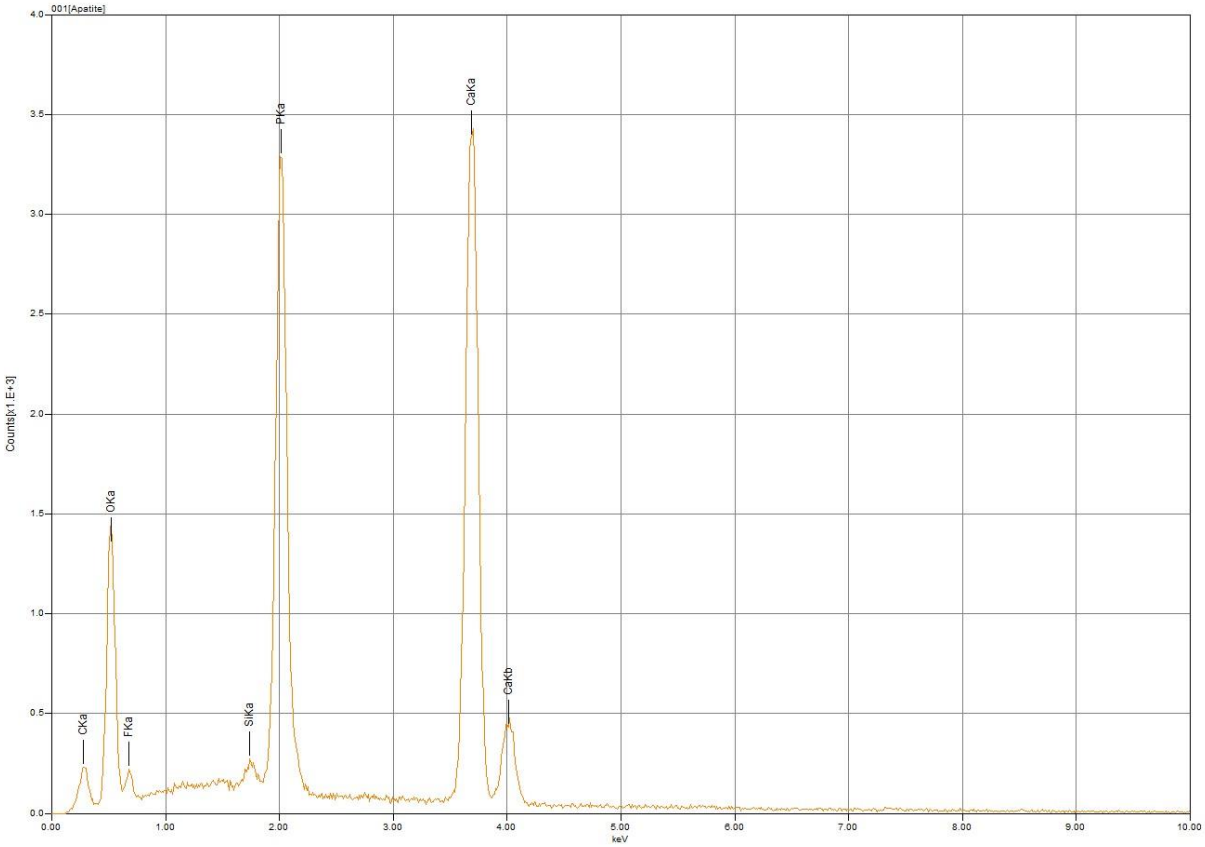
001[Apatite]
Counts[x1 E+3]
keV
CKa
OKa
FKa
SiKa
PKa
CaKa
CaKb

Grain 9

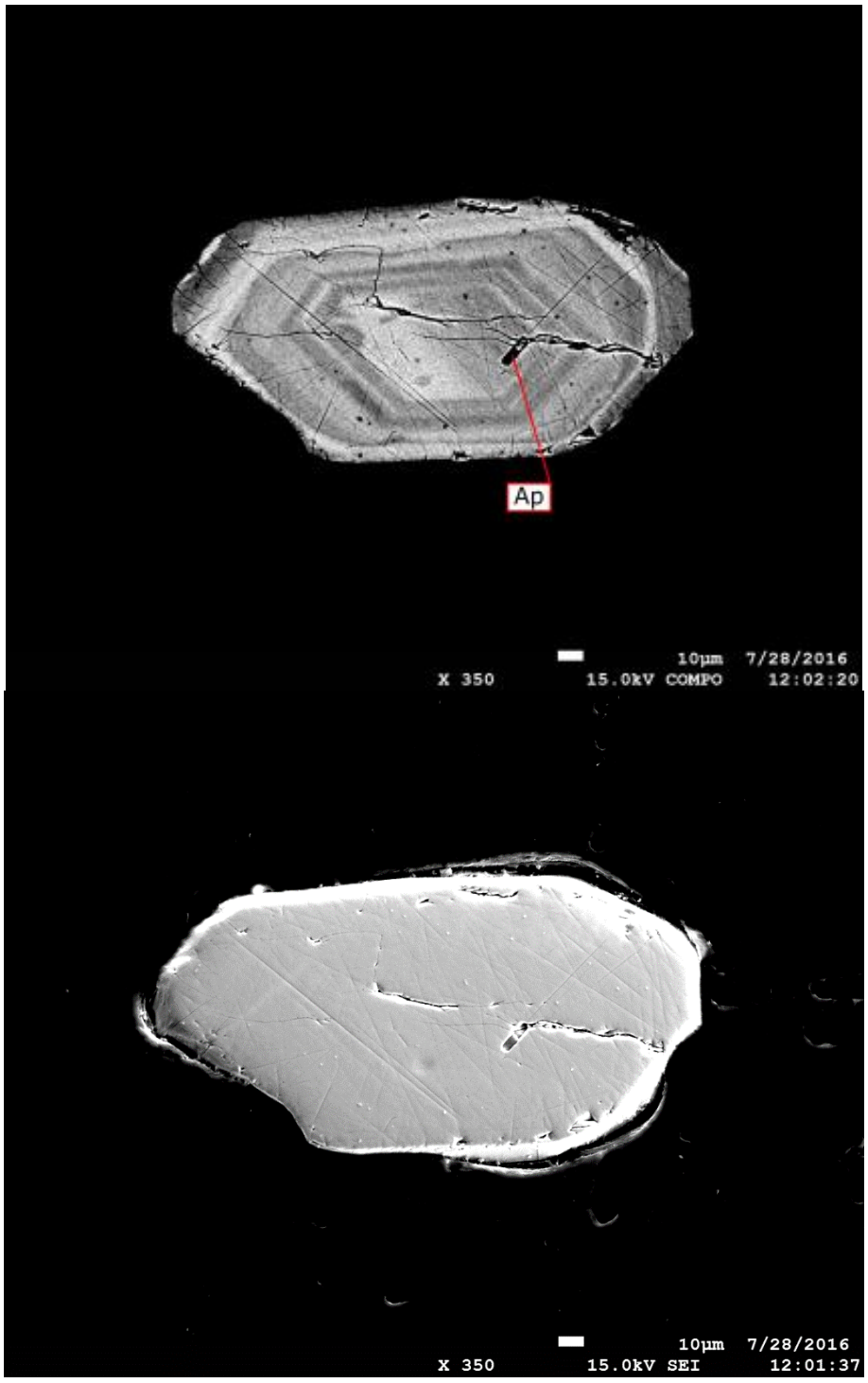
Ap
10µm 7/28/2016
X 350 15.0kV COMPO 12:02:20
10µm 7/28/2016
X 350 15.0kV SEI 12:01:37

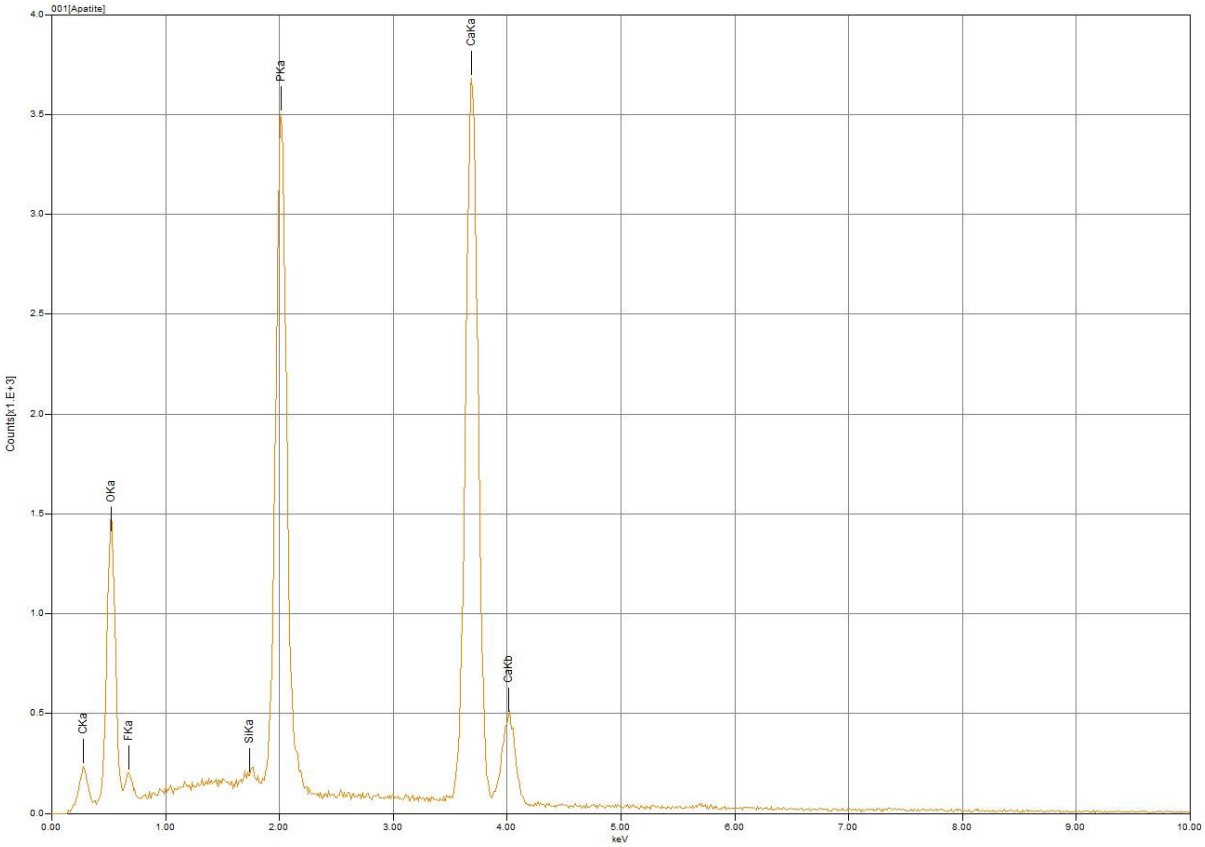
001[Apatite]
PKa
CaKa
OKa
CKa
FKa
SiKa
CaKb
Counts[x1 E+3]
keV
0.00
1.00
2.00
3.00
4.00
5.00
6.00
7.00
8.00
9.00
10.00
0.0
0.5
1.0
1.5
2.0
2.5
3.0
3.5
4.0

Grain 11

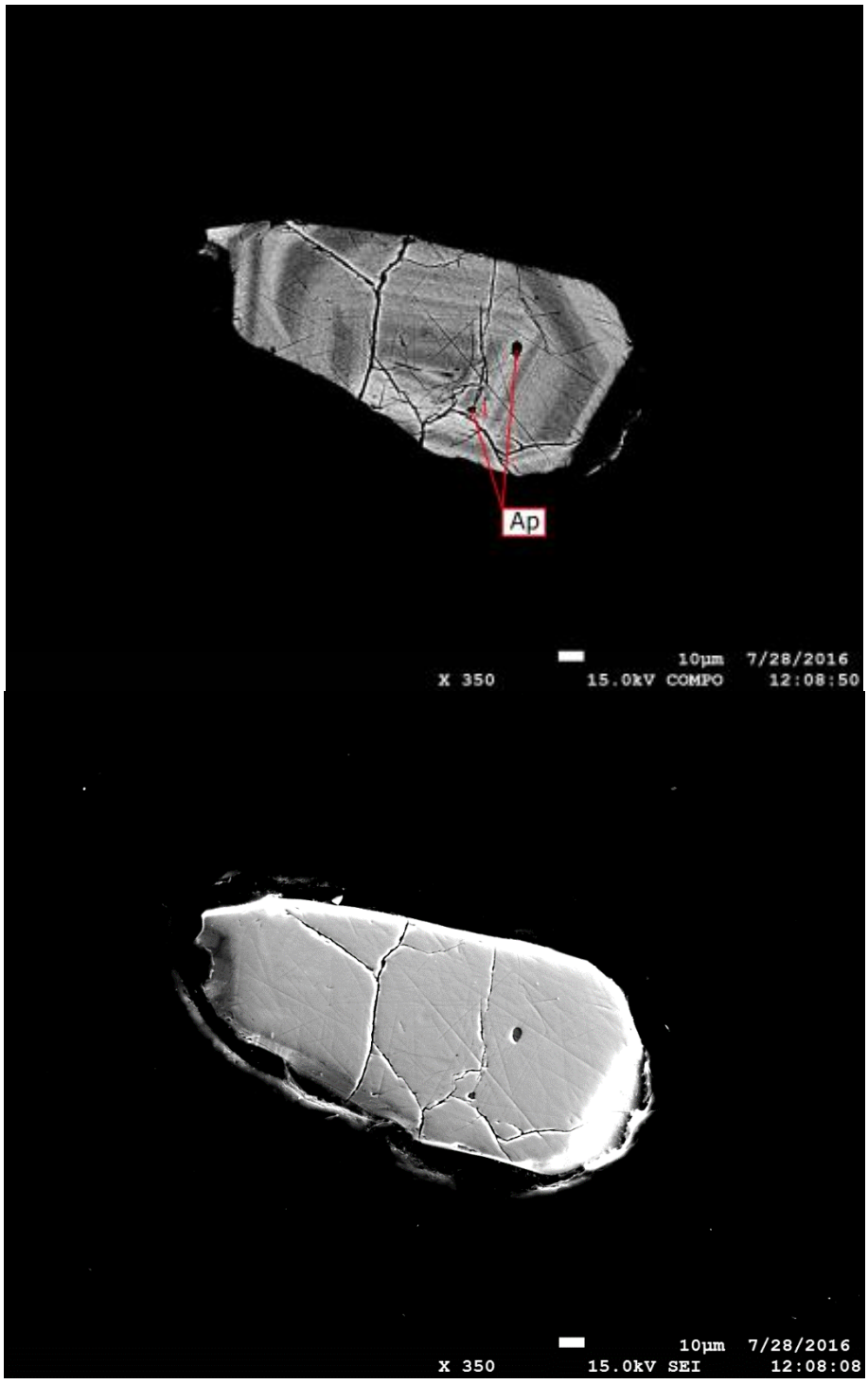
Ap
10µm 7/28/2016
X 350 15.0kV COMPO 12:08:50
10µm 7/28/2016
X 350 15.0kV SEI 12:08:08

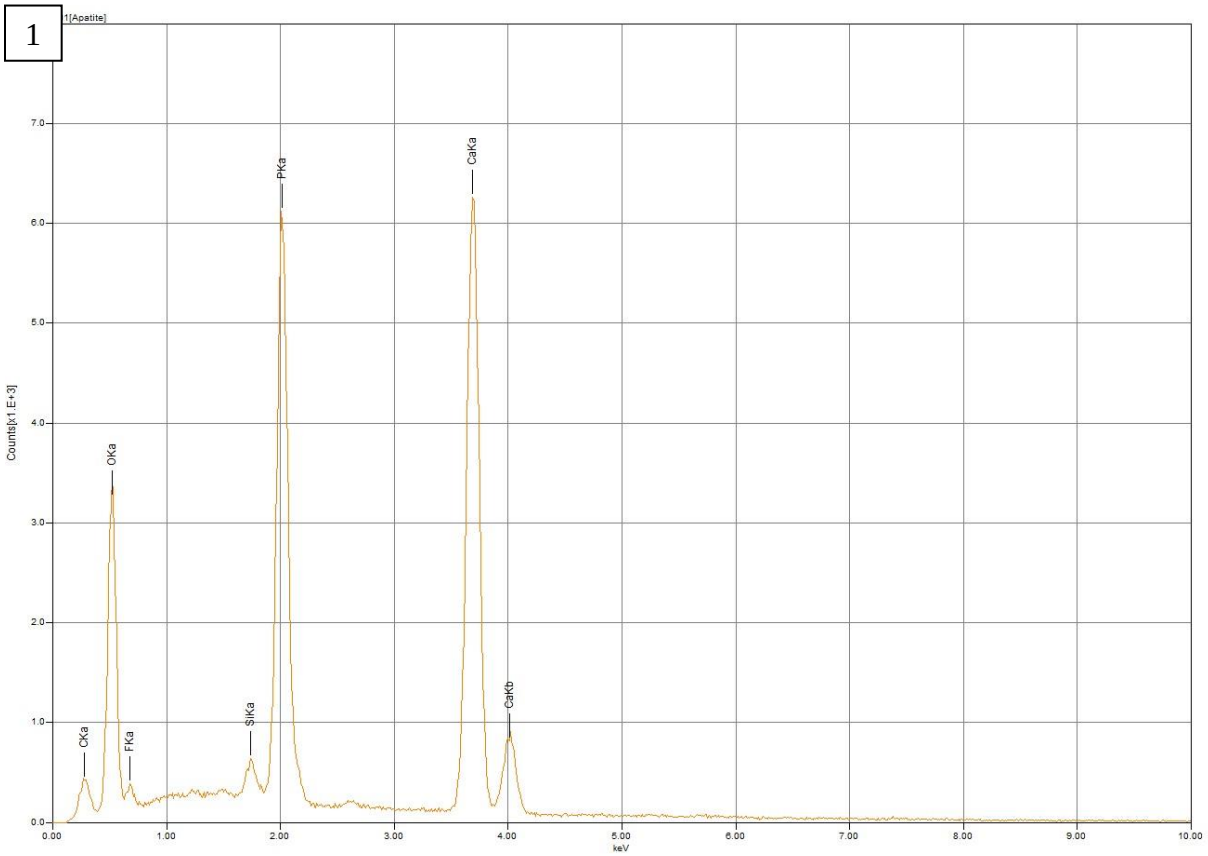
1
1[Apatite]
Counts[x1 E+3]
7.0
6.0
5.0
4.0
3.0
2.0
1.0
0.0
CKa
OKa
FKa
SiKa
PKa
CaKa
CaKb
0.00
1.00
2.00
3.00
4.00
5.00
6.00
7.00
8.00
9.00
10.00
keV

Grain 13

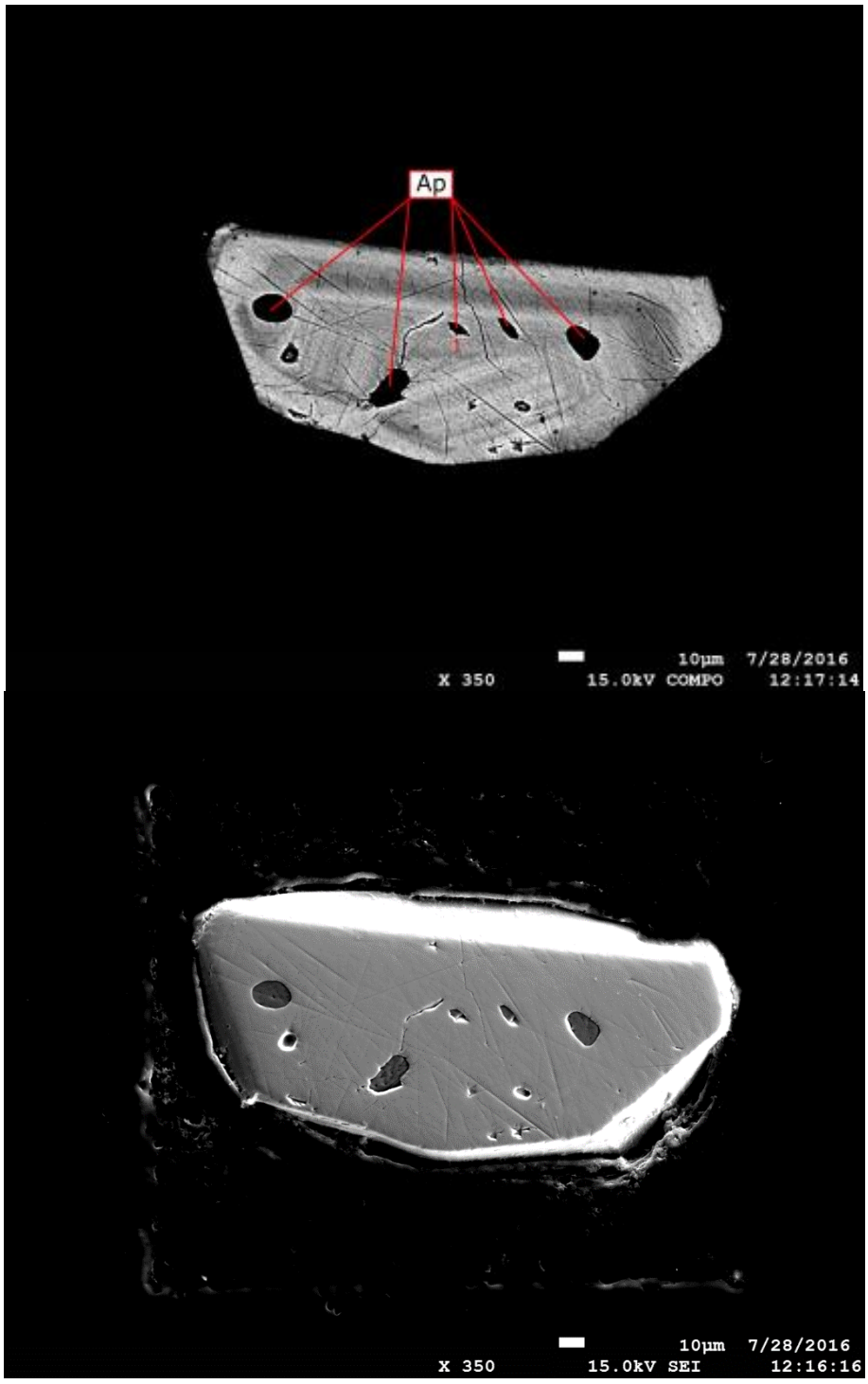
Ap
10µm 7/28/2016
X 350 15.0kV COMPO 12:17:14
10µm 7/28/2016
X 350 15.0kV SEI 12:16:16

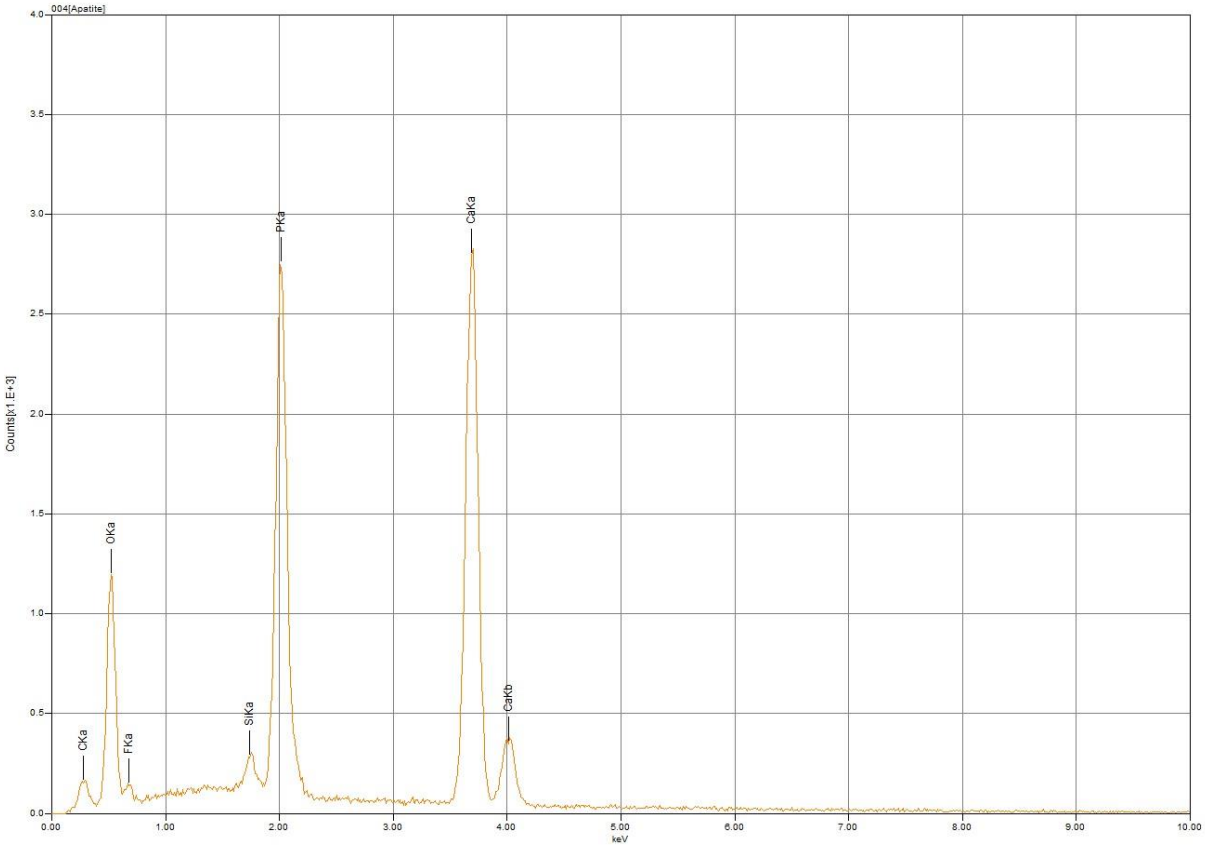
004[Apatite]
Counts[x1 E+3]
keV
CKa
OKa
FKa
SiKa
PKa
CaKa
CaKb

Grain 14


Ap
10µm 7/28/2016
X 350 15.0kV COMPO 12:21:24
10µm 7/28/2016
X 350 15.0kV SEI 12:20:39

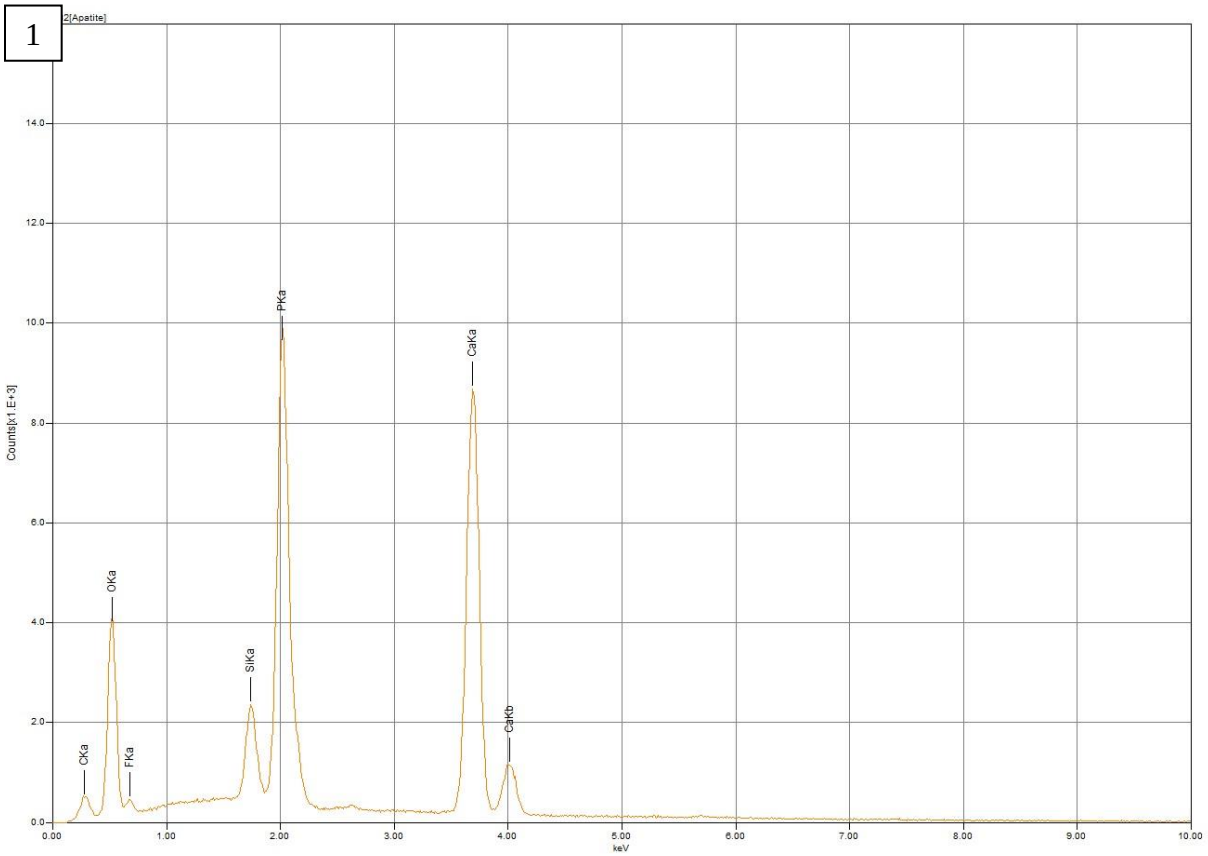
1
2[Apatite]
Counts[x1 E+3]
14.0
12.0
10.0
8.0
6.0
4.0
2.0
0.0
CKa
OKa
FKa
SiKa
PKa
CaKa
CaKb
0.00
1.00
2.00
3.00
4.00
5.00
6.00
7.00
8.00
9.00
10.00
keV

Grain 18

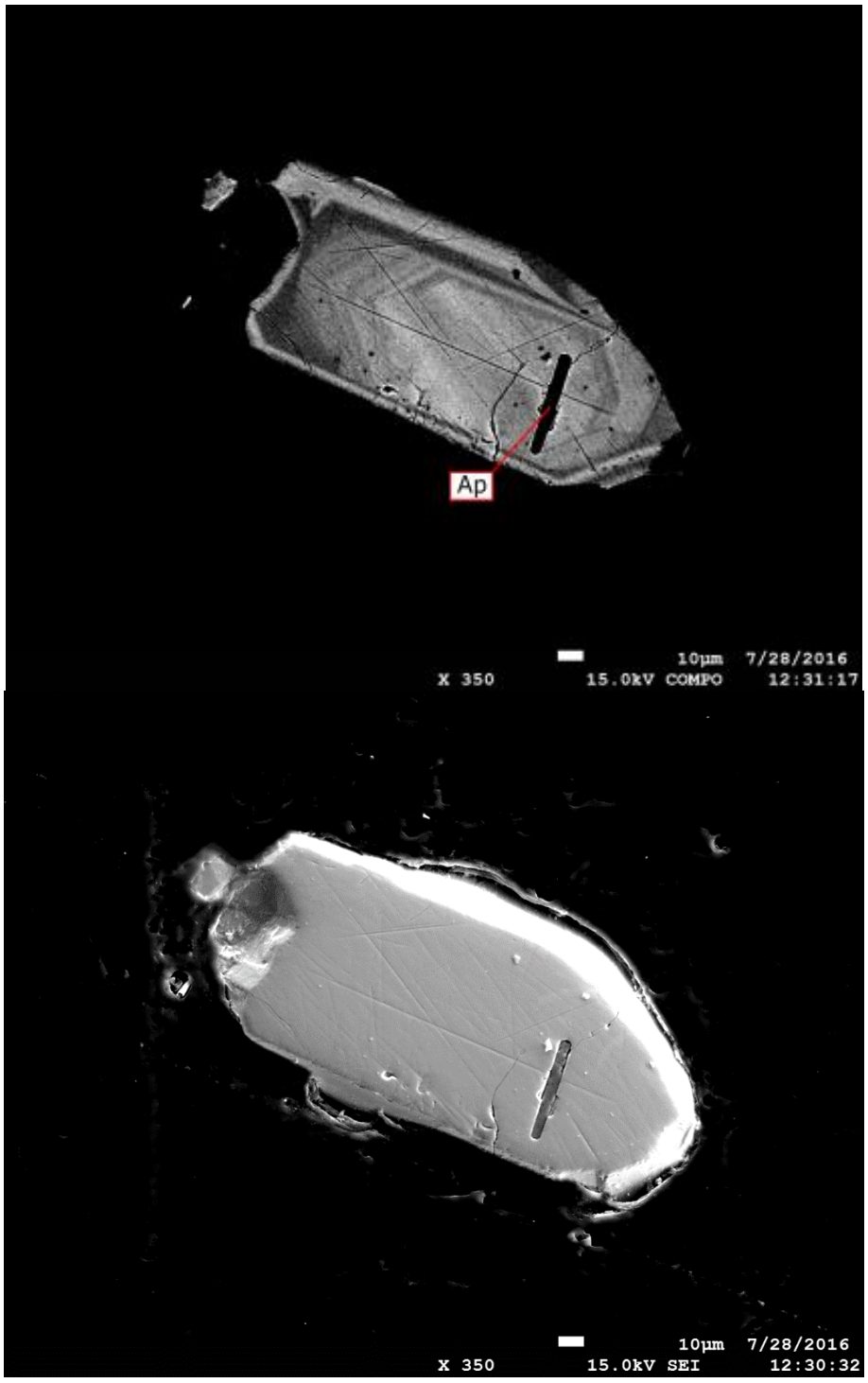
Ap
10µm 7/28/2016
X 350 15.0kV COMPO 12:31:17
10µm 7/28/2016
X 350 15.0kV SEI 12:30:32

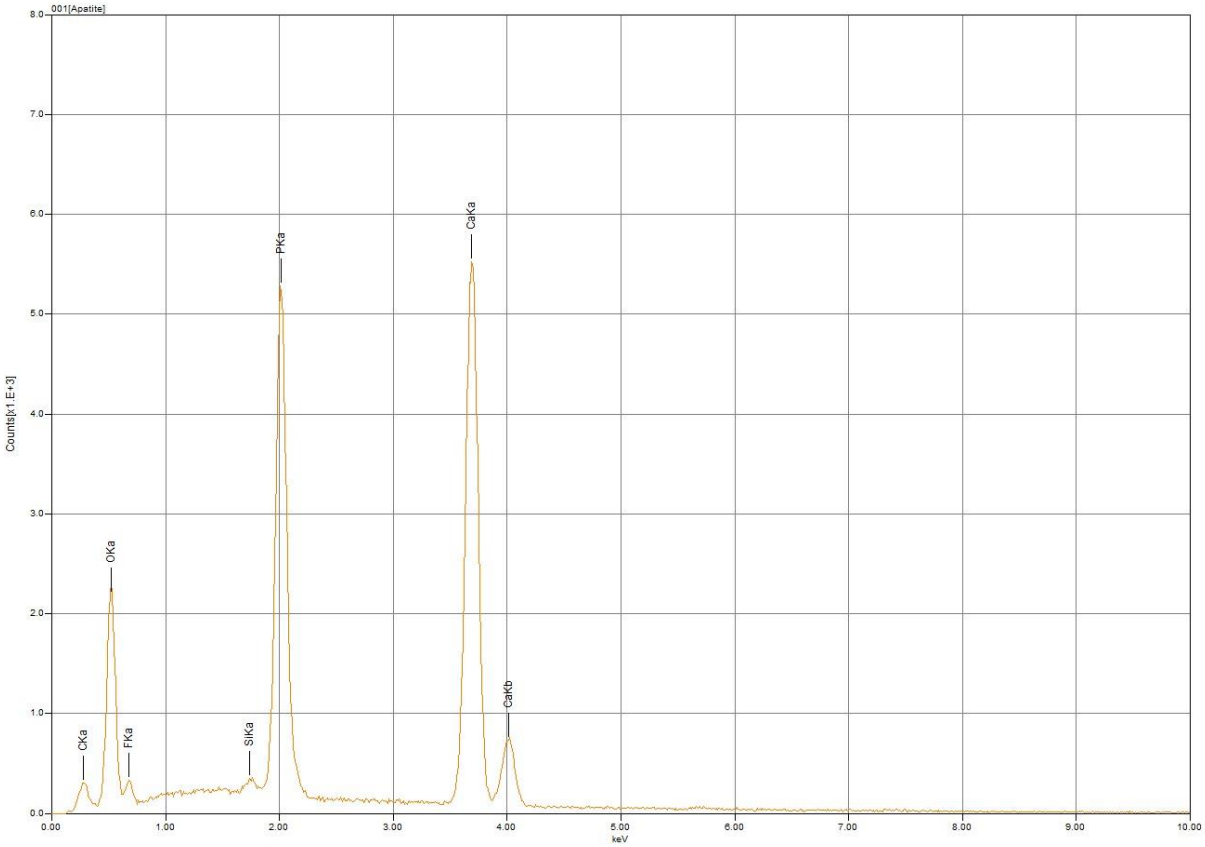
001[Apatite]
Counts[x1 E+3]
keV
CKa
OKa
FKa
SiKa
PKa
CaKa
CaKb

Grain 19


Ap
10µm 7/28/2016
X 350 15.0kV COMPO 12:34:15
10µm 7/28/2016
X 350 15.0kV SEI 12:33:29

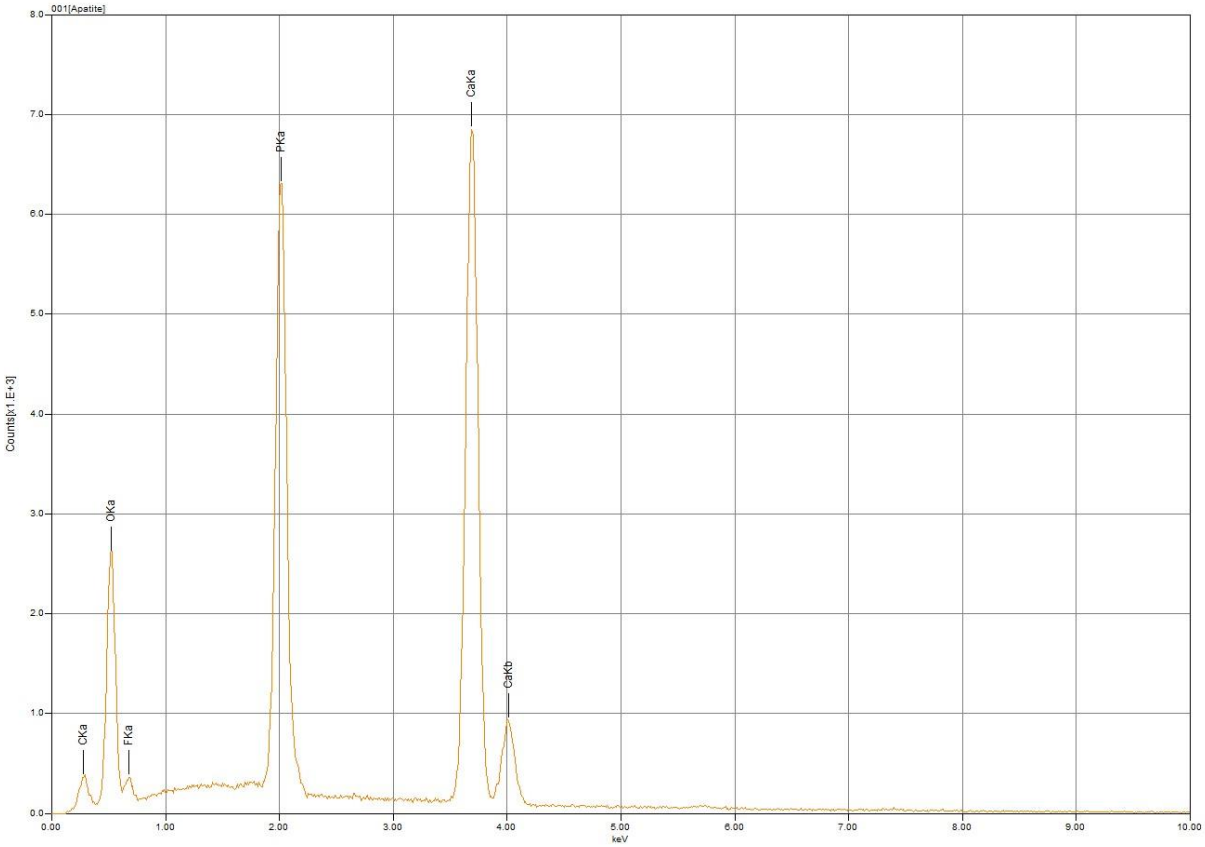
001[Apatite]
Counts[x1 E+3]
keV
CKa
OKa
FKa
PKa
CaKa
CaKb

Grain 3


Ep
10µm 7/15/2016
X 300 15.0kV COMPO 11:33:04

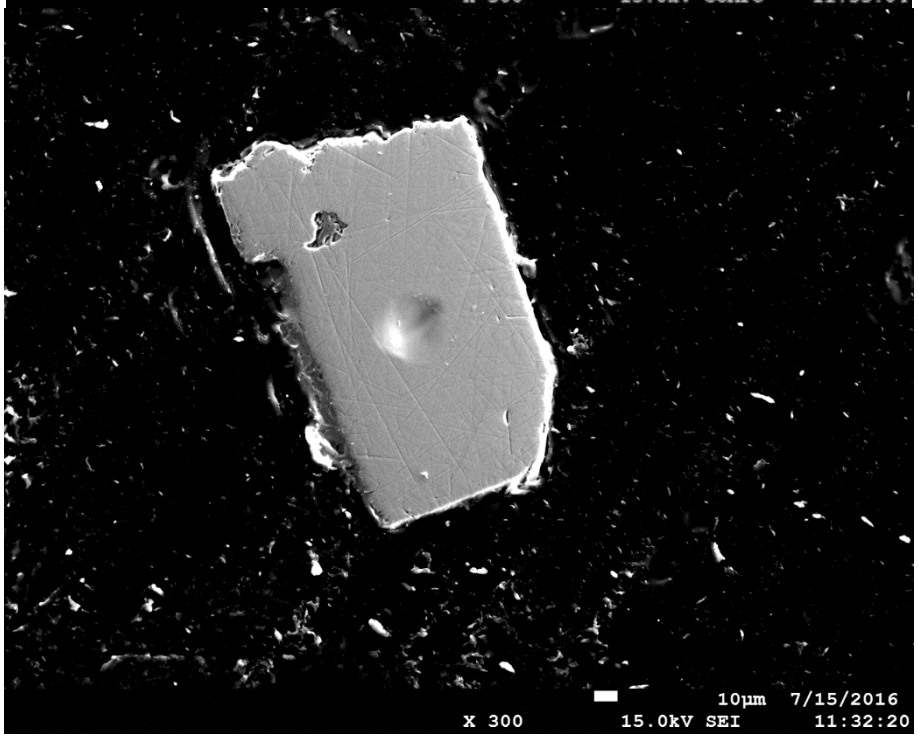
10µm 7/15/2016
X 300 15.0kV SEI 11:32:20

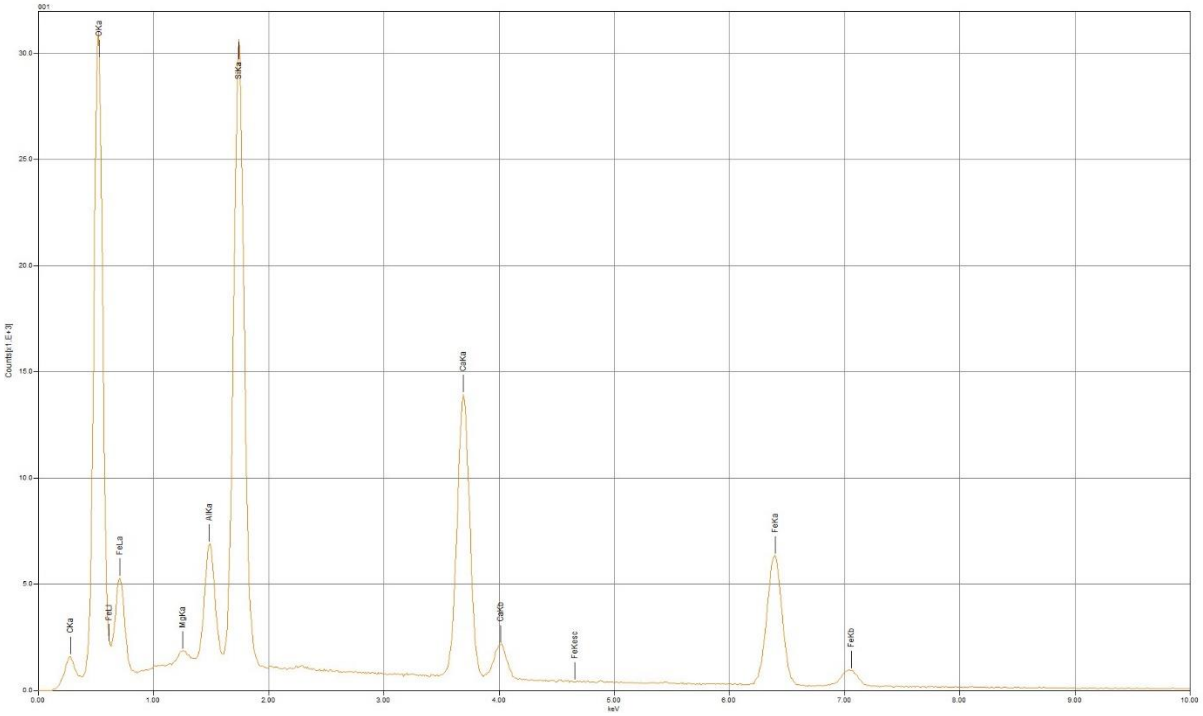
901
OKa
SiKa
CaKa
FeKa
AlKa
FeLa
FeLb
MgKa
CKa
CaKb
FeKes
FeKb
Counts[n.Ex.]
keV

Grain 5

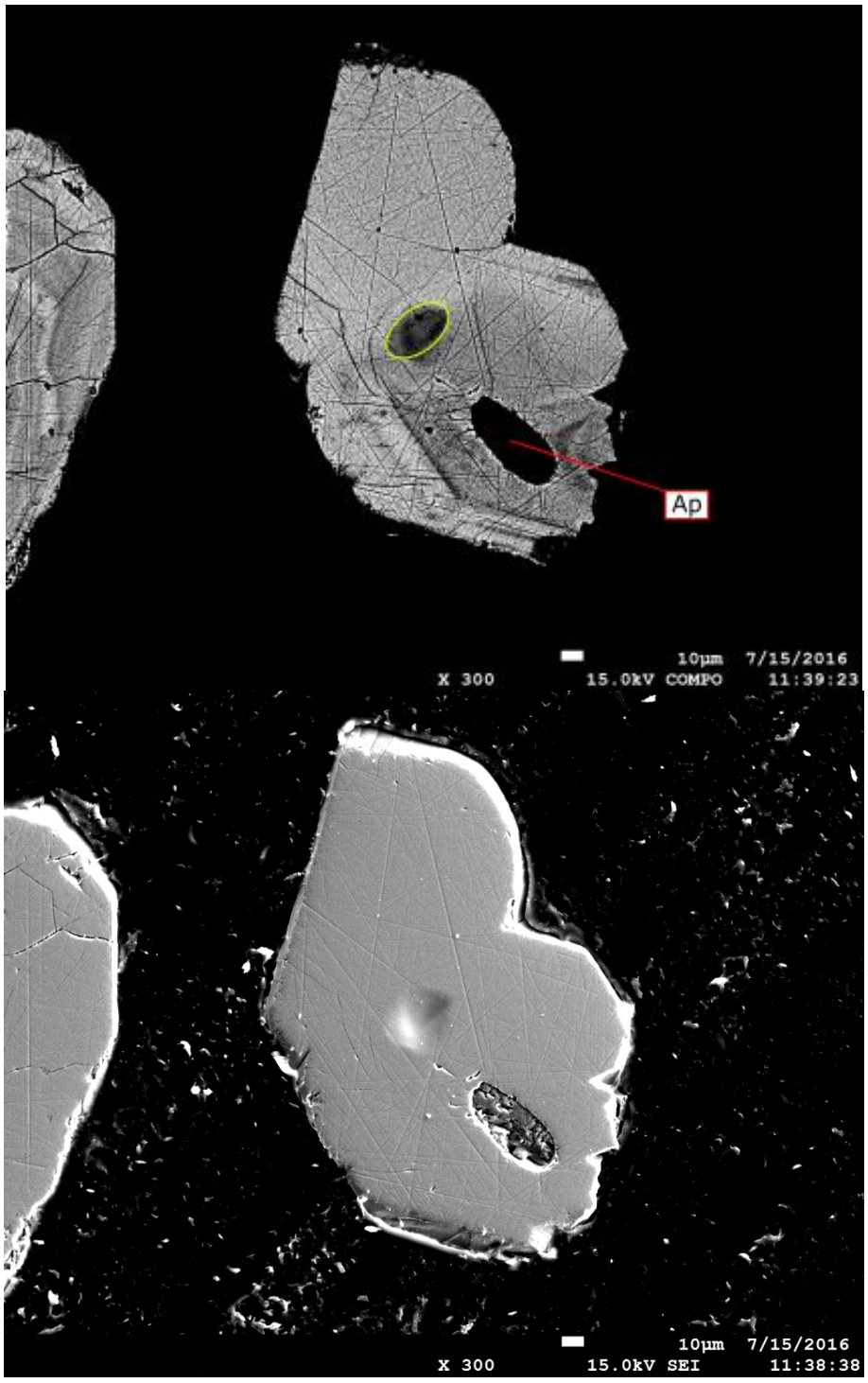
Ap
X 300
10µm 7/15/2016
15.0kV COMPO 11:39:23
X 300
10µm 7/15/2016
15.0kV SEI 11:38:38

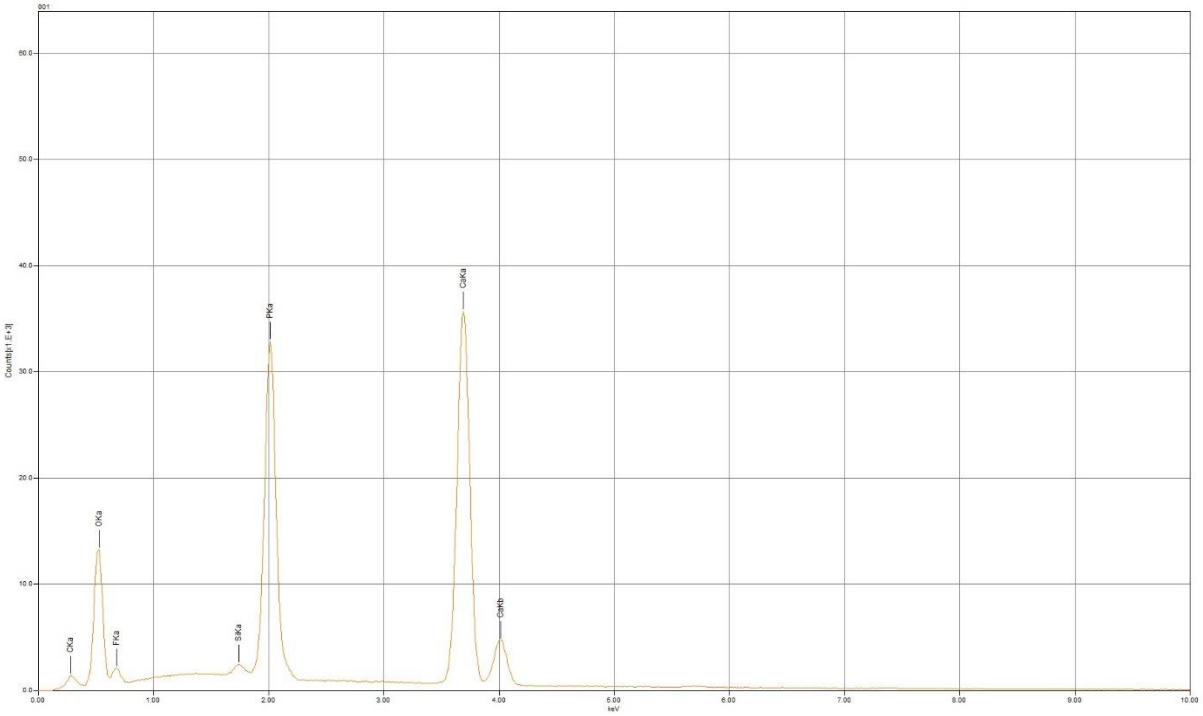
901
60.0
50.0
40.0
30.0
20.0
10.0
0.0
Counts[n.Ex3]
OKa
OKa
FKa
SiKa
PKa
CaKa
CaKb
0.00
1.00
2.00
3.00
4.00
5.00
6.00
7.00
8.00
9.00
10.00
keV

Grain 6

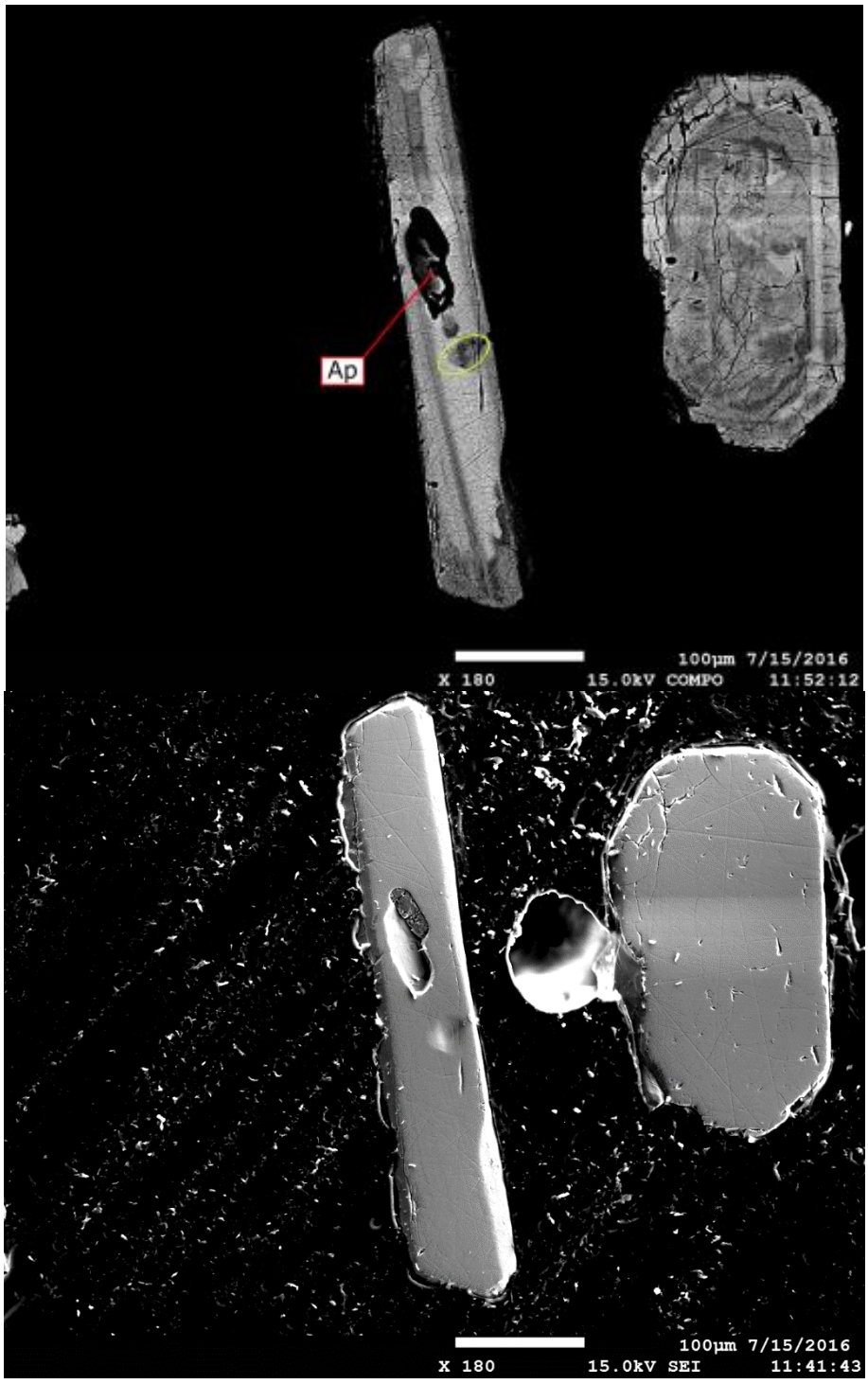
Ap
100µm 7/15/2016
X 180 15.0kV COMPO 11:52:12
100µm 7/15/2016
X 180 15.0kV SEI 11:41:43

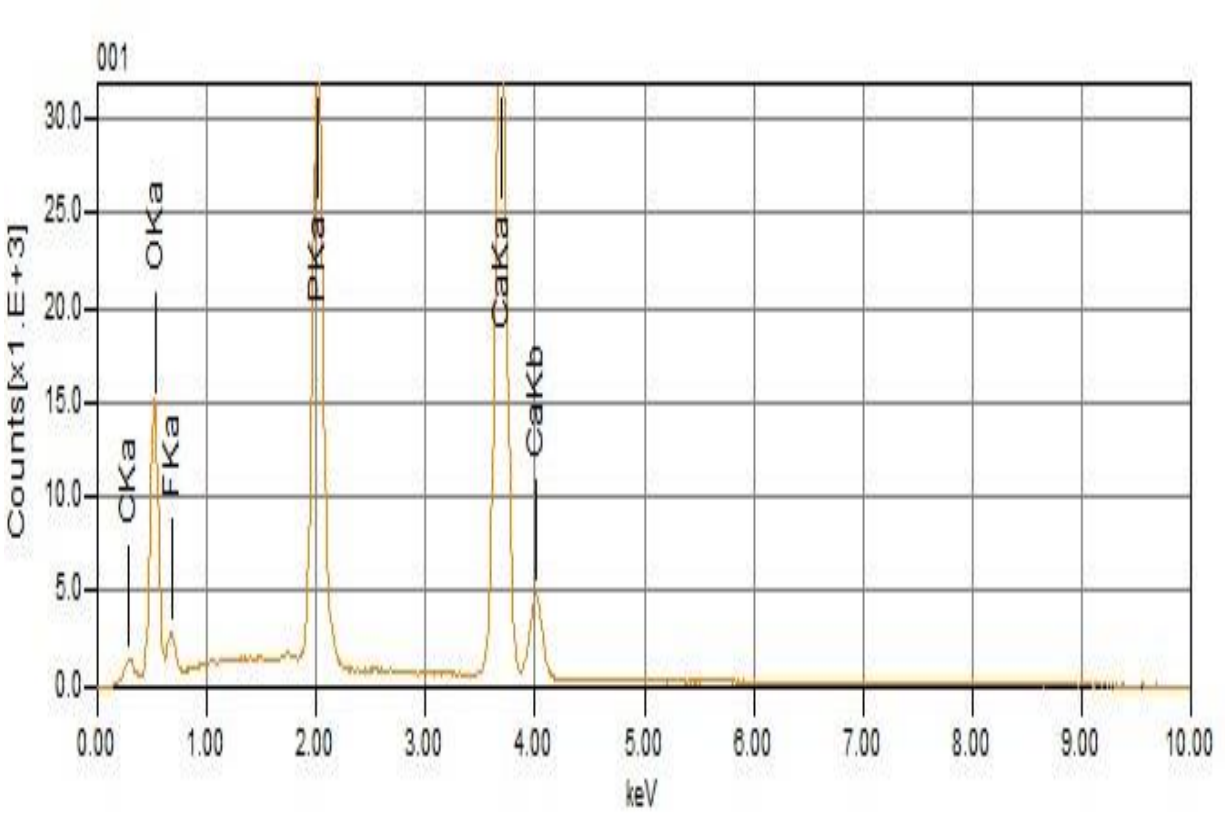
001
Counts[x1.E+3]
30.0
25.0
20.0
15.0
10.0
5.0
0.0
CKa
OKa
FKa
PKa
CaKa
CaKb
0.00
1.00
2.00
3.00
4.00
5.00
6.00
7.00
8.00
9.00
10.00
keV

Grain 12

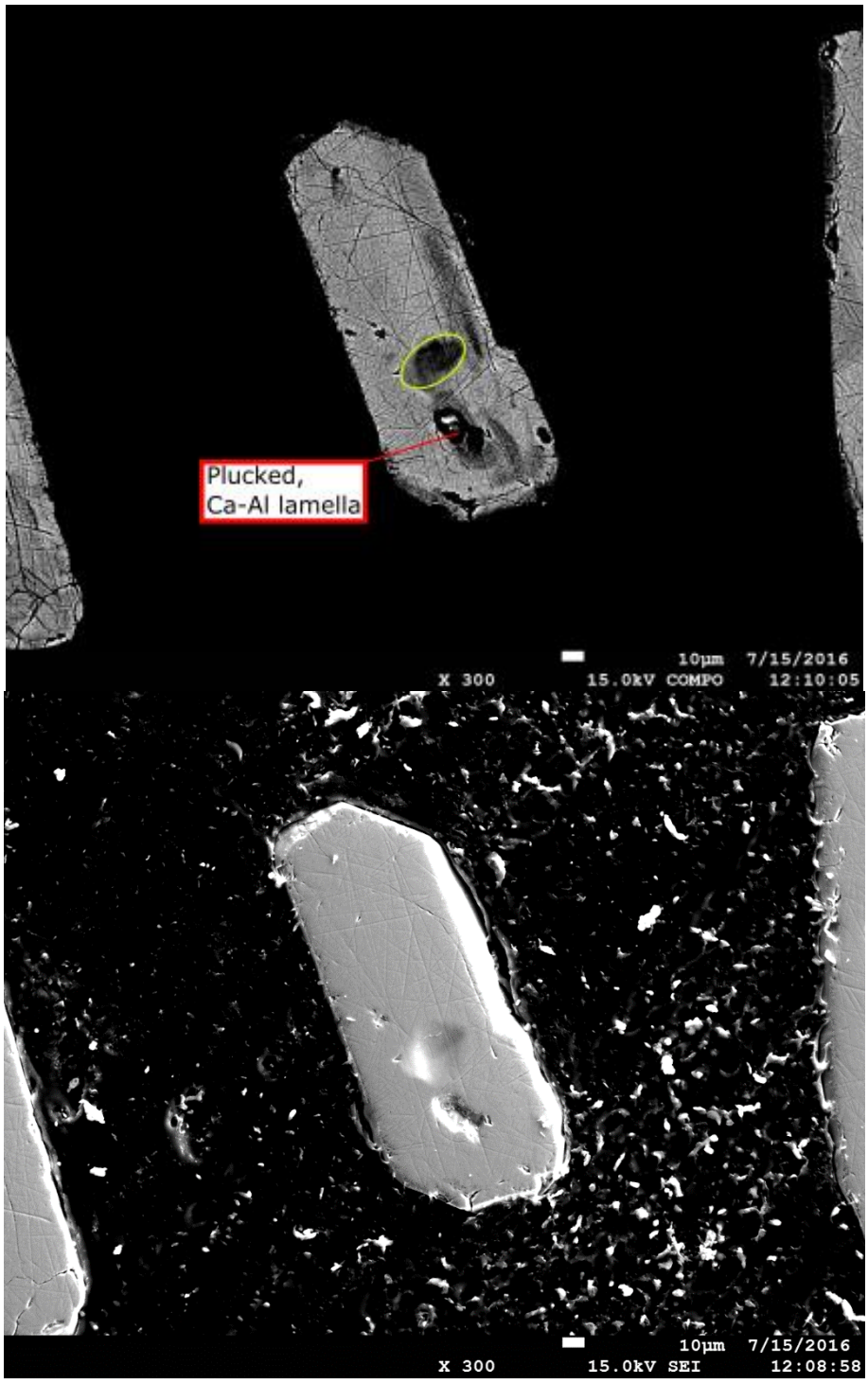
Plucked,
Ca-Al lamella
10µm 7/15/2016
X 300 15.0kV COMPO 12:10:05
10µm 7/15/2016
X 300 15.0kV SEI 12:08:58

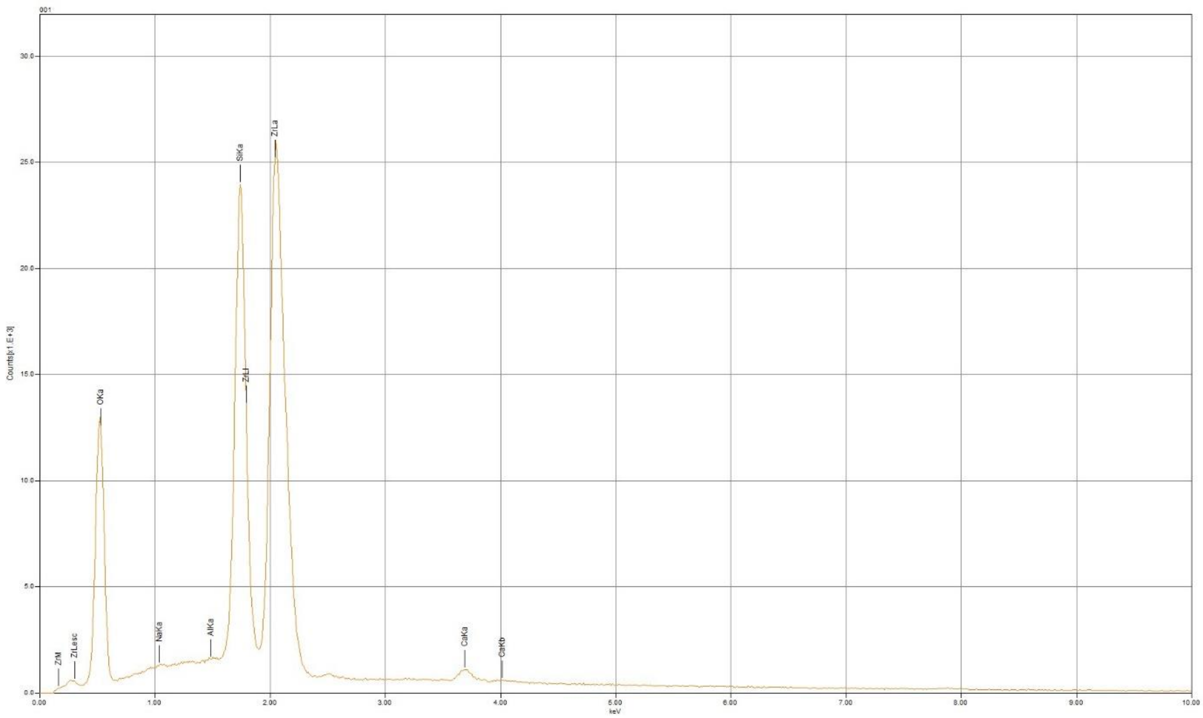
001
30.0
25.0
20.0
15.0
10.0
5.0
0.0
Counts[x1.E+3]
ZrLa
SiKa
ZrLl
OKa
ZrM
ZrLesc
NaKa
AlKa
CaKa
CaKb
0.00
1.00
2.00
3.00
4.00
5.00
6.00
7.00
8.00
9.00
10.00
keV

178084

Grain 3

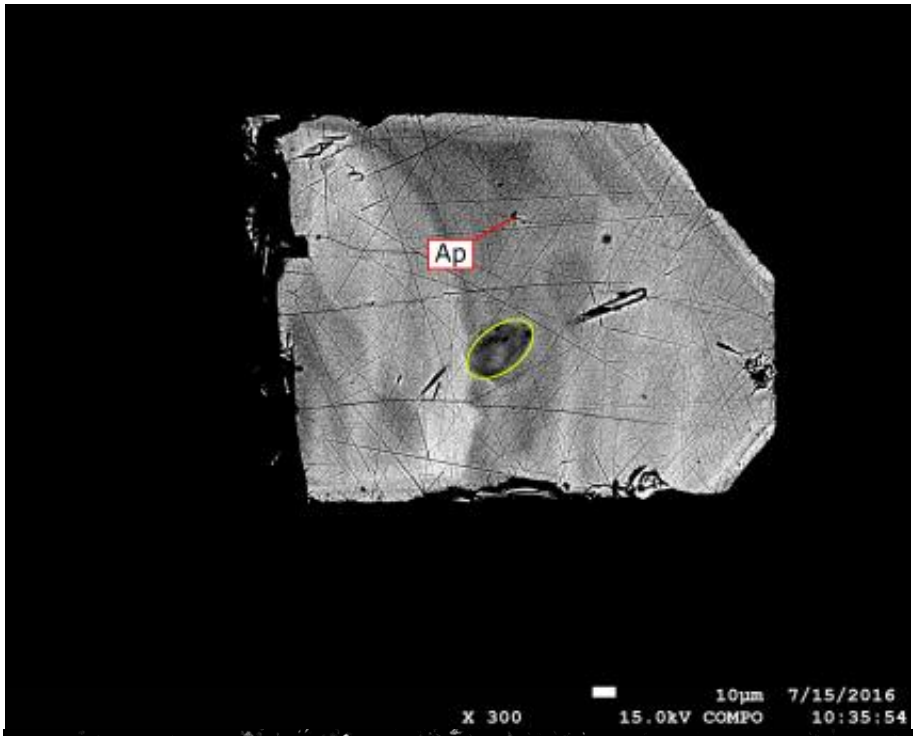

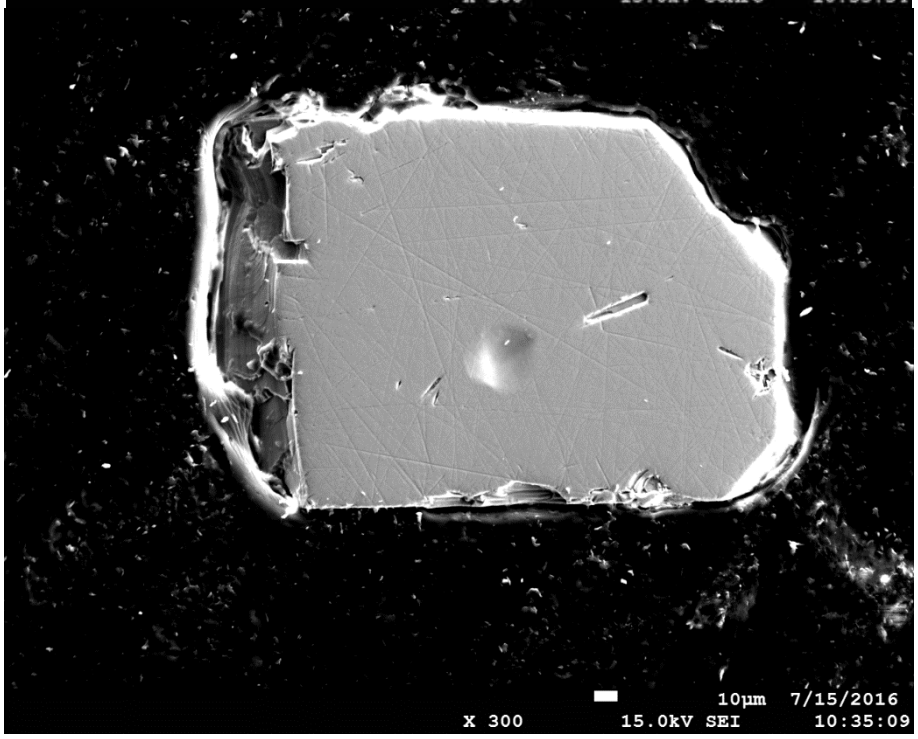

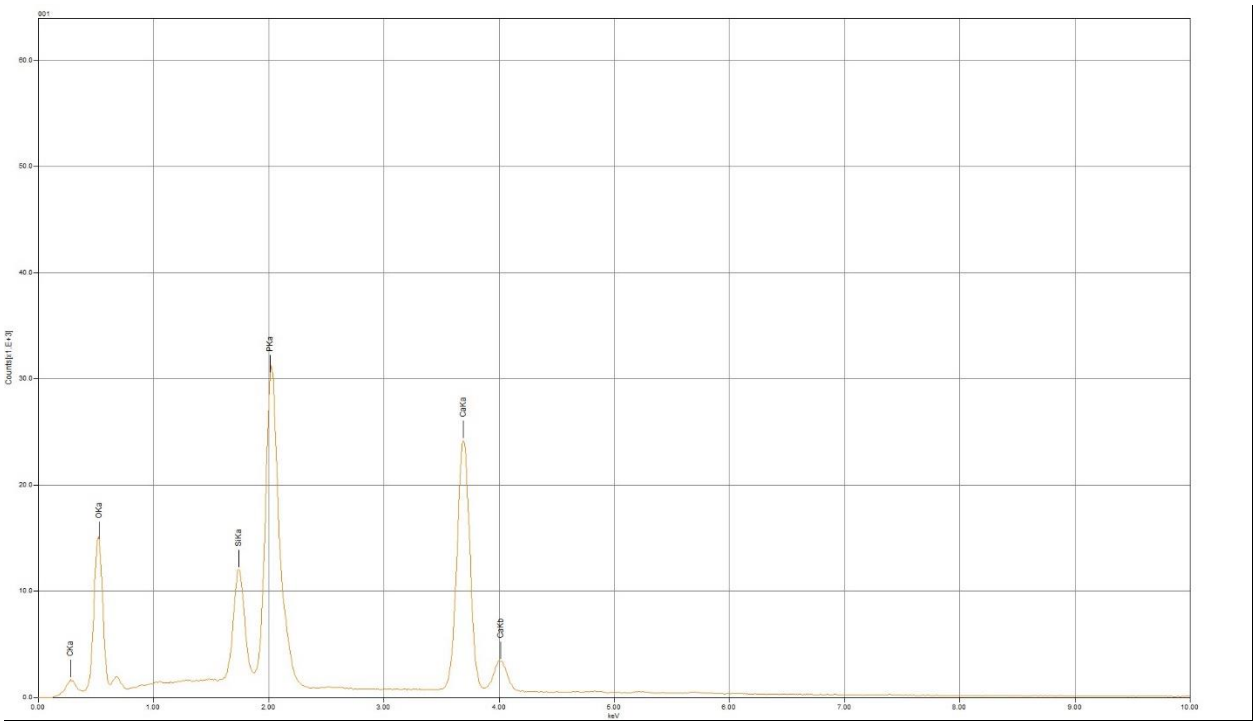
901
60.0
50.0
40.0
30.0
20.0
10.0
0.0
Counts[n.t.e.s]
OKa
OKa
SiKa
PKa
CaKa
CaKb
0.00
1.00
2.00
3.00
4.00
5.00
6.00
7.00
8.00
9.00
10.00
keV

Grain 7

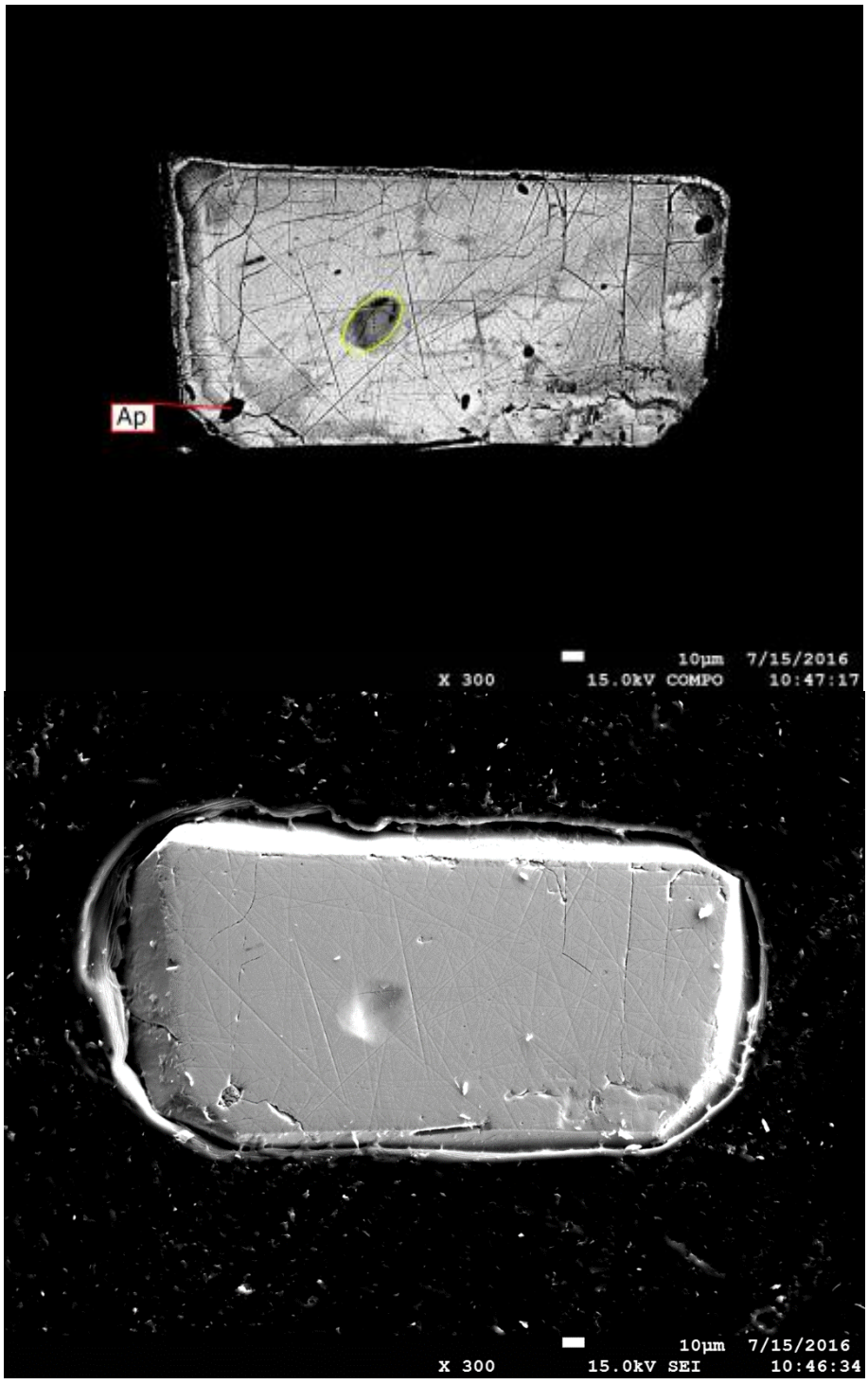
Ap
X 300
10µm
15.0kV COMPO
7/15/2016
10:47:17
X 300
10µm
15.0kV SEI
7/15/2016
10:46:34

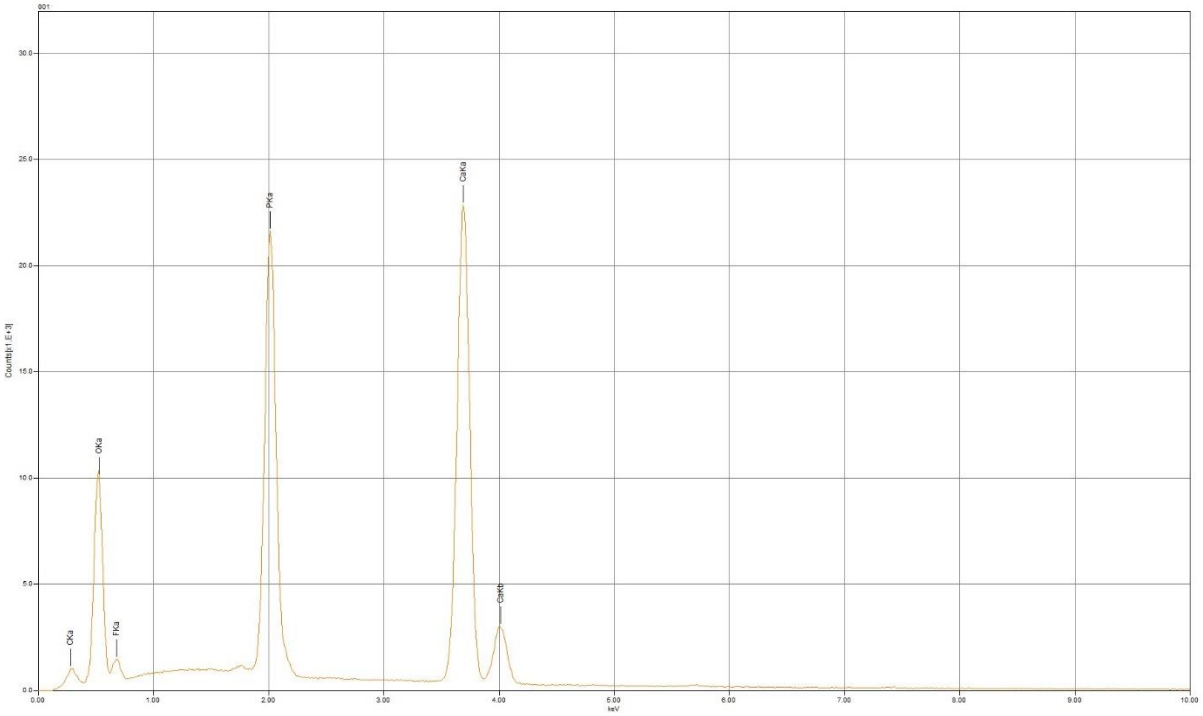
901
30.0
25.0
20.0
15.0
10.0
5.0
0.0
Counts[n.E.n]
OKa
OKa
FKa
PKa
CaKa
CaKb
0.00
1.00
2.00
3.00
4.00
5.00
6.00
7.00
8.00
9.00
10.00
keV

Grain 9

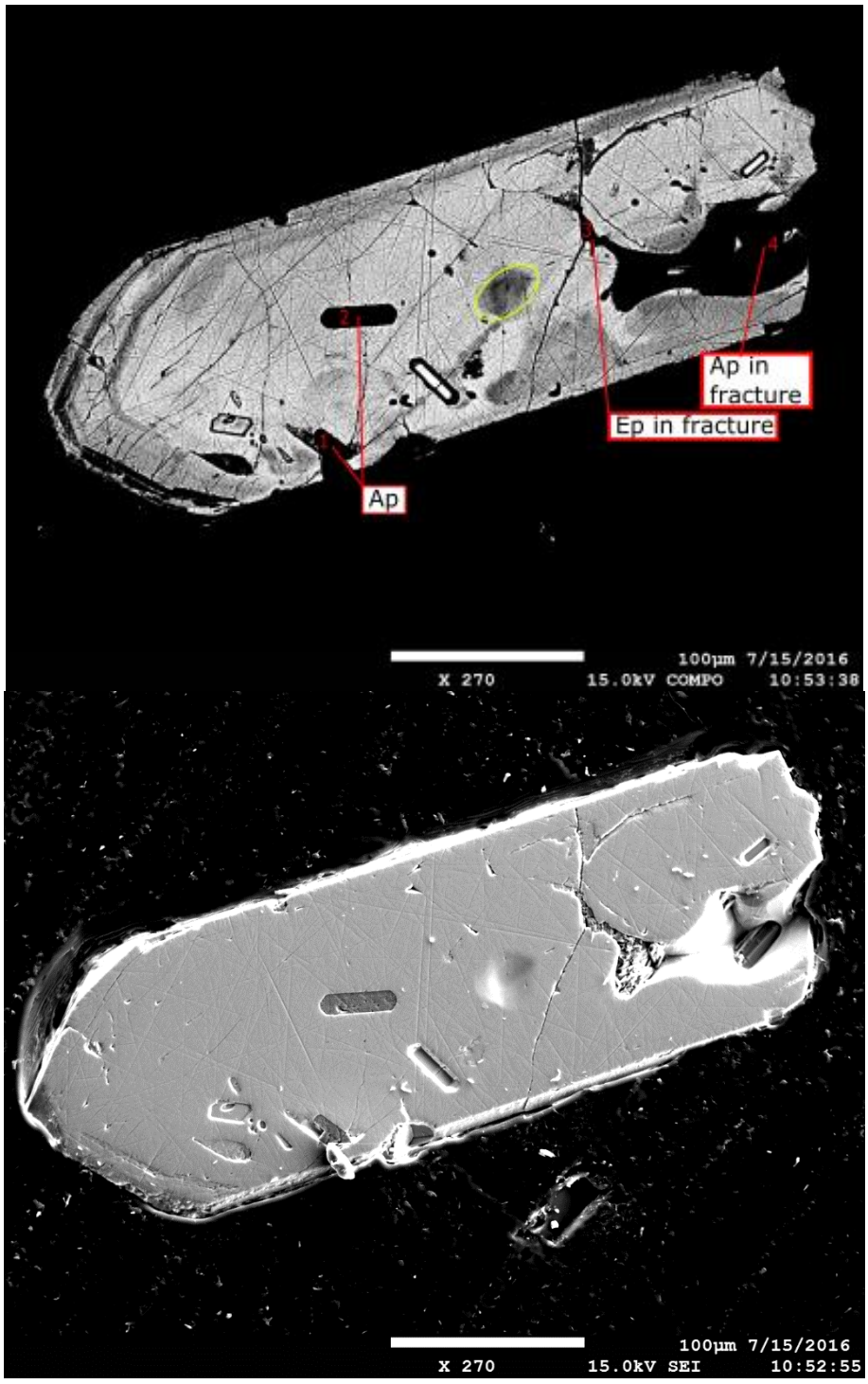
Ap in fracture
Ep in fracture
Ap
100µm 7/15/2016
X 270 15.0kV COMPO 10:53:38
100µm 7/15/2016
X 270 15.0kV SEI 10:52:55

1

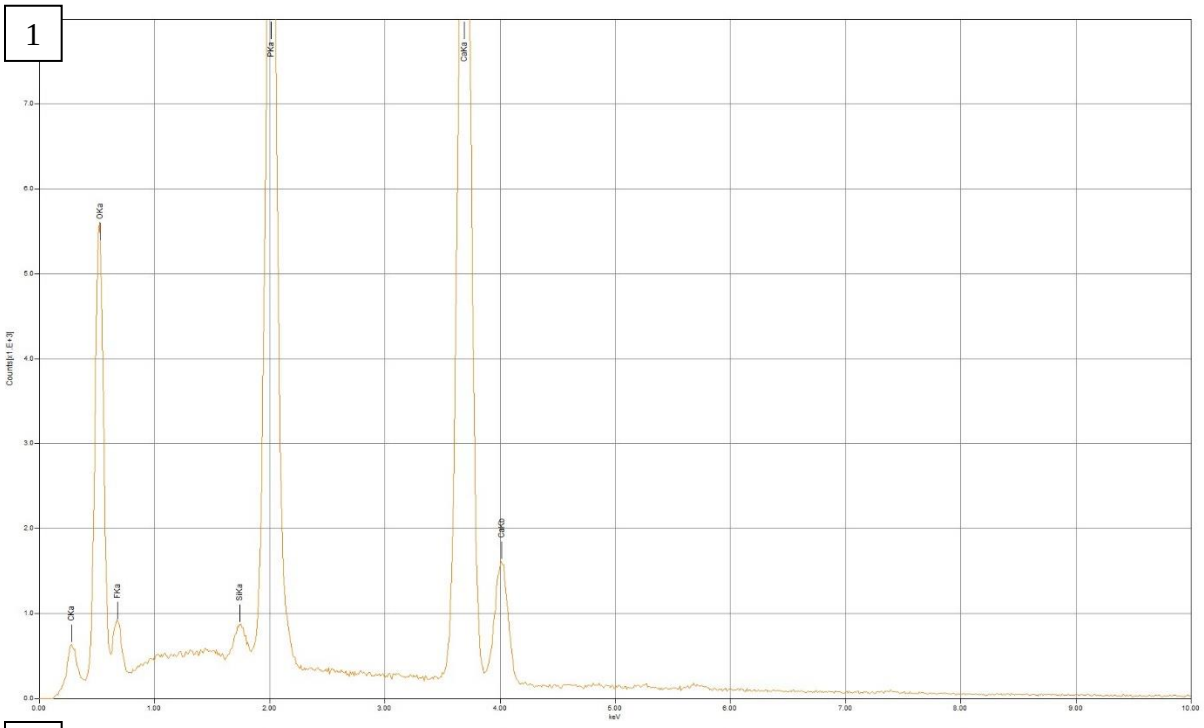
PKa
CaKa
OKa
CaKb
FKa
SiKa
OKa
keV

2

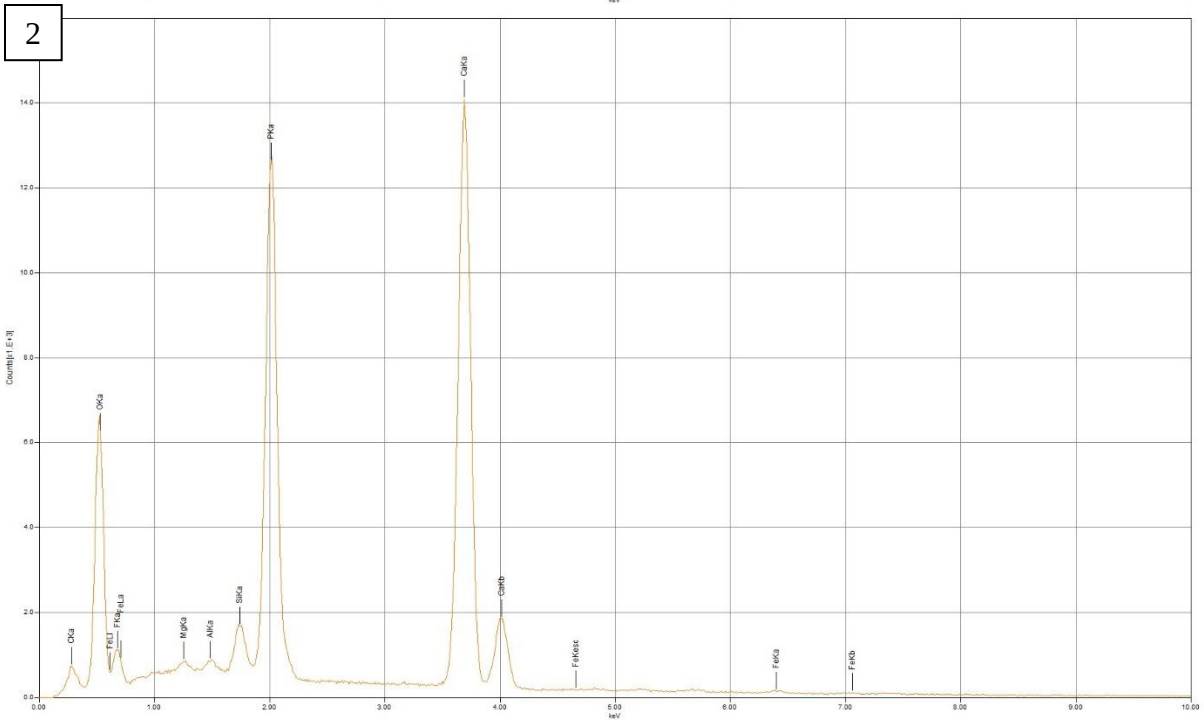
CaKa
PKa
OKa
CaKb
SiKa
OKa
FeLl
FKa
MgKa
AlKa
FeKesc
FeKa
FeKb
keV

4

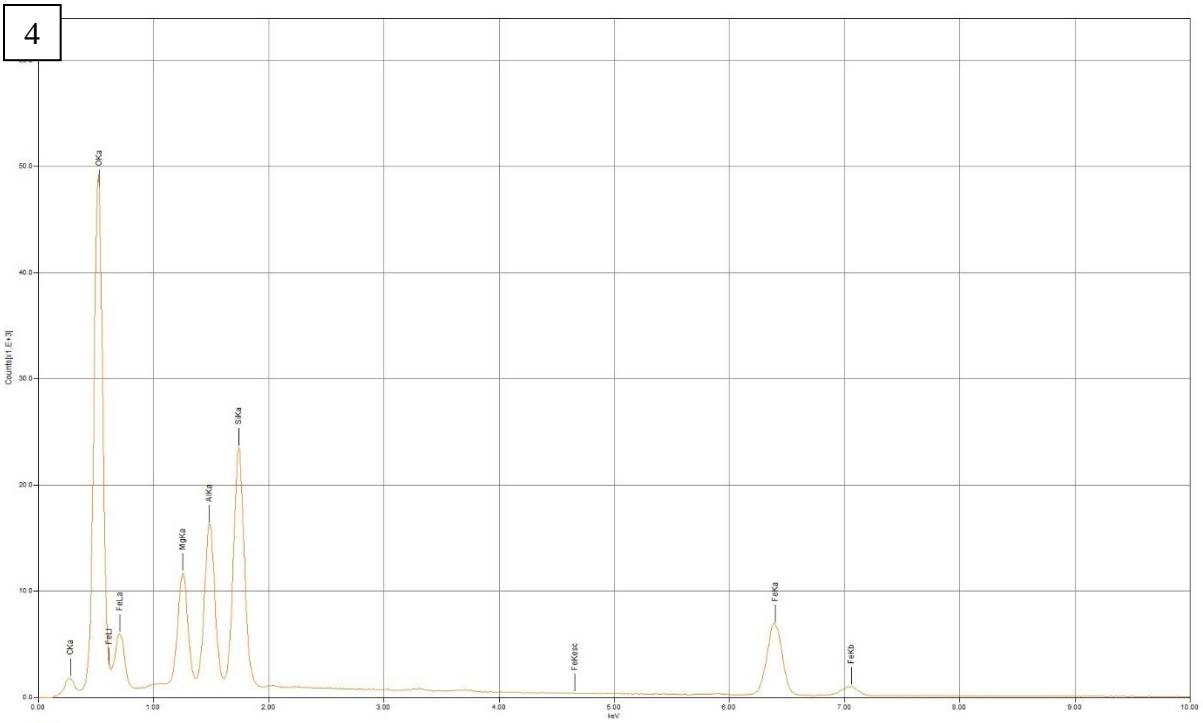
OKa
CKa
FeLl
FeLa
MgKa
AlKa
SiKa
FeKasc
FeKa
FeKb
Counts[n1 E+3]
keV

3

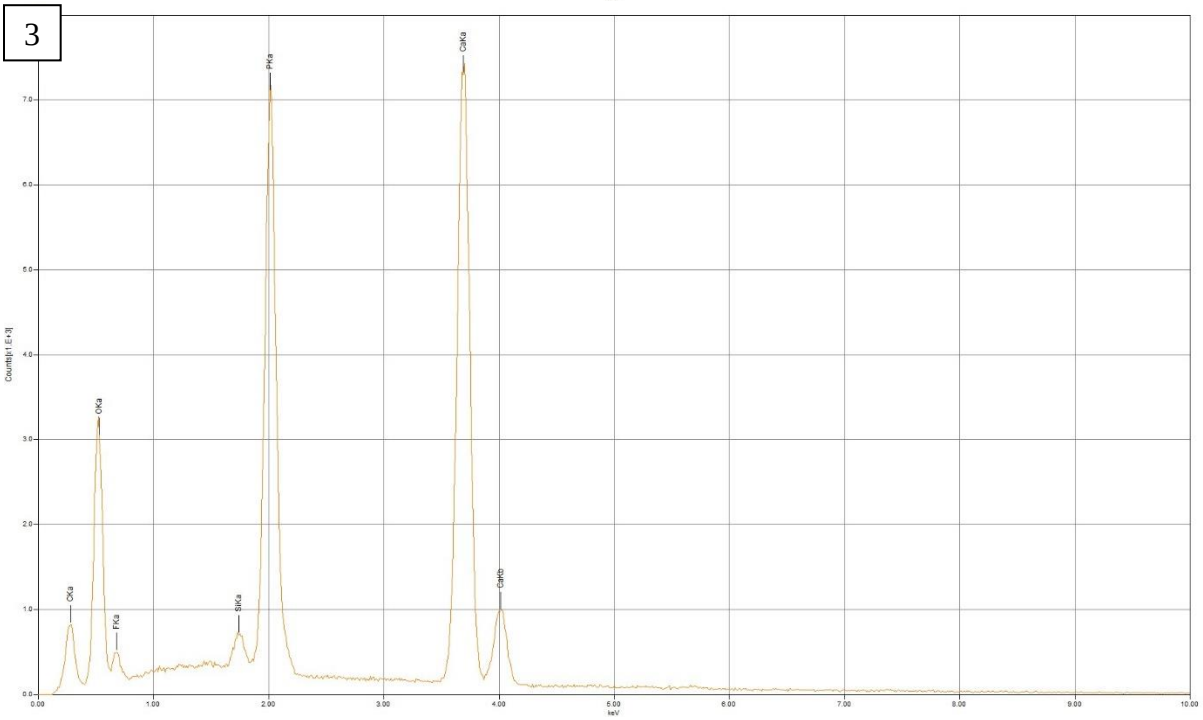
PKa
CaKa
OKa
CKa
FKa
SiKa
CaKb
Counts[n1 E+3]
keV

Grain 10

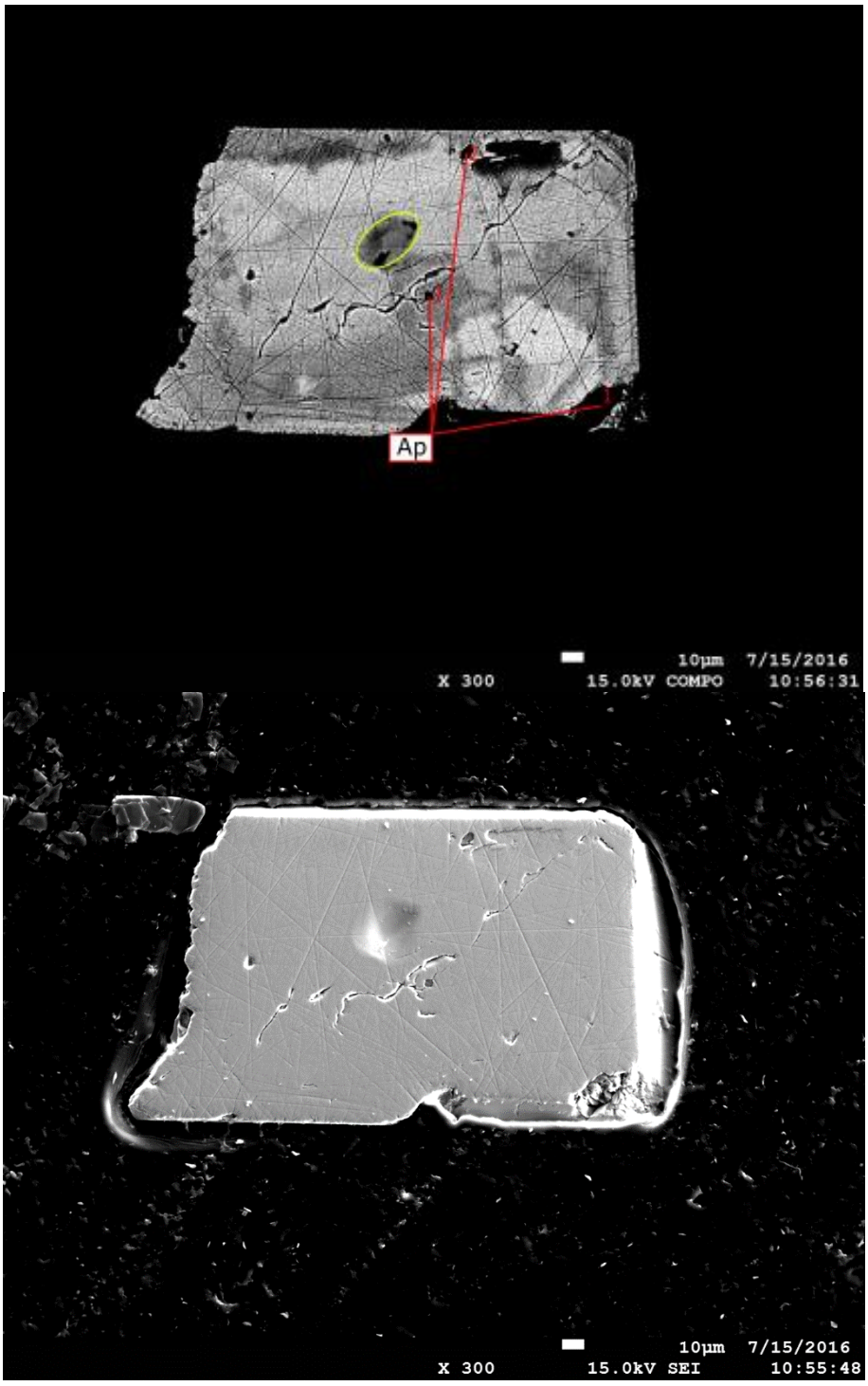
Ap
X 300
10µm
15.0kV COMPO
7/15/2016
10:56:31
X 300
10µm
15.0kV SEI
7/15/2016
10:55:48

1

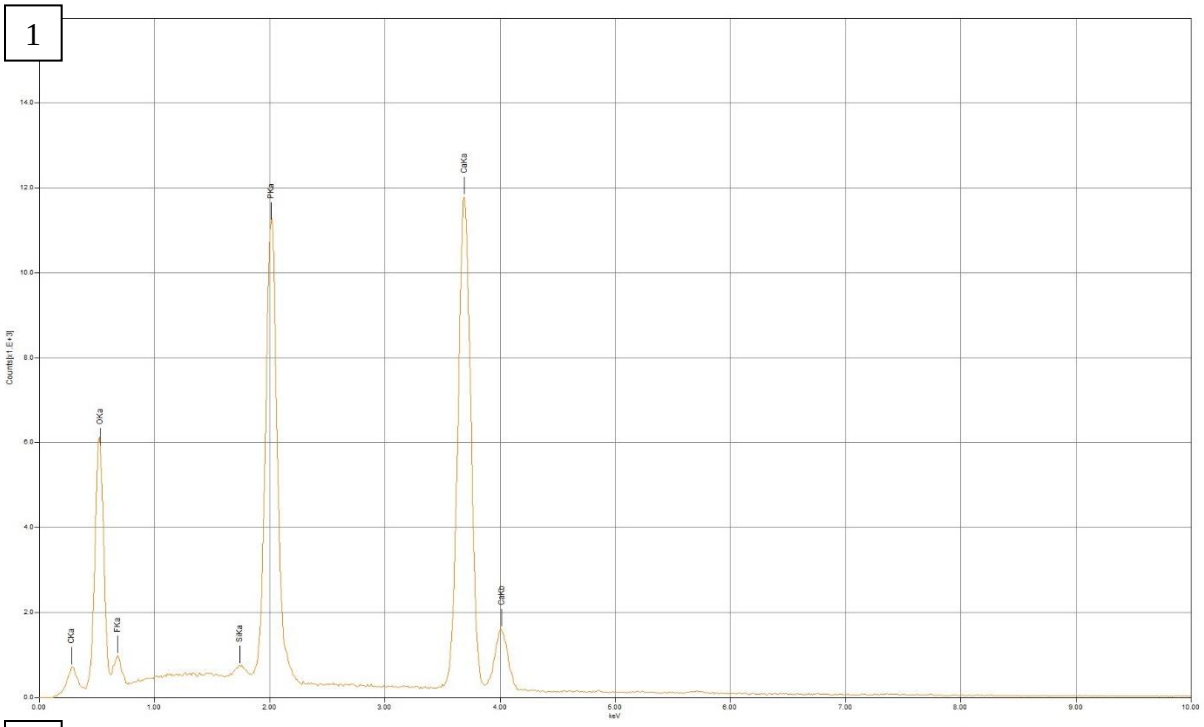

2

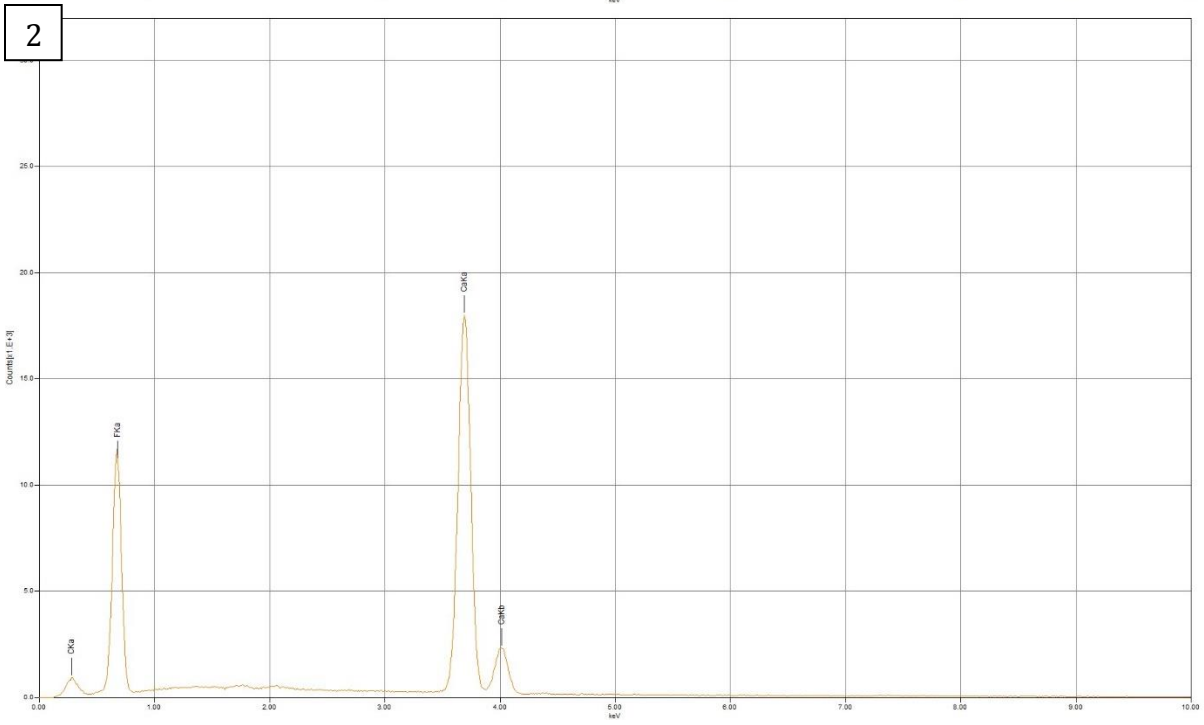

3

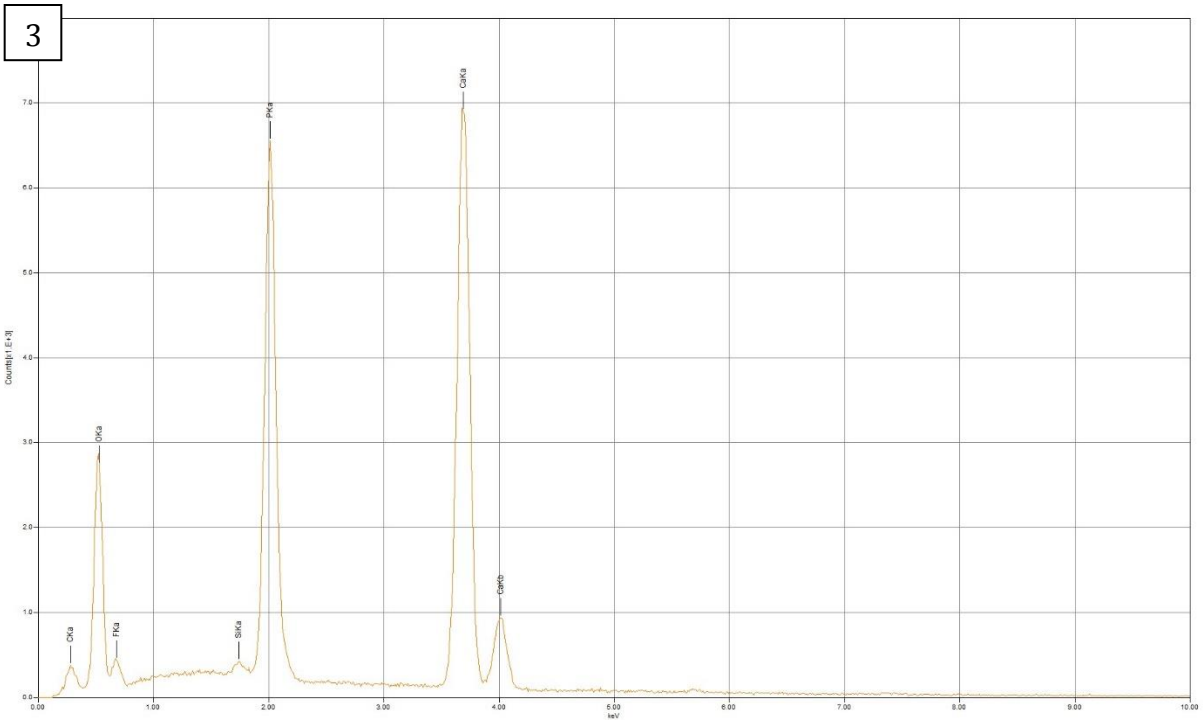

Grain 11

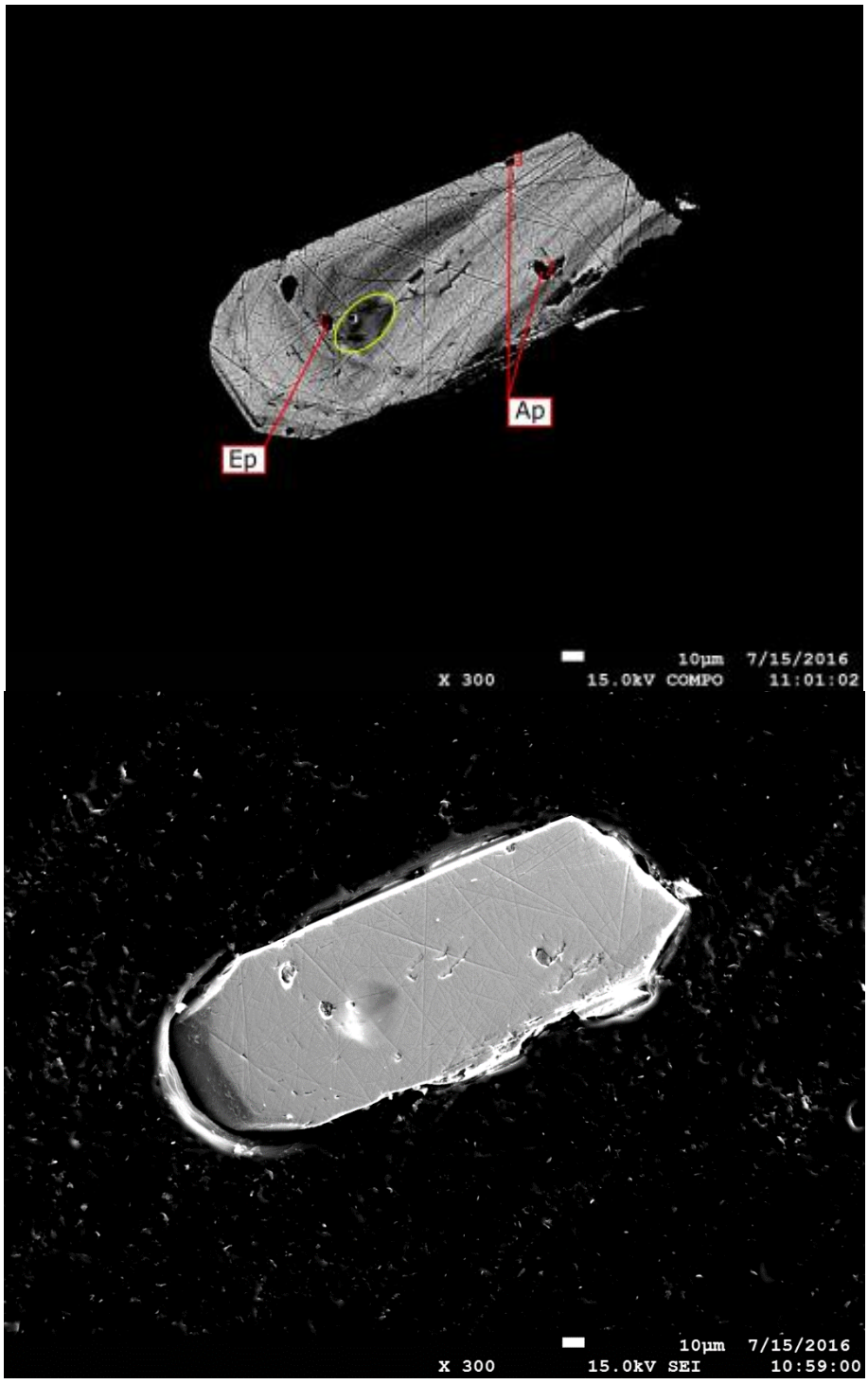
Ap
Ep
X 300
10µm
15.0kV COMPO
7/15/2016
11:01:02
X 300
10µm
15.0kV SEI
7/15/2016
10:59:00

1

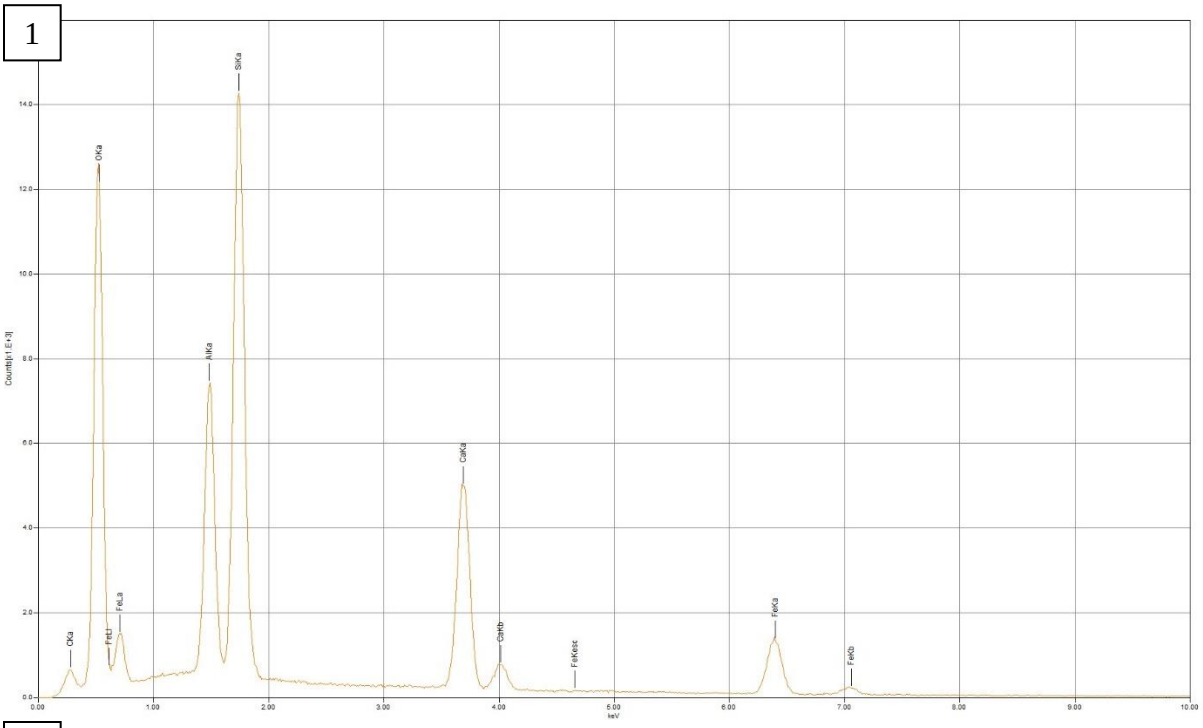
OKa
SiKa
AlKa
CaKa
CaKb
FeKa
FeKb
FeKesc
FeLa
FeLl
OKa
Counts[x1 E+3]
keV

2

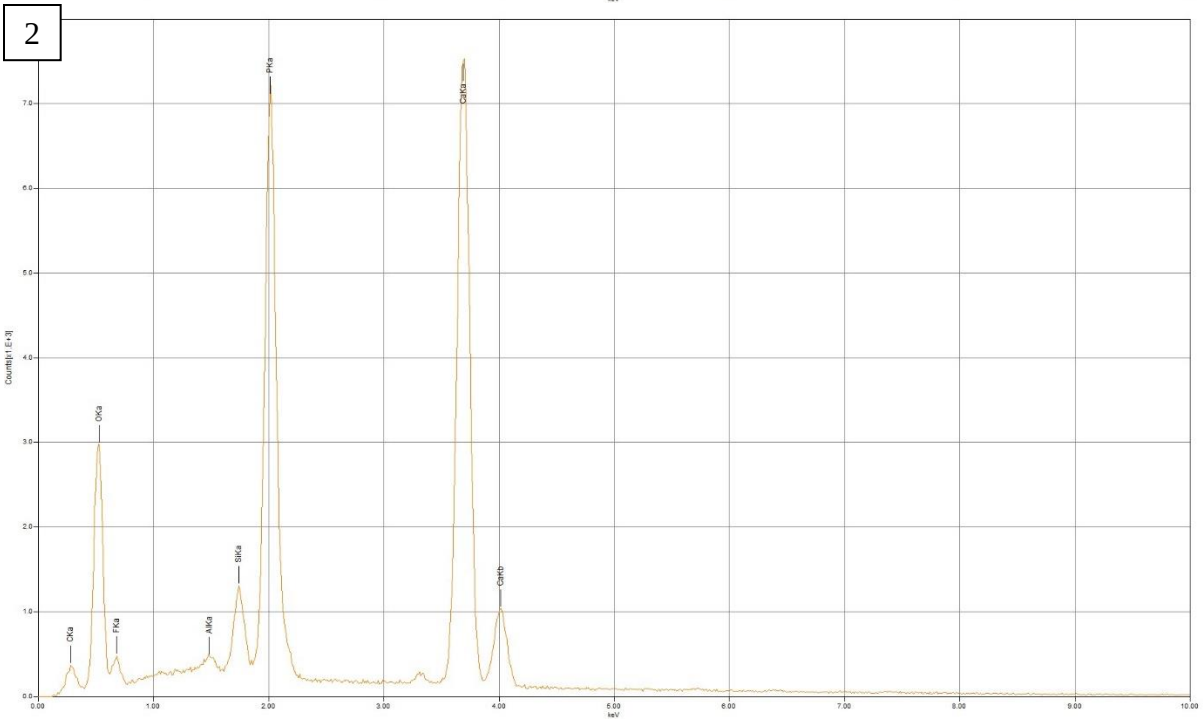
PKa
CaKa
OKa
SiKa
CaKb
FKa
AlKa
OKa
Counts[x1 E+3]
keV

3

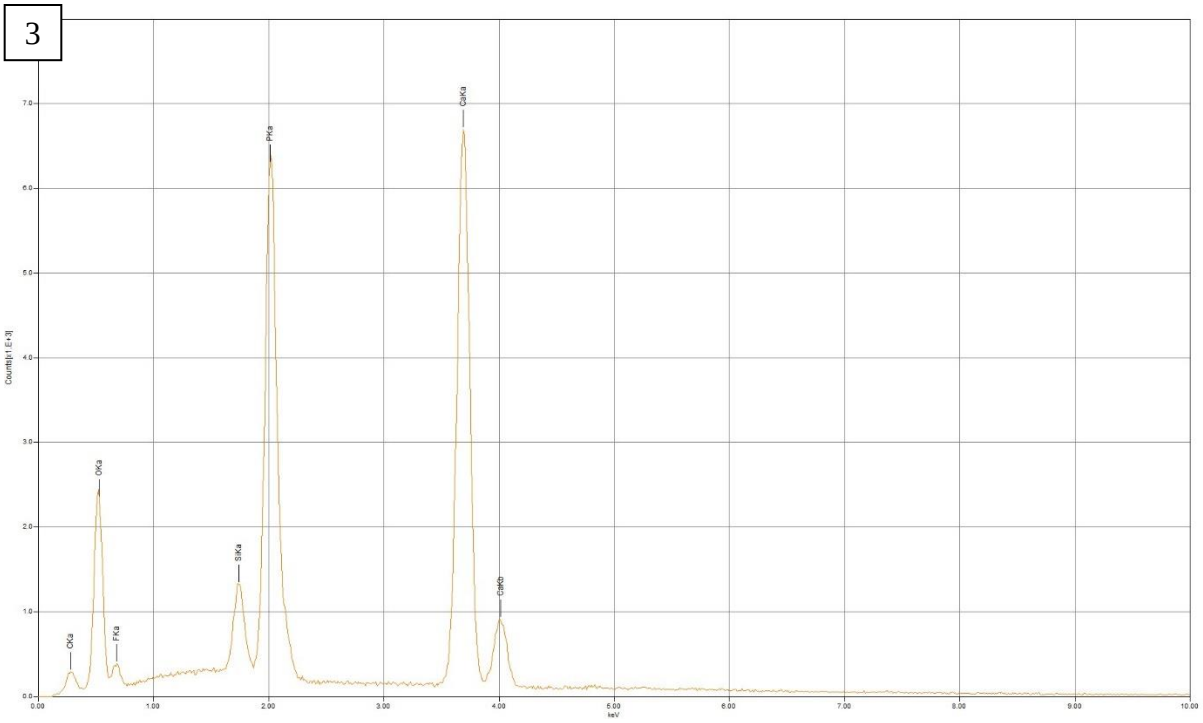

Vita

Andrew Webb was born on March 27, 1991 in Lafayette, Louisiana. He grew up in St. Tammy Parish, Louisiana and graduated high school from Fontainebleau High School in 2009. He then obtained a Bachelor's Degree in Geology at the Louisiana State University, and continued his education at LSU to earn a Master's of Science degree in Geology. He plans on continuing his education by earning a PhD with Dr. Carol Wicks.